Quantitative analysis of relationships

between fluxome and metabolome in *Escherichia coli*

Proefschrift

ter verkrijging van de graad van doctor
aan de Technische Universiteit Delft,
op gezag van de Rector Magnificus Prof. ir. K.C.A.M. Luyben,
voorzitter van het College voor Promoties,
in het openbaar te verdedigen op 4 oktober 2010 om 10:00 uur

door

Hilal TAYMAZ NİKEREL
Master of Science in Chemical Engineering
Boğaziçi University
geboren te Adana, Turkije

Dit proefschrift is goedgekeurd door de promotor:
Prof.dr.ir. J.J.Heijnen

Copromotor: Dr. W.M. van Gulik

Samenstelling promotiecommissie:

Rector Magnificus	voorzitter
Prof.dr.ir. J.J. Heijnen	Technische Universiteit Delft, promotor
Dr. W.M. van Gulik	Technische Universiteit Delft, copromotor
Prof.dr. J.H. de Winde	Technische Universiteit Delft
Prof.dr. M.J. Teixeira De Mattos	Universiteit van Amsterdam
Prof.dr.ing. M. Reuss	Universität Stuttgart
Prof.dr. B. Teusink	Vrije Universiteit Amsterdam
Prof.dr.ir. W. Soetaert	Universiteit Gent
Prof.dr. J.T. Pronk	Technische Universiteit Delft (reservelid)

to my family

Summary

Kinetic models, which predict the behaviour of metabolic reaction networks under different conditions, are indispensible to fully and quantitatively understand the relation between a product pathway and connected central metabolism. In this thesis the focus was to develop tools for future *in vivo* kinetic modeling in *Escherichia coli*. The relations between fluxome and metabolome at steady-state or transient state but where enzyme levels can be assumed constant are investigated. In addition, we aimed at stoichiometric and thermodynamic analyses that are also fundamental to comprehend the cellular systems.

Network stoichiometry is a significant aspect of kinetic models. Stoichiometric metabolic networks usually lack proper biomass composition and the exact stoichiometry of energy generating and consuming processes, e.g. the efficiency of ATP generation in oxidative phosphorylation (P/O ratio) and growth dependent and growth independent maintenance energy requirements (i.e. K_X and m_{ATP}). **Chapter 2** presents the determination of biomass composition of glucose-limited grown *E. coli* K12 cells, derivation of minimal network subsets from the genome-scale reconstruction for carbon-limited chemostat cultivations on minimal media and the estimation of the *in vivo* ATP stoichiometry parameters of this metabolic network. This allowed deriving Herbert-Pirt relations, which are of value, e.g. for quantification of transient growth rate (based on ATP balance), as was shown in Chapter 5.

Following in **Chapter 3**, the ATP related energy aspects of a stoichiometric metabolic network was studied within a thermodynamic framework. Case studies were production of dicarboxylic acids; fumaric (in eukaryotes) and succinic (in prokaryotes). Results point out the importance of black box analysis in learning the energy-related capabilities of the network of interest, e.g. Gibbs energy formation of the theoretical anaerobic reaction indicated that the maximal theoretical product yields are anaerobically feasible, also at low pH (< 3). Considering a required high extracellular total acid concentration, thermodynamically feasible active transport mechanisms were found to be H^+ antiport at pH 3 and H^+ symport at pH 7 for both acids. Subsequent detailed network analysis showed where biologically useful energy could be consumed, leading to novel metabolic engineering targets to enable fully anaerobic production at theoretical yields.

Given that a kinetic model needs information on metabolite concentrations, first a proper method is required to get accurate data. Measurement of intracellular metabolite concentrations requires rapid sampling, instantaneous quenching of metabolic enzymes activity with absence of leakage and removal of the extracellular medium as well as extraction of metabolites taking into account the high turnover rate of these compounds. In **Chapter 4** different quenching protocols that are variations of the most commonly applied method to remove extracellular metabolites, namely quenching with cold methanol and subsequent washing of the cell pellet, for arresting cellular metabolic activity in *E. coli* were investigated. From accurate LC-ESI-ID-MS/MS or GC-MS measurements of central metabolites, amino acids and adenine nucleotides, metabolite leakage during cold methanol quenching was quantified using a rigorous balancing approach. Consequently, a differential method, whereby broth samples are rapidly withdrawn from the

chemostat with a dedicated rapid sampling device and instantaneously quenched (< 180 ms) and culture filtrate is obtained by direct filtration of broth, was developed.

To gain information on *in vivo* enzyme kinetics, generally stimulus-response experiments are performed. In **Chapter 5** a quantitative analysis of flux and metabolite response during a perturbation of a glucose-limited grown *E. coli* culture with a glucose-pulse directly applied to the bioreactor, is presented. Flux quantification was based on the uptake/secretion rates, which are determined by mass balance equations and ATP balance. Metabolite quantification for 37 metabolites in glycolysis, tricarboxylic acid (TCA) cycle, pentose phosphate pathway (PPP), nucleotides and amino acids was carried out with the proposed differential method (in Chapter 4). A novel approach to resolve fluxes at seconds time scale was based on the calculation of $q_{O2}(t)$ from dynamic dissolved O_2 (DO) mass balance and measured DO levels. The obtained dynamic flux and metabolite concentration-time patterns in a time period of 50 s were highly corresponding. However, the observed remarkable increase in the growth rate (3-4 fold within 50 s), and hence protein synthesis rate was not reflected in changed amino acid concentrations. This suggested that the transcripts are increased in this short time frame. *In vivo* relations between growth rate and fructose-1,6-bisphosphate (FBP) concentration and between oxygen uptake rate and AMP/ATP ratio were found.

Since *E. coli* is shown to respond very quickly (to glucose perturbations), sampling at very short intervals is required. The device BioScope, designed by our group, fulfills this purpose with an additional advantage that pulses are given outside the bioreactor thus without disturbing the running culture and allowing multiple pulse response experiments. **Chapter 6** describes the characterization and application of the new BioScope II device, which was redesigned for *E. coli* perturbation experiments. Therefore the total observation time window as well as the sample intervals was decreased by shortening the BioScope channel, leading to a time window of 0 - 8 and 0 - 40 s for flow rates of 4 and 2 ml/min respectively. Furthermore the oxygen transfer characteristics were improved by increasing the ratio between the membrane area for gas transfer and the liquid volume. The performance of the modified BioScope is demonstrated by showing that the results of glucose perturbations carried out in the BioScope, coupled to a steady-state chemostat culture of *E. coli,* and results of similar perturbations carried out directly in the chemostat, are very comparable. Hereby it was ensured that oxygen non-limited conditions were maintained in both systems. For proper metabolite quantification we have applied the differential method, which we described in Chapter 4. The obtained results clearly showed the fast dynamic behaviour of the phosphotransferase system (PTS) in *E. coli.*

The BioScope does not allow flux quantification and therefore a pulse experiment should be performed both in the bioreactor (for flux quantification, Chapter 5) and in the BioScope (for fast metabolite dynamics, Chapter 6). In **Chapter 7** *in vivo* dynamic response of *E. coli*, grown at glucose-limited chemostat, to glycolytic (glucose) and gluconeogenic (pyruvate, succinate) substrates were investigated in both platforms. Time-resolved flux quantification at seconds time scale was based on the uptake/secretion rates, which are determined from dynamic mass balance equations and the degree of reduction balance. After each added different substrate the system (flux and metabolites) achieved pseudo-steady-state in about 30 - 40 s and a huge oxygen uptake

capacity of the cells was observed, and interestingly within 40 s the growth rate reached from its steady-state value of 0.13 h^{-1} to 0.3 h^{-1} for each different substrate pulse, indicating a capacity limit in e.g. ribosomes. The observed dynamic responses showed massive reorganization and flexibility (up to 12 - 100 fold change) of intracellular fluxes following the different pulses, which matches with the steep changes in metabolite levels leading to dynamic shifts in mass action ratio's of pseudo-/near-equilibrium reactions and flux inversions. From the dynamic intracellular metabolite and flux information, the *in vivo* kinetics was studied based on a simplified thermodynamic approach. It was found that several enzymes showed simple near-equilibrium kinetics as found before in baker's yeast (Q-linear kinetics).

In **Chapter 8** a comparative study of steady-state and dynamic metabolite and flux responses to localized pulses for succinate overproducing *E. coli* mutant is presented. In this mutant two transcription factors of glyoxylate pathway are deleted, which did not seem to affect this pathway but there was a significant effect on improved energy efficiency. The mutant had four functional mutations: increased succinate exporter, a deleted succinate importer, deletion of succinate dehydrogenase and a PEP carboxylase with increased capacity due to a point mutation. These mutations have a clear effect on steady-state and dynamic behaviour. In general the mutant showed much lower maximal uptake rates and succinate export was successfully implemented. Succinate import was 26 fold decreased. Also the mutant showed enormous dynamic flux flexibility. Compared to the wild type a considerable shift occurred from TCA cycle to oxidative PPP, including inversion of pyruvate kinase. Even more flexibility was observed on succinate uptake which seems only possible by an inverted TCA cycle. These flux shifts were in agreement with large and delocalized changes in metabolite levels. Clearly succinate dehydrogenase deletion caused large changes in metabolite levels close to and far from the deleted reaction. The mutant as the wild type showed extreme homeostatic behaviour for energy charge in the pulses. In contrast, large changes in redox level NAD^+/NADH occurred where the mutant showed even larger changes. This large redox change can be associated to reversal of flux direction.

In **Chapter 9** a different application area, which is large-scale mixing problems, of perturbation experiments is presented. Large-scale bioreactors are known to have heterogeneous conditions and several scale-down studies have reported the response of cells to glucose and DO gradients, whereby the glucose gradients have been attributed to cause DO depletion. The situation was mimicked with a two-compartment bioreactor system consisting of an *E. coli* chemostat culture connected to a BioScope. Fully aerobic transition from a glucose-limiting to a glucose-rich region triggered the overflow metabolism very rapidly (< 2 s). When the glucose gradient was created under anaerobic conditions, many other mixed-acid fermentation metabolites were detected with higher production rates. This study demonstrated that secretion of fermentative by-products occurs even from very short exposures of cells to gradients in large-scale bioreactors and this situation might induce unfavorable process performance.

Samenvatting

Kinetische modellen, die het gedrag van metabole reactienetwerken onder verschillende omstandigheden voorspellen, zijn onmisbaar om een kwantitatief en volledig inzicht te krijgen in de relatie tussen een productpad en het centraal metabolisme. De focus van dit proefschrift is het ontwikkelen van instrumentarium voor toekomstige *in vivo* kinetische modellering van het metabolisme in *Escherichia coli*. De relaties tussen het fluxoom en het metaboloom zijn onderzocht zowel in de steady-state als na een stapresponsie, waarbij enzymniveaus constant verondersteld kunnen worden. Daarnaast richten we ons op stoichiometrische en thermodynamische analyses die ook fundamenteel zijn voor het begrip van cellulaire systemen.

Netwerk stoichiometrie is een belangrijk onderdeel van kinetische modellen. Stoichiometrische metabole netwerken missen meestal de juiste biomassa samenstelling en de exacte stoichiometrie van de energie genererende en consumerende processen, bv. de efficiëntie van de ATP productie in de oxidatieve fosforylering (P/O ratio), de groei-afhankelijkheid van het onderhoud (K_X) en het groei-onafhankelijke deel van het onderhoud (m_{ATP}). **Hoofdstuk 2** presenteert de bepaling van de biomassasamenstelling van *E. coli* K12 cellen bij glucose-gelimiteerde groei, afleiding van minimale metabole netwerken voor koolstof gelimiteerde chemostaat groei op basis van het genoom en de schatting van *in vivo* ATP stoichiometrie parameters. Hieruit konden de Herbert-Pirt vergelijkingen afgeleid worden, die waardevol zijn voor de kwantificering van groei (gebaseerd op de ATP balans), zoals wordt aangetoond in hoofdstuk 5.

In **hoofdstuk 3**, worden de ATP gerelateerde energie aspecten van een stoichiometrisch metabool netwerk bestudeerd binnen een thermodynamisch context. Case studies zijn de productie van dicarbonzuren; fumaarzuur (in eukaryoten) en barnsteenzuur (in prokaryoten). De resultaten tonen het belang aan van "black box" analyse in het identificeren van energiegerelateerde capaciteiten van een netwerk. Een voorbeeld is de berekende Gibbs energie dissipatie voor de theoretische productvormings reactie onder anaërobe omstandigheden, die aangeeft, dat maximale theoretische productopbrengsten energetisch gezien haalbaar zouden moeten zijn, ook bij lage pH (< 3). Uitgaande van een vereiste hoge extracellulaire totale zuurconcentratie, blijken voor beide zuren de thermodynamisch haalbare transport mechanismen een H^+ antiport bij een pH van 3 en een H^+ symport bij een pH van 7 te zijn. De daaropvolgende detailanalyse van het netwerk toonde aan waar biologisch bruikbare energie kon worden ingezet. Dit leidde tot nieuwe metabolic engineering targets voor volledige anaërobe productie bij theoretisch maximaal rendement.

Een kinetisch model gebruikt informatie over metaboliet concentraties. Daarom is eerst een goede methode nodig om nauwkeurige gegevens hierover te krijgen. Voor betrouwbare meting van de intracellulaire metaboliet concentraties is een snelle bemonstering en het onmiddelijk stoppen (quenching) van alle enzymactiviteit noodzakelijk om verdere omzetting te voorkomen. Tijdens deze bemonstering dient lekkage van metabolieten te worden voorkomen en moeten extracellulaire metabolieten zo goed mogelijk verwijderd worden. In **hoofdstuk 4** worden verschillende quenching protocollen onderzocht, die varianten zijn van de meest toegepaste methode om extracellulaire metabolieten te verwijderen, namelijk quenchen met koude methanol,

voor het stoppen van cellulaire metabole activiteit en vervolgens het wassen van het cel pellet voor het verwijderen van extracellulaire metabolieten. Nauwkeurige LC-ESI-ID-MS/MS en GC-MS metingen van metabolieten, aminozuren en nucleotides zijn gebruikt om lekkage tijdens het koude methanol quenchen te kwantificeren met behulp van een zorgvuldige beschouwing van de component balansen. Hieruit bleek dat de lekkage van metabolieten tijdens quenching met koude methanol zo groot was dat alleen met behulp van een zogenaamde differentiële methode (waarbij de intracellulaire metaboliet hoeveelheden worden berekend aan de hand van metaboliet metingen in de totale cultuurvloeistof en het in filtraat) de enige betrouwbare procedure bleek te zijn.

Om informatie te verkrijgen over de *in vivo* enzymkinetiek, worden in het algemeen stimulus-respons experimenten uitgevoerd. In **hoofdstuk 5** wordt een kwantitatieve analyse gepresenteerd van de flux en de metaboliet respons op een verstoring van glucose-gelimiteerde groei van een *E. coli* cultuur met een glucose puls direct toegepast op de bioreactor. Flux bepaling is gebaseerd op de opname/secretie snelheden die worden bepaald door middel van massabalans vergelijkingen en het ATP evenwicht. Kwantificering van 37 metabolieten (in glycolyse, TCA-cyclus, pentose phosphate pathway (PPP)), nucleotiden en aminozuren werd uitgevoerd met de voorgestelde differentiële methode (in hoofdstuk 4). Een nieuwe aanpak voor fluxbepaling op een tijdschaal van secondes is gebaseerd op de berekening van $q_{O2}(t)$ uit de dynamische opgeloste O_2 (DO = dissolved oxygen) massabalans en het gemeten DO niveau. De verkregen dynamische flux en metaboliet concentratie-tijd profielen over een periode van 50 s bleken goed vergelijkbaar. De opmerkelijke stijging waargenomen in de groei (een factor 3-4 binnen 50 s), en daarmee de eiwitsynthese snelheid kwam niet tot uitdrukking in veranderende aminozuur concentraties. Dit suggereert dat de transcripten zijn toegenomen in deze korte tijd. *In vivo* zijn relaties gevonden tussen groeisnelheid en FBP concentratie en ook tussen zuurstofopname snelheid en AMP/ATP ratio.

Omdat het is gebleken dat *E. coli* zeer snel reageert op glucose verstoringen, is bemonstering op zeer korte tijdsintervallen vereist. De BioScope, een propstroom bioreactor ontworpen in de TUD biotechnologie afdeling, voldoet aan deze eisen met een extra voordeel dat verstoringen worden aangebracht buiten de bioreactor, dus zonder het verstoren van de lopende cultuur. De BioScope biedt tevens de mogelijkheid diverse typen verstoringen aan te brengen op een en dezelfde bioreactor cultuur. **Hoofdstuk 6** beschrijft de karakterisering en toepassing van de nieuwe BioScope II, dat werd herontworpen speciaal voor *E. coli* verstoringsexperimenten. In dit apparaat werden de totale observatie tijd evenals de meetintervallen verlaagd door het verkorten van het BioScope kanaal. Dit resulteerde in tijdsintervallen van 0 - 8 s en 0 - 40 s voor debieten van respectievelijk 4 en 2 ml/min. Verder werd de zuurstof overdracht verbeterd door een vergroting van de verhouding tussen membraanoppervlak voor overdracht van gas en het vloeistofvolume. De prestaties van de gewijzigde BioScope werden geverifieerd door experimenten met glucose verstoringen aan een BioScope gekoppeld met een chemostaat te vergelijken met experimenten aan een steady-state chemostaat cultuur van *E. coli*. Hierbij werd ervoor gezorgd dat er geen zuurstofbeperking optrad in beide systemen. Voor een goede metaboliet kwantificering hebben we de differentiële methode, beschreven in hoofdstuk 4,

toegepast. De verkregen resultaten toonden duidelijk het snelle dynamische gedrag aan van het phosphotransferase systeem (PTS) in *E. coli*.

De BioScope laat geen kwantitatieve bepaling van de fluxen toe. Dus een pulsexperiment moet worden uitgevoerd, zowel in een bioreactor (voor de flux bepaling, hoofdstuk 5) als in de BioScope (voor snelle metaboliet dynamica, hoofdstuk 6). In **hoofdstuk 7,** werd de *in vivo* dynamische respons van *E. coli* onderzocht, zowel in de BioScope als in de bioreactor, op verstoringen met glycolytische (glucose) en gluconeogenic (pyruvaat, succinaat) substraten. Flux als functie van tijd zijn berekend op basis van opname/secretie snelheden, die werden bepaald door dynamische massabalansvergelijkingen en het "degree of reduction" evenwicht. Na elke toevoeging van een substraat bereikte het systeem (flux en metabolieten) een pseudo-steady-state in ongeveer 30-40 s en een grote zuurstofopname capaciteit van de cellen werd waargenomen. Interessant was dat binnen 40 s de groeisnelheid een steady-state waarde van 0.13 h^{-1} tot 0.30 h^{-1} bereikt onafhankelijk van het substraat, waaruit blijkt dat de capaciteitsbeperking mogelijk in ribosomen plaatsvindt. Uit de waargenomen dynamische responses bleek dat grote intracellulaire flux variaties (tot 12 - 100 voudige verandering) aanwezig zijn, die past bij de veranderingen in metaboliet concentraties en verschuivingen in de dynamische massa-actie ratio's van pseudo-/bijna-evenwichtsreacties. Vanuit de dynamische intracellulaire metaboliet en flux informatie, werd de *in vivo* kinetiek bestudeerd op basis van een vereenvoudigde thermodynamische aanpak. Het bleek dat een aantal enzymen een bijna-evenwichtskinetiek vertoonden, zoals voorheen gevonden in bakkersgist (Q-lineaire kinetiek).

In **Hoofdstuk 8** wordt een vergelijkende studie gepresenteerd van de steady-state en dynamische metaboliet en flux responses op pulsen aan een succinaat overproducerende *E. coli* mutant. In deze mutant werden twee transcriptiefactoren van de glyoxylaat pathway verwijderd. Zij leken geen invloed op deze route te hebben, maar veroorzaakten een significant verbeterde energie-efficiëntie. De mutant had vier functionele mutaties: een verhoogde succinaat exporter, een verwijderde succinaat importer, het verwijderen van succinaat dehydrogenase en een PEP-carboxylase met een grotere capaciteit als gevolg van een genmutatie. Deze mutaties hadden een duidelijk effect op het steady-state en dynamische gedrag. Deze mutant vertoonde over het algemeen veel lagere maximale opname snelheden, terwijl de export van succinaat succesvol werd uitgevoerd. Succinaat invoer was 26 keer minder. De mutant vertoonde ook een grote dynamische flux flexibiliteit. In vergelijking met het wild type vond een aanzienlijke flux verschuiving plaats van de TCA-cyclus naar de oxidatieve PPP, met inbegrip van omkering van de pyruvaat kinase flux. Nog meer flexibiliteit werd waargenomen bij de succinaat opname die alleen mogelijk lijkt door een geïnverteerde TCA cyclus. Deze flux verschuivingen waren in overeenstemming met grote en gedelokaliseerde veranderingen in metaboliet niveaus. Knock-out van het succinaatdehydrogenase gen veroorzaakt grote veranderingen in metabolietconcentraties van intermediairen van het metabolisme die zowel dicht als ver van de verwijderde reactie liggen. De mutant en het wild-type vertoonden homeostatisch gedrag voor wat betreft de ATP, ADP en AMP niveaus tijdens de verstoringen. In tegenstelling daarmee, deden zich grote veranderingen in het redox-niveau NAD$^+$/NADH voor, waarbij de mutant de grootste veranderingen vertoonde. Deze grote redox verandering kan worden gerelateerd aan omkering van de flux richting.

In **hoofdstuk 9** wordt een ander toepassingsgebied van puls experimenten gepresenteerd namelijk naar meng problemen in bioreactoren. Grootschalige bioreactoren zijn bekend vanwege hun heterogene condities. In verschillende scale-down studies werd de reactie van de cellen op glucose en DO gradiënten onderzocht, waarbij de glucosegradiënten werden toegeschreven aan DO depletie. De situatie werd nagebootst met een bioreactor systeem van twee compartimenten, bestaande uit een *E. coli* chemostaat cultuur verbonden met een BioScope. Volledig aërobe overgang van een glucose-gelimiteerd naar een glucose-rijk domein initieerde zeer snel (< 2 s) het overflow metabolisme. Veel andere metabolieten werden aangetroffen met een hogere productiesnelheid, wanneer een glucose-gradiënt werd gecreëerd onder anaërobe omstandigheden. Deze studie toonde aan dat de secretie van fermentatie bijproducten plaatsvindt zelfs na zeer korte blootstelling van cellen aan gradiënten, die in grootschalige bioreactoren voorkomen, wat de product opbrengst in ongunstige zin beïnvloedt.

Özet

Metabolik reaksiyon ağlarının farklı koşullardaki davranışlarını öngören kinetik modeller herhangi bir ürün yolu ve ona bağlı merkez metabolizması arasındaki ilişkiyi tamamen ve nicel olarak anlamak için esastır. Bu tezde *Escherichia coli*'de canlı içi (*in vivo*) kinetik modelleme araçları geliştirmeye odaklanıldı. Enzim seviyelerinin sabit kabul edilebileceği kararlı veya geçici durumlarda flaksom ile metabolom arasındaki ilişkiler incelendi. Ayrıca hücresel sistemleri kavramakta temel olan stokiyometrik ve termodinamik analizler amaçlandı.

Kinetik modellerin temel taşlarından biri de ağ stokiyometrisidir. Stokiyometrik metabolik ağlarda genellikle doğru biyokütle kompozisyonu ve enerji üreten/tüketen süreçlerin kesin stokiyometrisi, örneğin oksidatif fosforilasyonda ATP üretimi verimliliği (P/O oranı) ve büyüme-bağımlı/büyüme-bağımsız bakım enerji gereksinimleri (K_X ve m_{ATP}) eksiktir. **2. Kısım** glukoz-sınırlı yetiştirilen *E. coli* K12 hücrelerinin biyokütle kompozisyonunun belirlenmesini, minimal ortamda büyütülmüş karbon-sınırlı kemostat için genom ölçekli minimal ağ altkümelerinin türetilmesini ve bu metabolik ağa ait *in vivo* ATP stokiyometri parametrelerinin tahminini sunar. Bu, örneğin 5. Kısım'da gösterilen geçici büyüme hızının (ATP dengesine dayalı) hesaplanmasında önemli olan Herbert-Pirt ilişkilerinin türetilmesine olanak sağlamıştır.

Bir sonraki **3. Kısım**'da, stokiyometrik bir metabolik ağın ATP ilişkili enerji özellikleri termodinamik çerçevede incelendi. Fumarik (ökaryotlarda) ve süksinik (prokaryotlarda) dikarboksilik asit üretimleri örnek çalışmalar olarak ele alındı. Sonuçlar ilgili ağın enerji ilişkili kapasitelerini öğrenmede kara kutu analizinin önemini işaret edip, örneğin teorik anaerobik reaksiyonun Gibbs enerji oluşumu maksimal teorik ürün verimlerinin anaerobik olarak uygun olduğunu (üstelik düşük pH(<3)' da) ortaya koydu. Gerekli yüksek hücre dışı toplam asit konsantrasyonu dikkate alındığında, her iki asit için termodinamik uygulanabilir aktif transport mekanizmaları pH 3'de H^+ antiport ve pH 7'de H^+ simport olarak bulundu. Daha sonraki detaylı ağ analizi enerjinin nerede biyolojik açıdan faydalı tüketilebiceğini, teorik verimlerde tam anaerobik üretimi sağlayacak yeni metabolik mühendislik hedeflerine de işaret ederek gösterdi.

Kinetik bir modelin metabolit konsantrasyonları bilgisine ihtiyacı göz önüne alındığında, öncelikle doğru deneysel verileri elde etmenin gerekliliği açıktır. Hücre içi metabolit konsantrasyonları ölçümü hızlı örnekleme, sızıntı yokluğunda anlık metabolik enzim aktivitesini dindirme ve hücre dışı ortamın kaldırılması ile birlikte metabolitlerin yüksek döngü hızları hesaba alınarak bu bileşiklerin özütlenmesini gerektirir. **4. Kısım**'da hücre dışı metabolitleri ayırmak için en sık uygulanan yöntem varyasyonları olan dört farklı dindirme protokolü, yani *E. coli*'de hücresel metabolik aktiviteyi durdurmak için soğuk metanolle dindirme ve müteakip hücre pelletinin yıkanması araştırıldı. Soğuk metanolle dindirme sırasındaki metabolit kaçağı merkez metabolitlerin, amino asitlerin ve adenin nükleotidlerin doğru LC-ESI-ID-MS/MS veya GC-MS ölçümlerinden titiz bir denge yaklaşımı kullanılarak hesaplandı. Sonuç olarak *broth* örneklerinin kemostattan hızlıca, bu iş için özel tasarlanmış hızlı bir örnekleme cihazı ile çekilip ve anlık durdurulup (< 180 milisaniye), kültür süzüntüsünün doğrudan filtrasyon ile elde edildiği diferansiyel bir yöntem geliştirildi.

In vivo enzim kinetiğine dair bilgi edinmek üzere kullanılan genel yöntem uyaran-tepki deneyleridir. **5. Kısım**'da glukoz sınırlı yetiştirilen *E. coli* kültürüne doğrudan biyoreaktörde uygulanan glukoz-puls sırasında akı ve metabolit yanıtının nicel analizi sunuldu. Akı hesabı kütle denge denklemleri ve ATP dengesi tarafından belirlenen alım/sekresyon hızlarına dayandırıldı. Glikoliz, TCA devri, pentoz fosfat yolu, nükleotidler ve amino asitlerden oluşan toplam 37 metabolitin miktarı 4. Kısım'da geliştirilen diferansiyel metod ile hesaplandı. Saniye zaman ölçekli akı hesabı yeni bir yaklaşımla, yani dinamik çözünmüş O_2 (DO) kütle dengesi ve ölçülmüş DO düzeyleri ile gerçekleştirilen $q_{O2}(t)$ hesaplanmasına dayandırıldı. 50 saniyelik bir zaman diliminde elde edilen dinamik akı ve metabolit konsantrasyon-zaman eğilimleri birbirine denkti. Mamafih, büyüme hızında ve dolayısıyla protein sentez hızında gözlenen belirgin artış (50 saniye içinde 3-4 kat) değişen amino asit konsantrasyonlarına yansımadı. Bu durum bu kısa zaman dilimi içinde transkriptlerde artış olabileceğini öne sürdü. Büyüme hızı ile fruktozbisfosfat konsantrasyonu ve oksijen alım hızı ile AMP/ATP oranı arasında *in vivo* ilişkiler tespit edildi.

E. coli (glukoz pulslarına) çok hızlı yanıt verdiğinden, çok kısa aralıklarla örnekleme gereklidir. Grubumuz tarafından tasarlanmış BioScope aleti, ek bir avantaj olan biyoreaktör dışında puls verme ve böylece mevcut kültürü bozmadan, çok sayıda puls-tepki deneylerine olanak sağlayarak, bu amacı yerine getirmektedir. **6. Kısım**'da *E. coli* pertürbasyon deneyleri için tasarlanan yeni BioScope II cihazının karakterizasyonu ve uygulaması açıklandı. BioScope kanalı kısaltılarak toplam gözlem süresi ve örnek aralıkları düşürülmüştür (4 ve 2 ml/dakika akış hızları için sırasıyla 0-8 ve 0-40 saniye). Buna ek olarak gaz transferi membran alanı ile sıvı hacmi arasındaki oran artırılarak oksijen transfer karakteristikleri geliştirildi. Tasarlanan BioScope'un performansı, kararlı durumdaki *E. coli* kemostat kültürüne bağlı BioScope'da ve doğrudan kemostatta benzer yürütülen glukoz pertürbasyon sonuçlarının çok benzer olduğu gösterilerek, açıklandı. Burada her iki sistemde de oksijen sınırlı olmayan koşulların korunması sağlandı. Doğru metabolit miktar hesabı için 4. Kısım'da açıklanan diferansiyel yöntemin uygulanmasıyla elde edilen sonuçlar açıkça *E. coli* phosphotransferase sisteminin (PTS) hızlı dinamik davranışını gösterdi.

BioScope akı ölçümüne izin vermediğinden bir puls deneyi hem biyoreaktörde (akı miktar hesabı için, 5. Kısım) hem de BioScope'da (hızlı metabolit dinamikleri için, 6. Kısım) yapılmalıdır. **7. Kısım**'da glukoz-sınırlı kemostatta yetiştirilen *E. coli*'nin glikolitik (glukoz) ve glikoneojenik (pirüvat, süksinat) substratlara gösterdiği *in vivo* dinamik tepki her iki platformda da araştırıldı. Saniye ölçekli akı hesabı dinamik kütle denge denklemleri ve redüksiyon derecesi dengesi ile belirlenen alım/sekresyon oranlarına dayandırıldı. Her eklenen farklı substrattan sonra sistem (akı ve metabolitler) yaklaşık 30-40 saniye içinde psödo-kararlı duruma ulaştı ve büyük bir oksijen kapasitesi gözlendi. İlginç olarak her farklı substrat için 40 saniye içinde büyüme oranı kararlı durumdaki 0,13 1/saat değerinden 0,3 1/saat'e ulaştı. Bu durum örneğin ribozomlarda bir kapasite sınırına işaret etti. Farklı pulsları takiben gözlenen dinamik yanıtlar büyük ölçekte reorganizasyon ve esneklik (12-100 kata kadar değişiklik) gösterdi. Bu durumun metabolit seviyelerindeki aşırı değişikliklerin yol açtığı psödo-/yakın-denge reaksiyonlarının kütle eylem oranlarındaki dinamik kaymalar ve akı yönlerinin tersine dönmesiyle uyumlu olduğu gözlendi. *In vivo* kinetiği hücre içi dinamik metabolit ve akı bilgileriyle basitleştirilmiş bir termodinamik

yaklaşıma dayanarak çalışıldı. Daha önce ekmek mayasında gözlendiği gibi (Q-lineer kinetik) burada da çeşitli enzimlerin basit yakın denge kinetiğine sahip olduğu bulundu.

8. Kısım'da yüksek miktarda süksinat üreten *E. coli* mutantının kararlı ve dinamik durumlarda lokalize pulslara gösterdiği metabolit ve akı yanıtları karşılaştırmalı bir çalışmayla sunuldu. Glyoksilat yoluna ait iki transkripsiyon faktörünün silindiği mutantta bu değişikliklerin bu yolu etkilemediği ancak gelişmiş enerji verimliliğine önemli bir etkisi olduğu gözlendi. Mutant artırılmış süksinat *exporter*, silinmiş süksinat *importer*, silinmiş süksinat dehidrojenaz ve bir nokta mutasyonuyla kapasitesi artırılmış PEP karboksilaz olmak üzere kararlı ve dinamik durum davranışlarına açık etkisi olan dört fonksiyonel mutasyona sahipti. Mutant genel olarak çok daha düşük maksimal alım oranları gösterdi ve süksinat sekresyonu başarılı bir şekilde gerçekleştirildi. Süksinat alımı 26 kat azaldı. Ayrıca mutant büyük ölçekte dinamik akı esnekliği gösterdi. Yaban tip ile karşılaştırıldığında piruvat kinazın yön değiştirmesi dahil TCA döngüsünden oksidatif pentoz fosfat yoluna önemli bir değişim oluştu. Ancak ters bir TCA döngüsü ile olası olan süksinat alımında daha fazla esneklik gözlendi. Bu akı değişimleri metabolit düzeylerindeki büyük ve delokalize olmuş değişiklikler ile uyumluydu. Açıkça, süksinat dehidrojenazın silinmesi silinmiş reaksiyona yakın ve uzak metabolit düzeylerinde büyük değişikliklere neden oldu. Yaban tip gibi mutant da pulslarda enerji yükü açısından aşırı homeostatik davranış gösterdi. Buna karşılık, redoks düzeyi $NAD^+/NADH$'de mutantta daha fazla gözlenen büyük değişiklikler oluştu. Bu büyük redoks değişikliği akı yönünün tersine dönmesiyle ilişkilendirilebilir.

9. Kısım'da pertürbasyon deneylerinin farklı bir uygulama alanı olan büyük ölçekli karıştırma problemleri sunuldu. Heterojen koşullara sahip olduğu bilinen büyük ölçekli biyoreaktörlerin çeşitli boyut küçültme çalışmalarında glukoz gradyanlarının DO'da tükenmeye sebep olduğuna atfedilerek hücrelerin glukoz ve DO geçişlerine yanıtı bildirilmiştir. Bu durum *E. coli* kemostat kültürünün bir BioScope'a bağlandığı iki bölmeli biyoreaktör sistemi ile taklit edildi. Tamamen aerobik ortamda glukoz sınırlı bölgeden glukoz zengin bölgeye geçiş, taşma metabolizmasını çok hızlı (< 2 saniye) tetikledi. Glukoz gradyanı anaerobik şartlar altında gerçekleştirildiğinde yüksek üretim oranlarında birçok karışık-asit-fermantasyon metabolitleri saptandı. Bu çalışma büyük ölçekli biyoreaktörlerde hücrelerin gradyanlara çok kısa süre maruz kaldığında bile olumsuz süreç performansına neden olabilecek fermentatif yan ürünleri salgıladığını gösterdi.

Contents

List of Abbreviations and Symbols

AcCoA	acetyl coenzyme A	FBP	fructose-1,6-bisphosphatase
Ace	acetate	FHL	formate hydrogen lyase
ACK	acetate kinase	*fnr*	fumarate-nitrate respiration regulatory gene
ACoNT	aconitase		
ADP	adenosine-5-diphosphate	FUM	fumarase
AK	adenylate kinase	Fum	fumarate
AKGDH	α-ketoglutarate dehydrogenase	G1P	glucose-1-phosphate
Ala	alanine	G3P	glycerol-3-phosphate
AMP	adenosine-5-monophosphate	G3PDH	G3P dehydrogenase
Asn	asparagine	G6P	glucose-6-phosphate
Asp	aspartate	G6PDH	glucose 6-phosphate dehydrogenase
ATP	adenosine-5-triphosphate	GAP	glyceraldehyde-3-phosphate
B	broth	GAPDH	GAP dehydrogenase
CDR	comprehensive data reconciliation	GC	gas chromatography
CE	capillary electrophoresis	gDW	gram of dry weight biomass
CER	carbon dioxide evolution rate	Gln	glutamine
cGMP	cyclic guanosine monophosphate	Glu	glutamate
Cit	citrate	Gluc	glucose
Cmol	moles of compound multiplied by number of Carbon it contains	Glx	glyoxylate
		Gly	glycine
CoA	coenzyme A	Glyc	glycerol
CS	citrate synthase	His	histidine
C_S	substrate concentration	HPLC	high-performance LC
Cys	cysteine	IC	intracellular
D	dilution rate	ICDH	isocitrate dehydrogenase
DHAP	dihyroxyacetone phosphate	ICL	isocitrate lyase
DO	dissolved oxygen	IDMS	isotope dilution mass spectrometry
DOT	dissolved oxygen tension	Ile	isoleucine
DSP	downstream processing	IsoCit	isocitrate
E4P	erythrose-4-phosphate	K_{eq}	equilibrium constant of the enzyme
EC	energy charge	$k_{overall}$	overall mass transfer coefficient
ED	Entner-Doudoroff pathway	K_X	growth dependent maintenance
ENO	enolase	LC	liquid chromatography
ETC	electron transport chain	LDH	lactate dehydrogenase
F	filtrate	Leu	leucine
F1P	fructose-1-phosphate	Lys	lysine
F2,6bP	fructose-2,6-bisphosphate	M6P	mannose 6-phosphate
F6P	fructose-6-phosphate	Mal	malate
FBA	flux balance analysis	MALS	malate synthase
FBA	fructose-biphosphate aldolase	Mannitol-1P	mannitol-1-phosphate
FBP	fructose-1,6-bisphosphate	MAR	mass action ratio

m_{ATP}	growth independent maintenance	S7P	sedoheptulose-7-phosphate
MDH	malate dehydrogenase	Ser	serine
Met	methionine	STR	stirred tank reactor
MFA	metabolic flux analysis	Suc	succinate
MS	mass spectrometry	SucCoA	succinyl-CoA
NDH	NADH dehydrogenase	SUCDH	succinate dehydrogenase
NMR	nuclear magnetic resonance	SUCoAS	succinyl-CoA synthetase
Oaa	oxaloacetate	T6P	trehalose-6-phosphate
Orn	ornithine	TCA	tricarboxylic acid
OUR	oxygen uptake rate	TEA	triethanolamine
PDH	pyruvate dehydrogenase	Thr	threonine
PEP	phosphoenolpyruvate	TOC	total organic carbon
PFK	6-phosphofructokinase	TPI	triosephosphate isomerase
PFL	pyruvate-formate lyase	Trp	tryptophan
PFR	Plug flow reactor	Tyr	tyrosine
PGI	phosphoglucose isomerase	v	reaction rate
PGK	phosphoglycerate kinase	Val	valine
PGM	phosphoglycerate mutase	WS	washing solution
PGP	3-Phospho-D-glyceroyl phosphate	X	biomass
Phe	phenylalanine	X5P	xylulose-5-phosphate
Pi	inorganic phosphate	Y	yield
pmf	proton motive force	13dPG	1,3-biphosphoglycerate
PMI	mannose-6-phosphate isomerase	2DGE	2-dimensional gel electrophoresis
P/O	the efficiency of ATP generation in oxidative phosphorylation	2PG	2-phospho-glycerate
		3PG	3-phospho-glycerate
PoxB	pyruvate oxidase	6PG	6-phospho-gluconate
PPC	PEP carboxylase	αKG	A-ketoglutarate
PPCK	PEP carboxykinase	γ	degree of reduction
PPP	pentose phosphate pathway	δ	P/O for NDH
Pro	proline	ΔG	Gibbs free energy change
pss	pseudo-steady-state	μ	specific growth rate
PTA	phosphotransacetylase	τ	turnover time (s)
PTS	phosphotransferase system	ψ	electrical potential
PYK	pyruvate kinase		
Pyr	pyruvate		
Q	reaction quotient (= MAR)		
q8	ubiquinone-8		
q8h2	ubiquinol-8		
q_i	biomass-specific rate of i (mmol/CmolX/h or mmol/g/h)		
QS	quenching solution		
R5P	ribose-5-phosphate		
RQ	respiratory quotient		
RTD	residence time distribution		
Ru5P	ribulose-5-phosphate		

Chapter 1
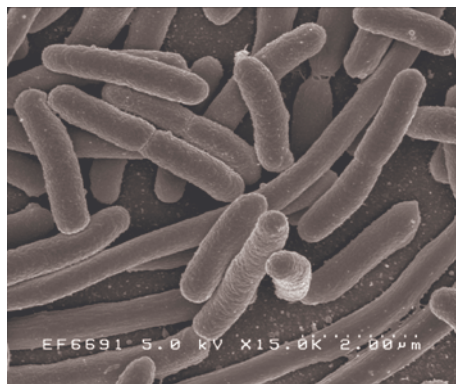
General Introduction

1.1. Industrial Microbial Biotechnology

"Industrial biotechnology", as a term, first commonly appeared in the literature in the early 1980s. Fermentation technology founded on microorganisms is used to produce pharmaceutical compounds (biologically active proteins, polypeptides such as hormones and vaccines), certain industrial enzymes, primary and secondary metabolites (common amino acids, vitamins, nucleotides, polysaccharides, organic acids, alcohols, antibiotics), fine and bulk chemicals, biocolorants, solvents, biopolymers, food additives, agricultural nutrients, biofuels, etc. In addition, microorganisms are used for bioconversions, in agriculture as biopesticides and fertilizers, for bioremediation to remove or degrade toxic wastes and other pollutants from the environment, and even for oil recovery and metal extraction. This diverse potential of microorganisms and the rapidly developing gene-based techniques promise that they will play a much more prominent role in the future. This allows greener and cleaner production based on renewable biological resources in response to concerns on the depletion of fossil resources and also on the environmental aspects. Also contributions to decreasing CO_2 emission and to more sustainable technologies are undeniable.

Industrial biotechnology aims to achieve the highest product concentration, the highest yield and the highest productivity of bulk or fine chemicals produced by microorganisms (Zhou *et al.* 2009). These optimum conditions are to be achieved through process optimization, scale-up and genetically-based strain improvement.

The first important step in the development of microbial production processes is the choice of the organism to be used. *Escherichia coli* is one of the best hosts for recombinant technology (see Box 1). Production of human insulin, which was marketed in 1982, was the first commercial application using *E. coli* (Goeddel *et al.* 1979). Afterwards, *E. coli* was also used in the production of other recombinant proteins, amino acids and other chemicals. *E. coli* is an attractive organism with its long history in research, its ability to grow rapidly on inexpensive substrates (also not auxotrophic) and its well-characterized genetics**.** These features motivated the choice for *E. coli* as the model system in this thesis, therefore the focus in examples and applications will be that of *E. coli* although the methodologies reported in this section/thesis are not limited to any given organism.

In this thesis attention is given to production of dicarboxylic acids. Microbial production of building block chemicals, which have multi functional groups, is of interest because some high-value bio-based chemicals/materials are derived from them. Dicarboxylic acids (e.g. succinic, fumaric) are used in the preparation of bulk chemicals that have applications in a broad range, from pharmaceuticals to paints, plastics, fuel additives, and fabrics and hence a large market.

Box 1: *Escherichia coli*

Figure 1.1: Scanning electron micro-graph of *E. coli*, (Rocky Mountain Laboratories, NIAID, NIH).

Escherichia coli belongs to the family *Entero bacteriaceae* (smaller than 1.5 μm) of gram-negative, rod shaped bacteria which can grow rapidly under both aerobic and anaerobic conditions (Figure 1.1). The group of organisms in the family *Entero bacteriaceae* share some features like: being oxidase negative, catalase positive, non-halophilic, non-spore -forming, usually motile by means of peritrichous flagella, and be able to reduce nitrate to nitrite and producing a common antigen (Neidhardt 1996). *Escherichia* are mostly found in the intestinal tract of humans and warm-blooded animals, some strains being pathogenic.

The cell envelope of gram-negative bacteria is composed of two membranes, the inner and outer, separated by a compartment, called the periplasm, that contains a thin peptidoglycan layer (Ruiz *et al.* 2006). Wild type *E. coli* strains are able to grow on a wide variety of carbon and energy sources, optimally on complete medium at neutral pH and 37 ^{o}C. Cox (2003) defined *E. coli* as an ultra-fast grower because, when it is growing at its maximum rate the generation time is less than the time needed to replicate the genome, leading to new-born cells possessing more than one genome equivalent per cell.

The *E. coli* strain used in this thesis is the K12 strain which is the primary model bacterium mainly because of the large number of studies so far that yield considerable knowledge on the physiology and genetics of this strain. The entire genome sequence of K12 strain MG1655 was first completed and annotated by Blattner *et al.* (1997) in the US and that of K12 strain W3110 was completed under the direction of Takashi Horiuchi in Japan (Hayashi *et al.* 2006).

The genome of *E. coli* K12 MG1655 consists of 4,639,675 bp of circular complex DNA. Of the total 4603 genes, protein-coding genes account for 4415 genes, 188 genes encode stable RNAs, and there are 115 pseudogenes as presented in January 2010 in the database EcoCyc: Encyclopedia of *E. coli* K12 genes and metabolism (Keseler *et al.* 2009). Nowadays such publicly available reference databases are visited to obtain information on genes, proteins, transcripts, metabolites and fluxes (e.g. KEGG: Kyoto Encyclopedia of Genes and Genomes, EcoProDB: *E. coli* protein database, *Escherichia coli* Multi-omics Database, etc.).

1.2. Strain Improvement: Systems Biology for Metabolic Engineering

Random methods (e.g. mutagenesis and selection), rational approaches, or combinatorial techniques have been used to improve industrial strains. The commonly used approach in metabolic pathway engineering is to make an educated guess based on biochemical knowledge of synthesis pathways whose genetic modification might improve or direct the metabolic flux to the compound of interest. By this approach, microorganisms can be improved to produce metabolites with a higher yield and can even be designed to produce new metabolites that they do not

naturally synthesize. Generally it takes a long time to obtain a microbial strain with a satisfactory product yield, due to the required testing of the modified strain and improving the strain in an iterative cycle (trial and error method). This process can be speeded up using the model-based approach (modeling cycle of systems biology). According to Nielsen and Jewett (2008) systems biology intends "to obtain new insight into the molecular mechanisms occurring in living cells or sub-systems of living cells for predicting the function of biological systems through the combination of mathematical modeling and experimental biology". This modeling cycle aims for quantitative understanding of the cell by using the experimental results as input to the model and the resulting output of the model is used to improve the next experimental design (Bailey 1991). The results of the model will allow defining the most promising genetic targets for metabolic pathway engineering, before actually performing the tedious genetic engineering work.

As mentioned in Petranovic and Vemuri (2009) the concept of this integration is not new, whereas our ability to accurately quantify cellular components at genome and whole system scale is. There are two kinds of approaches, being bottom-up and top-down. The bottom-up approach is based on existing biochemical knowledge. Such approaches involve describing part of a sub-system to form larger subsystems until the whole system is defined. The top-down approach does not require an *a priori* hypothesis, and is driven by the availability of high throughput data. High throughput analysis was initiated by sequencing of complete genomes, followed by quantifying other parts of the cells such as mRNA (transcriptome), proteins (proteome), and metabolites (metabolome) aiming to unravel the complexity of the cell, defined as the interactions between the "-omes". The genome is static, relatively independent of time and environment, whereas trancriptome, proteome, metabolome and fluxome may vary with genetic and environmental alterations. The interactions between and among these entities are referred to as interactome, e.g. protein-protein interactions, protein-metabolite interactions, regulatory interactions such as protein-DNA interactions or genetic interactions are to be quantified in systems biology.

1.2.1. The "-ome"s

Genome: The Oxford English Dictionary defines genome to be originally, a complete haploid set of chromosomes of an organism, species or gamete, and later, also as the complete set of genes of an organism, species, organelle, etc. After the development of DNA sequencing by Sanger and Coulson (1975), it took some time before the first complete genome, *Haemophilus influenzae* Rd, was presented (Fleischmann *et al.* 1995). Since then the speed at which whole genomes can be sequenced has rapidly increased. As of August 2009, there are approximately 106,533,156,756 bases in 108,431,692 sequence records in the traditional GenBank divisions and 148,165,117,763 bases in 48,443,067 sequence records in the WGS (Whole Genome Shutgun) division, meaning that genome sequences of about 3000 organisms are publicly available. Genomic knowledge is indispensable for optimization of strains for obvious targets such as the by-product routes, which should be removed. There are good examples of using this tool for improving product yield in this way, for example the constructed reduced-genome *E. coli* strain showed better growth and higher threonine production compared to the wild type (Mizoguchi *et al.* 2007). The idea behind

it was that a microorganism with a minimum genome is expected to show less by-product and regulation and is thus ideal for the systems biology approach.

Transcriptome: The transcriptome is the set of all mRNA molecules in a cell and reflects the genes that are being actively expressed at any given time. The transcript levels are quantified by several microarray techniques, oligonucleotide microarrays being the most popular because of their high specificity and sensitivity. In addition to quantifying gene expression, microarrays are also used in predicting the function of uncharacterized genes with the assumption that co-expressed genes are co-regulated. Klein-Marcuschamer *et al.* (2009) presented the use of transcriptional engineering studies for improving tolerance of *E. coli* to butanol and other solvents, for increasing titers of L-tyrosine and hyaluronic acid.

Proteome: The proteome is the set of all proteins in the system under defined conditions. Information on protein function and the pathways in which those proteins function is gained by protein analysis. The most conventional method is combination of two-dimensional gel electrophoresis (2DGE) (for protein separation) with mass spectrometry (MS) (for identification of protein). More recently MS-based methods are combined with liquid chromatography (LC), and proved to be a more efficient method. Besides these methods, protein arrays are becoming powerful tools to identify proteins, although there are still some issues to be solved, such as that recombinant production and purification of proteins is required. Ishii *et al.* (2007) measured the metabolite, protein and gene expression levels of wild type *E. coli* K12 and its 24 different single-gene (from glycolysis and pentose phosphate pathway) disruptants and compared these levels for metabolic pathways including glycolysis, pentose phosphate pathway and tricarboxylic acid cycle. These measurements allowed us to learn that *E. coli* has a central metabolic network that is robust against genetic perturbations, probably due to redundancy.

Metabolome: The metabolome represents the nature and abundance of each metabolite in the biological system. For a given physiological state, the concentration of metabolites gives a snapshot of the state of the cell. Kizer *et al.* (2008) showed a good example of making use of both transcriptomic and metabolic methods to optimize pathways for increased isoprenoid production in *E. coli*. Metabolome profiling is an important tool; however simultaneous determination of the complete metabolome with a single analytical technique is difficult due to the vast diversity in the chemical structure of the compounds. MS, preferably coupled with gas chromatography (GC) or LC, and nuclear magnetic resonance (NMR) are the most widespread approaches for metabolite profiling, the former (GC/LC-MS) being more promising due to much higher sensitivity.

Fluxome: Fluxome analysis aims at quantifying the complete set of *in vivo* fluxes in metabolic networks, i.e. *in vivo* activities of enzymes and pathways (Wittmann 2007). The metabolic fluxes are time-dependent and can be estimated using stoichiometric mass balance equations or combined with experimentally measured ^{13}C data using either NMR or MS. The most frequently used methods for fluxome analysis are based on GC-MS or NMR and recently LC-MS measurement of labeling pattern of metabolites from stable isotope tracer (such as ^{13}C-labeled substrates) studies (van Winden *et al.* 2005; van Winden *et al.* 2003). ^{13}C-flux methods have been applied for discovery and quantification of novel or unusual pathways within complex metabolic networks and have also been applied to less-characterized species (for a review: (Zamboni and

Sauer 2009)). An excellent example is combining dynamic metabolome analysis and ^{13}C-kinetics in the workz of Kwon *et al.* (2008) that demonstrates how these tools can unravel drug-enzyme interactions for the dihydrofolate reductase inhibitor in *E. coli*.

1.2.2. Stoichiometric network models

The stated experimental -omic tools will not be sufficient alone for strain improvement, but need to be combined with mathematical modeling as mentioned before. Mathematical models yield a higher level of understanding of mechanisms and the interactions therein, which allow selecting the best genetic interventions to improve a desired property of the system (Stephanopoulos *et al.* 2004). Mathematical models can be stochastic, graphical or deterministic. Metabolic networks (Box 2) are generally modeled through deterministic kinetic and stoichiometric methodologies. Stoichiometric approaches include metabolic flux analysis (MFA) and flux balance analysis (FBA) that can only be applied for (pseudo)-steady-state analysis of a system under a given condition while FBA requires an optimality constraint (Price *et al.* 2004).

Such constraint-based stoichiometric models have been used in the study of bacterial evolution and phenotypic behavior, analysis of network properties, biological discovery and metabolic engineering (Fleming *et al.* 2009). Mass and energy balances are the fundamental constraints with possible additional experimentally available data, e.g. transcript levels and/or thermodynamic information. Generally the resulting network is an underdetermined system that requires an optimization criterion (as mentioned above) for calculating the network fluxes. The most used objective is the maximization of growth yield. Schuetz *et al.* (2007) examined the effect of choosing different objective functions by evaluating the flux predictions and demonstrated that only different choices for an objective function described the fluxes under different conditions. Remarkably, optimization of biomass yield appeared to be the best objective function under nutrient limitation.

With the introduction of functional genomics and large scale datasets, metabolic reaction network reconstructions can be generated at genome-scale. In addition to the genome sequences, databases, textbooks and relevant publications are required in the reconstruction of biochemical networks (Feist *et al.* 2009). The growing scope of applications of genome-scale metabolic reconstructions has been recently reviewed (Feist and Palsson 2008). In addition to their valuable contributions in genome-scale metabolic networks, Palsson's group is recently developing networks for transcriptional regulation and transcriptional and translational processes at the genome-scale (Thiele *et al.* 2009). Moreover, Mendoza-Vargas *et al.* (2009) generated experimental data on transcription start sites (TSSs), promoters and regulatory regions at a genome-scale that will facilitate the understanding of the complex regulatory network of *E. coli*.

The production of L-valine using a metabolically engineered *E. coli* strain is a good example using integrative "omics" since improvement was based on transcriptome analysis and gene knockout simulation of an *in silico* genome-scale metabolic network (Park *et al.* 2007). All of the modifications in this strain are clearly defined because it was not a traditionally randomly

mutagenized strain. Another example of integrative analysis used for developing an overproducing strain is L-threonine production with *E. coli* using transcriptome profiling combined with *in silico* flux response analysis (Lee *et al.* 2007). Recently, Chemler *et al.* (2009) employed a stoichiometric-based model to identify combinations of gene knockouts for improving NADPH availability in *E. coli*.

Despite its valuable contribution to our understanding of the cellular metabolism, stoichiometric models have important deficiencies. The most important requirements in stoichiometric models are the knowledge on the ATP generation/consumption processes and the incorporation of a proper biomass composition of the studied microorganism. It has been reported that the biomass composition, which is known to be a function of the growth rate, has a significant effect on the flux distribution and must be accounted for in flux-based models (Pramanik and Keasling 1998).

Major ATP-related uncertainties are the amount of ATP generated in oxidative phosphorylation (P/O), ATP used for maintenance (m_{ATP}) and for biomass synthesis (K_X). Some of these parameters are known from *in vitro* (in test tubes) experiments (e.g. P/O) but their *in vivo* (inside the cells) values are questionable. Clearly, *in vivo* information on these ATP parameters is needed for a stoichiometric model, to be able to predict e.g. maximal yields of biomass and product on substrate and the maintenance coefficient (Roels 1983; van Gulik *et al.* 2001; van Gulik and Heijnen 1995). Such models provide the values of the parameters Y_{SX}^{max}, Y_{SP}^{max} and m_S, as a function of the ATP-stoichiomtery parameters, of the well-known linear Herbert-Pirt equation:

$$q_S = \frac{1}{Y_{SX}^{max}} \mu + \frac{1}{Y_{SP}^{max}} q_P + m_S.$$

This thesis will present an *in vivo* method to evaluate the ATP parameters for *E. coli*.

1.2.3. Thermodynamics of a product pathway

In addition to the balances and kinetics, thermodynamics is also more and more used for rational and efficient development of (bio)processes (Heijnen 1994; Heijnen 2002). Especially in the context of constraint-based analysis of genome-scale models of *E. coli*, the second law of thermodynamics starts to be incorporated (Feist *et al.* 2007; Henry *et al.* 2007; Henry *et al.* 2006). By applying the thermodynamic constraints, feasible directions of the biochemical reactions and feasible ranges for the concentrations of metabolites were calculated (Kummel *et al.* 2006). All these studies require information on the standard Gibbs free energy change of reaction ($\Delta_r G$) which can be calculated from the Gibbs energies of formation, $\Delta_f G$, of the products and reactants. Although the thermodynamic properties of a large number of biochemical compounds and reactions have been obtained experimentally under different conditions (Alberty 1998; Alberty 2003; Goldberg *et al.* 2004), values for most biochemical compounds are still unavailable (Kummel *et al.* 2006; Mavrovouniotis 1990). Therefore, the group contribution method (Benson 1976; Mavrovouniotis 1990; Mavrovouniotis 1991) can be used to estimate the

Gibbs energy of formation for the unknown compounds. The applicability of this method was recently expanded by improving the accuracy of the method (Jankowski *et al.* 2008).

A thermodynamic analysis provides an estimate of the energetic feasibility of potential pathways (Finley *et al.* 2009). In this thesis an example of this type of analysis is applied for the thermodynamic calculation of the maximum achievable succinic and fumaric acid yields on glucose for the succinate and fumarate production pathways, respectively.

1.2.4. Kinetic Models

However, stoichiometric and thermodynamic analysis is not sufficient to quantitatively predict the metabolic flux distributions under dynamic conditions or in genetically modified strains because the regulation effects, e.g. metabolite mass action effects, feedback inhibition, cofactor activation, allosteric effects, etc. are not considered. Additionally, kinetic properties of enzymes are required. A dynamic mathematical model of the central carbon metabolism, together with a product pathway would improve our understanding of cellular metabolism and shorten the development time of the engineered microorganism for the industrial production of useful chemicals from renewable resources. Detailed kinetic models should in principle provide a way of predicting metabolic system properties (fluxes and metabolite concentrations) based on the characteristics of the components of the system (enzyme levels, enzyme kinetics). However, the construction of such kinetic models is much more complicated than that of stoichiometric models. A dynamic metabolic model would comprise mathematical expressions representing the kinetic behavior of each enzyme. Enzymes can be described with mechanistic kinetics, e.g. Michaelis-Menten, or approximative e.g. linlog kinetics (Heijnen 2005). The pros and cons of these approaches are discussed extensively in Nikerel (2009).
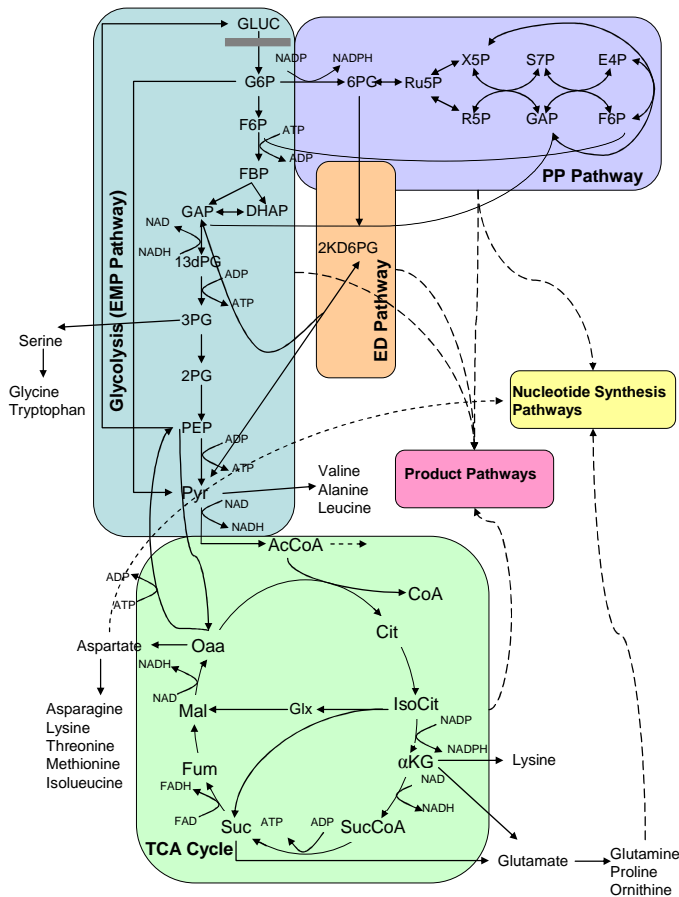
The major issue in kinetic modeling is the need for information on enzyme-kinetic rate laws and their parameters, which is most of the time not available. And even if it is available (Chang *et al.* 2009), it might be inadequate because of the *in vitro - in vivo* dilemma mentioned above, that frequently *in vitro* obtained enzyme-kinetic parameters are different from that of the actual *in vivo* value and consequently leading to erroneous predictions by the model (Teusink *et al.* 2000). Furthermore, enzymes which catalyze the same reaction in different organisms do seldomly have the same kinetics due to specific mutations. Therefore, there is an urgent need for accurate enzyme kinetic data which are valid under *in vivo* conditions in the organism of interest.

1.2.5. Rapid sampling, quenching, extraction and analysis techniques

An elegant solution to obtain such *in vivo* kinetic data is to use stimulus-response experiments where a well defined steady-state chemostat system (Box 3) is perturbed in such a way that the observed dynamic response can only be attributed to the perturbation performed. Transient data is collected on enzyme levels, fluxes and metabolite levels. Proper measurement of intracellular

metabolites requires that the applied sampling procedure should be fast enough to catch a snapshot of the culture, considering the fast turnover time of the intracellular metabolite pools. In addition to fast sampling, instantaneous quenching of enzyme activity and a proper extraction method that results in complete release of metabolites from the cells are required. Finally these protocols should be complemented with an accurate metabolite analysis method.

Box 2: Central carbon metabolism

The central metabolism, which is the key supplier of carbon precursors, energy and reducing power that are required for growth and product formation of *E. coli*, is the model system of this thesis. Central carbon metabolism consists of glycolysis (degradates sugars into pyruvate, meanwhile produces precursor metabolites that are used for the biosynthetic reactions), pentose phosphate pathway (supplies the precursors for amino acid and nucleotide synthesis and maintains the NADP$^+$/NADPH balance), Entner-Doudoroff (ED) pathway (joins the oxidative branch of pentose phosphate pathway to glycolysis) and TCA cycle (generates energy under aerobic conditions) with the glyoxylate shunt (replenishes the intermediate C$_4$-acids) and the anaplerotic reactions (converts TCA cycle intermediates into glycolytic intermediates during growth on TCA cycle intermediates).

Figure 1.2: The central carbon pathway with product, amino acid and nucleotide synthesis pathways.

Amino acid pathways, nucleotide synthesis pathways and product pathways are directly connected to the central metabolism (Figure 1.2).

When *E. coli* is aerobically grown on glucose at batch conditions, the main by-product acetate is secreted. Meanwhile, in glucose-limited chemostat cultures acetate secretion is not observed at dilution rates below 0.375 h^{-1} for the K12 strain (Kayser *et al.* 2005).

Box 3: Chemostat for reference steady-state

In the *in vivo* kinetic studies presented in this thesis, the chemostat was chosen to be the protocol for cultivation of cells because it provides a well-controlled environment in which the specific growth rate of the cells is set by the dilution rate of the chemostat and a reference steady-state can be realized. In kinetic studies this reference steady-state is perturbed. This steady-state should be fully characterized for which it is of utmost importance that black box analysis is carried out (Figure 1.3). Black box analysis applies balancing techniques based on conservation relations and thus enables checking the absence/presence of unknown products. In the experiments reported here, preferentially online measurements were used, such as the oxygen and carbon dioxide concentrations in the offgas, dissolved oxygen concentration, pH, temperature, reactor vessel weight, effluent vessel weight, and the added amounts of base + antifoam were monitored online. Additionally, offline measurements such as residual substrate concentration, biomass concentration, the concentration of total organic carbon in the culture broth and filtrate were accurately measured. These measurements are then used in black box analysis and subsequent data reconciliation with the constraint that the elemental conservation relations are satisfied.
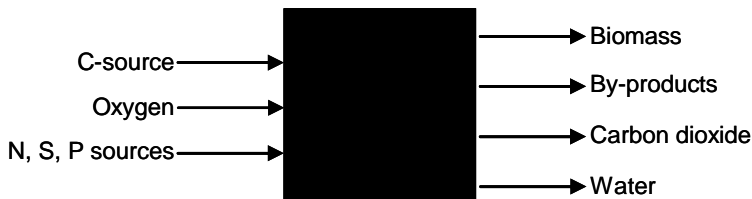
Figure 1.3: A black box system description of a fermentation process.

Rapid sampling: Theobald *et al.* (1993) were the first who established the rapid sampling technique where the total harvesting and inactivation time of a sample was 0.4 s, which further improved to 0.2 s in a later modification by the same group (Theobald *et al.* 1997). Schaefer *et al.* (1999) designed an automated rapid sampling device with a sampling time of 60 ms. Schaub *et al.* (2006) proposed an integrated sampling and extraction procedure whereby the sampling/ quenching/extraction is carried out through a helical single tube heat exchanger. Hiller *et al.* (2007a) established a fast sampling apparatus applicable to bioreactors which have sampling ports only at the lid. The details of these (and other) rapid sampling devices for metabolic engineering applications can be found in the reviews by Schadel and Franco-Lara (2009) and van Gulik (2010).

Lange *et al.* (2001) developed another system, which provides accurate sample weight as well as small sample size (< 1 ml) that avoids disturbance of the culture and ensures the ratio between the volumes of the quenching solution and the sample. This home-built rapid sampling system, with timer-controlled valves, is used for fast sampling (< 0.7 s) of *E. coli* in this thesis.

Quenching: The quenching of the metabolic/enzymatic activity in *E. coli* has e.g. been achieved by direct sampling into buffered/unbuffered cold aqueous 60 % (v/v) methanol (Buchholz *et al.* 2002; Buchholz *et al.* 2001; Hiller *et al.* 2007b; Schaefer *et al.* 1999), rapid freezing of the sample in liquid nitrogen (Chassagnole *et al.* 2002), rapid heating of the broth by means of a heat exchanger (Schaub *et al.* 2006) and a filter-culture methodology (Brauer *et al.* 2006). For proper

quantification of intracellular metabolites, the extracellular metabolites should be removed, which is generally performed by cold centrifugation, namely at < -20 ^{o}C (Schaefer *et al.* 1999). Quenching with liquid nitrogen or in a heat exchanger does not allow removal of extracellular metabolites. And although the filter-culture method allows quick separation of cells, this technique is not applicable to chemostat conditions.

In addition to these complications, application of the most widely used method in bacteria, i.e. cold aqueous methanol, has caused loss of intracellular metabolites due to leakage to the quenching liquid (Bolten *et al.* 2007; Wittmann *et al.* 2004). In contrast, Winder *et al.* (2008) concluded that 60 % cold methanol solution is a suitable quenching fluid and recommended 100 % methanol, with multiple freeze-thaw cycles for the extraction of metabolites. However this study was qualitative instead of being quantitative, making their conclusion questionable. Link *et al.* (2008) suggested using a cold mixture of methanol and glycerol as quenching solution for *E. coli* cells since they found that the leakage of adenine adenylates was significantly reduced with this method compared to cold aqueous methanol. But reduction of leakage is not sufficient to completely avoid the leakage problem. In another qualitative study (Spura *et al.* 2009), another cold quenching solution composed of 40 % ethanol and 0.8 % (w/v) sodium chloride was proposed. However as the authors confirmed, the cell leakage experiments were inconsistent, thus hindering to make clear statements on the applicability of the proposed method.

The metabolite leakage during quenching has also been observed in yeast cells (Canelas *et al.* 2008a; Villas-Boas and Bruheim 2007; Villas-Boas *et al.* 2005). By rigorous quantification of metabolites in different sample fractions from a yeast culture, Canelas *et al.* (2008a) confirmed that using 60 % cold methanol leads to leakage of metabolites. Villas-Boas and Bruheim (2007) suggested quenching with cold glycerol-saline solution. However, as mentioned in their work and experienced by Spura *et al.* (2009), it is difficult to remove glycerol from the samples, thus leading to problems in the analysis of metabolites.

To conclude, the sampling and quenching procedures used so far, in bacteria in general and *E. coli* in particular have not been appropriate, lacking quantification of leakage and/or degradation. Clearly, there is a need for a robust, reproducible and reliable method, which is one of the aims of this thesis.

Extraction: After the quenching step, intracellular metabolites are released by extraction, e.g. extraction with perchloric acid is a widely used procedure for *E. coli* (Buchholz *et al.* 2002; Buchholz *et al.* 2001; Chassagnole *et al.* 2002; Schaefer *et al.* 1999). In addition to the perchloric acid method, different methods using, e.g. cold methanol (Maharjan and Ferenci 2003), cold acidic solvent mixtures containing acetonitrile (Rabinowitz and Kimball 2007), buffered hot water (Hiller *et al.* 2007b) were proposed for the extraction of metabolites from *E. coli*.

An accurate extraction method should meet several criteria i.e. a wide range of metabolites should be extracted and degradation, conversion and/or leakage of metabolites should be minimal, or better, totally prevented. Partial losses during extraction can be corrected for, if internal standards (e.g. ^{13}C-labeled) are used. In this thesis *E. coli* cells are extracted with the hot ethanol method (Gonzalez *et al.* 1997) combined with addition of U-^{13}C-labeled cell extract to

the quenched sample (Mashego *et al.* 2004; Wu *et al.* 2005) that effectively reduces possible errors that might originate during the sample processing and analysis. With this method also laborious recovery checks (for each metabolite) are not required.

Analysis: Enzymatic and chromatographic (thin-layer, gas, liquid) methods are commonly used for quantification of intracellular metabolites. As a detection method, currently MS is most widely used. LC-MS/MS and GC-MS methods were shown to be well suited (Luo *et al.* 2007; van Dam *et al.* 2002) due to their robustness and high sensitivity. The use of stable isotope (e.g. ^{13}C) labeled internal standards highly improves the reproducibility of the analysis in the extracts (Mashego *et al.* 2004; Wu *et al.* 2005). Therefore this will be implemented to *E. coli* cells in this thesis work.

1.2.6. Perturbation studies for *in vivo* kinetic modeling

Rapid or slow: Perturbation of organisms in a steady-state (chemostat) can be achieved by changing extracellular concentrations from their steady-state values. A popular choice is to change the substrate concentration in a substrate-limited steady-state. Changes can be pulse-like (rapid, dynamic over a period of tens of minutes to hours) or the feed rate can be changed (slow, pseudo-steady-state over a range of substrate uptake rates). The observed effect of an external perturbation on the metabolite concentrations in a network depends on the kinetic properties and levels of the enzymes present. If perturbation experiments are rapid and carried out in a sufficiently short time frame (seconds to several minutes), the enzyme levels can be assumed not to change. In this case only intra- and extracellular metabolite concentrations as a function of time are required to obtain the rate of each reaction from the mass balances. The changing metabolite levels and reaction rates allow elaborating the *in vivo* kinetics for each enzyme. The slow approach has the disadvantage that enzyme levels are changed and hence must be quantified, in addition to extra/intracellular metabolites. Therefore the rapid perturbation approach is often preferred. These perturbations can be done inside and outside the bioreactor.

Rapid perturbations inside the bioreactor: Most of the rapid sampling devices mentioned above (Lange *et al.* 2001; Schaefer *et al.* 1999; Theobald *et al.* 1997; Theobald *et al.* 1993) were used for monitoring the fast dynamic response of *in vivo* concentrations of metabolites. The device designed by Schaefer *et al.* (1999), which allows sampling frequency of 4.5 samples.s^{-1}, was used to examine the dynamic response of intracellular concentrations to a glucose pulse in *E. coli* (Buchholz *et al.* 2002; Schaefer *et al.* 1999). Hoque *et al.* (2005) developed a rapid sampling device that enables taking a sample from the bioreactor every 1 s, and used this device for investigating the metabolic response of *E. coli* to a pulse addition of glucose/NH$_3$ in the limited continuous cultures.

The advantages of perturbation experiments inside the bioreactor are i) substrate and by-product flux measurements are possible due to possibly longer observation windows of extracellular metabolite measurements, ii) offgas measurements, which are required for O$_2$/CO$_2$ flux determinations, are possible.

Perturbations outside the bioreactor: In contrast to the above mentioned advantages, perturbation experiments inside the bioreactor have the disadvantage that the maintained chemostat steady-state might be disturbed. This limits the number of perturbations (that can be given to a single bioreactor) and the number of different kind of samples that can be taken. Thus multiple steady-states, which can be obtained either by awaiting for a new steady-state before each perturbation or running multiple bioreactors, are needed.

An option to circumvent the need for multiple steady-states is performing the perturbations outside the reactor. A stopped-flow technique (de Koning and van Dam 1992) was in the basis for the development of sampling/perturbation devices that serve for this purpose (Buziol *et al.* 2002; Visser *et al.* 2002). The sampling device of Buziol *et al.* (2002) was used in a glucose pulse study of *E. coli* (Chassagnole *et al.* 2002). A disadvantage of this system is the lack of continuous supply of oxygen in the device, consequently confining the sampling time (~ 20 s) for perturbations under aerobic conditions.

This oxygen depletion problem was overcome in the BioScope device (Mashego *et al.* 2006; Visser *et al.* 2002), which is a mini plug-flow reactor coupled to the cultivation bioreactor. The 1st generation BioScope (Visser *et al.* 2002) achieved that with oxygen permeable silicone tubing, however due to some drawbacks the device was improved to 2nd generation BioScope where gas exchange is ensured by a silicone membrane separating a gas and a broth channel (Mashego *et al.* 2006). Furthermore, theoretically the amount of sample that can be taken from the BioScope is unlimited because the perturbation is applied outside the bioreactor and hence there is no disturbance of the steady-state in the bioreactor.

Several different stimulus-response experiments in *Saccharomyces cerevisiae* (Kresnowati *et al.* 2007; Kresnowati *et al.* 2008; Mashego *et al.* 2007b; Mashego *et al.* 2006) and *Penicillium chrysogenum* (Nasution *et al.* 2006) were performed with the BioScope devices. In this thesis the BioScope application in *E. coli* cultures will be demonstrated.

Although the BioScope has attractive features, there is a limitation in terms of calculating dynamic uptake/secretion rates which are required for description of *in vivo* kinetics. The time window of samples taken from the BioScope does not allow accurate calculation of substrate uptake rate from the slightly decreased extracellular substrate concentration. Since offgas and dissolved oxygen concentrations during the dynamic experiments in the BioScope cannot be measured, oxygen consumption rate and carbon dioxide production rate cannot be obtained. A way to obtain these fluxes is to perform pulses in the bioreactor whereby samples are followed in a longer time frame than for the pulse experiments in the BioScope, which will be shown in this thesis.

1.2.7. Perturbation studies for large-scale mixing problems

After the reconstruction of genome-scale metabolic and regulatory networks, the uptake/secretion rates of the cells in response to chemical/physical conditions in the extracellular environment can

be integrated with a transport model of large-scale for the bioprocess optimization/control and scale-up (Wang *et al.* 2009). Processes developed at laboratory-scale should be precisely translated to industrial scale in order to achieve the high-quality products that the industry demands. Clearly, the conditions at pilot-plant and production scales will be different from laboratory-scale. Large-scale might result in extracellular gradients. Most relevant gradients that have been measured or predicted in large-scale cultures are dissolved oxygen (DO), pH, dissolved carbon dioxide, substrate or inducer, shear stress and temperature (Lara *et al.* 2006a).

Transient changes in these extracellular concentrations can have a significant effect on cell growth/uptake/secretion. It was experimentally observed that the respiratory activity of *E. coli* was increased when cells cycled between a nutrient-deprived region and a nutrient-rich region (Bylund *et al.* 1998; Larsson and Tornkvist 1996; Larsson *et al.* 1996). The temporary increase in substrate and respiration resulted in a transient formation of product of overflow metabolism, such as acetic acid. The accumulation of by-products can generate zones of low pH, and the transient increase in respiratory activity can cause oxygen depletion in nutrient-rich regions. This illustrates the complex gradients which occur on a large-scale, and which may result in phenotypic changes and genetic instability, occurring in large-scale bioreactors (Lara *et al.* 2006a). To solve these problems, we need information on the response of the cells exposed to such fast gradients. Computational fluid dynamics (CFD) is one of the important tools and used to simulate mixing characteristics of the agitated bioreactors and calculate these gradients. The ability to accurately imitate these concentration gradients at the laboratory-scale is then needed to better understand the response of the exposed cells. The approach used in the work presented in Chapter 9 is an example of an application of such scale-down studies.

1.3. Thesis outline

The complexity of metabolic systems and their regulation demands a structured approach towards their understanding. The main sources of complexity, the topology and the non-linearity of interactions among enzyme-catalyzed reactions were described by Rossell (2007). In this complex network numerous processes occur simultaneously, which require large-scale dynamic mathematical models to unravel the complexity, performing further simulations, design and optimization of the modeled system. One of the challenges to construct such a model is related with the quality of the available data. Throughout this thesis **proper**ly measured **comprehensive** sets of *in vivo* data, providing **rich stoichiometric/kinetic** information on central metabolism of *E. coli* **K12 MG1655** was aimed for (see Figure 1.4).

One of the previously mentioned uncertainties in the metabolic networks is the exact stoichiometry of energy generating and consuming processes. This problem was focused at in **Chapter 2**. Comprehensive data reconciliation (after incorporation of the growth rate dependent biomass composition) using a metabolic network model derived from the genome-scale model for *E. coli* MG1655 of Reed *et al.* (2003), was applied to successfully estimate the *in vivo* ATP
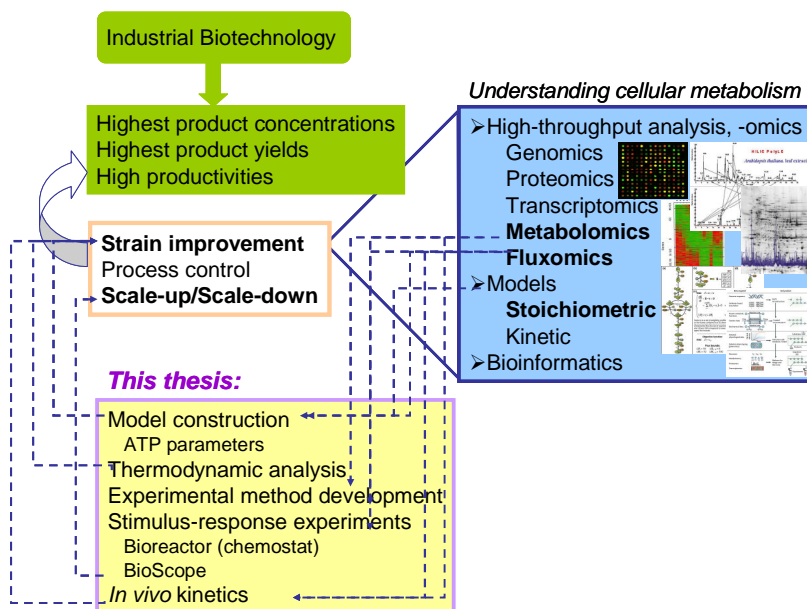
Figure 1.4: An outline of the goals and tools applied in this thesis.

stoichiometry parameters. With these parameters, actual maximum yields were determined. In addition to this stoichiometric study, maximum yields were studied using a thermodynamic approach with a focus on dicarboxylic organic acid production in **Chapter 3**.

Different techniques for rapid sampling and quenching for quantification of intracellular metabolites in microorganisms have been reported in the literature. However, the applicability of a method highly depends on the microorganism for which it is employed. **Chapter 4** investigates the applicability of the most commonly used quenching method, i.e. cold methanol quenching, for *E. coli* cells. Sampling was performed using a home-built rapid sampling system (Lange *et al.* 2001) and metabolite quantification was carried out with Isotope Dilution Mass Spectrometry (IDMS) (Wu *et al.* 2005) using LC-ESI-MS/MS (Seifar *et al.* 2009; van Dam *et al.* 2002) and GC-MS methods. The results showed that the conventional quenching method was not applicable to *E. coli* cells due to leakage and a new method, wherein metabolite leakage was circumvented, is presented.

Stimulus-response experiments are performed to monitor metabolite responses, by which *in vivo* enzyme kinetic parameters can be identified with the help of dynamic metabolic models. In **Chapter 5** a glucose-pulse, directly applied to the reactor, containing a glucose-limited *E. coli* culture is examined. Carbon, redox and ATP balances were checked to obtain a more comprehensive time-resolved (rate and metabolite levels) characterization of the dynamic responses.

Perturbing the culture in the reactor has some disadvantages, such as that a subsequent pulse cannot be applied directly, but a new steady-state should be awaited for. The BioScope is a

recently developed tool in which pulses can be performed outside the reactor. Although the BioScope's performance in its present configuration has been successful for eukaryotic organisms, it is not suitable to prokaryotes which have much faster response. **Chapter 6** describes the development and characterization of the new BioScope II device, designed for *E. coli* perturbation experiments at much shorter time frames. **Chapter 7** investigates the response of the cells to the different carbon sources by measurements of extra-/intracellular metabolites and fluxes through pulses in the BioScope and in the reactor. In **Chapter 8** these responses are further compared for the wild type and for a mutant *E. coli* strain which is a succinate overproducer, with the aim to find new targets for metabolic engineering that would further improve the succinate production.

Chapter 9 deals with the problems associated with the concentration gradients that exist in large-scale bioreactors. The situation was mimicked with two-compartment bioreactor system consisting of a stirred tank reactor (STR) connected to a mini plug-flow reactor (BioScope). The response of *E. coli* to transient exposures to glucose gradients under controlled aerobic and anaerobic conditions was investigated and analyzed.

In **Chapter 10,** an outlook into the future of kinetic modeling of metabolic reaction networks is presented.

Chapter 2

Genome-derived minimal metabolic models with estimated *in vivo* ATP stoichiometry

Abstract

Metabolic network models describing growth of *Escherichia coli* on glucose, glycerol and acetate were derived from a genome-scale model of *E. coli*. One of the uncertainties in the metabolic networks is the exact stoichiometry of energy generating and consuming processes. Accurate estimation of biomass and product yields requires correct information on the ATP stoichiometry. The unknown ATP stoichiometry parameters of the constructed *E. coli* network were estimated from experimental data of eight different aerobic chemostat experiments carried out with *E. coli* MG1655, grown at different dilution rates (0.025, 0.05, 0.1, 0.3 h^{-1}) and on different carbon substrates (glucose, glycerol, acetate). Proper estimation of the ATP stoichiometry requires proper information on the biomass composition of the organism as well as accurate assessment of net conversion rates under well defined conditions. For this purpose a growth rate dependent biomass composition was derived, based on measurements and literature data. After incorporation of the growth rate dependent biomass composition in a metabolic network model, an effective P/O ratio of 1.49 ± 0.26 mol of ATP/mol of O, K_X (growth dependent maintenance) of 0.46 ± 0.27 mol of ATP/Cmol of biomass and m_{ATP} (growth independent maintenance) of 0.075 ± 0.015 mol of ATP/Cmol of biomass/h were estimated using a newly developed Comprehensive Data Reconciliation (CDR) method, assuming that the three energetic parameters were independent of the growth rate and the used substrate. The resulting metabolic network model only requires the specific rate of growth, μ, as an input in order to accurately predict all other fluxes and yields.

2.1. Introduction

Quantitative understanding of cellular reaction networks and their regulation is essential for the efficient employment of industrial microorganisms for new and improved product formation from renewable resources. Hereby mathematical modeling of metabolism is an important tool in a systems biology approach to obtain this understanding. In the last decade particularly stoichiometric modeling has become increasingly popular to guide metabolic engineering of microbes (Kim *et al.* 2008). An important reason for this is that stoichiometric modeling only requires information on the structure of the metabolic network and not on the kinetics of the individual biochemical reactions involved.

Complete genome-scale metabolic networks can be constructed from annotated genome sequences and subsequent curation based on biochemical and physiological information of the corresponding organism (Durot *et al.* 2009). Genomic reconstruction is an ongoing process and e.g. the genome-scale metabolic model of *Escherichia coli* has been expanded several times (Feist *et al.* 2007).

It should be realized, however, that for specific well defined growth conditions, it is not always necessary to incorporate the complete database of possible reactions in the metabolic model. It has been shown that by using appropriate model reduction techniques genome-scale reaction databases can be reduced to dedicated metabolic network models for specific conditions (Burgard *et al.* 2001).

Although the stoichiometry of the majority of the metabolic pathways is known, some uncertainties remain, for example with respect to substrate transport mechanisms, compartmentation and the *in vivo* stoichiometry of energy generating and consuming processes, e.g. the efficiency of ATP generation in oxidative phosphorylation (P/O ratio) and growth dependent and growth independent maintenance energy requirements (i.e. K_X and m_{ATP}). In many cases the values of these parameters have either been assumed on a theoretical basis (Kayser *et al.* 2005; Stouthamer 1973; Varma and Palsson 1993) or obtained from *in vitro* experiments (Hempfling and Mainzer 1975).

Van Gulik and Heijnen (1995) introduced a method to obtain the ATP stoichiometry parameters under *in vivo* conditions. They estimated P/O ratio and K_X for the yeasts *Saccharomyces cerevisiae* and *Candida utilis* using literature data obtained from carbon-limited chemostat cultures at the same growth rate but on different substrates. The fact that the experimental data were collected at a single growth rate prevented the distinction between growth dependent and growth independent maintenance energy requirements. Furthermore it was assumed that the parameters were independent of the growth-limiting substrate. This approach has been successfully applied in predicting the flux distributions through central metabolism of *S. cerevisiae* for growth on glucose/ethanol mixtures, prediction of operational yields for the overproduction of amino acids, derivation of equations for network derived irreversibility limits, etc. (van Gulik and Heijnen 1995).

The approach was extended to a metabolic network for growth and penicillin production in *Penicillium chrysogenum* (van Gulik *et al.* 2000). From the results of carbon-limited chemostat experiments on different substrates and carried out at a range of different dilution rates, they estimated the growth and non-growth associated maintenance, the efficiency of oxidative phosphorylation as well as the additional amount of ATP dissipation associated with the production of β-lactam compounds (van Gulik *et al.* 2001). Such stoichiometric models, containing proper estimates of the ATP stoichiometry coefficients are highly relevant because they are able to provide flux predictions for a given substrate and given growth and product formation rates. Moreover, such models provide realistic predictions of theoretical maximum biomass and product yields on substrate, thereby taking into account the stoichiometric and thermodynamic constraints. An important requirement for meaningful estimation of the ATP stoichiometry of metabolic network models is the incorporation of the proper biomass composition of the studied microorganism. It has been reported that the biomass composition, which is known to be a function of the growth rate, has a significant effect on the flux distribution and must be accounted for in flux-based models (Pramanik and Keasling 1998).

To our knowledge, *in vivo* estimation of the ATP stoichiometry parameters of metabolic network models for *E. coli* under *in vivo* conditions has not been carried out previously. In this work determined metabolic network models were derived for aerobic, carbon-limited growth of *E. coli* MG1655 on a chemically defined medium with glucose, glycerol and acetate as carbon sources. The obtained models consisted of subsets of reactions selected from the genome-scale model of Reed *et al.* (2003) whereby maximization of the yield of biomass on substrate was used as objective function. Subsequently, steady-state chemostat cultivations were carried out to obtain *in vivo* data for growth on three different substrates at different dilution rates. Measurements of the elemental and biochemical composition of the biomass were combined to obtain a consistent biomass composition as a function of the growth rate. Simultaneous data reconciliation, with the constraint that the elemental conservation relations are satisfied, and parameter estimation was carried out to obtain the ATP stoichiometry parameters from the chemostat data, achieving the purpose of the present work.

2.2. Materials and Methods

2.2.1. Strain and growth conditions

The *E. coli* K12 MG1655 [λ⁻, F⁻, rph^{-1}, (*fnr*⁻ 267)del] strain was obtained from The Netherlands Culture Collection of Bacteria (NCCB). Cells were grown to stationary phase in shake-flasks on Luria-Bertani (LB) medium. Culture aliquots containing 50 % (v/v) glycerol were kept at -80 ^{o}C until they were used as inoculum of the precultures for chemostat experiments. Precultures were grown at 37 ^{o}C and 220 rpm in shake flasks on minimal medium with the following composition per liter: 5.0 g $(NH_4)_2SO_4$, 2.0 g KH_2PO_4, 0.5 g $MgSO_4.7H_2O$, 0.5 g NaCl, 2.0 g NH_4Cl, 5.5 g glucose.$1H_2O$, 0.001 g thiamine.HCl, 1 ml of trace elements solution (Verduyn *et al.* 1992), and 40 mM MOPS. The pH of the medium was adjusted to 7.0 with 1 M K_2HPO_4 before filter

sterilization (FP 30/0.2 CA-S, pore size 0.2 μm, cellulose acetate, Whatman GmbH, Dassel, Germany).

Aerobic carbon-limited chemostat cultures were carried out on minimal medium on three different carbon sources, namely glucose, acetate and glycerol. The glucose-limited chemostats were carried out at dilution rates (D) of 0.025, 0.05, 0.1 and 0.3 h^{-1}. The acetate and glycerol-limited chemostats were performed at a dilution rate of 0.1 h^{-1}. All chemostat experiments were carried out in 7 l laboratory fermentors with a working volume of 4 l, controlled by weight (Applikon, Schiedam, The Netherlands). Apart from the carbon source, the composition of the minimal medium was the same for all chemostat experiments and contained per liter: 5.0 g $(NH_4)_2SO_4$, 2.0 g KH_2PO_4, 0.5 g $MgSO_4.7H_2O$, 0.5 g NaCl, 2.0 g NH_4Cl, 0.001 g thiamine-HCl, 2.0 ml of trace elements solution (Verduyn *et al.* 1992) and 0.2 ml silicone-based antifoaming agent (BDH, Poole, UK). The carbon source was either glucose, at a concentration of 37.9, 75.8 or 151.5 mmol/l, glycerol (75.8 mmol/l) or acetate (113.6 mmol/l) (Table 2.1). The medium preparation procedure and the cultivation conditions were the same as described previously (Taymaz-Nikerel *et al.* 2009). The dissolved oxygen tension (DOT) of the culture was measured online with an autoclavable DOT sensor (Mettler-Toledo, Greifensee, Switzerland) but not controlled. During the experiments the DOT never dropped below 50 % of air saturation.

Chemostat cultivation was preceded by a batch phase which was carried out on a medium identical to the feed medium. Medium feeding was started directly after the batch phase was finished which was indicated by a steep decline of the carbon dioxide evolution rate (CER) and the oxygen uptake rate (OUR). The chemostat was assumed to be in steady-state after five residence times which was verified from the measured biomass concentration and the online measurements of dissolved oxygen and the oxygen and carbon dioxide concentrations in the offgas.

2.2.2. Analytical procedures

The carbon dioxide and oxygen volume fractions in dried (permapure, Perma Pure LLC, Toms River, NJ) offgas were monitored online with a combined carbon dioxide (infrared) and oxygen (paramagnetic) gas analyzer (NGA 2000, Rosemount Analytical, Hasselroth, Germany).

Samples of the supernatant were obtained by rapid sampling of broth into syringes containing cold stainless steel beads (-20 ^{o}C) followed by immediate filtration through disposable membrane filters with a pore size of 0.45 μm (MILLEX-HV, Millipore, Carrigtwohill, Co. Cork, Ireland) as described by Mashego *et al.* (2003). Measurement of the concentrations of cell dry weight, residual glucose and total organic carbon (TOC) content in the broth and filtrate were carried out as described previously (Taymaz-Nikerel *et al.* 2009). Residual acetate and residual glycerol concentrations in the supernatant were analyzed with enzymatic kits (R-Biopharm, Boehringer Mannheim, Darmstadt, Germany).

Table 2.1: Overview of the conditions (substrate, substrate concentration in the feed vessel (C$_{S,in}$) and dilution rate (D)) and the purpose of the chemostat experiments carried out

Chemostat Name	Substrate	C$_{S,in}$ [mM]	D [h^{-1}]	Purpose
gluc1	glucose	37.9	0.102	P
gluc2	glucose	37.9	0.099	B, P
gluc3	glucose	37.9	0.314	B, P
gluc4	glucose	37.9	0.049	B, P
gluc5	glucose	37.9	0.025	P
glyc1	glycerol	75.8	0.102	P
glyc2	glycerol	75.8	0.099	P
ace1	acetic acid	113.6	0.097	P
gluc6	glucose	75.8	0.100	B
gluc7	glucose	151.5	0.102	B

B: determination of the biomass composition, P: parameter estimation and flux analysis.

2.2.3. Biomass Macromolecular and Elemental Composition

E. coli biomass was harvested from glucose-limited cultures at steady-state. The broth was centrifuged (5000 g, 4 ^{o}C, 5 min) and the cells were washed twice with 0.9 % NaCl solution. The biomass pellet was stored at -80 ^{o}C and then freeze-dried for 24 h at 10 Pa (Edwards Modulyo, Sussex, UK). The freeze-dried biomass was then stored at room temperature in a desiccator until further analysis.

The biomass contents of C, H, N, S and O were determined with an elemental analyzer (Elementar, Vario EL III, Hanau, Germany). Total protein content was determined using the Biuret method (Herbert *et al.* 1971).

2.2.4. Calculation of uptake/secretion rates

The substrate consumption rate (q$_S$), oxygen consumption rate (q$_{O2}$) and carbon dioxide production rate (q$_{CO2}$) were calculated from the mass balances of substrate for the liquid phase and oxygen and carbon dioxide for the gas phase, respectively. The rate of cell lysis (q$_{lysis}$) was calculated from the carbon balance for the culture filtrate, whereby the total amount of carbon produced in the form of dissolved compounds was determined by measuring TOC of the filtrate. The obtained net conversion rates, calculated from the raw measurements, are referred to as "unbalanced rates".

2.2.5. Theoretical Aspects

Oxidative Phosphorylation in *E. coli*

The aerobic respiratory chain of *E. coli* is branched and consists of two different membrane bound NADH dehydrogenases (NDH1 and NDH2), a quinone pool and two ubiquinol oxidases (bo-type and bd-type) (Calhoun *et al.* 1993; Neijssel and Teixeira de Mattos 1994).

Of the two NADH dehydrogenases NDH1 is the homolog of the eukaryotic mitochondrial complex I and is assumed to have a H^+/e^- ratio of 2. NDH2 does not contribute to the generation of the proton motive force (pmf) (i.e. $H^+/e^- = 0$) (Calhoun *et al.* (1993) and references therein).

The two terminal oxidases (bo-type and bd-type) differ in their H^+/e^- translocation ratios, the bd-type, which predominates at low oxygen levels, has an H^+/e^- ratio of 1, the bo-type, which predominates at high oxygen levels, has an H^+/e^- ratio of 2 (Calhoun *et al.* (1993) and references therein).

Under aerobic conditions succinate dehydrogenase delivers its electrons in the form of $FADH_2$ to the quinone pool. Furthermore, there is a strong evidence that formate dehydrogenase generates pmf across the cytoplasmic membrane. Ingledew and Poole (1984) suggested that the formate-to-quinone segment of the respiratory chain translocates 2 protons.

Another reaction that donates electrons to the quinone pool is dihydroorotic acid dehydrogenase, a reaction in the purine-pyrimidine biosynthesis pathway. The contribution of this reaction is, however, very small. Under oxygen non-limiting conditions the quinone pool in *E. coli* was found to consist almost entirely of ubiquinone (Calhoun *et al.* 1993; Ingledew and Poole 1984).

The glycerol-3-phosphate dehydrogenase reaction, which is required for growth on glycerol as carbon source, is ubiquinone-8 dependent (Keseler *et al.* 2009).

From the above it becomes clear that the efficiency of oxidative phosphorylation in *E. coli*, i.e. the P/O ratio, depends on the exact composition of the respiratory chain, which is strongly dependent on the availability of oxygen. With a H^+/ATP stoichiometry of the ATP synthase of 4 (Stahlberg *et al.* 2001) it can be calculated that the theoretical maximum value for the P/O ratio is equal to 2. The proton translocation stoichiometry of each dehydrogenase involved in the network is summarized in Table 2.2.

ATP Stoichiometry

The ATP balance of the complete metabolic network model can be written as

$$q_{ATP,ox} - \sum q_i^{ATP} - K_X \mu - m_{ATP} = 0, \tag{2.1}$$

where the first term represents the production of ATP in oxidative phosphorylation and the second term represents the net rate of ATP consumption in the part of the metabolic network model of which the ATP stoichiometry is known, including substrate level phosphorylation, μ is

the specific growth rate and the parameters K_X and m_{ATP} represent the growth dependent and growth independent maintenance coefficients, respectively (van Gulik *et al.* 2001).

As outlined above, the division of the electron flux over the different components of the respiratory chain is a function of the growth conditions (e.g. substrate and growth rate). If the known generation of the pmf for the different electron sources are included (see Table 2.2), the ATP production in oxidative phosphorylation can be represented by:

$$q_{ATP,ox} = \sum_{i=1}^{n} P/O^i \ q_{2e}^i. \tag{2.2}$$

For *E. coli* this can be expressed as:

$$q_{ATP,ox} = \delta(q_{NDH} + \alpha_1 q_{SUCD4} + \alpha_2 q_{FDH2} + \alpha_3 q_{DHORD2} + \alpha_4 q_{G3PD5}), \tag{2.3}$$

wherein the parameter δ can be considered as the P/O ratio for NADH dehydrogenase (with maximum $\delta = 2$) and α_1 to α_4 represent the relative contributions of the other dehydrogenases to proton translocation. Because the two NADH dehydrogenases NDH1 and NDH2 operate in parallel, the flux distribution between them cannot be observed. Therefore, only the total flux through both dehydrogenases (q_{NDH}) is considered. From the maximum P/O values for the different electron sources (Table 2.2) it follows that:

$$q_{ATP,ox} = \delta(q_{NDH} + 0.5q_{SUCD4} + 0.75q_{FDH2} + 0.5q_{DHORD2} + 0.5q_{G3PD5}). \tag{2.4}$$

It should be noted that q_{G3PD5} is only relevant for growth on glycerol as carbon source.

Table 2.2: Stoichiometry of proton translocation and maximum theoretical P/O ratio of each dehydrogenase involved in the *E. coli* metabolic network

Dehydrogenase		Proton translocation		max P/O[a]
NDH1	NADH dehydrogenase	$8H^+/2e^-$	$4 + 4$	$2 \ (\delta)$
NDH2	NADH dehydrogenase	$4H^+/2e^-$	$0 + 4$	1
SUCD4	Succinate dehydrogenase	$4H^+/2e^-$	$0 + 4$	$1 \ (\alpha_1. \delta)$
FDH2	Formate dehydrogenase	$6H^+/2e^-$	$2 + 4$	$1.5 \ (\alpha_2. \delta)$
DHORDT	dihydroorotic acid dehydrogenase	$4H^+/2e^-$	$0 + 4$	$1 \ (\alpha_3. \delta)$
G3PD5	glycerol-3-phosphate dehydrogenase	$4H^+/2e^-$	$0 + 4$	$1 \ (\alpha_4. \delta)$

[a] For the calculation of the maximal P/O ratios the H^+/ATP stoichiometry of the ATP synthase was considered to be equal to 4.

Comprehensive Data Reconciliation (CDR) and estimation of energetic parameters

The primary measurements that are obtained from each chemostat experiment are measured or set gas and liquid flow rates as well as the concentrations of compounds in both phases, including their experimental errors. Given the interaction matrix of the complete network, we find by

standard data reconciliation techniques the relevant fluxes and their covariance matrix for the whole metabolic network (van der Heijden *et al.* 1994; Verheijen 2010). The obtained fluxes for chemostat cultivations carried out under different conditions (e.g. dilution rates and growth-limiting substrates) can subsequently be substituted in the ATP balance (Eq. 2.1) yielding a linear equation for each condition. Finally the best estimates of the ATP stoichiometry parameters, representing the efficiency of oxidative phosphorylation (P/O ratio) and growth dependent and growth independent maintenance energy requirements, can be obtained by linear regression (van Gulik *et al.* 2001).

We have extended this approach. For each chemostat experiment, we have the basic flux balances on each node determined by the interaction matrix, and we add Eq. (2.1) as an extra constraint in the data reconciliation procedure. This is directly solvable, and gives a weighted sum-of-squares $SS_i(P/O,K_X,m_{ATP})$ for each chemostat experiment, i = 1,...,n. Subsequently, we add the sums-of-squares for the all different experiments simultaneously, in this case n = 8, to obtain a total sum-of-squares

$$SS_T(\delta,K_X,m_{ATP})=\sum_{i=1}^{n} SS_i(\delta,K_X,m_{ATP}). \tag{2.5}$$

Minimization of this objective as a function of the three energy parameters yields the best estimate for these parameters and the local curvature of the objective provides an estimate of the covariance matrix of the three energy parameters δ, K_X and m_{ATP}.

The advantage of this approach is that it is based directly on the raw measurements, and that each experiment is taken along with its own weight. Secondly, we take along in the data reconciliation the fact that we apply the ATP balance (Eq. 2.1) as well. This is one assumption underlying the method of finding the energy parameters, but it is now applied comprehensively throughout the analysis. The obtained best estimates of the fluxes are consistent with this assumption and the error in the estimated fluxes is reduced as well.

2.3. Results and Discussion

2.3.1. Construction of a genome-derived minimal metabolic network model

To determine the metabolic reaction fluxes in the CDR step for obtaining the fluxes through the network and simultaneous estimation of the ATP stoichiometry parameters, either an objective function (e.g. maximum biomass yield on the supplied substrate) or reduced reaction sets representing determined metabolic sub-models for the different substrates are required. It should be noted that both procedures lead to the same result if the same objective function is used to obtain the reduced models. For this work we choose to derive reduced determined metabolic models.

A minimal metabolic network model for carbon-limited growth of *E. coli* K12 MG1655 was derived from the genome-scale reconstruction published by Reed *et al.* (2003), containing 904 genes and 931 biochemical reactions. In this reconstruction biomass growth is represented by one single reaction wherein biosynthetic constituents and ATP are drained from the network. However, this approach does not allow modifying the biomass composition, which is known to be a function of the growth rate, in a straightforward way. Therefore separate reactions were introduced for the biosynthesis of the major biomass constituents (i.e. protein, carbohydrates, lipids, RNA and DNA) and a reaction to synthesize biomass from these constituents. This resulted in the addition of 14 reactions to the genome-scale model of Reed *et al.* (2003).

Subsequently model reduction was applied to obtain a minimum reaction set for the description of aerobic glucose-limited growth on a defined medium. The first step was to remove all 150 transport reactions which were irrelevant for the applied cultivation conditions because the compounds involved were neither present in the cultivation medium nor produced by the cells. This resulted in 264 dead-end reactions, which were also removed, resulting in a reduced model containing 531 reactions.

As the second step, linear programming was applied to obtain the flux distribution with as objective maximum biomass yield on the supplied substrate. This resulted in 276 non-zero fluxes for glucose, as sole carbon source. The removal of the zero flux reactions finally resulted in a minimal metabolic network model for aerobic growth on glucose. The obtained reaction set is listed in Appendix 2.5.1.

To compare the flux predictions of the reduced and the genome-scale versions of the model, the flux distribution through central metabolism for growth on glucose calculated with the reduced model was compared with the published genomewide optimal metabolic flux distribution for $q_S = 6.6$, $q_{O2} = 12.4$ and $q_{Acetate} = 1.5$ mmol/g/h (Edwards and Palsson 2000). This yielded an identical flux distribution for lower glycolysis and TCA cycle and only minor deviations for the upper glycolysis and pentose phosphate pathway. This is most likely caused by the fact that the biomass composition used in our reduced model (see section on biomass composition below) was slightly different from the one used in Edwards and Palsson (2000).

Similar models for growth on glycerol and acetate were derived from the model for growth on glucose by addition of the appropriate catabolic reactions (see Appendix 2.5.1).

2.3.2. Chemostat cultivations

To estimate the ATP stoichiometry parameters δ, K_x and m_{ATP} a minimum of three independent ATP balance equations (Eq. 2.1) and thus three independent datasets for $q_{ATP,ox}$, Σq_i^{ATP} and μ are required. These can be obtained by cultivating *E. coli* in chemostat cultures under different conditions (substrates and growth rates). Additional datasets, in this case more than the minimum of three, will improve the accuracy of the estimated parameters. Therefore eight different carbon-limited chemostat cultivations were carried out on glucose, glycerol and acetate as carbon

sources, for which the substrate concentration in the feed medium was for all cultivations the same on a Cmol basis (227 mCmol/l) (see Table 2.1). The glucose-limited chemostats (gluc1 - gluc5) were carried out at four different dilution rates (0.025, 0.05. 0.1 and 0.31 h^{-1}), the glycerol (glyc1 - glyc2) and acetate (ace1) limited chemostats were carried out at a single dilution rate of 0.1 h^{-1}. It was confirmed from the measurement of the biomass concentration and the oxygen and carbon dioxide concentrations in the offgas that the cultures reached a steady-state after a period of approximately 5 residence times. Measurement of the residual substrate concentrations confirmed that all cultures were substrate-limited during steady-state growth. For the glucose-limited cultures the residual glucose concentration varied between 4.5 ± 1.5 - 12.7 ± 1.2 mg/l for dilution rates between 0.025 and 0.31 h^{-1}. For the glycerol-limited cultures the residual glycerol concentration was 2.97 ± 0.31 mg/l, for the acetate-limited culture the residual acetate concentration was 2.86 ± 0.07 mg/l.

The measured concentrations in the gas and the liquid phase as well as the liquid and gas flow rates allowed calculating the net conversion rates of biomass, substrate, oxygen and carbon dioxide for all chemostat experiments. It was confirmed by HPLC measurements that by-product formation (acetate, formate, lactate, succinate) was negligible in these well aerated carbon-limited cultures. Nevertheless, it appeared from measurement of the TOC content that the culture filtrate still contained a significant amount of carbon. For the glucose-limited cultures carried out at a dilution rate of 0.1 h^{-1} the TOC content of the filtrate was approximately 16 mM of carbon and increased to values of 20 and 29 mM of carbon for dilution rates of 0.05 and 0.025 h^{-1}, respectively. The TOC content of the filtrate of the glycerol and acetate-limited chemostats was similar as for the glucose-limited chemostats (15 and 13 mM respectively).

Increasing the glucose concentration in the feed vessel of glucose-limited chemostats with a factor of four did not result in a significant increase in the residual glucose concentration (results not shown), confirming that growth was still glucose-limited. However, this fourfold increase led to a fourfold increase in the steady-state biomass concentration and also resulted in a fourfold increase in the TOC content of the filtrate. The above findings (increase of the filtrate TOC content with increased biomass concentration and decreased dilution rate) strongly suggest that the organic carbon present in the filtrate was a result of cell lysis, as has been reported previously (Taymaz-Nikerel *et al.* 2009).

The occurrence of cell lysis implies that the specific growth rate (μ) of the cells is not identical to the dilution rate of the chemostat but is equal to the sum of the dilution rate and the biomass-specific rate of cell lysis (q_{lysis}). It should be realized that neglecting cell lysis leads to serious errors in the flux calculations and subsequent estimation of the ATP stoichiometry coefficients because growth is a major ATP sink.

The biomass-specific conversion rates calculated from the primary measurements as well as the recoveries of carbon and redox are shown in Table 2.3. It can be seen from this table that the carbon recoveries were between reasonable limits. However, for some of the glucose-limited chemostats serious deviations were found for the redox balances (recoveries up to 123 %). The most probable cause for this is a deviating oxygen concentration measurement in the offgas,

Table 2.3: Unbalanced (calculated from the raw measurement data) uptake and secretion rates, q_i, expressed per Cmol of biomass [mmol/CmolX/h] of the steady-state aerobic carbon-limited chemostat cultivations of *E. coli*, carried out at different dilution rates with different substrates

Chemostat	D [h⁻¹]	C_X [gDW/l]	q_X	$-q_S$	$-q_{O2}$	q_{CO2}	q_{lysis}	Carbon recovery	Redox recovery
gluc1	0.102	2.90±0.27	115.2±2.7	30.6±3.1	88.09	81.59	13.0±1.4	107.0	115.3
gluc2	0.099	2.63±0.05	113.7±2.3	32.6±1.3	97.09	87.54	14.53±0.59	102.8	112.0
gluc3	0.314	2.99±0.22	362.8±8.1	93.6±7.8	211.49	196.41	48.5±4.1	99.5	105.4
gluc4	0.049	2.47±0.10	58.8±1.3	16.99±0.90	61.46	51.05	9.38±0.71	107.7	123.3
gluc5	0.025	1.96±0.09	33.70±0.78	10.73±0.61	42.63	37.16	8.45±0.54	110.1	123.8
glyc1	0.102	2.91±0.06	113.8±2.3	60.3±2.5	98.22	69.53	11.83±0.46	101.4	104.6
glyc2	0.099	3.05±0.09	110.2±2.5	56.3±2.6	94.70	65.83	11.1±1.1	104.2	108.1
ace1	0.097	1.44±0.26	117.7±4.5	176±32	229.48	224.29	20.7±3.9	97.2	101.2
gluc6	0.100	5.34±0.07	114.1±2.6	32.50±1.2	88.69	87.30	14.0±1.3	103.3	108.4
gluc7	0.102	10.24±0.15	119.4±2.6	33.55±1.3	92.94	92.57	17.5±1.3	105.3	109.9

q_X = biomass formation rate, q_S =substrate consumption rate, q_{O2} = oxygen consumption rate, q_{CO2} = carbon dioxide production rate and q_{lysis} = biomass lysis rate. Carbon and redox recoveries are given in %.

27

resulting in a too high value for the oxygen uptake rate. For aerobic glucose-limited growth the oxygen uptake rate is expected to be slightly lower than the carbon dioxide production rate, which was in several cases not observed in our chemostat cultures. Deviating oxygen measurements were not used in the subsequent data reconciliation and parameter estimation procedure.

2.3.3. Biomass Composition

Elemental Composition

The elemental compositions of freeze dried biomass samples from the different aerobic glucose-limited cultures were analyzed with respect to their C, H, O, N and S content. The results showed (Table 2.4) that the elemental compositions were similar for the different growth rates and substrate concentrations in the feed. The carbon and nitrogen contents appeared comparable with published values for aerobic growth on glucose (Bratbak and Dundas 1984; Han *et al.* 2003; Heldal *et al.* 1985).

Because the measured elemental compositions for the different growth rates and substrate concentrations in the feed were very similar, the measurements were averaged, the average elemental composition being $CH_{2.01}N_{0.23}O_{0.48}S_{0.004}$ (γ_X = 4.37). These elements represent 93 % of the biomass. The remaining part consists of phosphorus and various metal ions and is designated to be ash content.

The typical biomass yield on glucose varies in the range 1.93 – 3.00 Cmol biomass/mol glucose and typical RQ measurements are between 1.03 – 1.11 for aerobic glucose-limited *E. coli* K12 cultures run at 0.09 – 0.22 h^{-1} dilution rate (Emmerling *et al.* 2002; Fischer and Sauer 2003; Hua *et al.* 2003; Johansson *et al.* 2005; Sauer *et al.* 1999). The mentioned range of biomass yields and RQ analysis indicate γ_X to be in the range of 4.23 – 4.41 for *E. coli* (see Appendix 2.5.2). Our elementally measured γ_X of 4.37 nicely lies in this range.

Macromolecular Composition

Published data on the biomass composition of *E. coli* K12 grown in aerobic carbon-limited chemostat cultures are scarce; instead most authors refer to Neidhardt (1987). He measured the biochemical composition of *E. coli* B/r during balanced aerobic growth at 37 ^{o}C (with a mass doubling time of 40 min) on glucose minimal medium. It was reported that the dried biomass consisted of 55 % protein, 20.5 % RNA, 3.1 % DNA, 9.1 % lipids, 3.4 % lipopolysaccharides (LPS), 2.5 % peptidoglycan (PG), 2.5 % glycogen (= polysaccharide (PS)), 0.4 % polyamines (0.3 % putrescine and 0.1 % spermidine), and 3.5 % other metabolites, cofactors and ions resulting in a calculated elemental composition of $CH_{1.61}N_{0.27}O_{0.41}S_{0.006}P_{0.019}$ (γ_x = 4.12).

Table 2.4: Measured elemental composition (% of dry weight) of *E. coli* biomass at different dilution rates (D) and glucose concentrations in the feed (C$_{S,in}$) with their standard errors

Chemostat code	D [h^{-1}]	C$_{S,in}$ [mM]	C [%]	H [%]	N [%]	O [%]	S [%]
gluc4	0.049	37.9	44.36±0.08	7.57±0.03	11.81±0.02	NA	0.41±0.01
gluc6	0.100	75.8	43.91±0.05	7.29±0.04	12.25±0.01	28.36±0.29	0.58±0.02
gluc2	0.099	37.9	43.46±0.06	7.35±0.05	12.06±0.01	27.66	0.47±0.003
gluc2	0.099	37.9	45.09±0.01	7.43±0.03	12.38±0.01	29.17	0.50±0.03
gluc7	0.102	151.5	45.47±0.03	7.63±0.02	12.42±0.03	NA	0.47±0.01
gluc3	0.314	37.9	43.71±0.03	7.34±0.04	11.93±0.03	NA	0.45±0.02
Average			44.33±0.02	7.44±0.01	12.14±0.01	28.40±0.40	0.48±0.01

Apart from the study of Neidhardt (1987) some macromolecules have been measured in other studies, but for the unmeasured molecules the composition published by Neidhardt was used.

The macromolecular composition of the biomass is known to change with environmental conditions and specific growth rate (Bremer and Dennis 1996). However, our measurements of the protein content of *E. coli* cells grown in glucose-limited chemostats showed that the protein content did not change significantly with changes in specific growth rate. The measured protein content agreed well with published data (Table 2.5).

Unfortunately the performed RNA measurements did not yield reproducible results; therefore published data (Table 2.5), yielding a linear relation between RNA content and specific growth rate (Emmerling *et al.* 2002), were used to calculate the RNA content as a function of the specific growth rate. The DNA content was estimated from the RNA/DNA ratio published before (Neidhardt 1987). The amino acid composition under glucose-limited aerobic chemostat conditions were obtained from Pramanik and Keasling (1998). Investigating the published data on the amino acid composition of *E. coli* protein revealed that variations between different strains and/or growth conditions were small. The ribonucleotide composition of RNA should not differ significantly because the amino acid composition of the protein does not change with growth rate (Pramanik and Keasling 1998). The composition of the deoxyribonucleotides in DNA should not change as well although the total DNA content would change with growth rate (Pramanik and Keasling 1998). The remaining organic biomass fraction was assigned to lipids, LPS, PS, PG, putrescine and spermidine at fixed ratios (Neidhardt 1987). Also the ash content, calculated in elemental analysis part, was assumed to be independent of the growth rate.

From the obtained biochemical composition the average elemental composition was calculated as $CH_{1.63}N_{0.25}O_{0.38}S_{0.006}$, with generalized degree of reduction $\gamma_x = 4.18$. The calculated elemental composition appeared to be significantly different from the average measured elemental composition which was calculated from the data presented in Table 2.4 as $CH_{2.01}N_{0.23}O_{0.48}S_{0.004}$, with $\gamma_x = 4.37$.

Table 2.5: Published values of protein and RNA contents (% of dry weight) of *E. coli* grown in aerobic glucose-limited chemostat cultures

E. coli strain	D [h^{-1}]	Protein [%]	RNA [%]	Reference
JM101	0.09	69.8	7.2	(Emmerling *et al.* 2002)
JM101	0.4	61.7	15.4	(Emmerling *et al.* 2002)
K12 W3110	0.1	70	7	(Hua *et al.* 2003)
K12 MG1655	0.12	70.1	4.7	(Fischer and Sauer 2003)

The observed difference in the degree of reduction calculated from the measured elemental and the above obtained biochemical composition of the biomass indicates that the latter cannot be correct. Considering the degrees of reduction (expressed per Cmol) of the individual biomass components, only the degree of reduction of lipids is higher than 4.2. This implies that the lipid content of the cells cultivated under our conditions must have been significantly higher than the 9.1 % which was measured by Neidhardt for cells growing at a much higher growth rate (1.0 h^{-1}) than in our chemostats (between 0.03 and 0.4 h^{-1}). It is known that the total lipid content of bacteria increases with decreasing growth rate, as has been reported e.g. for *Bacillus megaterium* (Sud and Schaechter 1964), *E. coli* (Ballesta and Schaechter 1972) and *Streptococcus faecium* (Carson *et al.* 1979). It can be calculated that the degree of reduction of 4.37, obtained from the measured average elemental composition, corresponds with a lipid content of the biomass of 14.5 %. Comparison of the elemental composition calculated from the biochemical composition after increasing the lipid content with the measured one revealed that there were still small differences in the contents of hydrogen and oxygen. This is most probably caused by some residual H_2O which might still be present in the freeze dried biomass. This phenomenon was observed before in yeast samples (Lange and Heijnen 2001).

Table 2.6 shows the obtained macromolecular and corresponding elemental biomass compositions for specific growth rates between 0.025 and 0.3 h^{-1}. These compositions have subsequently been used in the data reconciliation and parameter estimation procedure using the minimal metabolic network models described above. It should be noted that the γ_x of 4.12 calculated from the biomass composition published by Neidhardt falls well within the obtained trend of the decreasing γ_x at increasing growth rate (see Table 2.6). This is not surprising because the biomass was harvested at a high growth rate (late exponential phase) in that work.

2.3.4. Simultaneous data reconciliation and estimation of energetic parameters

Experimental data from eight steady-state carbon-limited chemostat cultures at different dilution rates on three different substrates (glucose, glycerol and acetate) (see Table 2.1) of which the amount of supplied carbon in the feed was the same (227 mCmol/l) were used for the simultaneous data reconciliation and parameter estimation.

Table 2.6: The macromolecular biomass composition of *E. coli,* grown in aerobic glucose-limited cultures, as a function of dilution rate. The macromolecules are given in % of cell dry weight

	D=0.025 h^{-1}	D=0.05 h^{-1}	D=0.1 h^{-1}	D=0.3 h^{-1}
Protein	63.95	64.81	68.19	65.43
RNA	5.21	5.86	7.26	13.06
DNA	0.79	0.89	1.10	1.98
Total Lipids	20.18	18.80	14.54	11.20
glyc	6.30	5.87	4.54	3.49
etha	3.79	3.53	2.73	2.11
hdca	4.34	4.04	3.12	2.41
hdcea	3.33	3.10	2.40	1.85
ocdcea	2.42	2.26	1.74	1.34
Lipopolysaccharides	1.18	1.10	0.85	0.65
Polysaccharide	0.87	0.81	0.62	0.48
Peptidoglycan	0.87	0.81	0.62	0.48
Putrescine	0.40	0.37	0.29	0.22
Spermidine	0.13	0.12	0.10	0.07
Ash	6.43	6.43	6.43	6.43
SUM	100.00	100.00	100.00	100.00
Biomass Composition	$CH_{1.74}N_{0.24}O_{0.34}$ $S_{0.006}P_{0.005}$	$CH_{1.73}N_{0.24}O_{0.35}$ $S_{0.006}P_{0.005}$	$CH_{1.69}N_{0.25}O_{0.35}$ $S_{0.007}P_{0.007}$	$CH_{1.64}N_{0.27}O_{0.37}$ $S_{0.007}P_{0.012}$
γ_X	4.41	4.38	4.31	4.21

Protein content was measured.
RNA content was estimated from the data in Table 2.5.
DNA content was estimated from the RNA/DNA ratio published by Neidhardt (1987).
Lipid components are glyc: glycerol, etha: ethanolamine, hdca: C16:0 fatty acid, hdcea: C16:1 fatty acid, ocdcea: C18:1 fatty acid. Ash content was assumed to be 6.43 % and independent of growth rate.

The complete set of primary data (measured concentrations, flow rates and volumes) of the eight chemostat experiments was reconciled with the CDR procedure as described in the materials and methods section. This procedure yields the best estimates of the primary measurements and the net conversion rates (i.e. balanced conversion rates) under the constraint that the elemental conservation relations are satisfied, as well as the best estimates of the three ATP stoichiometry parameters δ, K_X and m_{ATP}. To verify whether the growth rate and the carbon source would have a significant influence on the values of these parameters, we have also performed additional parameter estimations. For example, we allowed δ having distinct values for the four different growth rates while K_X and m_{ATP} were treated as before, namely as single universal parameters. This process was repeated for each of the three ATP parameters and for both the growth rate and the carbon source. In all the six cases it was found that the simpler model with three universal ATP parameters independent of growth rate and carbon source could not be rejected, with a P-

value of the associated F-test of 58 % or higher. Therefore the ATP stoichiometry parameters were considered to be independent of the growth rate and the substrate used.

The obtained balanced biomass-specific net conversion rates μ, q_S, q_{O2}, etc. are shown in Table 2.7. The applied statistical criterion (χ^2 test with a null hypothesis of significant measurement deviations at a significance level of 0.1 %) indicated that there was no proof for significant errors in the calculated rates and/or in the system definition.

Table 2.7: Balanced (reconciled) uptake and secretion rates, q_i, expressed per Cmol of biomass [mmol/CmolX/h] of steady-state aerobic carbon-limited chemostat cultivations of *E. coli*, carried out at different dilution rates; q_X = biomass formation rate, q_S = substrate consumption rate, q_{O2} = oxygen consumption rate, q_{CO2} = carbon dioxide production rate and q_{lysis} = biomass lysis rate

Chemostat	q_X	$-q_S$	$-q_{O2}$	q_{CO2}	q_{lysis}
gluc1	116.0 ± 2.7	33.3 ± 0.7	74.7 ± 1.2	83.6 ± 1.5	13.9 ± 0.8
gluc2	113.0 ± 2.5	32.51 ± 0.65	73.4 ± 1.2	82.0 ± 1.4	14.22 ± 0.51
gluc3	365.1 ± 8.5	95.9 ± 2.1	192 ± 4	210 ± 4	50.6 ± 2.1
gluc4	59.0 ± 1.4	18.82 ± 0.37	48.3 ± 0.7	53.9 ± 0.8	9.8 ± 0.7
gluc5	34.5 ± 0.9	12.52 ± 0.22	37.1 ± 0.4	40.6 ± 0.5	9.29 ± 0.47
glyc1	113.7 ± 2.5	61.2 ± 1.2	91.6 ± 1.5	69.8 ± 1.1	11.89 ± 0.36
glyc2	110.2 ± 2.7	59.5 ± 1.3	89.5 ± 1.6	68.2 ± 1.2	11.3 ± 1.1
ace1	116.3 ± 2.9	162 ± 4	199 ± 4	208 ± 4	19.2 ± 1.2

The estimated ATP stoichiometry parameters are shown in Table 2.8. It can be seen from this table that the estimated δ is significantly lower than the maximum theoretical value (2.0). Although under high oxygen levels (as was the case in our chemostat cultures) the predominant terminal oxidase is the of the bo-type with a H^+/e^- ratio of 2, under these conditions also the NDH2 dehydrogenase, which does not contribute to the pmf, is known to be expressed (see section Theoretical Aspects above). This implies that the expected δ under these conditions would be between 1.0 and 2.0, which corresponds well with the estimated value of 1.49.

A comparison of the *in vivo* P/O results for *E. coli* with reported values is not useful because as explained in the introduction section P/O was always theoretically assumed or taken from *in vitro* experiments. The estimated m_{ATP} value (0.075 ± 0.015 mol/Cmol/h = 3.2 ± 0.7 mmol/g/h) compares reasonably well with reported values of 2 mmol/g/h (Farmer and Jones 1976) and 2.81 mmol/g/h (Kayser *et al.* 2005) assuming that they have a similar error estimate. Feist *et al.* (2007) reported estimated values for the growth independent (m_{ATP}) and growth dependent maintenance parameters of 8.4 mmol/gDW/h and 59.8 mmol/gDW respectively, for the complete genome-scale reconstruction of *E. coli* K12 MG1655. Both values are significantly higher than our estimates of 3.2 ± 0.7 mmol/g/h and 19.8 ± 12 mmol/g for the growth independent and dependent maintenance parameters respectively. These differences might originate from the fact that Feist *et al.* (2007) used published chemostat data from several different *E. coli* strains cultivated on

different minimal media and/or because the authors used a value of the P/O ratio which was much higher than the value we estimated. Unfortunately Feist *et al.* (2007) did not report which value of the P/O ratio was used for their estimations.

It is also worthwile to compare our *in vivo E. coli* results with those for *S. cerevisiae* (van Gulik and Heijnen 1995) and *P. chrysogenum* (van Gulik *et al.* 2001) which are of the same order of magnitude (Table 2.8). Our estimation of the δ of *E. coli* lies between the values for *S. cerevisiae* and *P. chrysogenum*. The growth related maintenance coefficient for *E. coli* was similar as for *P. chrysogenum* whereas the growth independent maintenance coefficient was two times higher for *E. coli*.

The obtained metabolic network model with the simultaneously estimated energetic parameters allows calculating operational biomass yields on substrate as a function of the growth rate. Calculated and measured operational biomass yields on substrate are presented in Figure 2.1. It can be seen from this figure that the experimental biomass yields on substrate are close to the calculated values for all different growth conditions applied. This shows that our assumption that these ATP coefficients are independent of the growth rate and the substrate used is justified.

Table 2.8: Estimated ATP stoichiometry parameters for *E. coli* metabolic network with their standard errors and comparison with published parameters for *S. cerevisiae* (van Gulik and Heijnen 1995) and *P. chrysogenum* (van Gulik *et al.* 2001)

	δ	K_X	m_{ATP}
	mol ATP/½mol O_2	mol ATP/CmolX	mol ATP/CmolX/h
E. coli	1.49 ± 0.26	0.46 ± 0.27	0.075 ± 0.015
S. cerevisiae[a]	1.20	0.80	-
P. chrysogenum[b]	1.84 ± 0.08	0.38 ± 0.11	0.033 ± 0.012

[a] To express K_X per Cmol of biomass a protein content of 50 % and a molecular weight of 26.4 g/Cmol was used (Lange and Heijnen 2001), m_{ATP} was not determined.
[b] Errors were given as 95 % confidence intervals.

2.3.5. Flux Analysis

As has been described above the fluxes through the metabolic network of *E. coli* were simultaneously estimated for growth on glucose, glycerol and acetate while estimating the parameter values of δ, K_X, m_{ATP} using the CDR procedure (see Supplementary Material for fluxes). The flux distribution through central carbon metabolism at a dilution rate of 0.1 h⁻¹ (biomass production rate q_X of about 115 mCmol/CmolX/h which corresponds to a specific growth rate μ of 0.115 h⁻¹) is shown in Figure 2.2.

Under glucose-limited conditions the split ratio between glycolysis and pentose phosphate pathway (PPP) at the G6P node often shows discrepancies in literature. At D = 0.1 h⁻¹ this ratio was reported ranging from 28% / 71% (Chassagnole *et al.* 2002; Schmid *et al.* 2004) to 72% /

27% (Schmid *et al.* 2004). Our finding of 56% / 44% (Figure 2.2) is in good agreement with the ratio of 55% / 44% determined by Schaub *et al.* (2008) with ID-^{13}C MFA in wild type *E. coli* W3110 at D = 0.10 h^{-1}and with the ratio of 54% / 44% determined by Emmerling *et al.* (2002) with NMR based IS-^{13}C MFA in wild type *E. coli* JM101 at D = 0.09 h^{-1}. Similar split ratios between glycolysis and PPP were observed before: 53% / 46% (Schmidt *et al.* 1999), 57% / 41% for *E. coli* K12 TG1 at D = 0.066 h^{-1} (Kayser *et al.* 2005), 65% / 34% for *E. coli* K12 at D = 0.10 h^{-1} (Siddiquee *et al.* 2004).
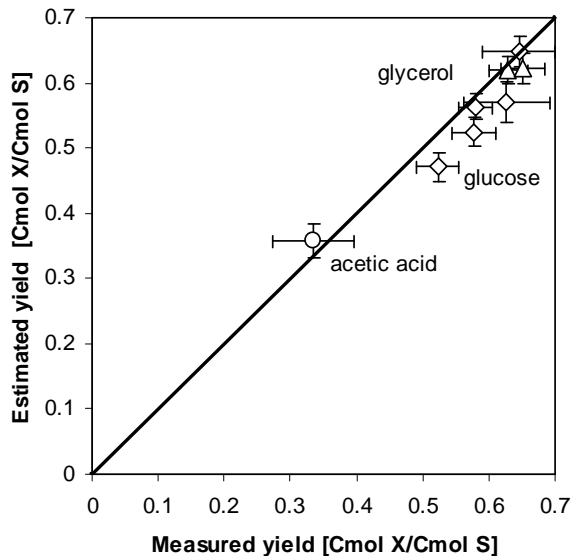
Figure 2.1: Comparison of the measured biomass yields on substrate with the calculated yields using the best estimates of the ATP-stoichiometry parameters (diamonds: glucose-limited, triangles: glycerol-limited, circle: acetate-limited).

When acetate is the sole source of carbon, there is an important branch point at isocitrate with isocitrate dehydrogenase (ICDH) and isocitrate lyase (ICL). When fluxes are expressed on a molar basis and are normalized with respect to the acetate uptake rate, the distribution of ICDH/ICL is 55% / 20% in our findings (Figure 2.2). This agrees well with the reported 53% / 21% values at D = 0.11 h^{-1} for *E. coli* K12 (Zhao and Shimizu 2003). Pramanik and Keasling (1997) found 71% / 13%, which indicates a higher flux towards α-ketoglutarate instead of glyoxylate, which might be due to the fact that the isocitrate dehydrogenase reaction was assumed to be dependent on NADH instead of NADPH.

Under glycerol-limited conditions the flux through the gluconeogenetic enzyme fructose bisphosphatase (FBP) is equal to 13 % of the glycerol consumption rate (Figure 2.2). At the junction of GAP, flux through 13dPG is 80 % of the glycerol consumption rate which is very well comparable with the value of 81 % reported by (Holms 1996) for *E. coli* ML308 grown in batch culture.

2.3.6. Herbert-Pirt relations

The Herbert-Pirt equation for substrate consumption is a linear relation describing the substrate consumption rate q_S as a function of the specific growth rate μ and specific product formation rate q_P (if any). It can be considered as a black box model that describes how the consumed substrate is distributed over growth, maintenance and product formation under different conditions (growth and product formation rates). The parameters of these relations are the maximum yield coefficients of biomass and product on substrate and the maintenance coefficient. Similar relations can be derived for the rates of oxygen consumption and carbon dioxide production. These linear relations can be derived from a given metabolic model (van Gulik *et al.* 2001). Table 2.9 presents the derived Herbert-Pirt equations for substrate, O_2 and CO_2 for the three different carbon sources. The reciprocal of the coefficient of μ represents the maximum yield. Maximal yields of biomass on substrate were found to be 0.66 Cmol X/Cmol glucose, 0.70 Cmol X/Cmol glycerol, 0.39 Cmol X/Cmol acetate. Maximal yields of 2.27, 1.71, 0.69 Cmol X/mol O_2 and 1.93, 2.36, 0.65 Cmol X/Cmol CO_2 were found for glucose, glycerol and acetate, respectively.

Table 2.9: Herbert-Pirt relations derived from the constructed *E. coli* metabolic networks for each substrate (all rates are expressed in mol/CmolX/h)

Substrate	Herbert-Pirt relations		
Glucose	$-q_S=0.25\mu+0.0036$	$-q_{O2}=0.44\mu+0.022$	$q_{CO2}=0.52\mu+0.022$
Glycerol	$-q_S=0.47\mu+0.0066$	$-q_{O2}=0.58\mu+0.023$	$q_{CO2}=0.42\mu+0.020$
Acetate	$-q_S=1.27\mu+0.018$	$-q_{O2}=1.46\mu+0.023$	$q_{CO2}=1.54\mu+0.036$

2.4. Conclusions

In this work it was shown that from a large genome-scale model, determined minimal metabolic network models can be derived for the description of growth on a minimal medium under well defined conditions. The obtained minimal models were used to study the growth stoichiometry of *E. coli* K12 for three substrates (glucose, glycerol and acetate) in aerobic substrate-limited chemostats at different dilution rates using redundant measurements and a comprehensive network-based reconciliation approach. In the chemostat cultivations significant cell lysis (10 - 25 %) occurred, which was taken into account in the flux calculations. Additionally, the proper biomass composition was incorporated into the metabolic networks whereby the protein content was measured, the relation between RNA and DNA contents and growth rate were obtained from literature data and the lipid and carbohydrate contents of the biomass was estimated from the measured elemental composition of the biomass. With the accurate growth rate and the corresponding biomass compositions, the presented CDR method allowed simultaneous estimation of the ATP energetic parameters (δ, K_X and m_{ATP}) of the *E. coli* K12 metabolic network for aerobic carbon-limited growth. The estimated *in vivo* values for δ, K_X and m_{ATP} showed an excellent fit and good accuracy and compared well with such parameter values in

other organisms. The assumption of independence of these parameters of the specific growth rate and on the substrate was justified.
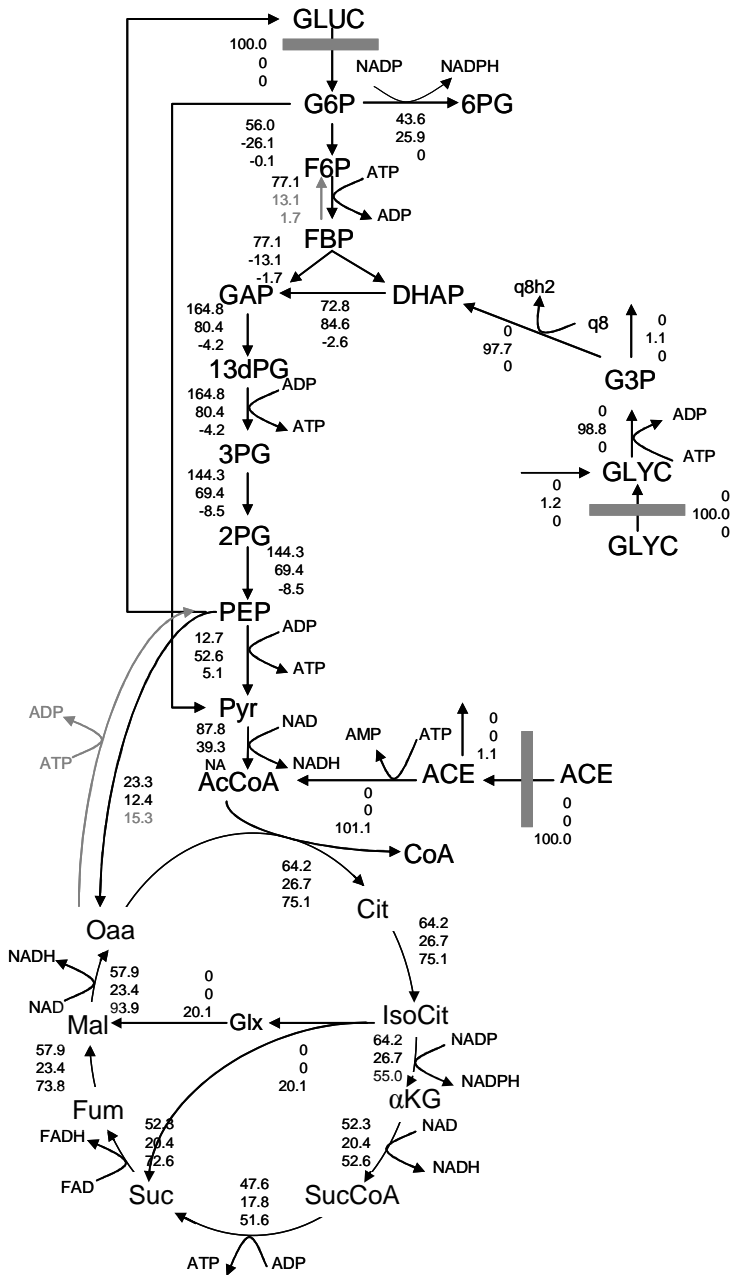
Figure 2.2: Calculated metabolic flux patterns of central carbon metabolism for aerobic growth of *Escherichia coli* on glucose, glycerol and acetate at a dilution rate of 0.1 h⁻¹. All fluxes are given as % relative to the uptake rate of the substrate. First values represent growth on glucose, second values represent growth on glycerol and third values represent growth on acetate. The reactions indicated with gray arrows (and gray values for the fluxes) are reversed in comparison to growth on glucose.

The network model allowed calculating all fluxes, using only μ as input. For the three substrates the obtained flux pattern / split ratios agreed very well with the published data based on labeled C experiments which is an accurate way for measuring fluxes. Furthermore, the metabolic network model allows calculating maximum biomass yields on substrate from the derived Herbert-Pirt relations.

2.5. Appendix

2.5.1. Reaction List

Glycolysis/Gluconeogenesis

1	PGI	glucose6-phosphate isomerase	g6p <==> f6p
2	PFK	phosphofructokinase	atp + f6p => adp + fdp + h
3	FBA	fructose-bisphosphate aldolase	fdp <==> dhap + gap
4	TPI	triose-phosphate isomerase	dhap <==> gap
5	GAPD	glyceraldehyde-3-phosphate	gap + nad + pi <==> 13dpg + h + nadh
6	PGK	phosphoglycerate kinase	3pg + atp <==> 13dpg + adp
7	PGM	phosphoglycerate mutase	2pg <==> 3pg
8	ENO	enolase	2pg <==> h2o + pep
9	PYK	pyruvate kinase	adp + h + pep => atp + pyr
10	PDH	pyruvate dehydrogenase	coa + nad + pyr => accoa + co2 + nadh
11	GLGC	glucose-1-phosphate	atp + g1p + h => adpglc + ppi
12	GLCS1	glycogen synthase (ADPGlc)	adpglc => adp + glycogen + h

TCA Cycle

13	AKGDH	2-oxogluterate dehydrogenase	akg + coa + nad => co2 + nadh + succoa
14	ACONT	aconitase	cit <==> icit
15	CS	citrate synthase	accoa + h2o + oaa => cit + coa + h
16	FUM	fumarase	fum + h2o <==> mal-L
17	ICDHyr	isocitrate dehydrogenase (NADP)	icit + nadp <==> akg + co2 + nadph
18	MDH	malate dehydrogenase	mal-L + nad <==> h + nadh + oaa
19	SUCD1i	succinate dehydrogenase	fad + succ => fadh2 + fum
20	SUCOAS	succinyl-CoA synthetase	atp + coa + succ <==> adp + pi + succoa
21	DHFR	dihydrofolate reductase	dhf + h + nadph <==> nadp + thf

Anaplerotic Reactions

22	PPA	inorganic diphosphatase	h2o + ppi => h + (2) pi
23	PPC	phosphoenolpyruvate carboxylase	co2 + h2o + pep => h + oaa + pi

Pentose Phosphate Cycle

24	G6PDH2r	glucose6phosphate dehydrogenase	g6p + nadp <==> 6pgl + h + nadph
25	PGL	6-phosphogluconolactonase	6pgl + h2o => 6pgc + h
26	GND	phosphogluconate dehydrogenase	6pgc + nadp => co2 + nadph + ru5p-D
27	RPI	ribose-5-phosphate isomerase	r5p <==> ru5p-D
28	RPE	ribulose 5-phosphate 3-epimerase	ru5p-D <==> xu5p-D
29	TALA	transaldolase	gap + s7p <==> e4p + f6p
30	TKT1	transketolase	r5p + xu5p-D <==> gap + s7p
31	TKT2	transketolase	e4p + xu5p-D <==> f6p + gap

Oxidative Phosphorylation

32	ATPS4r	ATP synthase	adp + (4) h:ext + pi <==> atp + (3) h + h2o
33	CYTBO4	cytochrome oxidase	(2δ) h + (0.5) o2 + q8h2 => (2δ) h:ext + h2o + q8
34	NDH1	NADH dehydrogenase	(2δ) h + (nadh + h) + q8 => (2δ) h:ext + nad + q8h2
35	SUCD4	succinate dehyrdogenase	fadh2 + q8 <==> fad + q8h2
36	FDH2	formate dehydrogenase	for + (δ+1) h + q8 => co2 + (δ) h:ext + q8h2
37	TRDR	thioredoxin reductase (NADPH)	h + nadph + trdox => nadp + trdrd

Pyruvate Metabolism

38	ADHEr	acetaldehyde dehydrogenase	accoa + (2) h + (2) nadh <==> coa + etoh + (2) nad
39	ACKr	Acetate kinase	ac + atp <==> actp + adp
40	LDH_D	D-lactate dehydrogenase	lac-D + nad <==> h + nadh + pyr
41	PTAr	phosphotransacetylase	accoa + pi <==> actp + coa

Alternate Carbon Metabolism

42	A5PISO	arabinose-5-phosphate isomerase	ru5p-D <==> ara5p
43	DRPA	deoxyribose-phosphate aldolase	2dr5p => acald + gap
44	G3PD2	glycerol-3-phosphate dehydrogenase	glyc3p + nadp <==> dhap + h + nadph
45	PGMT	phosphoglucomutase	g1p <==> g6p
46	PPM	phosphopentomutase	r1p <==> r5p
47	PPM2	phosphopentomutase2 (deoxyribose)	2dr1p <==> 2dr5p

Transport

48	ACALDt	acetaldehyde reversible transport	acald:ext <==> acald
49	ACt2r	acetate reversible transport via proton symport	ac:ext + h:ext <==> ac + h
50	NH3t	ammonia reversible transport	nh4:ext <==> nh4
51	CO2t	CO_2 transporter via diffusion	co2:ext <==> co2
52	GLCpts	D-glucose transport via PEP:Pyr PTS	glc-D:ext + pep => g6p + pyr
53	D-LACt2	D-lactate transport via proton symport	h:ext + lac-D:ext <==> h + lac-D
54	ETOHt2r	ethanol reversible transport	etoh:ext <==> etoh
55	FORt	formate transport via diffusion	for:ext <==> for
56	GLYCt	glycerol transport via channel	glyc <==> glyc:ext
57	H2Ot	H_2O transport via diffusion	h2o:ext <==> h2o
58	O2t	O_2 transport (diffusion)	o2:ext <==> o2
59	PIt2r	phosphate reversible transport via symport	h:ext + pi:ext <==> h + pi
60	SUCCt2b	succinate efflux via proton symport	h + succ => h:ext + succ:ext
61	SULabc	sulfate transport via ABC system	atp + h2o + so4:ext => adp + h + pi + so4

Alanine and Aspartate Metabolism

62	ALAR	alanine racemase	ala-L <==> ala-D
63	ASNS2	asparagine synthetase	asp-L + atp + nh4 => amp + asn-L + h + ppi
64	ASPTA	aspartate transaminase	akg + asp-L <==> glu-L + oaa
65	ALATA_L	L-alanine transaminase	akg + ala-L <==> glu-L + pyr

Arginine and Proline Metabolism

66	DKMPPD	2,3-diketo-5-methylthio-1-phosphopentane degradation reaction	dkmpp + h2o + o2 => 2kmb + for + (2) h + pi
67	UNK3	2-keto-4-methylthiobutyrate transamination	2kmb + glu-L => akg + met-L
68	MDRPD	5-methylthio-5-deoxy-D-ribulose1-phosphate dehydratase	5mdru1p => dkmpp + h2o
69	MTRK	5-methylthioribose kinase	5mtr + atp => 5mdr1p + adp + h
70	MTRI	5-methylthioribose-1-phosphate isomerase	5mdr1p <==> 5mdru1p
71	ACGK	acetylglutamate kinase	acglu + atp => acg5p + adp
72	ACODA	acetylornithine deacetylase	acorn + h2o => ac + orn
73	ACOTA	acetylornithine transaminase	acorn + akg <==> acg5sa + glu-L
74	ADMDCr	adenosylmethionine decarboxylase	amet + h <==> ametam + co2
75	ARGSL	argininosuccinate lyase	argsuc <==> arg-L + fum
76	ARGSS	argininosuccinate synthase	asp-L + atp + citr-L => amp + argsuc + h + ppi
77	CBPS	carbamoyl-phosphate synthase (glutamine-hydrolysing)	(2) atp + gln-L + h2o + hco3 => (2) adp + cbp + glu-L + (2) h + pi
78	GLU5K	glutamate 5-kinase	atp + glu-L => adp + glu5p
79	G5SD	glutamate-5-semialdehyde dehydrogenase	glu5p + h + nadph => glu5sa + nadp + pi

80	G5SADs	L-glutamate 5-semialdehyde dehydratase (spontaneous)	glu5sa => 1pyr5c + h + h2o
81	MTAN	methylthioadenosine nucleosidase	5mta + h2o => 5mtr + ade
82	AGPR	N-acetyl-g-glutamyl-phosphate reductase	acg5sa + nadp + pi <==> acg5p + h + nadph
83	ACGS	N-acetylglutamate synthase	accoa + glu-L => acglu + coa + h
84	OCBT	ornithine carbamoyltransferase	cbp + orn <==> citr-L + h + pi
85	ORNDC	ornithine decarboxylase	h + orn => co2 + ptrc
86	P5CR	pyrroline-5-carboxylate reductase	1pyr5c + (2) h + nadph => nadp + pro-L
87	SPMS	spermidine synthase	ametam + ptrc => 5mta + h + spmd

Cysteine Metabolism

88	BPNT	3',5'-bisphosphate nucleotidase	h2o + pap => amp + pi
89	ADSK	adenylyl-sulfate kinase	aps + atp => adp + h + paps
90	CYSS	cysteine synthase	acser + h2s => ac + cys-L + h
91	PAPSR	phosphoadenylyl-sulfate reductase (thioredoxin)	paps + trdrd => (2) h + pap + so3 + trdox
92	SERAT	serine O-acetyltransferase	accoa + ser-L <==> acser + coa
93	SADT2	sulfate adenyltransferase	atp + gtp + h2o + so4 => aps + gdp + pi + ppi
94	SULR	sulfite reductase (NADPH2)	(3) h2o + h2s + (3) nadp <==> (5) h + (3) nadph + so3

Glutamate Metabolism

| 95 | GLUDy | glutamate dehydrogenase (NADP) | glu-L + h2o + nadp <==> akg + h + nadph + nh4 |
| 96 | GLNS | glutamine synthetase | atp + glu-L + nh4 => adp + gln-L + h + pi |

Glycine and Serine Metabolism

97	GHMT2	glycine hydroxymethyltransferase	ser-L + thf => gly + h2o + mlthf
98	PGCD	phosphoglycerate dehydrogenase	3pg + nad => 3php + h + nadh
99	PSP_L	phosphoserine phosphatase (L-serine)	h2o + pser-L => pi + ser-L
100	PSERT	phosphoserine transaminase	3php + glu-L => akg + pser-L

Histidine Metabolism

101	PRMICIi	1-(5-phosphoribosyl)-5-[(5-phosphoribosylamino)methylideneamino)imidazole-4-carboxamide isomerase (irreversible)	prfp => prlp
102	ATPPRT	ATP phosphoribosyltransferase	atp + prpp => ppi + prbatp
103	HISTD	histidinol dehydrogenase	h2o + histd + (2) nad => (3) h + his-L + (2) nadh
104	HISTP	histidinol-phosphatase	h2o + hisp => histd + pi
105	HSTPT	histidinol-phosphate transaminase	glu-L + imacp => akg + hisp
106	IG3PS	imidazole-glycerol-3-phosphate synthase	gln-L + prlp => aicar + eig3p + glu-L + h
107	IGPDH	imidazoleglycerol-phosphate dehydratase	eig3p => h2o + imacp
108	PRAMPC	phosphoribosyl-AMP cyclohydrolase	h2o + prbamp => prfp
109	PRATPP	phosphoribosyl-ATP pyrophosphatase	h2o + prbatp => h + ppi + prbamp
110	PRPPS	phosphoribosylpyrophosphate synthetase	atp + r5p <==> amp + h + prpp

Methionine Metabolism

111	CYSTL	cystathionine b-lyase	cyst-L + h2o => hcys-L + nh4 + pyr
112	HSST	homoserine O-succinyltransferase	hom-L + succoa => coa + suchms
113	METAT	methionine adenosyltransferase	atp + h2o + met-L => amet + pi + ppi
114	METS	methionine synthase	5mthf + hcys-L => met-L + thf
115	SHSL1	O-succinylhomoserine lyase (L-cysteine)	cys-L + suchms => cyst-L + h + succ

Threonine and Lysine Metabolism

116	ASPK	aspartate kinase	asp-L + atp <==> 4pasp + adp
117	ASAD	aspartate-semialdehyde dehydrogenase	aspsa + nadp + pi <==> 4pasp + h + nadph
118	DAPDC	diaminopimelate decarboxylase	26dap-M + h => co2 + lys-L
119	DAPE	diaminopimelate epimerase	26dap-LL <==> 26dap-M

120 DHDPRy	dihydrodipicolinate reductase (NADPH)	23dhdp + h + nadph => nadp + thdp
121 DHDPS	dihydrodipicolinate synthase	aspsa + pyr => 23dhdp + h + (2) h2o
122 HSDy	homoserine dehydrogenase (NADPH)	hom-L + nadp <==> aspsa + h + nadph
123 SDPDS	succinyl-diaminopimelate desuccinylase	h2o + sl26da => 26dap-LL + succ
124 SDPTA	succinyldiaminopimelate transaminase	akg + sl26da <==> glu-L + sl2a6o
125 THDPS	tetrahydropicolinate succinylase	h2o + succoa + thdp => coa + sl2a6o
126 THRAr	threonine aldolase	thr-L <==> acald + gly

Tyrosine, Tryptophan and Phenylalanine Metabolism

127 DHQD	3-dehydroquinate dehydratase	3dhq <==> 3dhsk + h2o
128 DHQS	3-dehydroquinate synthase	2dda7p => 3dhq + pi
129 DDPA	3-deoxy-D-arabino-heptulosonate 7-phosphate synthetase	e4p + h2o + pep => 2dda7p + pi
130 PSCVT	3-phosphoshikimate 1-carboxyvinyltransferase	pep + skm5p <==> 3psme + pi
131 ANPRT	anthranilate phosphoribosyltransferase	anth + prpp => ppi + pran
132 ANS	anthranilate synthase	chor + gln-L => anth + glu-L + h + pyr
133 CHORM	chorismate mutase	chor => pphn
134 CHORS	chorismate synthase	3psme => chor + pi
135 IGPS	indole-3-glycerol-phosphate synthase	2cpr5p + h => 3ig3p + co2 + h2o
136 PHETA1	phenylalanine transaminase	akg + phe-L <==> glu-L + phpyr
137 PRAIi	phosphoribosylanthranilate isomerase (irreversible)	pran => 2cpr5p
138 PPNDH	prephenate dehydratase	h + pphn => co2 + h2o + phpyr
139 PPND	prephenate dehydrogenase	nad + pphn => 34hpp + co2 + nadh
140 SHK3Dr	shikimate dehydrogenase	3dhsk + h + nadph <==> nadp + skm
141 SHKK	shikimate kinase	atp + skm => adp + h + skm5p
142 TRPS3	tryptophan synthase (indole glycerol phosphate)	3ig3p => g3p + indole
143 TRPAS2	tryptophanase (L-tryptophan)	h2o + trp-L <==> indole + nh4 + pyr
144 TYRTA	tyrosine transaminase	akg + tyr-L <==> 34hpp + glu-L

Valine, Leucine and Isoleucine Metabolism

145 ACHBS	2-aceto-2-hydroxybutanoate synthase	2obut + h + pyr => 2ahbut + co2
146 IPPMIb	2-isopropylmalate hydratase	2ippm + h2o <==> 3c3hmp
147 IPPS	2-isopropylmalate synthase	3mob + accoa + h2o => 3c3hmp + coa + h
148 OMCDC	2-oxo-4-methyl-3-carboxy pentanoate decarboxylation	3c4mop + h => 4mop + co2
149 IPPMIa	3-isopropylmalate dehydratase	3c2hmp <==> 2ippm + h2o
150 IPMD	3-isopropylmalate dehydrogenase	3c2hmp + nad => 3c4mop + h + nadh
151 KARA1i	acetohydroxy acid isomero reductase	alac-S + h + nadph => 23dhmb + nadp
152 ACLS	acetolactate synthase	h + (2) pyr => alac-S + co2
153 DHAD1	dihydroxy-acid dehydratase (2,3-dihydroxy-3-methylbutanoate)	23dhmb => 3mob + h2o
154 DHAD2	dihydroxy-acid dehydratase (2,3-dihydroxy-3-methylpentanoate)	23dhmp => 3mop + h2o
155 ILETA	isoleucine transaminase	akg + ile-L <==> 3mop + glu-L
156 KARA2i	ketol-acid reductoisomerase (2-aceto-2-hydroxybutanoate)	2ahbut + h + nadph => 23dhmp + nadp
157 LEUTAi	leucine transaminase (irreversible)	4mop + glu-L => akg + leu-L
158 THRD_L	L-threonine deaminase	thr-L => 2obut + nh4
159 VALTA	valine transaminase	akg + val-L <==> 3mob + glu-L

Cell Envelope Biosynthesis

160 KDOPS	3-deoxy -D-manno-octulosonic - acid 8-phosphate	ara5p + h2o + pep => kdo8p + pi

161 MOAT	3-deoxy-D-manno-octulosonic acid transferase	ckdo + lipidA => cmp + h + kdolipid4
162 MOAT2	3-deoxy-D-manno-octulosonic acid transferase	ckdo + kdolipid4 => cmp + h + kdo2lipid4
163 KDOCT2	3-deoxy-manno-octulosonate cytidylyltransferase	ctp + kdo => ckdo + ppi
164 KDOPP	3-deoxy-manno-octulosonate-8-phosphatase	h2o + kdo8p => kdo + pi
165 AACPS2	acyl-[acyl-carrier-protein] synthetase (n-C14:1)	ACP + atp + ttdcea => amp + ppi + tdeACP
166 AACPS3	acyl-[acyl-carrier-protein] synthetase (n-C16:0)	ACP + atp + hdca => amp + palmACP + ppi
167 AACPS4	acyl-[acyl-carrier-protein] synthetase (n-C16:1)	ACP + atp + hdcea => amp + hdeACP + ppi
168 AACPS5	acyl-[acyl-carrier-protein] synthetase (n-C18:1)	ACP + atp + ocdcea => amp + octeACP + ppi
169 AACPS1	acyl-[acyl-carrier-protein] synthetase (n-C14:0)	ACP + atp + ttdca => amp + myrsACP + ppi
170 AGMHE	ADP-D-glycero-D-manno-heptose epimerase	adphep-D,D => adphep-L,D
171 ALAALAr	D-alanine-D-alanine ligase (reversible)	(2) ala-D + atp <==> adp + alaala + h + pi
172 GMHEPAT	D-glycero-D-manno-hepose 1-phosphate adenyltransferase	atp + gmhep1p + h => adphep-D,D + ppi
173 GMHEPPA	D-glycero-D-manno-heptose 1,7-bisphosphate phosphatase	gmhep17bp + h2o => gmhep1p + pi
174 GMHEPK	D-glycero-D-manno-heptose 7-phosphate kinase	atp + gmhep7p => adp + gmhep17bp + h
175 DAGK_EC	diacylglycerol kinase	(0.02) 12dgr_EC + atp => adp + h + (0.02) pa_EC
176 EDTXS1	endotoxin synthesis (lauroyl transferase)	ddcaACP + kdo2lipid4 => ACP + kdo2lipid4L
177 EDTXS2	endotoxin synthesis (myristoyl transferase)	kdo2lipid4L + myrsACP => ACP + lipa
178 PEPT_EC	ethanolamine phosphotransferase	cmp + h + (0.02) pe_EC <==> (0.02) 12dgr_EC + cdpea
179 G1PACT	glucosamine-1-phosphate N-acetyltransferase	accoa + gam1p => acgam1p + coa + h
180 GLUR	glutamate racemase	glu-D <==> glu-L
181 GF6PTA	glutamine-fructose-6-phosphate transaminase	f6p + gln-L => gam6p + glu-L
182 GPDDA2	glycerophosphodiester phosphodiesterase	g3pe + h2o => etha + glyc3p + h
183 GPDDA4	glycerophosphodiester phosphodiesterase	g3pg + h2o => glyc + glyc3p + h
184 LPADSS	lipid A disaccaride synthase	lipidX + u23ga => h + lipidAds + udp
185 LPSSYN_EC	lipopolysaccharide synthesis	(3) adphep-L,D + (2) cdpea + (3) ckdo + lipa + (2) udpg => (3) adp + (2) cdp + (3) cmp + (10) h + lps_EC + (2) udp
186 LPLIPA2	lysophospholipase L (acyl-glycerophosphoethanolamine)	(0.02) agpe_EC + h2o => g3pe + h + (0.36) hdca + (0.07) hdcea + (0.5) ocdcea + (0.02) ttdca + (0.05) ttdcea
187 LPLIPA1	lysophospholipase L (acyl-glycerophosphoglycerol)	(0.02) agpg_EC + h2o => g3pg + h + (0.36) hdca + (0.07) hdcea + (0.5) ocdcea + (0.02) ttdca + (0.05) ttdcea
188 PPTGS	peptidoglycan subunit synthesis	uaagmda => h + peptido_EC + udcpdp
189 PLIPA2	phosphlipase A (phosphatidylethanolamine)	h2o + (0.02) pe_EC => (0.02) agpe_EC + h + (0.36) hdca + (0.07) hdcea + (0.5) ocdcea + (0.02) ttdca + (0.05) ttdcea
190 PGAMT	phosphoglucosamine mutase	gam1p <==> gam6p
191 PLIPA1	phospholipase A (phosphatidylglycerol)	h2o + (0.02) pg_EC => (0.02) agpg_EC + h + (0.36) hdca + (0.07) hdcea + (0.5) ocdcea + (0.02) ttdca + (0.05) ttdcea
192 PAPPT3	phospho-N-acetylmuramoyl-pentapeptide-transferase	udcpp + ugmda => uagmda + ump
193 S7PI	sedoheptulose 7-phosphate isomerase	s7p => gmhep7p
194 TDSK	tetraacyldisaccharide 4'kinase	atp + lipidAds => adp + h + lipidA
195 U23GAAT	UDP-3-O-(3-hydroxymyristoyl) glucosamine acyltransferase	3hmrsACP + u3hga => ACP + h + u23ga

196	UHGADA	UDP-3-O-acetylglucosamine deacetylase	h2o + u3aga => ac + u3hga
197	UAPGR	UDP-N-acetylenolpyruvoyl glucosamine reductase	h + nadph + uaccg => nadp + uamr
198	UAGCVT	UDP-N-acetylglucosamine 1-carboxyvinyltransferase	pep + uacgam => pi + uaccg
199	UAGAAT	UDP-N-acetylglucosamine acyltransferase	3hmrsACP + uacgam <==> ACP + u3aga
200	UAGDP	UDP-N-acetylglucosamine diphosphorylase	acgam1p + h + utp => ppi + uacgam
201	UAGPT3	UDP-N-acetylglucosamine-N-acetylmuramyl-(pentapeptide) pyrophosphoryl-undecaprenol N-acetylglucosamine transferase	uacgam + uagmda => h + uaagmda + udp
202	UAMAS	UDP-N-acetylmuramoyl-L-alanine synthetase	ala-L + atp + uamr => adp + h + pi + uama
203	UAMAGS	UDP-N-acetylmuramoyl-L-alanyl-D-glutamate synthetase	atp + glu-D + uama => adp + h + pi + uamag
204	UAAGDS	UDP-N-acetylmuramoyl-L-alanyl-D-glutamyl-meso-2,6-diaminopimelate synthetase	26dap-M + atp + uamag => adp + h + pi + ugmd
205	UGMDDS	UDP-N-acetylmuramoyl-L-alanyl-D-glutamyl-meso-2,6-diaminopimeloyl-D-alanyl-D-alanine synthetase	alaala + atp + ugmd => adp + h + pi + ugmda
206	USHD	UDP-sugar hydrolase	h2o + u23ga => (2) h + lipidX + ump
207	UDCPDP	undecaprenyl-diphosphatase	h2o + udcpdp => h + pi + udcpp
208	GALU	UTP-glucose-1-phosphate uridylyltransferase	g1p + h + utp <==> ppi + udpg

Folate Metabolism

209	MTHFR2	5,10-methylenetetrahydrofolate reductase (NADH)	h + mlthf + nadh => 5mthf + nad
210	FTHFD	formyltetrahydrofolate deformylase	10fthf + h2o => for + h + thf
211	MTHFC	methenyltetrahydrofolate cyclohydrolase	h2o + methf <==> 10fthf
212	MTHFD	methylenetetrahydrofolate dehydrogenase (NADP)	mlthf + nadp <==> h + methf + nadph

Membrane Lipid Metabolism

213	KAS16	3-hydroxy-myristoyl-ACP synthesis	ddcaACP + (2) h + malACP + nadph => 3hmrsACP + ACP + co2 + nadp
214	ACCOACr	acetyl-CoA carboxylate, reversible reaction	accoa + atp + hco3 <==> adp + h + malcoa + pi
215	KAS15	b-ketoacyl synthase	accoa + h + malACP => actACP + co2 + coa
216	DASYN_EC	CDP-diacylglycerol synthetase	ctp + h + (0.02) pa_EC <==> (0.02) cdpdag1 + ppi
217	C120SN	fatty acid biosynthesis (n-C12:0)	actACP + (14) h + (4) malACP + (10) nadph => (4) ACP + (4) co2 + ddcaACP + (5) h2o + (10) nadp
218	C140SN	fatty acid biosynthesis (n-C14:0)	actACP + (17) h + (5) malACP + (12) nadph => (5) ACP + (5) co2 + (6) h2o + myrsACP + (12) nadp
219	C160SN	fatty acid biosynthesis (n-C16:0)	actACP + (20) h + (6) malACP + (14) nadph => (6) ACP + (6) co2 + (7) h2o + (14) nadp + palmACP
220	C161SN	fatty acid biosynthesis (n-C16:1)	actACP + (19) h + (6) malACP + (13) nadph => (6) ACP + (6) co2 + (7) h2o + hdeACP + (13) nadp
221	C181SN	fatty acid biosynthesis (n-C18:1)	actACP + (22) h + (7) malACP + (15) nadph => (7) ACP + (7) co2 + (8) h2o + (15) nadp + octeACP
222	MCOATA	malonyl-CoA-ACP transacylase	ACP + malcoa <==> coa + malACP
223	PASYN_EC	phosphatidic acid synthase	glyc3p + (0.14) hdeACP + (0.04) myrsACP + octeACP + (0.72) palmACP + (0.1) tdeACP => (2) ACP + (0.02) pa_EC
224	PGPP_EC	phosphatidylglycerol phosphate phosphatase	h2o + (0.02) pgp_EC => (0.02) pg_EC + pi
225	PGSA_EC	phosphatidylglycerol synthase	(0.02) cdpdag1 + glyc3p <==> cmp + h + (0.02) pgp_EC
226	PSD_EC	phosphatidylserine decarboxylase	h + (0.02) ps_EC => co2 + (0.02) pe_EC
227	PSSA_EC	phosphatidylserine syntase	(0.02) cdpdag1 + ser-L <==> cmp + h + (0.02) ps_EC

Nucleotide Salvage Pathways

228	NTD6	5'-nucleotidase (dAMP)	damp + h2o => dad-2 + pi
229	ADNK1	adenosine kinase	adn + atp => adp + amp + h
230	ADK1	adenylate kinase	amp + atp <==> (2) adp
231	CYTK1	cytidylate kinase (CMP)	atp + cmp <==> adp + cdp
232	CYTK2	cytidylate kinase (dCMP)	atp + dcmp <==> adp + dcdp
233	DADK	deoxyadenylate kinase	atp + damp <==> adp + dadp
234	DGK1	deoxyguanylate kinase (dGMP:ATP)	atp + dgmp <==> adp + dgdp
235	GK1	guanylate kinase (GMP:ATP)	atp + gmp <==> adp + gdp
236	NDPK3	nucleoside-diphosphate kinase (ATP:CDP)	atp + cdp <==> adp + ctp
237	NDPK6	nucleoside-diphosphate kinase (ATP:dUDP)	atp + dudp <==> adp + dutp
238	NDPK1	nucleoside-diphosphate kinase (ATP:GDP)	atp + gdp <==> adp + gtp
239	NDPK2	nucleoside-diphosphate kinase (ATP:UDP)	atp + udp <==> adp + utp
240	PUNP1	purine-nucleoside phosphorylase (Adenosine)	adn + pi <==> ade + r1p
241	PUNP2	purine-nucleoside phosphorylase (Deoxyadenosine)	dad-2 + pi <==> 2dr1p + ade
242	RNDR1	ribonucleoside-diphosphate reductase (ADP)	adp + trdrd => dadp + h2o + trdox
243	RNDR3	ribonucleoside-diphosphate reductase (CDP)	cdp + trdrd => dcdp + h2o + trdox
244	RNDR2	ribonucleoside-diphosphate reductase (GDP)	gdp + trdrd => dgdp + h2o + trdox
245	RNTR4	ribonucleoside-triphosphate reductase (UTP)	trdrd + utp => dutp + h2o + trdox
246	TMDS	thymidylate synthase	dump + mlthf => dhf + dtmp
247	UMPK	UMP kinase	atp + ump <==> adp + udp
248	URIDK2r	uridylate kinase (dUMP)	atp + dump <==> adp + dudp

Purine and Pyrimidine Biosynthesis

249	ADSL2r	adenylosuccinate lyase	25aics <==> aicar + fum
250	ADSS	adenylosuccinate synthase	asp-L + gtp + imp => dcamp + gdp + (2) h + pi
251	ADSL1r	adenylsuccinate lyase	dcamp <==> amp + fum
252	ASPCT	aspartate carbamoyltransferase	asp-L + cbp => cbasp + h + pi
253	CTPS2	CTP synthase (glutamine)	atp + gln-L + h2o + utp => adp + ctp + glu-L + (2) h + pi
254	DHORD2	dihydoorotic acid dehydrogenase	dhor-S + q8 => orot + q8h2
255	DHORTS	dihydroorotase	dhor-S + h2o <==> cbasp + h
256	GLUPRT	glutamine phosphoribosyl diphosphate amidotransferase	gln-L + h2o + prpp => glu-L + ppi + pram
257	GMPS2	GMP synthase	atp + gln-L + h2o + xmp => amp + glu-L + gmp + (2) h + ppi
258	IMPC	IMP cyclohydrolase	h2o + imp <==> fprica
259	IMPD	IMP dehydrogenase	h2o + imp + nad => h + nadh + xmp
260	ORPT	orotate phosphoribosyltransferase	orot5p + ppi <==> orot + prpp
261	OMPDC	orotidine-5'-phosphate decarboxylase	h + orot5p => co2 + ump
262	AIRC2	phosphoribosylaminoimidazole carboxylase	air + atp + hco3 => 5caiz + adp + h + pi
263	AIRC3	phosphoribosylaminoimidazole carboxylase (mutase rxn)	5aizc <==> 5caiz
264	PRAIS	phosphoribosylaminoimidazole synthase	atp + fpram => adp + air + (2) h + pi
265	AICART	phosphoribosylaminoimidazole carboxamide formyltransferase	10fthf + aicar <==> fprica + thf
266	PRASCS	phosphoribosylaminoimidazole succinocarboxamide synthase	5aizc + asp-L + atp <==> 25aics + adp + h + pi
267	PRFGS	phosphoribosylformylglycin amidine synthase	atp + fgam + gln-L + h2o => adp + fpram + glu-L + h + pi

268	GARFT	phosphoribosylglycinamide formyltransferase	10fthf + gar <==> fgam + h + thf
269	PRAGSr	phosphoribosylglycinamide synthase	atp + gly + pram <==> adp + gar + h + pi

Unassigned

270	ATPM	ATP maintenance requirement	atp + h2o => adp + h + pi
271	HCO3E	HCO$_3$ equilibration reaction	co2 + h2o <==> h + hco3

Anabolism

272	Aaprotsyn	average amino acid synthesis for protein	(0.113) ala-L + (0.0512) arg-L + (0.0532) asn-L + (0.0532) asp-L + (0.0176) cys-L + (0.0599) gln-L + (0.0599) glu-L + (0.0872) gly + (0.0182) his-L + (0.0493) ile-L + (0.0541) leu-L + (0.0605) lys-L + (0.0259) met-L + (0.0350) phe-L + (0.0416) pro-L + (0.0501) ser-L + (0.0545) thr-L + (0.0114) trp-L + (0.0290) tyr-L + (0.0752) val-L => Aaprot
273	Biomform	biomass formation	(0.7400) Biom_Prot + (0.00865) DNA + (0.0109) etha + (0.0122) glyc + (0.000956) glycogen + (0.00304) hdca + (00.00235) hdcea + (0.0000543) lps_EC + (0.00154) ocdcea + (0.000156) peptido_EC + (0.000784) ptrc + (0.0535) RNAtot + (0.000159) spmd => Biom_01
274	Protsyn	biomass protein synthesis	Aaprot + (4) atp + (3) h2o => (4) adp + (4.77) Biom_Prot + (4) h + (4) pi
275	DNA_pol	DNA polymerization;	(2) atp + (0.246) damp + (0.254) dcmp + (0.254) dgmp + (0.246) dtmp + h2o => (2) adp + (9.75) DNA + (2) h + 2 pi
276	RNA_pol_tot	RNA polymerization	(0.262) amp + (2) atp + (0.2) cmp + (0.322) gmp + h2o + (0.216) ump => (2) adp + (2) h + (2) pi + (9.58) RNAtot

Additional reactions for growth on glycerol

277	GLYK	glycerol kinase	atp + glyc => adp + glyc3p + h
278	G3PD5	glycerol-3-phosphate dehydrogenase (ubiquinone-8)	glyc3p + q8 <==> dhap + q8h2
279	FBP	fructose-bisphosphatase	fdp + h2o => f6p + pi

Additional reactions for growth on acetate

279	FBP	fructose-bisphosphatase	fdp + h2o => f6p + pi
280	PPCK	PEP carboxykinase	atp + oaa => adp + co2 + pep
281	ICL	isocitrate lyase	icit => glx + succ
282	MALS	malate synthase	accoa + glx + h2o => coa + h + mal-L
283	ACS	acetyl-CoA synthetase	ac + atp + coa => accoa + amp + ppi
284	THD2	NAD(P) transhydrogenase	(2) h + nad + nadph <==> (2) h:ext + nadp + nadh

Components

10fthf	10-Formyltetrahydrofolate	acglu	N-Acetyl-L-glutamate
12dgr_EC	1,2-Diacylglycerol (E.coli)	acorn	N2-Acetyl-L-ornithine
13dpg	3-Phospho-D-glyceroyl phosphate	ACP	acyl carrier protein
1pyr5c	1-Pyrroline-5-carboxylate	acser	O-Acetyl-L-serine
23dhdp	2,3-Dihydrodipicolinate	actACP	Acetoacetyl-ACP
23dhmb	(R)-2,3-Dihydroxy-3-methylbutanoate	actp	Acetyl phosphate
23dhmp	(R)-2,3-Dihydroxy-3-methylpentanoate	ade	Adenine
25aics	(S)-2-[5-Amino-1-(5-phospho-D-ribosyl) imidazole-4-carboxamido] succinate	adn	Adenosine
		adp	ADP
26dap-LL	LL-2,6-Diaminoheptanedioate	adpglc	ADPglucose
26dap-M	meso-2,6-Diaminoheptanedioate	adphep-D,D	ADP-D-glycero-D-manno-heptose
2ahbut	(S)-2-Aceto-2-hydroxybutanoate	adphep-L,D	ADP-L-glycero-D-manno-heptose
2cpr5p	1-(2-Carboxyphenylamino)-1-deoxy-D-ribulose-5-phosphate	agpe_EC	acyl-glycerophosphoethanolamine (E.coli)
		agpg_EC	acyl-glycerophosphoglycerol (E.coli)
2dda7p	2-Dehydro-3-deoxy-D-arabino-heptonate7-phosphate	aicar	5-Amino-1-(5-Phospho-D-ibosyl) imidazole-4-carboxamide
2dr1p	2-Deoxy-D-ribose 1-phosphate	air	5-amino-1-(5-phospho-D-ribosyl)imidazole
2dr5p	2-Deoxy-D-ribose 5-phosphate	akg	2-Oxoglutarate
2ippm	2-Isopropylmaleate	alaala	D-Alanyl-D-alanine
2kmb	2-keto-4-methylthiobutyrate	alac-S	(S)-2-Acetolactate
2obut	2-Oxobutanoate	ala-D	D-Alanine
2pg	D-Glycerate 2-phosphate	ala-L	L-Alanine
34hpp	3-(4-Hydroxyphenyl)pyruvate	amet	S-Adenosyl-L-methionine
3c2hmp	3-Carboxy-2-hydroxy-4-methylpentanoate	ametam	S-Adenosylmethioninamine
3c3hmp	3-Carboxy-3-hydroxy-4-methylpentanoate	amp	AMP
3c4mop	3-Carboxy-4-methyl-2-oxopentanoate	anth	Anthranilate
3dhq	3-Dehydroquinate	aps	Adenosine 5'-phosphosulfate
3dhsk	3-Dehydroshikimate	ara5p	D-Arabinose 5-phosphate
3hmrsACP	R-3-hydroxy-myristoyl-ACP	arg-L	L-Arginine
3ig3p	C'-(3-Indolyl)-glycerol 3-phosphate	argsuc	N(omega)-(L-Arginino)succinate
3mob	3-Methyl-2-oxobutanoate	asn-L	L-Asparagine
3mop	(S)-3-Methyl-2-oxopentanoate	asp-L	L-Aspartate
3pg	3-Phospho-D-glycerate	aspsa	L-Aspartate 4-semialdehyde
3php	3-Phosphohydroxypyruvate	atp	ATP
3psme	5-O-(1-Carboxyvinyl)-3-phosphoshikimate	Biom_Prot	Biomass protein
4mop	4-Methyl-2-oxopentanoate	biom3	biomass3
4pasp	4-Phospho-L-aspartate	cbasp	N-Carbamoyl-L-aspartate
5aizc	5-amino-1-(5-phospho-D-ribosyl) imidazole-4-carboxylate	cbp	Carbamoyl phosphate
		cdp	CDP
5caiz	5-phosphoribosyl-5-carboxyaminoimidazole	cdpdag1	CDPdiacylglycerol (E coli)
		cdpea	CDPethanolamine
5mdr1p	5-Methylthio-5-deoxy-D-ribose1-phosphate	chor	Chorismate
5mdru1p	5-Methylthio-5-deoxy-D-ribulose 1-phosphate	cit	Citrate
		citr-L	L-Citrulline
5mta	5-Methylthioadenosine	ckdo	CMP-3-deoxy-D-manno-octulosonate
5mthf	5-Methyltetrahydrofolate	cmp	CMP
5mtr	5-Methylthio-D-ribose	co2	CO_2
6pgc	6-Phospho-D-gluconate	coa	Coenzyme A
6pgl	6-phospho-D-glucono-1,5-lactone	ctp	CTP
Aaprot	Averige amino acid composition for protein synthesis	cys-L	L-Cysteine
		cyst-L	L-Cystathionine
ac	Acetate	dad-2	Deoxyadenosine
acald	Acetaldehyde	dadp	dADP
accoa	Acetyl-CoA	damp	dAMP
acg5p	N-Acetyl-L-glutamyl 5-phosphate	dcamp	N6-(1,2-Dicarboxyethyl)-AMP
acg5sa	N-Acetyl-L-glutamate 5-semialdehyde	dcdp	dCDP
acgam1p	N-Acetyl-D-glucosamine 1-phosphate	dcmp	dCMP

ddcaACP	Dodecanoyl-ACP (n-C12:0ACP)	hdca	Hexadecanoate (n-C16:0)
dgdp	dGDP	hdcea	hexadecenoate (n-C16:1)
dgmp	dGMP	hdeACP	Hexadecenoyl-ACP (n-C16:1ACP)
dhap	Dihydroxyacetone phosphate	his-L	L-Histidine
dhf	7,8-Dihydrofolate	hisp	L-Histidinol phosphate
dhor-S	(S)-Dihydroorotate	histd	L-Histidinol
dkmpp	2,3-diketo-5-methylthio-1-phosphopentane	hom-L	L-Homoserine
DNA	Deoxyribonucleic acid	icit	Isocitrate
dtmp	dTMP	ile-L	L-Isoleucine
dudp	dUDP	imacp	3-(Imidazol-4-yl)-2-oxopropyl phosphate
dump	dUMP	imp	IMP
dutp	dUTP	Indole	Indole
e4p	D-Erythrose 4-phosphate	kdo	3-Deoxy-D-manno-2-octulosonate
eig3p	D-erythro-1-(Imidazol-4-yl)glycerol3-phosphate	kdo2lipid4	KDO(2)-lipid IV(A)
		kdo2lipid4L	KDO(2)-lipid IV(A) with laurate
etha	Ethanolamine	kdo8p	3-Deoxy-D-manno-octulosonate 8-phosphate
etoh	Ethanol		
f6p	D-Fructose 6-phosphate	kdolipid4	KDO-lipid IV(A)
fad	FAD	lac-D	D-Lactate
fadh2	FADH2	leu-L	L-Leucine
fdp	D-Fructose 1,6-bisphosphate	lipa	KDO(2)-lipid (A)
fgam	N2-Formyl-N1-(5-phospho-D-ribosyl)glycinamide	lipidA	2,3,2'3'-Tetrakis(beta-hydroxymyristoyl)-D-glucosaminyl-1,6-beta-D-glucosam
for	Formate	lipidAds	Lipid A Disaccharide
fpram	2-(Formamido)-N1-(5-phospho-D-ribosyl)acetamidine	lipidX	2,3-Bis(3-hydroxytetradecanoyl)-beta-D-glucosaminyl 1-phosphate
fprica	5-Formamido-1-(5-phospho-D-ribosyl)imidazole-4-carboxamide	lps_EC	lipopolysaccharide (Ecoli)
fum	Fumarate	lys-L	L-Lysine
g1p	D-Glucose 1-phosphate	malACP	Malonyl-[acyl-carrier protein]
gap	Glyceraldehyde 3-phosphate	malcoa	Malonyl-CoA
g3pe	sn-Glycero-3-phosphoethanolamine	mal-L	L-Malate
g3pg	Glycerophosphoglycerol	methf	5,10-Methenyltetrahydrofolate
g6p	D-Glucose 6-phosphate	met-L	L-Methionine
gam1p	D-Glucosamine 1-phosphate	mlthf	5,10-Methylenetetrahydrofolate
gam6p	D-Glucosamine 6-phosphate	myrsACP	Myristoyl-ACP (n-C14:0ACP)
gar	N1-(5-Phospho-D-ribosyl)glycinamide	nad	Nicotinamide adenine dinucleotide
gdp	GDP	nadh	Nicotinamide adenine dinucleotide-reduced
glc-D	D-Glucose	nadp	Nicotinamide adenine dinucleotide phosphate
gln-L	L-Glutamine	nadph	Nicotinamide adenine dinucleotide phosphate- reduced
glu5p	L-Glutamate 5-phosphate	nh4	ammonium
glu5sa	L-Glutamate 5-semialdehyde	o2	O_2
glu-D	D-Glutamate	oaa	Oxaloacetate
glu-L	L-Glutamate	ocdcea	octadecenoate (n-C18:1)
gly	Glycine	octeACP	Octadecenoyl-ACP (n-C18:1ACP)
glyc	Glycerol	orn	Ornithine
glyc3p	Glycerol 3-phosphate	orot	Orotate
glycogen	glycogen	orot5p	Orotidine 5'-phosphate
gmhep17bp	D-Glycero-D-manno-heptose 1,7-bisphosphate	pa_EC	phosphatidate (E.coli)
		palmACP	Palmitoyl-ACP (n-C16:0ACP)
gmhep1p	D-Glycero-D-manno-heptose 1-phosphate	pap	Adenosine 3',5'-bisphosphate
gmhep7p	D-Glycero-D-manno-heptose 7-phosphate	paps	3'-Phosphoadenylyl sulfate
gmp	GMP	pe_EC	Phosphatidylethanolamine (Ecoli)
gtp	GTP	pep	Phosphoenolpyruvate
h	H+	peptido_EC	Peptidoglycan subunit of *Escherichia coli*
h2o	H2O	pg_EC	Phosphatidylglycerol (Ecoli)
h2s	Hydrogen sulfide	pgp_EC	Phosphatidylglycerophosphate (Ecoli)
hco3	Bicarbonate	phe-L	L-Phenylalanine
		phpyr	Phenylpyruvate
hcys-L	L-Homocysteine	pi	Phosphate

pphn	Prephenate	trp-L	L-Tryptophan
ppi	Diphosphate	ttdca	tetradecanoate (n-C14:0)
pram	5-Phospho-beta-D-ribosylamine	ttdcea	tetradecenoate (n-C14:1)
pran	N-(5-Phospho-D-ribosyl)anthranilate	tyr-L	L-Tyrosine
prbamp	1-(5-Phosphoribosyl)-AMP	u23ga	UDP-2,3-bis(3-hydroxytetradecanoyl)
prbatp	1-(5-Phosphoribosyl)-ATP		glucosamine
prfp	1-(5-Phosphoribosyl)-5-[(5-phosphoribosyl amino)methylideneamino] imidazole-4	u3aga	UDP-3-O-(3-hydroxytetradecanoyl)- N-acetylglucosamine
prlp	5-[(5-phospho-1-deoxyribulos-1-ylamino) methylideneamino]-1-(5-phosphoribosy	u3hga	UDP-3-O-(3-hydroxytetradecanoyl)- D-glucosamine
pro-L	L-Proline	uaagmda	Undecaprenyl-diphospho-N-acetylmuramoyl-(N-acetylglucosamine)-L-alanyl-D-glutamyl-meso-2,6-diaminopimeloyl-D-alanyl-D-alanine
prpp	5-Phospho-alpha-D-ribose 1-diphosphate		
ps_EC	phosphatidylserine (Ecoli)		
pser-L	O-Phospho-L-serine		
ptrc	Putrescine	uaccg	UDP-N-acetyl-3-O-(1-carboxyvinyl)- D-glucosamine
pyr	Pyruvate		
q8	Ubiquinone-8	uacgam	UDP-N-acetyl-D-glucosamine
q8h2	Ubiquinol-8	uagmda	Undecaprenyl-diphospho-N-acetyl muramoyl -L -alanyl-D-glutamyl-meso-2,6-diaminopimeloyl-D-ala-D-ala
r1p	alpha-D-Ribose 1-phosphate		
r5p	alpha-D-Ribose 5-phosphate		
RNAtot	Ribonucleic acid total	uama	UDP-N-acetylmuramoyl-L-alanine
ru5p-D	D-Ribulose 5-phosphate	uamag	UDP-N-acetylmuramoyl-L-alanyl-D-glutamate
s7p	Sedoheptulose 7-phosphate		
ser-L	L-Serine	uamr	UDP-N-acetylmuramate
skm	Shikimate	udcpdp	Undecaprenyl diphosphate
skm5p	Shikimate 5-phosphate	udcpp	Undecaprenyl phosphate
sl26da	N-Succinyl-LL-2,6-diaminoheptanedioate	udp	UDP
sl2a6o	N-Succinyl-2-L-amino-6-oxoheptanedioate	udpg	UDPglucose
so3	Sulfite	ugmd	UDP-N-acetylmuramoyl-L-alanyl- D-gamma-glutamyl-meso-2,6-diaminopimelate
so4	Sulfate		
spmd	Spermidine		
succ	Succinate	ugmda	UDP-N-acetylmuramoyl-L-alanyl- D-glutamyl-meso-2,6-diaminopimeloyl-D-alanyl-D-alanine
succoa	Succinyl-CoA		
suchms	O-Succinyl-L-homoserine		
tdeACP	Tetradecenoyl-ACP (n-C14:1ACP)	ump	UMP
thdp	2,3,4,5-Tetrahydrodipicolinate	utp	UTP
thf	5,6,7,8-Tetrahydrofolate	val-L	L-Valine
thr-L	L-Threonine	xmp	Xanthosine 5'-phosphate
trdox	Oxidized thioredoxin	xu5p-D	D-Xylulose 5-phosphate
trdrd	Reduced thioredoxin		

2.5.2. Relation of biomass composition and respiratory quotient (RQ) for cultures that utilize glucose as substrate

In the absence of product formation the carbon balance is written as

$$q_{CO_2} + \mu = 6q_S \tag{2.6}$$

and the generalized degree of reduction balance is written as

$$24q_S - 4q_{O_2} = \gamma_x\mu. \tag{2.7}$$

The respiratory quotient (RQ) is defined as: $RQ = q_{CO2}/q_{O2}$. Combining this with the observed biomass yield, $Y = \mu/q_S$ yields

$$\gamma_x = \frac{4}{Y}\left[6 - \frac{(6-Y)}{RQ}\right].$$

$$(2.8)$$

Eq. (2.8) shows the relation between yield of biomass on substrate (Y), degree of reduction of biomass (γ_X) and RQ. This implies that under the conditions of no by-product formation, the available measurements of offgas and measurement of biomass yield would give the degree of reduction of biomass produced. As an example, filling in a typical yield of 3 Cmol X/mol glucose, and RQ = 1.05 (Sauer *et al.* 1999) for aerobic glucose-limited chemostat cultures of *E. coli*, gives $\gamma_X = 4.2$.

Acknowledgements

Supplementary Material

The supplementary material can be accessed online at http://www3.interscience.wiley.com/journal/123443492/suppinfo.

Chapter 3

A thermodynamic analysis of fermentative dicarboxylic acid production

Abstract

Production of dicarboxylic acids from microorganisms, and hence searching for genetic engineering targets to achieve the maximal product yields, especially at low pH, has recently received substantial interest. Therefore it is of importance that the theoretical limits of the production pathways are known. This can be analyzed stoichiometrically and thermodynamically as shown here for the production of succinic and fumaric acids from glucose at 25 ^{o}C for pH 1 - 8. Taking into consideration the different species (solid, undissociated, dissociated) of the organic acids at each pH, very negative Gibbs energy formation of the theoretical anaerobic reaction (-22 to -70 kJ/mol fumaric acid and -125 to -159 kJ/mol succinic acid) were found, indicating that the maximal theoretical product yields (1.71 and 2.00 mol/mol for succinic and fumaric, respectively) are anaerobically feasible, also at low pH (< 3). Considering a required high extracellular total acid concentration, thermodynamically feasible active transport mechanisms were found to be 1 H^+ antiport at pH 3 and 1 H^+ symport at pH 7 for both acids, to achieve sufficient driving force for export of the organic acid, assuming an intracellular pH of 7. Taking this transport energy into account shows that fumaric acid production at low pH requires aerobic conditions. Alternative aerobic (pH 3) and anaerobic (pH 3 and 7) networks for fumaric acid and anaerobic network for succinic acid (pH 3 and 7) are proposed with energy (ATP) characteristics considered. The effect of acid back diffusion, which occurs at low pH by the undissociated organic acid, on the product yield was found to be different for the studied organic acids, being positively correlated with succinic acid (due to growth) and negatively correlated with fumaric acid. Taking these energy aspects of the optimal network into account, genetic engineering targets are suggested.

3.1. Introduction

The production of chemicals from renewable feedstocks using microorganisms receives considerable attention due to the ever increasing possibilities of genetic engineering and the contribution to decreasing CO_2 emissions. Especially multifunctional molecules, containing alcoholic and carboxylic acid groups, are of interest because of their application in polymer production, which represents a very large market (Sauer *et al.* 2008). Four carbon 1,4-diacids (succinic, fumaric, and malic) are considered as one of 12 top chemical building blocks manufactured from bio-feed-stocks in a report from the USDOE (US Department of Energy, 2004).

As a consequence, the biotechnological processes will occur on very large-scale, where from a cost point of view one desires the highest yield of product on substrate, low cost of auxiliary chemicals (e.g. pH control) and low cost of down stream processing (DSP). A general approach to evaluate these aspects, leading to relevant targets for genetic engineering, is therefore of interest and is the focus of this contribution. The approach will be illustrated using two dicarboxylic acids (succinic and fumaric acid) and will be thermodynamically-based, ensuring its general applicability to any other product of interest.

Outline of the approach

For dicarboxylic acids, one has to consider several aspects:

- There is production of acid, which requires the consumption of alkali for pH control in the fermentation process. In DSP the conventional method to obtain the undissociated acid (needed in the final polymerization processes) requires the addition of an inorganic acid solution. Overall, this leads to the consumption of stoichiometric amounts of alkali (e.g. $CaCO_3$) and acid (e.g. H_2SO_4) leading to production of stoichiometric amounts of salt (e.g. $CaSO_4$). Purchase of the alkali and acid and disposal of the salt pose a significant cost factor of about € 0.30 per kg acid (see Appendix 3.4.1). Economically it is therefore desirable to perform the fermentation process at low pH, producing the undissociated acid, which avoids the need for these auxiliary agents.
- The dicarboxylic acids are produced in metabolic reaction networks, which require that the product is exported over the membrane. While this is no problem for alcohols (passive diffusion is possible), the intracellular present organic acid anions (charge -2) require special transporters which must achieve the required large out/in concentration ratio of the acid which is typical order of 10^3 (because typical intracellular concentrations of the dicarboxylic acid anions are order 10^{-3} M, and an economically viable process requires about 1 M concentration in the broth). Therefore, the export of the acid has an energy aspect. This energy aspect is even augmented because all the produced H^+ must also be exported against the H^+ gradient (proton motive force).
- Organic acids, especially at the preferred low extracellular pH, can only be exported using energy consuming active transport mechanisms as explained above. However at low pH, the richly available extracellular undissociated organic acid can freely diffuse

back into the cell, leading to an energy consuming (futile) cycle of export and import of undissociated acid. This energy drain leads to a changed product yield.

- At low pH organic acids often reach a solubility limit.

Our approach uses a thermodynamic framework to analyze the production of dicarboxylic acids (succinic and fumaric) from glucose at low pH with respect to stoichiometry and energy aspects of the black box theoretical product reaction and of candidate metabolic networks.

3.2. Black Box thermodynamic analysis of the theoretical dicarboxylic acid product reaction

This analysis will present for the two organic acids the maximal theoretical yield, the theoretical product reaction, the consumption of alkali, the osmotic strength and the amount of solid product as function of pH, and finally the calculation of ΔG_r as function of pH.

3.2.1. Maximal theoretical product yield

A product made by microorganisms is the result of a metabolic network. Theoretically, the highest product yield is obtained when the organism does not spend substrate for growth, maintenance or external electron acceptor (as O_2). This leads to a theoretical situation where one envisages that the cell only makes the intended product under **anaerobic conditions** where all electrons from the substrate end in the product. The theoretical maximal yield then follows from a simple balance of degree of reduction (Roels 1983):

$$Y_{SP}^{theor} \left(\frac{mol\ P}{mol\ S} \right) = \frac{\gamma_S}{\gamma_P}. \tag{3.1}$$

Assuming glucose ($C_6H_{12}O_6$, $\gamma_S = 24$) as a renewable substrate and considering succinic acid ($C_4H_6O_4$, $\gamma_P = 14$) or fumaric acid ($C_4H_4O_4$, $\gamma_P = 12$) as products gives $24/14 = 1.71$ and $24/12 = 2.00$ as maximal theoretical molar yields for succinic and fumaric acid per mol glucose. This theoretical maximal yield would be achieved anaerobically and is not based on any metabolic reaction network assumption. In principle, this black box result poses a theoretical maximum for any conceivable network, which starts with glucose and produces the acid as only product. The feasibility of this yield needs however first to be checked from a thermodynamic point of view, for which the stoichiometry of the theoretical product reaction is needed.

3.2.2. Stoichiometry of the theoretical product reaction

A dicarboxylic acid in aqueous solution is composed of 4 different species which are undissociated acid dissolved in water (aq), due to a limited solubility (see Figure 3.1) there is

solid undissociated acid (s) present and the dissolved undissociated acid dissociates at increasing pH into its mono (-1) and di (-2) anion.
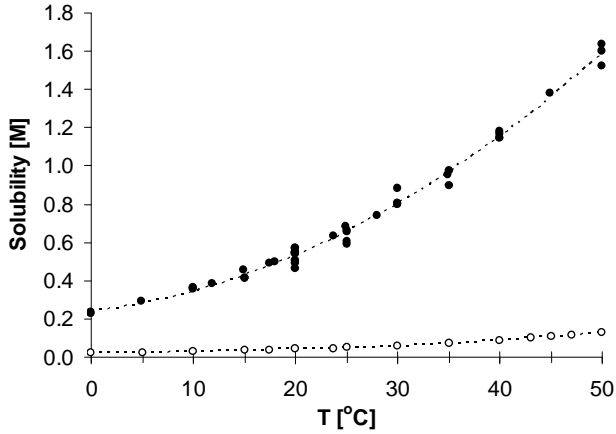
Figure 3.1: Solubility of undissociated fumaric acid (open symbols) and succinic acid (closed symbols) (Yalkowsky and He 2003) as function of temperature.

Considering the four product species, and using succinic acid as an example, we can write the product reaction as (note that consumed compounds have negative coefficients and that CO_2 is assumed to be in equilibrium with the gas phase):

$$a\ C_6H_{12}O_6(aq) + b\ CO_2(g) + c\ C_4H_6O_4\ (s) + d\ C_4H_6O_4(aq) + e\ C_4H_5O_4^{-1}(aq) \tag{3.2}$$

$$+ f\ C_4H_4O_4^{2-}(aq) + g\ H_2O + h\ H^+$$
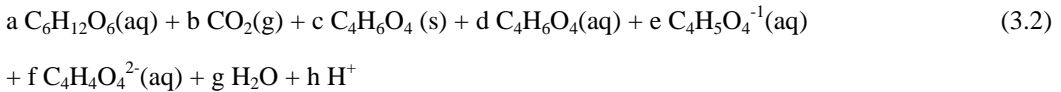
The 8 coefficients (a to h) can be calculated as follows, where we distinguish two regimes.

Dissolved acid regime

In this regime there is absence of solid product, hence $c = 0$ in equation (3.2). 7 stoichiometric coefficients remain to be calculated. The required 7 equations are:

- 4 conservation (C, H, O, charge) equations:

$$6a + b + 4(d+e+f) = 0 \tag{3.3a}$$

$$12a + 6d + 5e + 4f + 2g + h = 0 \tag{3.3b}$$

$$6a + 2b + 4(d+e+f) + g = 0 \tag{3.3c}$$

$$-e - 2f + h = 0 \tag{3.3d}$$

- The product sum relation:

We assume that the sum of all acid species equals 1 mol (knowing c = 0).

$$d + e + f = 1 \qquad (3.3e)$$

- Two dissociation equilibrium relations:

The dicarboxylic acids have two dissociation equilibria with dissociation equilibrium constants of pK_1 and pK_2.

$$H_2A \leftrightarrow HA^- + H^+$$

$$HA \leftrightarrow A^{2-} + H^+$$

This gives the following two relations when we consider a situation where the stoichiometric coefficients of the succinic species become identical to their concentrations (which require that the sum of all organic acid is equal to 1 mol/l):

$$\frac{e}{d} = 10^{pH-pK_1} \qquad (3.3f)$$

$$\frac{f}{e} = 10^{pH-pK_2} \qquad (3.3g)$$

Table 3.1 shows the pK values for succinic and fumaric acid at an assumed temperature of 25 °C.

Table 3.1: pK_1 and pK_2 values for fumaric and succinic acid dissociation at 25 °C (Alberty 2003)

Compound	pK_1	pK_2
Fumaric acid	3.09	4.60
Succinic acid	4.21	5.64

The above 7 relations (3.3a to 3.3g) can be used to obtain the 7 coefficients a, b, d, e, f, g, h as function of pH. h represents the molar amount of H^+ produced per mol of total dicarboxylic acid, which equals 2 at higher pH. d, e, f represent the amount of the three organic acid species. If we assume that the fermentation process needs (for economic DSP) a total product concentration of e.g. 1 mol/l, then d, e and f represent the concentrations of the three acid species (dissolved undissociated, mono- and di-dissociated). b represents the consumed CO_2 and a is the consumed glucose. Assuming glucose-limited continuous fermentation, where the residual glucose concentration can be neglected, the coefficient a represents then the concentration of glucose in the feed solution (assuming equal in and out flow rates).

Solving the 7 equations shows that coefficients a and b are independent of pH. b follows from the C-balance and a follows from the balance of degree of reduction as shown in Eq. (3.1), a = $(Y_{SP}^{theor})^{-1}$. The theoretical minimal glucose consumption per mol acid is a = 1/1.71 = 0.58 mol glucose (succinic acid) and a = 1/2.00 = 0.50 mol glucose (fumaric acid).

Interestingly, there is also pH independent CO_2-consumption, b = 0.50 and 1.00 mol CO_2 per mol succinic and fumaric acid, respectively.

d, e, f and h depend on pH. At high pH the amount of produced H^+ (h) = 2.0, because the only acid species is the -2 acid (f = 1). At decreasing pH the stoichiometric coefficient h (-2 species) decreases monotonously, f (-1 species) increases and then decreases, and d (undissociated acid) increases monotonously (see Figure 3.2).

Solid acid regime

Below a certain pH the concentration of undissociated acid will rise beyond its solubility (Figure 3.1). At 25 °C for succinic acid this solubility limit of 0.64 mol/l is reached at pH = 3.95, for fumaric acid the solubility limit (0.047 mol/l) is reached at pH = 4.11.

Below these pH values, we enter another regime, where solid acid is present. In this regime the stoichiometric coefficient c ≠ 0 but the dissolved undissociated acid (d) remains constant at its solubility limit, hence now d = 0.64 and 0.047 for succinic and fumaric acid, respectively. The above 7 equations can then be solved again to obtain the other coefficients which apply to the low pH range (see Figure 3.2). Figure 3.2 shows that at a low pH of about 3 most (90 %) of fumaric acid is present as solid, making DSP very attractive. At low pH most succinic acid is present as dissolved acid.

3.2.3. Alkali consumption, osmotic stress and ionic strength

The theoretical product reaction stoichiometry (Figure 3.2) shows that at different pH there is a different amount of H^+ produced meaning that different amounts of alkali needs to be added. Usually NaOH or $CaCO_3$ is used, and the cost of alkali (in fermentation) and acid (in DSP) is considerable and is calculated at about € 0.30/kg acid (Appendix 3.4.1). The addition of alkali to the bioreactor for pH control leads then to accumulation of Na^+ at higher pH, which causes a steep increase in osmotic and ionic strength. Figure 3.3 shows the results. It appears that increase of pH from 1 to 8 leads to steep increase in osmotic stress with maximum (at pH ~ 6) osmotic strength equalling 3 mol/l. Also the ionic strength increases and given 1 M of total dicarboxylic acid, the maximal ionic strength equals also 3. Interestingly at low pH (~ 3) the ionic strength becomes close to zero for both acids but the osmotic strength is different, being low (~ 0) for fumaric acid (low solubility) and much higher (~ 0.6 M) for succinic acid.

Clearly, a low pH is not only economically advantageous due to absence of alkali need in fermentation and acid need in DSP, but the cells are also exposed to much lower ionic/osmotic stress. Especially for the low soluble fumaric acid, the osmotic/ionic stress at low pH is marginal.
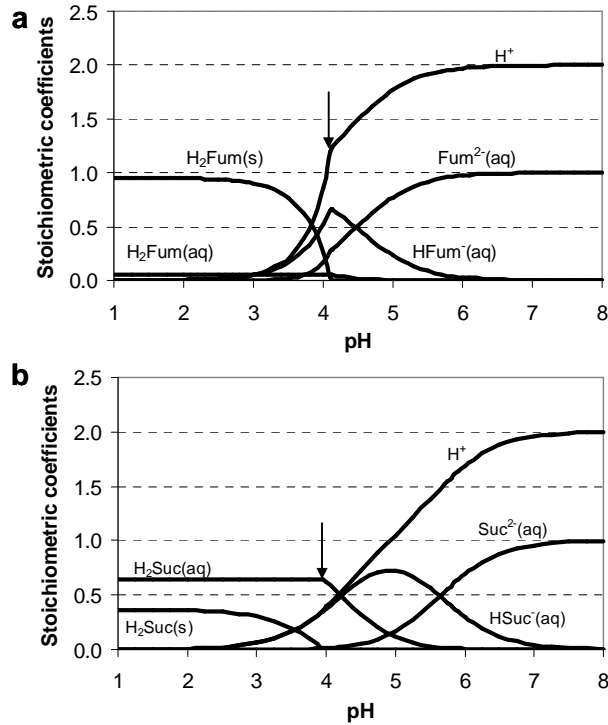
Figure 3.2: Stoichiometry of organic acid species and H$^+$ in the theoretical product reaction for 1 mol total organic acid as function of pH at 25 ^{o}C (a) fumaric acid, (b) succinic acid. The arrows indicate the solubility limit.

3.2.4. Thermodynamics of product formation

Having elaborated the theoretical product reaction stoichiometry as function of pH (Figure 3.2), it is easy to calculate ΔG_r. Here the standard ΔG_f° values were used (25 $^\circ$, see Appendix 3.4.2). In addition, we assumed that the residual glucose concentration is 1 mM and that the CO_2 is supplied as gas at 1 bar pressure (standard condition).

ΔG_r depends also on temperature and ionic strength. Our calculation shows that the effects are minor (only a few kJ difference, results not shown), which agrees with the conclusion of Maskow and von Stockar (2005).

Using the results of Figure 3.2, the value of ΔG_r follows (Figure 3.4), which shows three main results:

1. For both dicarboxylic acids ΔG_r (kJ/mol acid) is very negative. Therefore the theoretical, anaerobic product reaction could allow production of biochemical useful energy (ATP, pmf).
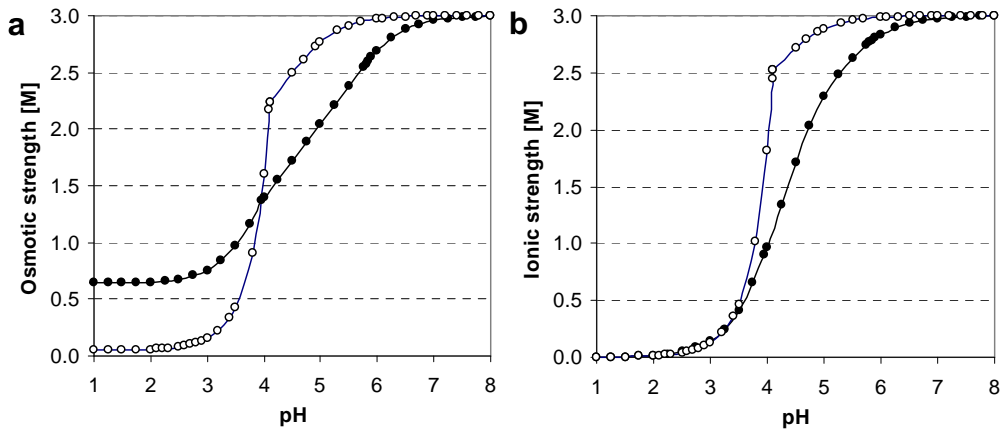
Figure 3.3: Osmotic (a) and ionic (b) strength of broth as function of pH for succinic acid (closed symbols) and fumaric acid (open symbols).

2. ΔG_r becomes less negative with decreasing pH until about pH ~ 4. Below pH ~ 4 most of acid is in the undissociated form and the pH effect disappears. Clearly a low pH leads to less energy production potential. The economic advantage for fermentation and DSP at low pH obviously is at the expense of the energy production potential for the organism.

3. ΔG_r for fumarate is, in the whole pH trajectory, significantly less negative than for succinate. This shows that much easier DSP of fumaric acid (solid product) is at the expense of the energy production potential for the organism.

These results shows a general trade-off behaviour with respect to the total available Gibbs energy, between the Gibbs energy available for the organism, the Gibbs energy consequences of low pH (in the fermentation and DSP) and presence/absence of solid product (DSP); there is no such thing as a free lunch, somebody has to pay!

3.2.5. Thermodynamics of dicarboxylic acid transport

Thermodynamically feasible transport mechanisms

In the previous paragraph, it has been shown for succinic and fumaric acid, also at low pH (~ 3), that the theoretical anaerobic product reaction is thermodynamically very feasible from an overall (black box) point of view.

This means that in principle the proposed theoretical product reaction under anaerobic conditions could function as sole source of biological energy (ATP, pmf) for the producing organism. The amount of biological useful energy harvested from the available Gibbs energy (ΔG_r) however depends on the metabolic pathways employed. These pathways can be very diverse, but they all have in common that the produced acid (anions and H^+) must be exported. Therefore, part of the
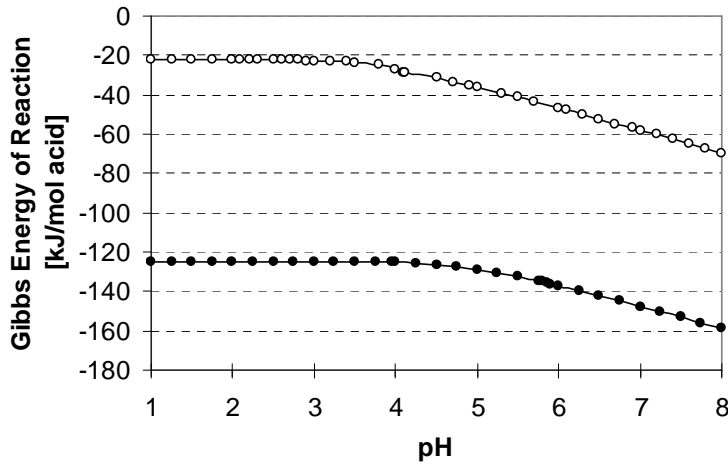
Figure 3.4: ΔG_r [kJ/mol acid] of succinic acid (closed symbols) and fumaric acid (open symbols) as function of pH.

ATP or pmf produced in the network is needed for acid export, diminishing the ATP available for growth and/or maintenance. This export is common to all acids and therefore it is useful to consider this separately from metabolic pathway considerations. Metabolism occurs inside the cells where pH is considered to be constant at around $pH_i = 7$. This shows (Figure 3.2) that the pathway produces the -2 charged dicarboxylate anion and 2 H^+. Anion and H^+ need to be exported from the cytosol by transport mechanisms. To enable proper transport thermodynamic calculations, we first need to define the intracellular and extracellular conditions.

- The extracellular conditions cover a range of outside pH_o between 1 and 8. For succinic acid (Figure 3.2a), the total dissolved organic acid concentration decreases from 1 mol/l at high pH_o to about 0.64 mol/l at low pH_o due to the presence of solid acid. For fumaric acid (Figure 3.2b) the total dissolved organic acid concentration decreases from 1 mol/l at high pH_o to only 0.047 mol/l at low pH_o due to the low solubility of the undissociated fumaric acid (Figure 3.1).

- The intracellular conditions are characterized by a neutral intracellular pH_i (= 7). In addition, the intracellular concentration of dicarboxylic acid is needed. Recent measurements in *Escherichia coli* (Taymaz-Nikerel *et al.* 2009) or *Saccharomyces cerevisiae* (Canelas *et al.* 2009) show concentrations of order 1×10^{-3} M.

- A most important aspect for transport of charged molecular species is that the intracellular space has an electrical potential, ψ. Its value depends on the extracellular pH_o in such a way that the so-called proton motive force (pmf) remains constant (homeostasis) when the extracellular pH changes. This pmf homeostasis concept leads to the following relation between ψ (in Volt) and extracellular pH_o

$$\psi = -pmf - \frac{2.303RT}{F}(pH_o - pH_i). \tag{3.4}$$

In this relation R and F are the gas constant (8.314×10^{-3} kJ/molK) and Faradays constant (96.5 kJ/Volt e-mol), leading for T = 298 K to a value of $2.303RT/F = 0.059$ V. A typical value for the proton motive force is, pmf = 0.15 V.

Equation 3.4 shows that the electrical potential inside is negative ($\psi = -0.15$ V) when $pH_o = pH_i$, whereas at lower outside pH (e.g. $pH_o = 3$), the potential becomes positive ($\psi = +0.084$ V).

The above defined situation around the membrane shows that we need a mechanism, which can transport the dicarboxylic acid from a low (0.001 M) total acid concentration inside to a much higher outside dissolved total acid concentration of 0.047 M (fumarate) and 0.64 M (succinate). This usually requires active transport where H^+ transport is coupled to the acid export of one of the three acid-species (undissociated, A^- or A^{2-}). At $pH_i = 7$ and an intracellular total dicarboxylic acid concentration of 1×10^{-3} M, one can calculate from the dissociation equilibria that the concentration of undissociated acid is 6.78×10^{-8} M (succinic) and 4.90×10^{-10} M (fumaric acid), while the concentration of monodissociated acid equals 4.18×10^{-5} M and 1.23×10^{-7} M, respectively. Clearly nearly all intracellular acid is present as the dicarboxylate, while the other species are in general present at less than μM level. Therefore we assume that the anion (-2) species is exported, together with export of n H^+/mol A^{2-}. The anion export process can now be written as:

$$A_{in}^{2-} + n\,H_{in}^+ \ \rightarrow\ A_{out}^{2-} + n\,H_{out}^+ \qquad (3.5)$$

This transport process shows that the transport protein exports the (-2) anion (A^{2-}) together with n protons. n has different values for the different possible transport mechanisms. For uniport n = 0, for symport and double symport n = 1 and 2, for antiport and double antiport n = -1 and -2.

Using standard thermodynamics, and recognizing that there is an intracellular electric potential ψ, leads to ΔG_r for the transport process defined in Eq. (3.5) as

$$\Delta G_r = 2.303\,RT \log\,(A_o^{2-}/A_i^{2-}) - 2.303\,n\,RT\,(pH_o - pH_i) - (n-2)\,F\psi. \qquad (3.6)$$

We have already seen that the electrical potential ψ depends on the extracellular pH_o (Eq. 3.4) and the pmf. Elimination of ψ leads to the achievable equilibrium out/in ratio of anions (A_o^{2-}/A_i^{2-}) as ($\Delta G_r = 0$):

$$\log(A_o^{2-}/A_i^{2-})^{eq} = 2(pH_o - pH_i) + \frac{(n-2)(-pmf)F}{2.303RT} \,. \qquad (3.7)$$

In this equation pmf is the proton motive force in Volts which is considered to have a typical value of + 0.15 V and $2.303RT/F = 0.059$ V at 25 °C. Equation (3.7) gives the equilibrium out/in ratio of the (-2) anion. In practice, one measures the total acid ratio. The equilibrium relation between the (-2) anion acid ratio (Eq. 3.7) and the total acid ratio $(A_o/A_i)^{eq}$ follows from the dissociation relations (see also e.g. Eq. 3.3f and Eq. 3.3g) as

$$\left(\frac{A_o}{A_i}\right)^{eq} = \left(\frac{10^{pK_1+pK_2-2pH_o}+10^{pK_2-pH_o}+1}{10^{pK_1+pK_2-2pH_i}+10^{pK_2-pH_i}+1}\right)\left(\frac{A_o^{2-}}{A_i^{2-}}\right)^{eq}. \tag{3.8}$$

Elimination of the (-2) anion acid ratio from Eq. (3.7) and Eq. (3.8) gives the equilibrium out/in ratio of total acid A_o/A_i. The equilibrium total acid ratio, assuming a constant pH_i and a constant pmf, then only depends on pH_o, the $pK_{1,2}$ values of the acid and the number of protons (n) involved in the transporter mechanism (n = 1, 2 for symport of 1 or 2 protons, n = 0 for uniport, n = -1, -2 for antiport of 1 or 2 protons).

Figure 3.5 shows that the achievable A_o/A_i equilibrium ratio drops steeply with decreasing pH_o until pH 3 and increases steeply with decreasing n (from symport (n = 1) to uniport (n = 0) to antiport (n = -1)). Using Figure 3.5 we can select, for each acid, the thermodynamic feasible transport mechanism (number of protons involved), which yields the required A_o/A_i ratio at two relevant pH values (7 and 3). For *succinic acid* (Figure 3.5a) the total acid concentration outside decreases from 1 M (pH = 7) to 0.64 M (pH = 3). Assuming 1 mM as inside concentration leads to a required ratio A_o/A_i as function of pH as indicated (horizontal dashed lines) in Figure 3.5. To achieve sufficient driving force it is required that the transport mechanism should allow an A_o/A_i equilibrium ratio above the dashed line. At pH = 3, Figure 3.5a shows that this requires a mechanism where 1 H^+ is antiported (n = -1), and at pH = 7 symport (n = 1) is suitable. For *fumaric acid* (Figure 3.5b) the total dissolved acid decreases strongly with decreasing pH, due the low solubility of the undissociated acid. At pH = 7 all acid is dissolved and A_o/A_i = 1000 is required, leading to symport (n = 1) as thermodynamically feasible mechanism. At pH = 3 the required total acid ratio is about A_o/A_i = 100, showing that antiport of 1 H^+, assuming A_i=3 x 10^{-3} M, is sufficient. We can conclude with respect to thermodynamically feasible transport mechanisms that for both acids at pH = 7 a symport (n = 1) mechanism and at pH = 3 a 1 H^+ antiport (n = -1) mechanism is required to achieve sufficient driving force for export of the organic acid.

Metabolic energy required for dicarboxylic acid export

Previously the thermodynamically feasible mechanisms for export of the dicarboxylic anion (A^{2-}) are considered. However, also the produced 2 H^+ must be exported. At pH = 7 symport is a feasible mechanism and the anion export takes care of export of 1 H^+, leaving 1 H^+ to be exported otherwise. At pH = 3 an antiport mechanism of 1 H^+ is needed for the anion export, leading to 3 H^+ per anion which needs to be exported otherwise. H^+ export (which occurs against the proton motive force) requires a source of metabolic energy. Under the here-considered anaerobic conditions, ATP is this source. It is now relevant to distinguish pro- and eukaryotes. In *prokaryotes* H^+ is exported by a cell membrane bound H^+-ATPase at the expense of ATP. The stoichiometry (H^+ expelled per mol ATP consumed) is not completely certain but can be set conservatively at 3 (see Appendix 3.4.3). This leads then at pH = 7 to 1/3 mol ATP cost and at pH = 3 to 1 mol ATP cost for export of 1 mol organic acid.

In *eukaryotes*, such as yeast or fungi which are considered as excellent production platforms at low pH, H^+ is expelled by a H^+ exporter which requires 1 ATP per H^+ (Burgstaller 1997; Serrano 1991). This leads in eukaryotes at pH = 7 to 1 mol ATP cost and at pH = 3 to 3 mol ATP cost per mol of exported organic acid.

In summary the export of dicarboxylic acid, using thermodynamically feasible transport mechanisms, requires the net export of 1 H^+ (pH = 7) and 3 H^+ (pH = 3) per mol acid. For prokaryotes (e.g. *E. coli*) this translates per mol organic acid at pH = 7 and 3 into a consumption of 1/3 and 1 mol ATP, for eukaryotes (*S. cerevisiae*) into 1 and 3 mol ATP. The massive ATP-consumption for acid export in eukaryotes is completely due to the energetically very wasteful H^+-ATPase for H^+ transport over the cell membrane (1 ATP only expels 1 H^+ compared to 3 H^+ in prokaryotes).

This clearly provides a genetic engineering target in eukaryotes (introduce a cell membrane H^+-ATPase for H^+ export with H^+/ATP stoichiometry of 3 instead of 1).

3.2.6. Converting Gibbs energy of the theoretical product reaction into ATP for growth

The previous thermodynamic analysis of the theoretical product reaction (Figure 3.4) shows that for both acids at pH = 7 as well as at pH = 3, there is a large Gibbs energy release (58 (pH = 7) to 23 kJ (pH = 3) per mol fumaric and 148 (pH = 7) to 125 kJ (pH = 3) per mol succinic acid). Only a part of this potentially available energy is converted into biological useful energy (ATP) depending on the metabolic network used for acid production. The biological energy (ATP) is needed for acid export, cell maintenance and growth. A key issue is to analyze whether the product pathway, with the theoretical maximal product yield, after taking the ATP need for product export into account, provides a surplus of ATP to allow growth, because then an anaerobic process with only acid (fumaric or succinic) production, leading to the highest theoretical yield, can be performed. Even more important then evolutionary approaches can be used to improve the rate of product formation of engineered strains with this pathway because faster production leads to faster growth due to ATP-based coupling between product formation and growth (Kuyper *et al.* 2004; Wisselink *et al.* 2009).

Fumaric acid

Figure 3.6a shows *for pH = 7* the network which anaerobically converts glucose to fumaric acid. We will discuss first the energetically most favourable anaerobic network which uses malic enzyme to reductively carboxylate pyruvate to malate without ATP consumption (the other energetically more expensive possibility is carboxylation of Pyr or PEP to Oaa, which requires 1 ATP per mol C_4-acid). The pathway is redox neutral because the glycolytic NADH is consumed by the NADH coupled malic enzyme. The fumarate anion export (1 H^+ symport) requires the additional export of $2 - 1 = 1$ H^+/fumarate which is performed by a prokaryotic H^+-ATPase
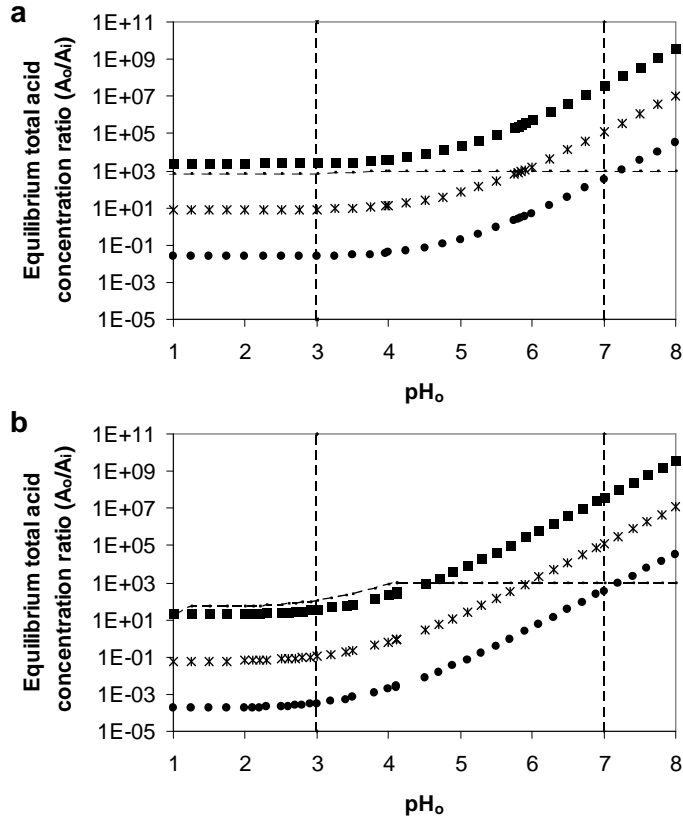
Figure 3.5: Out/in equilibrium total acid concentration ratio (A_o/A_i) as function of pH_o, for antiport n=-1 (squares), uniport n=0 (stars) and symport n=1 (circles). (a) Succinic acid, (b) Fumaric acid. Horizontal dashed line is the minimal required ratio ($A_i = 10^{-3}$ M).

(stoichiometry of 3 H^+/ATP, see Appendix 3.4.3), demanding 1/3 ATP per mol acid. The net ATP production is then 2/3 ATP per mol produced fumaric acid, as indicated in the overall reaction (Figure 3.6a). This amount is available for growth and maintenance and is equivalent to 2/3 x 45 = 30 kJ of biological energy, which is about 50 % of the potentially available energy (~ 58 kJ, Figure 3.4 at pH = 7). The difference, 30 kJ per mol produced acid, is needed to provide thermodynamic driving force for each of the 13 reactions in the network.

Figure 3.6b shows *for pH = 3* the network, which is only different from Figure 3.6a in the exporter used, which is now a 1 H^+ antiporter. This results in a required export of 3 H^+ per mol acid, which consumes 1 ATP by the prokaryotic cell membrane H^+-ATPase. The end result is that the pathway produces 0 ATP, showing that the 23 kJ theoretical available Gibbs energy (Figure 3.4) does not allow any ATP synthesis. We could conclude that in the fumarate product network 20 - 30 kJ/mol product is needed to assure thermodynamic driving force for the 13 reactions. The ATP analysis shows that at pH = 7 one can perform an anaerobic fumaric acid process with 2 mol fumaric acid/mol glucose as catabolic reaction with 2/3 ATP yield. At pH = 3 this is not possible.

The above anaerobic network at pH = 3 (Figure 3.6b) uses rather optimistic choices such as the use of malic enzyme and a H^+/ATPase stoichiometry of 3. More realistic choices at this low pH are:

- a eukaryotic H^+/ATPase with H^+/ATP = 1, because at pH = 3 eukaryotes (yeast, fungi) are known to be much more acid tolerant than prokaryotes
- use of an ATP-consuming reaction for the carboxylation of C_3 (Pyr or PEP) to C_4 (oxaloacetic acid), e.g. pyruvate carboxylase.

This (Figure 3.6c) then leads at pH = 3 to a *consumption* of 3 ATP per mol secreted fumaric acid which then raises the question of how to generate the required ATP at pH = 3.

Under *anaerobic* conditions, ATP production requires the production of other organic acids or ethanol which is economically highly undesirable because the fumaric acid yield decreases steeply and one obtains a product mixture (acids, alcohols), which poses extra costs in DSP. The *aerobic* production of ATP is far more favourable because there are no additional products (except CO_2 and H_2O) and the extra consumption of glucose to produce ATP is about 5 - 10 times less than under anaerobic conditions.

The aerobic fumarate production (Figure 3.7) requires an excess production of NADH, which is converted to ATP in the electron transport chain (ETC). Therefore, in addition to the reductive

-1gluc -2CO₂ + 2(Fum²⁻)ₒᵤₜ + 2H₂O + 4(H⁺)ₒᵤₜ +4/3ATP   -1gluc -2CO₂ + 2(Fum²⁻)ₒᵤₜ + 2H₂O + 4(H⁺)ₒᵤₜ +0ATP   -1gluc -2CO₂ -6ATP + 2(Fum²⁻)ₒᵤₜ + 2H₂O + 4(H⁺)ₒᵤₜ
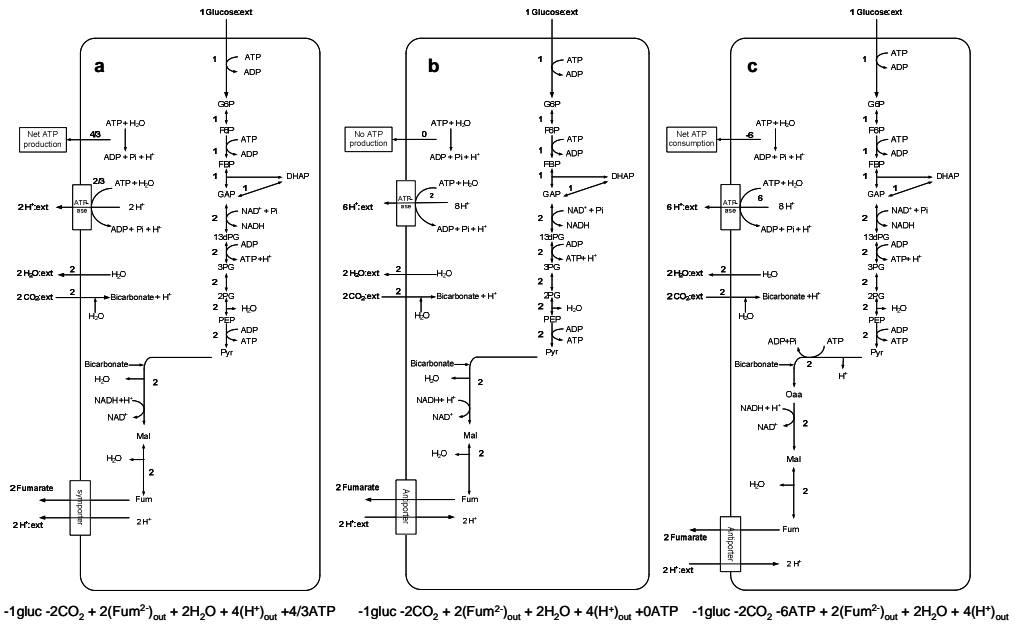
Figure 3.6: ATP-analysis for the anaerobic fumarate network. (a) pH = 7, symport for acid export, malic enzyme, H^+/ATP = 3 (prokaryotic), (b) pH = 3, antiport for acid export, malic enzyme, H^+/ATP = 3 (prokaryotic), (c) pH = 3, antiport for acid export, pyruvate carboxylase, H^+/ATP = 1 (eukaryotic).

(NADH consuming) fumarate pathway (Figure 3.6) one needs an oxidative (NADH producing) fumarate pathway. This oxidative pathway to fumarate involves the conversion of pyruvate to Acetyl-CoA followed by the glyxolate pathway over succinate to fumarate.

Figure 3.7 shows the aerobic fumarate network at pH 3 which consists of a reductive branch, the oxidative glyoxylate branch, and the electron transport chain to convert $NADH/FADH_2$ from the oxidative branch and the extracellular electron acceptor O_2 to produce the required ATP by oxidative phosphorylation. Furthermore (pH = 3) fumarate is exported by H^+ antiport and the cytosolic H^+ is exported using a eukaryotic H^+-ATPase with $H^+/ATP = 1$.

The produced NADH and $FADH_2$ are consumed by the ETC, where for the eukaryotic organism (yeast) it is assumed that 1 NADH gives 1.25 ATP and 1 $FADH_2$ gives 0.75 ATP (van Gulik and Heijnen 1995).

The aerobic fumarate network (combined reductive/oxidative path) with balanced ATP then shows the following stoichiometry:

$$-2 \text{ glucose} - 3 \text{ O}_2 + 3 \text{ (Fum}^{2-})_{out} + 6 \text{ H}_2\text{O} + 6 \text{ (H}^+)_{out} \tag{3.9}$$
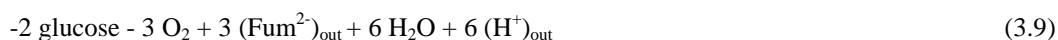
leading to a theoretical stoichiometry of 1.5 mol fumarate/mol glucose. This network requires that α-ketoglutarate dehydrogenase is knocked out from the TCA cycle.

Succinic acid

The black box thermodynamic result of succinic acid (Figure 3.4) shows that the available Gibbs energy is much more than for fumaric acid.

The anaerobic metabolic network for succinic acid consists of a combination of a reductive route (which requires a net input of NADH for the reduction of fumarate to succinate) and the oxidative route which converts pyruvate to succinate and NADH using the glyoxylate route (Clark 1989).

NADH-balancing of oxidative and reductive route, leads then to the previous theoretical black box reaction, with a yield of 24/14 mol succinic acid per mol glucose. The key question is now about ATP aspects of succinate production, which has surprisingly received little attention.

For the reductive path one usually makes traditional choices such as ATP needed for carboxylation of pyruvate to oxaloacetate and a cytosolic dehydrogenase which reduces fumarate to succinate. This gives as overall *reductive reaction*:

$$-1 \text{ glucose} - 2 \text{ NADH} - 2 \text{ CO}_2 + 2 \text{ (Suc}^{2-})_{in} + 4 \text{ (H}^+)_{in}$$

For the *oxidative (glyoxylate) path* it follows

$$-1 \text{ glucose} + 1\text{(Suc}^{2-})_{in} + (2\text{H}^+)_{in} + 2 \text{ ATP} + 5 \text{ NADH} + 2 \text{ CO}_2$$
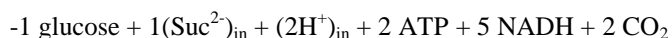
Multiplication of these reactions with 5 respectively 2 gives as overall reaction the black box reaction, but now also the ATP stoichiometry is obtained for production of 12 succinic acid:

$$-2gluc -3O_2 + 3(Fum^{2-})_{out} + 6H_2O + 6(H^+)_{out} + 0ATP$$
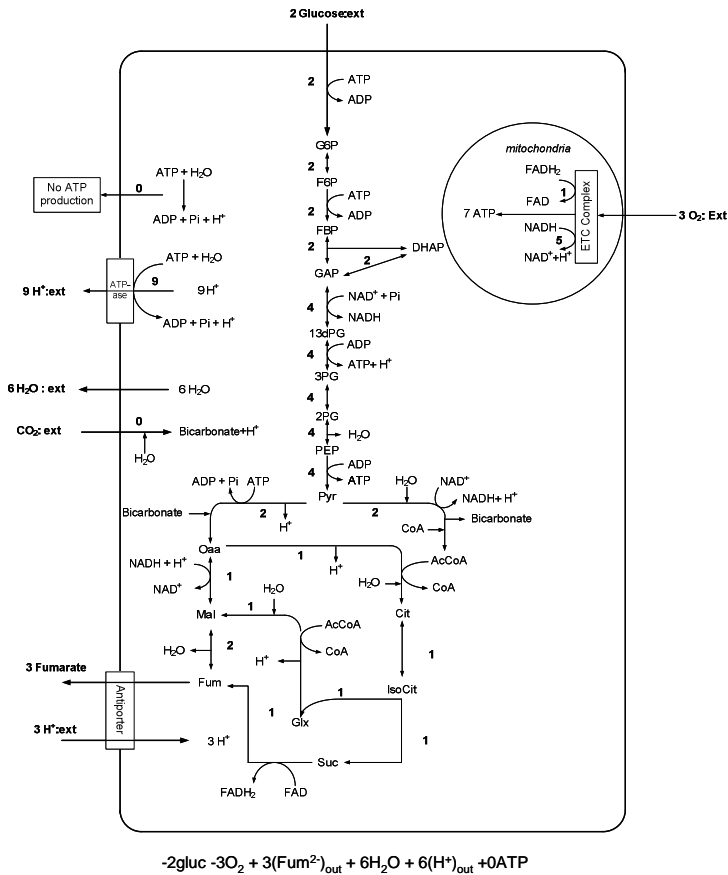
Figure 3.7: Network and stoichiometry for aerobic fumarate production at pH = 3. Aerobic combined reductive and oxidative (glyoxylate path) fumarate pathway with ETC (NADH gives 1.25 ATP, 1 FADH$_2$ gives 0.75 ATP), eukaryotic H$^+$-ATPase (H$^+$/ATP=1) and ATP requiring carboxylation of pyruvate. There is no growth and no net ATP production.

-7 glucose – 6 CO$_2$ + 12 (Suc^{2-})$_{in}$ + 24 (H$^+$)$_{in}$ + 4 ATP
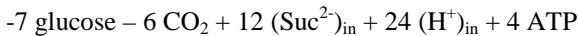
However for a full ATP-balance we need to take energy for acid export into account.

At pH = 7, 1 H$^+$-symport represents a thermodynamically feasible export mechanism, leaving 12 H$^+$ to be exported by H$^+$-ATPase. Assuming a prokaryotic ATPase, which exports 3 H$^+$ at the cost of 1 ATP requires 12/3 = 4 ATP for export of H$^+$, leading to 0 ATP per mol secreted succinic acid. Hence anaerobic succinate production at pH 7 using this traditional network *does not provide ATP*. This means that ATP must be produced using traditional pathways (leading to ethanol, acetate secretion). Indeed all published prokaryotic succinate producing systems at pH = 7 show production of these by-products (Hong and Lee 2001; Jantama *et al.* 2008; Millard *et al.* 1996; Sanchez *et al.* 2005a; Sanchez *et al.* 2005b; Stols and Donnelly 1997; Vemuri *et al.* 2002a; Vemuri *et al.* 2002b; Wang *et al.* 2006; Wu *et al.* 2007). This, according to our analysis, is completely due to a need to generate ATP for maintenance and growth.

At pH = 3 the H^+-antiport transport mechanism leads to 36 mol H^+ which need to be exported. At low pH it is generally accepted that eukaryotes are more acid-tolerant than prokaryotes and it is therefore useful to assume the presence of a eukaryotic H^+-ATPase (H^+/ATP = 1), which leads to the consumption of 36 mol ATP to export 12 succinate, leading to an overall need of 36 - 4 = 32 mol ATP for 12 succinic acid.

We observe now a tremendous discrepancy between the potentially available (Figure 3.4) Gibbs energy (which would maximally allow production of about 2 ATP (pH = 3) or 3 ATP (pH = 7) per mol secreted succinate) and the net ATP balance of the conventional network (0 ATP at pH = 7 and at pH = 3 a consumption of 32/12 mol ATP per succinic acid).

This indicates that there occur major losses of Gibbs energy in the network. Global inspection of reaction thermodynamics points at 3 reactions, which are the eukaryotic H^+-ATP-ase, the ATP requiring carboxylation of pyruvate and the fumarate reduction to succinate (Appendix 3.4.3).

Figure 3.8a and 3.8b shows (for pH = 3 and 7) alternative networks where the cytosolic fumarate reduction with NADH is replaced by a membrane bound menaquinone-based electron transport chain which exports H^+ using the large Gibbs energy release of the fumarate reduction reaction.

Appendix 3.4.3 shows that we can expect an export of 3 H^+ per fumarate which is reduced. This proton export partly replaces the use of the highly unfavourable eukaryotic H^+-ATPase for H^+ export and is therefore of crucial importance. In addition it is assumed that the excess exported H^+ is imported by a reversible H^+ consuming ATPase (with prokaryotic 3 H^+/ATP) to make ATP.

It is clear that with this modification succinate production is possible with ATP-production under anaerobic conditions at pH = 3 and pH = 7 with 2/12 (pH = 3) and 10/12 (pH = 7) mol ATP/mol secreted acid. These networks then conserve per mol succinic acid an amount of 2/12 x 45 = 8 kJ (pH = 3) to 10/12 x 45 = 38 kJ in ATP (pH = 7), which is only about 6 - 25 % of the available energy (Figure 3.4). Of course the ATP yield will increase when the ATP-requiring carboxylation (pyruvate carboxylase) is replaced by e.g. malic enzyme. This will increase the produced ATP per succinate to 12/12 (pH = 3) and to 20/12 (pH = 7), increasing the Gibbs energy efficiency to about 36 - 51 %. The Gibbs energy loss in this much more complex network of 20 reactions is then around 75 kJ/mol succinate.

3.2.7. Acid back diffusion at low pH

A final energy aspect at low pH is that the secreted undissociated organic acid diffuses back at a rate determined by the extracellular concentration of the undissociated acid. For fumaric acid at low pH this fumaric acid concentration is constant (solubility limit) and therefore this back diffusion flux is constant (= 20.0 mmol acid/CmolX/h measured, (Jamalzadeh *et al.* 2010)). Assuming q_F^{bd} = 20 mmol/CmolX/h, Figure 3.9a shows the relation between fumarate specific productivity q_F and the glucose and O_2 consumption per mol fumarate using the network of Figure 3.7, but now extended with acid back diffusion (see Appendix 3.4.4 for detailed calculations). Obviously this back diffused acid must be exported again at high energy cost,
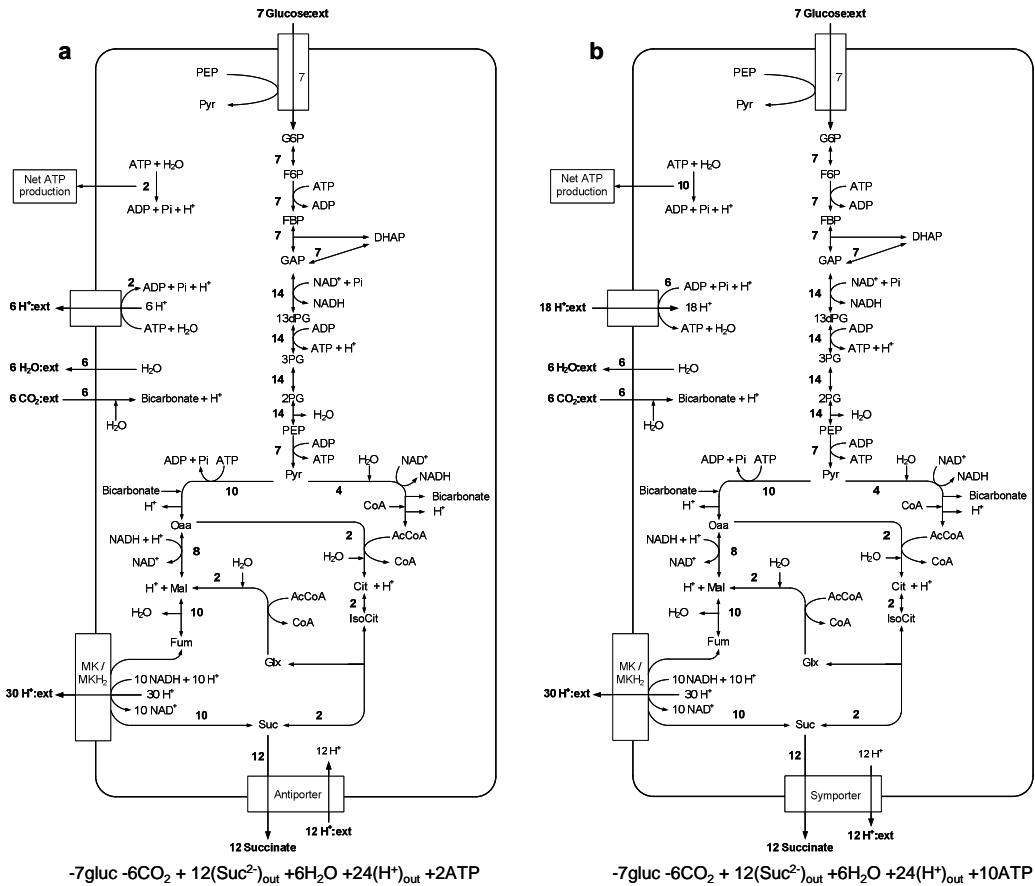
Figure 3.8: Succinic acid production network using a membrane bound, H$^+$ translocating, menaquinone-mediated fumarate reduction to succinate and ATP-generation from pmf (prokaryotic 3H$^+$ uptake per ATP) at (a) pH = 3 (using H$^+$ antiport for A^{2-} export), (b) pH = 7 (using H$^+$ symport for A^{2-} export).

increasing the glucose and O_2 consumed per mol fumarate at lower q_F. For $q_F \geq 80$ mmol fumaric acid/CmolX/h the O_2 and glucose stoichiometry approaches the theoretical limit.

Also undissociated succinic acid can diffuse back, leading to extra ATP need to export this acid (see Appendix 3.4.4). Now, in contrast to fumaric acid, this leads to increase in succinic acid yield on glucose because less ATP can be consumed by growth. Figure 3.9b shows that at decreasing q_{Suc} the glucose consumed per mol succinate decreases, albeit slightly.

3.2.8. Genetic engineering targets

For real networks the harvested ATP-energy must be less then the available Gibbs energy. It is therefore of interest to inspect the Gibbs energy losses which occur per reaction. This approach is
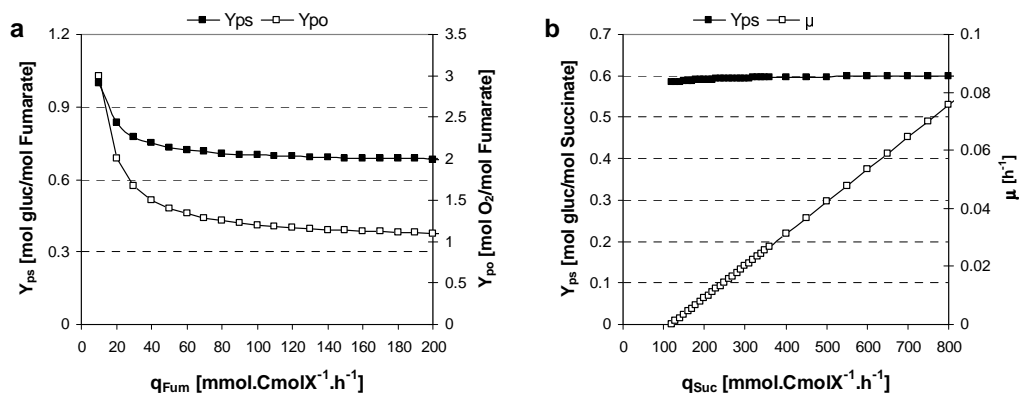
Figure 3.9: (a) Glucose and O₂ required per mol fumarate as function of specific fumarate production rate assuming the aerobic/pH=3 network of Figure 3.7 and fumarate back diffusion rate of 20 mmol/CmolX/h, (b) Growth rate μ [h⁻¹] and required glucose per mol succinate as function of specific succinate production rate assuming anaerobic/pH=3 network of Figure 3.8a and succinate back diffusion rate of 20 mmol/CmolX/h.

highly useful to find genetic engineering targets for more energy conservation.

A clear genetic engineering target in eukaryotes is the introduction of a cell membrane bound H⁺-ATPase with H⁺/ATP stoichiometry of 3 (as in prokaryotes) instead of 1 (as in ABC transporter), for H⁺ export.

For succinic acid an important target is to couple fumarate reduction to proton motive force generation. For both acids replacing pyruvate carboxylase by malic anzyme for anaplerosis will increase the ATP production, thus decrease ATP cost. With all these modifications around 30 - 50 % of the available Gibbs free energy can be converted to ATP.

3.3. Conclusions

The microbial production of dicarboxylic acids, succinic and fumaric, from glucose at low pH at 25 °C was analyzed using a thermodynamic approach. First the black box anaerobic theoretical product reaction was studied with respect to the stoichiometry of the individual species of dicarboxylic acids and Gibbs energy formation of the theoretical reaction was obtained as a function of pH (1 - 8). The results were very promising with very negative ΔG_r (kJ/mol acid) for both dicarboxylic acids. The thermodynamically feasible mechanisms for product export were discussed, including their energy need and candidate metabolic networks were analyzed with respect to conversion of available Gibbs energy into ATP.

Here we show that analysis on energy aspects of both the theoretical product reaction and then the metabolic network, including transport, is vital because it provides the strong and weak points

of the network, in terms of energy conservation and directly suggests genetic engineering targets to further improve the product yield, achieving ultimately anaerobic production.

The energy analysis shows that it seems possible (after implementing the suggested genetic modifications) that succinic acid (at pH 3 and 7) and fumaric acid (at pH 7) can be produced anaerobically as sole catabolic product with net ATP production. At low pH (3) fumaric acid production must be performed aerobically. Finally the consequences for acid back diffusion at low pH (3) are found to be different for both acids.

3.4. Appendix

3.4.1. Acid/alkali cost

The cheapest alkali is $CaCO_3$, which costs about € 270/ton (98 % pure, a high purity is needed to produce high purity acid.) The cheapest acid for down stream processing is sulphuric acid (H_2SO_4), which costs about € 90/ton (98 % pure). This leads for 1 mol H^+ to a cost of 0.0045 € and for 1 mol OH^- to 0.0135 €. The total acid/alkali cost per kg dicarboxylic acid is then € 0.30/kg. In addition there are costs for disposal of the produced $CaSO_4$.

3.4.2. Standard ΔG_f^o values

Table 3.2: Standard Gibbs energy of formation (ΔG_f^o, kJ/mol) of species at 25 ^{o}C and zero ionic strength (Alberty 2003)

Compound	ΔG_f^o
Glucose	-915.90
H_2Fum (s) [a]	-645.68
H_2Fum (aq)	-645.80
$HFum^-$ (aq)	-628.14
Fum^{2-} (aq)	-601.87
H_2Suc (s) [a]	-747.75
H_2Suc (aq)	-746.64
$HSuc^-$ (aq)	-722.62
Suc^{2-} (aq)	-690.44
H_2O	-237.19
H^+	0
CO_2 (g)	-394.36

[a] ΔG_f^o of solid form of fumaric and succinic acids are obtained by the knowledge that solid form is in equilibrium with the aqueous form when the concentration of aqueous form reaches the solubility concentration: $\Delta G_{f,H_2A(s)}^o = \Delta G_{f,H_2A(aq)}^o + RT\ln(c^*_{H_2A(aq)})$, $c^*_{H_2A(aq)}$ is the solubility [M] of fumaric or succinic acid in water at 25 ^{o}C.

3.4.3. *In vivo* energy aspects of ATP, proton motive force and fumarate reductase

ATP

ATP is synthesized according to ADP + P_i →ATP.

The Gibbs energy (kJ/mol ATP) of reaction follows as ($\Delta G_R^o = 30.9$ kJ/mol (Panke and Rumberg 1997))

$$\Delta G_{ATP} = +30.9 + RT \ln\left(\frac{ATP}{ADP\ P_i}\right).$$

The indicated concentrations are given in Table 3.3. This shows that the value of ATP/(ADP P_i) ~ 100, leading to an *in vivo* value (25 °C) of ΔG_{ATP} ~ 45 kJ/mol.

Table 3.3: Concentrations [mM] of nucleotides and P_i in aerobic glucose-limited *S. cerevisiae* and *E. coli*

	S. cerevisiae	*E. coli*
ATP	2.9 ± 0.1[a]	3.36 ± 0.03[c]
ADP	0.71 ± 0.04[a]	1.30 ± 0.01[c]
P_i	43[b]	-

[a] taken from Canelas *et al.* (2009). Concentrations were converted to mM using the factor 2.38 ml cell/gDW (Theobald *et al.* 1997).
[b] taken from Wu *et al.* (2006).
[c] taken from Taymaz-Nikerel *et al.* (2009). Concentrations were converted to mM using the factor 1.77 mlcell/gDW (Chassagnole *et al.* 2002).

Proton motive force (pmf)

A typical pmf value is 0.15 Volt, which translates, using Faradays constant of 96.5 kJ/V e mol, to 0.15 x 96.5 = 14.5 kJ Gibbs energy needed to export 1 mol H^+.

With the above result for ΔG_{ATP} it follows that 3 H^+ can be exported per 1 mol ATP hydrolysis by the reversible H^+-ATPase.

Fumarate reductase in succinate production

Fumarate reductase reduces fumarate to succinate using NADH as electron donor. This reaction is of particular importance because it is a potential rich source of biological energy. This requires that the reduction occurs by a set of membrane coupled proteins which form an electron transport chain where fumarate acts as electron acceptor with NADH as electron donor leading to succinate. This chain expels H^+.
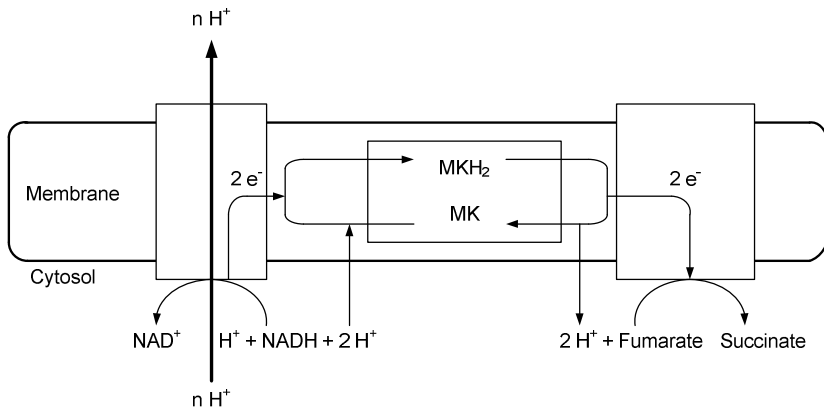
Figure 3.10: The scheme of fumarate respiratory chain (adapted from EcoCyc database (Keseler *et al.* 2009)).

Figure 3.10 shows the proposed mechanism which consists of two reactions:

- The first reaction reduces fumarate to succinate using reduced menaquinone as electron donor. The equilibrium constant follows then from the respective standard redox potentials as $K_{eq} = 6895$ (25°). Measurements of fumarate and succinate show a typical succinate/fumarate concentration ratio of about 0.10 (Taymaz-Nikerel *et al.* 2009), leading to a maximal ratio of $MK/MKH_2 \sim 690$ showing that nearly all menaquinone is oxidized.

- The second reaction regenerates MKH_2 from MK using NADH and expels H^+
$$NADH + MK + mH^+_{in} \rightarrow NAD^+ + MKH_2 + mH^+_{out}$$

We first consider ΔG_R in absence of H^+ expulsion. The ΔG_R^o of this reaction is -47.5 kJ/mol (using $\Delta E_o^1 = -0.32$ V for NADH/NAD$^+$ (Tran *et al.* 1997) and $\Delta E_o^1 = -0.074$ V for MKH$_2$/MK (Leger *et al.* 2001)).

Under *in vivo* conditions NADH/NAD$^+ \sim 0.01$ in *S. cerevisiae* (Canelas *et al.* 2008b) and 0.02 in *E. coli* (Taymaz-Nikerel *et al.* 2009), which gives an average NAD$^+$/NADH ~ 75.
Also (see above) $MK/MKH_2 \sim 690$. This gives for the *in vivo* Gibbs energy of reaction

$$\Delta G_R = -47.5 + RT \ln\left(\frac{75}{690}\right) = -52 \text{ kJ/mol.}$$

This amount of Gibbs energy is available to expel protons. For export of 1 mol H^+, given the pmf value of 0.15 Volts, one needs 14.5 kJ, hence the maximal possible stoichiometry is 3 mol H^+ expulsion per mol NADH (which consumes 3 x 14.5 = 43.5 kJ from the available 52 kJ). The conclusion is that membrane coupled fumarate reductase using NADH can lead to the export of 3 mol H^+.

3.4.4. Effect of acid back diffusion on product yield of dicarboxylic acid

Fumaric acid

Fumaric acid, at pH = 3, shows back diffusion (at a rate of 20 mmol/h/CmolX) which is constant due to the solubility limit (47 mM) of undissociated fumaric acid (Jamalzadeh *et al.* 2010).

At pH 3 the acid is exported by an H^+-antiporter leading to 3 H^+ per mol fumaric acid which need to be exported. Assuming a eukaryotic H^+-ATPase (H^+/ATP = 1 mol/mol), acid back diffusion and its export create a futile cycle, which requires 3 x 20 = 60 mmol ATP/h/CmolX.

The *catabolic reaction* of glucose with O_2 (assuming P/NADH = 1.25 and P/FADH$_2$ = 0.75) leads to 4 (substrate phosphorylation) plus 10 x 1.25 + 2 x 0.75 = 14 (oxidative phosphorylation), leading to 18 mol ATP, hence we can write

-1 gluc - 6 O_2 + 6 CO_2 + 6 H_2O + 18 ATP
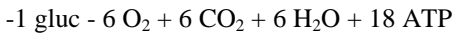
Figure 3.7 shows the stoichiometry of the aerobic *fumaric acid formation reaction*:

-2 glucose - 3 O_2 + 3 $(Fum^{2-})_{out}$ + 6 H_2O + 6 $(H^+)_{out}$
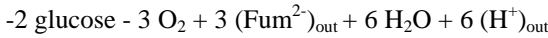
This gives for substrate and O_2 consumption as function of q_F:

$$-q_S = \frac{60}{18} + \frac{2}{3} q_F,$$

$$-q_{O2} = 6x \frac{60}{18} + \frac{3}{3} q_F.$$

The glucose and O_2 consumption per mol fumarate produced then becomes:

$$\frac{\text{mol glucose}}{\text{mol fumarate}} = \frac{60/18 + (2/3)q_F}{q_F},$$

$$\frac{\text{mol } O_2}{\text{mol fumarate}} = \frac{6x \dfrac{60}{18} + (3/3)q_F}{q_F}.$$

These yields are shown in Figure 3.9a as function of q_F. At high productivity one achieves asymptotically the lowest consumption of 0.667 mol glucose/mol fumarate and 1 mol O_2/mol fumarate.

Succinic acid

It is expected that succinic acid also diffuses back at pH = 3. The back diffusion rate is assumed to be same as in the fumaric acid case (constant at 20 mmol/h/CmolX), since succinic acid has much higher solubility but on the other hand has lower membrane permeability.

The acid is exported by an H^+-antiporter and in addition 2 H^+ per mol succinic acid needs to be exported (in total 3 H^+). Using a prokaryotic H^+-ATPase ($3H^+$/ATP) (Figure 3.8a), acid back diffusion and its export requires 1 ATP per mol succinic acid. Then the *back diffusion reaction* occurs with a rate of 20 mmol succinate/h/CmolX:

$-(Suc^{2-})_{in} - 1$ ATP $+ (Suc^{2-})_{out}$

The catabolic *anaerobic production reaction* at pH = 3 (as in Figure 3.8a), with a rate q_{Suc}:

-7 gluc $- 2 CO_2 + 12 (Suc^{2-})_{out} + H_2O + (H^+)_{out} + 2$ ATP
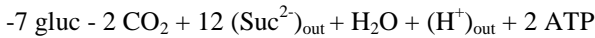
Growth reaction, with a rate μ:

$-1/6$ gluc $- 1.5$ ATP $-\ldots+ 1$ Biomass $+ \ldots$
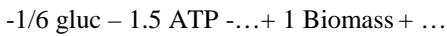
The ATP balance is:

$$\frac{2}{12} q_{Suc} - 1.5\mu - 20 = 0.$$

This relation can be rewritten (with μ in mCmolX/h/CmolX) as $q_{Succ} = 9\mu + 120$ and shows that this minimal succinate production rate is needed.

The substrate uptake rate will be:

$$-q_S = \frac{7}{12} q_{Suc} + \frac{1}{6} \mu.$$

At $\mu = 0$ there is a minimal $q_{Suc} = 120$ mmol/h/CmolX and the stoichiometry follows as

$$\frac{\text{mol glucose}}{\text{mol succinate}} = \frac{7/12 \text{x} 120}{120} = \frac{7}{12}.$$

For $\mu > 0$ elimination of μ from the q_S-relation gives q_S as function of q_{Suc}:

$$-q_S = \frac{65}{108} q_{Suc} - \frac{20}{9}.$$

The stoichiometric ratio of mol glucose/mol succinic acid follows as

$$\frac{\text{mol glucose}}{\text{mol succinate}} = \frac{(65/108)q_{Suc} - (20/9)}{q_{Suc}}.$$

This relation shows that the stoichiometric ratio slightly increases with q_{Suc}, reaching an asymptotic value of 7.222/12 mol glucose/mol succinate where 0.222/12 mol glucose is used for biomass formation.

Development and application of a differential method for reliable metabolome analysis

Abstract

Quantitative metabolomics of microbial cultures requires well-designed sampling and quenching procedures. We successfully developed and applied a differential method to obtain a reliable set of metabolome data for *Escherichia coli* K12 MG1655 grown in steady-state, aerobic, glucose-limited chemostat cultures. From a rigorous analysis of the commonly applied quenching procedure based on cold aqueous methanol, it was concluded that it was not applicable because of release of a major part of the metabolites from the cells. No positive effect of buffering or increasing the ionic strength of the quenching solution was observed. Application of a differential method in principle requires metabolite measurements in total broth and filtrate for each measurement. Different methods for sampling of culture filtrate were examined, and it was found that direct filtration without cooling of the sample was the most appropriate. Analysis of culture filtrates revealed that most of the central metabolites and amino acids were present in significant amounts outside the cells. Because the turnover time of the pools of extracellular metabolites is much larger than of the intracellular pools, the differential method should also be applicable to short-term pulse response experiments without requiring measurement of metabolites in the supernatant during the dynamic period.

4.1. Introduction

Metabolic engineering of microorganisms requires comprehensive knowledge and understanding of the functionality and control of the metabolic reaction network as a whole. Quantitative metabolomics plays an important role in obtaining information on the *in vivo* regulation of enzymes. Hereby, metabolite measurements are carried out under steady-state conditions, as well as dynamic conditions, during which a steady-state chemostat culture is perturbed and the subsequent response in both extracellular and intracellular metabolites is monitored (Chassagnole *et al.* 2002; Theobald *et al.* 1997; Visser *et al.* 2002; Wu *et al.* 2006). Taking into account the high turnover rate of most intracellular metabolites, proper measurement of their concentrations requires rapid sampling and instantaneous quenching of enzyme activity. The significance of correct measurement of intracellular concentrations of metabolites is obvious from the fact that wrong determinations will lead to unrealistic conclusions on the status of the metabolism and, hence, on the kinetic properties of the enzymes.

There have been several attempts to develop reliable sampling methods for quantification of intracellular metabolites in bacteria. Lowry *et al.* (1971) published one of the first most comprehensive metabolite concentration datasets for *Escherichia coli* during logarithmic growth. Tweeddale *et al.* (1998) and Liu *et al.* (2000) investigated the *E. coli* metabolome using qualitative analysis. Table 4.1 presents the different published sampling, quenching and extraction methods which have until now been applied for metabolite analysis in chemostat-grown *E. coli* K12 cells.

Rapid sampling of cells from a bioreactor with the aim to capture highly dynamic changes of intracellular metabolites in pulse response studies has been achieved by developed fast techniques comprising immediate withdrawal of culture broth into syringes or tubes containing a certain quenching fluid. Theobald *et al.* (1993) developed a fast manual sampling technique in which samples could be withdrawn in a fraction of a second with intervals of 2 to 5 s between samples. A comparable system was developed by Lange *et al.* (2001). To achieve shorter intervals between samples, an automated sampling device with a maximum sampling frequency of 4.5 samples.s^{-1} was constructed (Schaefer *et al.* 1999). Another sampling device introduced was based on the stopped-flow technique, where dynamic responses in the millisecond range could be captured (Buziol *et al.* 2002). Recently, an integrated sampling procedure was proposed, whereby the sampling is carried out through a helical single tube heat exchanger (Schaub *et al.* 2006).

The most commonly used method for fast quenching of all metabolic activity in culture samples has been direct sampling into cold aqueous 60 % (v/v) methanol at -40 ^{o}C. This method was firstly applied for yeast (de Koning and van Dam 1992). In general, removal of the extracellular metabolites present in the broth is performed by centrifugation of the quenched broth/quenching liquid solution to obtain a cell pellet. To be sure that no conversion of metabolites occurs, centrifugation of the broth/quenching liquid mixture is normally performed at temperatures below -20 ^{o}C (Schaefer *et al.* 1999). Shimizu and coworkers (Hoque *et al.* 2005; Peng *et al.* 2004; Siddiquee *et al.* 2004) applied a similar method for batch cultures as well as for continuous cultures.

Table 4.1: Methods used for determination of intracellular metabolites in aerobic glucose-limited chemostat grown *E. coli* K12 cells

	(Schaefer *et al.* 1999)	(Buchholz *et al.* 2001)	(Buchholz *et al.* 2002)	(Chassagnole *et al.* 2002)	(Schaub *et al.* 2006)	(Hiller *et al.* 2007b)
***E. coli* strain**	K12 DSM 498	K12	K12	K12 W3110	K12 W3110	K12 DSM 498
Dilution rate [h⁻¹] (Reactor volume, Cultivation temp.)	0.125 (7 l, 37 °C)	0.125 (0.4 l)[a]	0.125 (7 l, 37 °C)	0.1 (1.5 l, 35 °C)	0.1 (1.5 l, 37 °C)	0.125 (3 l)[a]
Biomass concn. [gDW/l]	10.7	10	10	8.7	2.3	10
Sampling	Rapid sampling device, 5 ml broth	Pre-cooled syringes, 5 ml broth	Rapid sampling device, 5 ml broth	Rapid sampling device, 2.6-3.7 ml broth	Heat exchanger, 1 ml broth	Rapid sampling device,~6 g broth
Quenching	60% (v/v) methanol (-50°C, 15 ml)	60%(v/v) methanol+ 70 mM HEPES (-50°C, 15 ml)	60%(v/v) methanol+ 70 mM HEPES (-50°C, 15 ml)	Liquid nitrogen (-196°C, 10 ml) or perchloric acid (-25°C, %35w/w)	Heat exchanger	60%(v/v) methanol + 30 mM TEA (-40°C, 25 g)
Separation	Centrifugation (-20°C)	Centrifugation (-20°C)	Centrifugation (-20°C)	No	No	Centrifugation (-19°C)
Washing	No	No	No	No	No	No
Internal standard	No	0.5 mM cGMP	No	No	Naphthyl-P and carboxyphenyl-P	Std mixture (200 µl)
Extraction	Perchloric acid (2 ml, %35w/v) -18°C	Perchloric acid (2 ml, %35w/v)	Perchloric acid (2 ml, %35v/v)	Perchloric acid (2 ml, Tris-H₂SO₄/EDTA (0.5 sv), KOH (0.3N, -25°C), perchloric acid (-25°C, %35w/w)	Heat exchanger	water + 30 mM TEA (95°C, 4 ml)
Concentration	No	No	No	No	No	Lyophilization
Analysis Method	Enzymatic/ HPLC	ESI LC-MS	Enzymatic/HPLC/LC-MS	Enzymatic/ HPLC	IC-MS	Enzymatic/LC-MS

[a] Cultivation temperature was not mentioned.

75

Alternative methods that have been used for quenching of *E. coli* include rapid freezing of the sample in liquid nitrogen (Chassagnole *et al.* 2002) and the above-mentioned rapid heating of the broth by means of a heat exchanger (Schaub *et al.* 2006). The disadvantage of these methods is that removal of extracellular metabolites is not possible.

Removal of extracellular metabolites is a prerequisite for proper quantification of the intracellular metabolite levels. It should be realized here that although the extracellular concentrations of most metabolic intermediates are generally much lower than the intracellular concentrations, the amounts present in the supernatant may still be very significant because the volume of the supernatant in laboratory cultivations is typically two orders of magnitude larger than the total cell volume. It has indeed been shown by Bolten *et al.* (2007) that in batch cultures of different bacterial species significant amounts of several central metabolites and amino acids are present in the culture filtrate.

It has been reported that application of the currently most used quenching method allowing removal of extracellular metabolites, based on cold aqueous methanol (Table 4.1), for bacteria results in loss of intracellular metabolites due to leakage to the quenching liquid (Bolten *et al.* 2007; Wittmann *et al.* 2004). Bolten *et al.* (2007) compared the cold methanol quenching method with separation and washing of the cells by means of filtration for different gram-positive and gram-negative bacteria including *E. coli* K12 (DSMZ 2670) grown in shake-flasks. Depending on the microorganism and the metabolites measured, cold methanol quenching either resulted in either higher or lower concentrations compared with filtration. Because the filtration procedure took about 30 s per sample, this method does not appear to be suitable either for rapid sampling in dynamic experiments or for steady-state measurements of metabolites with short turnover times. Even for yeast cells which are thought to be more robust, leakage of metabolites during quenching has been observed to occur (Villas-Boas *et al.* 2005). Villas-Boas and Bruheim (2007) applied a quenching method whereby cold glycerol-saline is used as the quenching solution. They compared it with the conventional aqueous methanol solution and showed that the metabolite levels were much higher when samples were quenched with the cold glycerol-saline solution. However, as they also mentioned in their work, the application of glycerol leads to additional problems because it is difficult to remove from the samples.

Rabinowitz and coworkers (Brauer *et al.* 2006) developed filter-culture methodology that involves growing cells directly on filters on top of an agarose-media support. This method enables quick quenching of metabolism by transferring a filter from an agarose plate into cold organic solvent, separating cells from their extracellular environment.

Subsequently, the quenched cells have to be extracted to release the intracellular metabolites. For *E. coli*, perchloric acid extraction has been the most widely used procedure (Buchholz *et al.* 2002; Buchholz *et al.* 2001; Chassagnole *et al.* 2002; Schaefer *et al.* 1999). In some cases, different methods have been used for the extraction of different classes of metabolites, for example, alkaline extraction for NADH and NADPH (Chassagnole *et al.* 2002). Maharjan and Ferenci (2003) investigated the influence of different extraction methods i.e. hot ethanol, cold and hot methanol, perchloric acid, alkaline and methanol-chloroform, on the quantification of metabolites extracted from *E. coli*. They proposed the use of cold methanol because of its simplicity and the

fact that it allowed more components to be extracted. Rabinowitz and Kimball (2007) proposed the use of cold acidic solvent mixtures containing acetonitrile for extraction of the *E. coli* metabolome. Hiller *et al.* (2007b) used buffered hot water (30 mM TEA, pH 7.5, 95 °C) that was claimed to result in more reliable metabolite extraction compared with buffered ethanol, unbuffered hot water or perchloric acid for *E. coli*. Clearly, a proper extraction method should result in complete release of metabolites from the cells, whereby degradation and/or conversion of compounds should be minimal. The use of cold extraction methods has been advocated to avoid chemical degradation of compounds. However, to avoid enzymatic conversion of metabolites, efficient protein denaturation should be accomplished, and this is not always ensured with cold extraction methods (Kimball and Rabinowitz 2006).

For the quantification of the metabolites in the cell extracts, different kinds of analytical techniques have been applied, such as enzymatic assays, thin-layer chromatography, gas chromatography (GC), nuclear magnetic resonance (NMR) and high-performance liquid chromatography (HPLC). Presently mass spectrometry (MS) is the most widely used detection method, thereby coupled to GC, capillary electrophoresis (CE) or HPLC as initial separation step. Advanced LC-MS/MS methods allow more accurate, robust and sensitive analyses (Luo *et al.* 2007; van Dam *et al.* 2002). For application of LC-MS/MS especially the rigorous use of stable isotope (e.g., ^{13}C) labeled internal standards is a prerequisite to obtain reproducible and reliable results (Mashego *et al.* 2004; Wu *et al.* 2005).

The aim of the current study was to obtain a fast and reliable method for sampling and quenching of *E. coli* K12 cells that would also be applicable to highly dynamic pulse response studies carried out in chemostat cultures. Having shown that considerable amounts of metabolites are present outside the cells, different variations of a quenching protocol based on cold aqueous methanol were investigated. A rigorous approach was used to quantify metabolite leakage. This approach was based on demonstration that decrease in amounts of metabolites present in the cell pellets is matched quantitatively with a corresponding increase in metabolites in the quenching and washing fluids. Glycolytic, pentose phosphate pathway (PPP) and TCA cycle intermediates, as well as amino acids and adenine nucleotides, were measured to quantify leakage of these compounds into the quenching and washing fluids. As an alternative, we applied a differential method whereby from the quantification of metabolites in both the broth and the supernatant a reliable metabolite dataset was obtained for steady-state cultivated *E. coli* in aerobic glucose-limited chemostat culture.

4.2. Materials and Methods

4.2.1. Strain and preculture conditions

The *E. coli* K12 MG1655 [λ⁻, F⁻, rph⁻¹, (*fnr⁻* 267)del] strain was obtained from The Netherlands Culture Collection of Bacteria (NCCB). Cells were grown to stationary phase in shake-flasks on LB medium. Culture aliquots containing 50 % (v/v) glycerol were kept at -80 °C until they were used as inoculum of the precultures for chemostat experiments.

Precultures were grown on minimal medium with the following composition per liter: 5.0 g $(NH_4)_2SO_4$, 2.0 g KH_2PO_4, 0.5 g $MgSO_4.7H_2O$, 0.5 g NaCl, 2.0 g NH_4Cl, 5.5 g glucose.$1H_2O$, 0.001 g thiamine-HCl, 1 ml of trace elements solution (Verduyn *et al.* 1992) and 40 mM MOPS. The pH of the medium was adjusted to 7.0 with 1M K_2HPO_4 before filter sterilization (pore size 0.2 μm, cellulose acetate, Whatman GmbH, Germany).

4.2.2. Chemostat cultivation

Aerobic glucose-limited chemostat cultures were carried out on minimal medium at a dilution rate (D) of 0.1 h^{-1} either in 7 l laboratory fermentors with a working volume of 4 l, controlled by weight, or in 1 l laboratory fermentors with a working volume of 0.5 l, controlled by means of an overflow system (Applikon, Schiedam, The Netherlands). The composition of the minimal medium was as follows (per liter): 1.25 g $(NH_4)_2SO_4$, 1.15 g KH_2PO_4, 0.5 g $MgSO_4.7H_2O$, 0.5 g NaCl, 6.75 g NH_4Cl, 30 g glucose.$1H_2O$, 0.001 g thiamine-HCl, 2 ml of trace elements solution (Verduyn *et al.* 1992) and 0.2 ml silicone-based antifoaming agent (BDH, Poole, UK). This medium allowed a steady-state biomass concentration of approximately 11 gDW/l. The medium was filter sterilized (pore size 0.2 μm, polyethersulfone, Sartorius, Goettingen, Germany) without pH adjustment; the final pH of the medium was 4.90. The cultivation temperature was controlled at 37 °C, and the pH was controlled at 7.0 with 4 M KOH. The 7 l fermentor was operated at 0.3 bar overpressure, a stirrer speed of 500 rpm (two six-bladed Rushton turbine stirrers, D = 85 mm) and an aeration rate of 100 l/h. The 1 l fermentor was operated at 0.1 bar overpressure, a stirrer speed of 700 rpm (two six-bladed Rushton turbine stirrers, D = 45 mm) and an aeration rate of 30 l/h. Under these conditions, oxygen transfer was sufficient because the dissolved oxygen tension (DOT) never dropped below 50 % of air saturation that was measured online with a DOT sensor (Mettler-Toledo GmbH, Switzerland).

During all chemostat experiments the oxygen and carbon dioxide concentrations in the offgas, DOT, pH, temperature, reactor vessel weight (only for the 7 l fermentor), effluent vessel weight and the added amounts of base + antifoam were monitored online. The carbon dioxide and oxygen volume fractions in dried offgas (permapure, Perma Pure, USA) were monitored online with a combined carbon dioxide (infrared) and oxygen (paramagnetic) gas analyzer (NGA 2000, Fisher-Rosemount, Germany).

Medium feeding was started when the carbon dioxide evolution rate (CER) and the oxygen uptake rate (OUR) during the batch phase preceding the chemostat cultivation, which was carried out on a medium identical to the feed medium, declined to nearly zero. The chemostat was assumed to be in steady-state after five residence times, and this was verified from the measured biomass concentration and the online measurements of dissolved oxygen and the oxygen and carbon dioxide concentrations in the offgas.

4.2.3. Measurement of cell dry weight

From a broth sample, 4x10 g was transferred to centrifuge tubes, the cells were spun down (5000 g, 4 °C, 5 min), and the cells were washed twice with 0.9 % NaCl solution. The centrifuge tubes containing the cell pellets were dried in an oven at 70 °C for 48 h until constant weight. The cell dry weight was obtained gravimetrically; the tubes were cooled in a desiccator prior to weighing.

4.2.4. Determination of residual glucose and total organic carbon

Samples of the supernatant were obtained by rapid sampling of broth into syringes containing cold stainless steel beads followed by immediate filtration (pore size 0.45 μm, cellulose acetate), according to the procedure described by Mashego *et al.* (2003). The glucose concentration in these samples was analyzed enzymatically (Boehringer Mannheim/R-Biopharm, Roche). The total amount of organic carbon (TOC) in the broth and filtrate were quantified with a TOC Analyzer (TOC-5050A, Shimadzu).

4.2.5. Rapid sampling

Broth sampling: Using a home-built rapid sampling system (Lange *et al.* 2001), which was coupled to the fermentor, samples of 1 ml broth were withdrawn from the fermentor within 0.5 s. Samples were withdrawn directly into tubes containing 5 ml of quenching solution precooled at -40 °C that were immediately mixed after sampling by vortexing. The exact sample sizes were quantified gravimetrically by weighing the tubes before and after sampling.

Filtrate sampling: Samples of extracellular culture fluid were obtained with three different methods: (F_1) syringe filtration (pore size 0.45 μm, cellulose acetate) with cold stainless steel beads (Mashego *et al.* 2003): quenching of the broth sample with cold stainless steel beads and subsequent filtration, (F_2) syringe filtration (pore size 0.45 μm, cellulose acetate) at room temperature without beads: direct filtration of the broth sample, (F_3) centrifugation of the broth sample at 5000 g, 4 °C, for 5 min. After removal of the cells with one of these three methods, the obtained filtrate or supernatant was immediately mixed with 5 ml of quenching solution to process these samples in the same way as the broth samples. Also in this case, the exact amount of sample obtained was quantified gravimetrically.

4.2.6. Quenching procedure

The quenching solutions that were used were: (i) 60 % (v/v) aqueous methanol, (ii) 60 % (v/v) aqueous methanol + 70 mM HEPES, (iii) 60 % (v/v) aqueous methanol + 0.9 % NaCl and (iv) 60 % (v/v) aqueous methanol + 10 mM tricine. After quenching of broth samples in one of these quenching solutions, precooled at -40 °C, the sample/quenching solution mixture was centrifuged

for 5 min at 8000 g in a cooled centrifuge (-20 °C) using a rotor that was precooled at -40 °C. After decanting, the supernatant (QS) was stored at -40 °C until extraction. Subsequently, the cell pellets were resuspended in 5 ml of -40 °C quenching solution and again centrifuged. Also, this second supernatant (WS) was stored at -40 °C until extraction. For measurement of metabolites in total broth as well as in the culture filtrate, the same quenching procedure was applied; however, the quenched total broth mixtures (B) or quenched culture filtrates (F) were not centrifuged, but after thorough vortexing, 500 μl of these mixtures was withdrawn for metabolite extraction.

4.2.7. Metabolite extraction procedure

Extraction of metabolites from the cell pellets as well as from the 500 μl samples from the quenched total broth was performed with the hot ethanol method (Gonzalez *et al.* 1997). To analyze the metabolites in the supernatants obtained from the quenching and washing procedure (QS and WS) and quenched culture filtrate (F), 500 μl of each of these solutions was subjected to the same procedure as for cell pellets. In all cases 100 μl of a U-^{13}C labeled cell extract of *Saccharomyces cerevisiae* was added to the pellets and samples before extraction. The cell extract was prepared as described in Wu *et al.* (2005). Subsequently the cell pellets and samples were extracted in 75 % boiling ethanol (3 min, 90 °C). After cooling, the thus obtained extracts were evaporated to dryness in a RapidVap (Labconco, Kansas City, MO, USA) during 110 min under vacuum. After resuspension of each residue in 500 μl of H_2O, cell debris was removed by centrifugation during 5 min at 5000 g. After decanting, the supernatants were stored at -80 °C until further analysis.

The reason why the same quenching and extraction procedure was applied in all cases (cell pellets, filtrates and supernatants) was to obtain analytes with the same sample matrix to the greatest extent possible. In addition, the boiling ethanol step ensured the destruction of any enzymatic activity which could cause conversion of metabolites before or during the analysis procedure.

4.2.8. Metabolite analysis

Metabolites of the glycolysis, TCA cycle and PPP were quantified with Isotope Dilution Mass Spectrometry (IDMS) using the method described by Wu *et al.* (2005). Amino acids were quantified with IDMS applying GC-MS, using the EZ:Faast® Free (Physiological) kit (Phenomenex, Torrance, CA, USA). Derivatization of the amino acids in the samples was carried out according to the manufacturer's instructions. The derivatized samples were analyzed with a Trace GC Ultra equipped with a programmed temperature vaporizer (PTV) injector and auto sampler AI 3000, which was directly coupled to a Trace DSQ single quadrupole mass spectrometer with an electron ionisation source, all from Thermo Finnigan (Boston, MA, USA).

The concentrations of the adenine nucleotides AMP, ADP and ATP were also analyzed with IDMS. LC separation of the adenine nucleotides was accomplished with ion-pair reversed phase LC using an AllianceHT pump 2795 system (Waters, Milford, MA, USA) and an XTerra MS C18 column (3.5 µm, 100 x 1 mm i.d., Waters, Ireland). The mobile phase consisted of 10 mM dibutylammonium acetate (DBAA) and a linearly increasing acetonitrile content (9 - 29 % v/v). The MS/MS data were acquired with a Waters Quatro Ultima TM Pt (Micromass, UK). The electrospray ionization was operated in negative mode (ESI-) and the data were collected in the multiple reaction monitoring (MRM) mode. Further details of the applied LC-ESI-MS/MS procedure have been described elsewhere (Seifar *et al.* 2009).

For each compound group to be analysed, i.e. central metabolites, amino acids and adenine nucleotides, 10 different dilutions of a standard mixture were prepared. To each of these dilutions the same amount of ^{13}C extract was added. The analysis of these mixtures allowed us to quantify the amounts of ^{13}C metabolites in the ^{13}C extract so as to convert the measured ^{12}C/^{13}C peak area ratios to absolute concentrations.

4.3. Results and Discussion

4.3.1. Chemostat cultivations

The aim of this work was to develop a reliable sampling method for quantification of intracellular metabolites in *E. coli* applicable to steady-state chemostat cultures as well as to highly dynamic pulse response experiments. In this study, all cultivations were aerobic glucose-limited chemostats on a minimal medium, carried out at a dilution rate of 0.1 h^{-1}. For all chemostat cultivations, measurements of residual glucose, biomass concentration, oxygen and carbon dioxide concentrations in the offgas and medium inflow and culture outflow rates were performed during steady-state growth. In addition, the concentration of TOC in the culture filtrate was measured in order to verify whether significant amounts of by-products were formed. From these measurements, the biomass-specific rates of glucose consumption, biomass growth, oxygen consumption and carbon dioxide production were calculated (see Table 4.2). Chemostat cultivations were carried out in two different bioreactors with working volumes of 4 and 0.5 l. All chemostat experiments appeared to be reproducible and no significant differences were observed between the 4 and the 0.5 l. cultivations with respect to the biomass-specific conversion rates, as can be inferred from the average rates calculated for the three 4 l and the two 0.5 l chemostat cultivations which were carried out (see Table 4.2).

Although the growth conditions were aerobic and carbon-limited, it appeared from the TOC measurements that the culture filtrate still contained a significant amount of organic carbon (about 20 % of the TOC in the broth). It was verified from the residual glucose measurement and HPLC analysis of the filtrate, however, that concentrations of glucose and organic acids were negligible (results not shown). Therefore, the measured residual organic carbon was attributed to cell lysis. An indication of this was that the measured carbon to nitrogen (C/N) ratio of the filtrate, corrected for the residual ammonia present, was very similar to the C/N ratio of the

biomass (results not shown). If all organic carbon in the filtrate is considered as originating from lysed biomass, the calculated specific rate of biomass decay was considerable (approx. 0.02 h^{-1}), implying that the specific growth rate (μ') in the chemostat, being the sum of the dilution rate and the rate of cell decay, was higher than the dilution rate, namely $\mu' \sim 0.12$ h^{-1}.

The measured biomass yield in our chemostat cultivations was $Y_{SX} = 3.2$ CmolX/mol glucose which is very similar to published biomass yields of this *E. coli* strain under similar conditions (Nanchen *et al.* 2006; Pramanik and Keasling 1997). From the last two columns of Table 4.2, it can be seen that the recoveries of carbon and redox, which are indicative for possible measurement errors (Roels 1983), were close to 100 % for both the 4 l and the 0.5 l chemostats.

Table 4.2: Average net conversion rates (q_i), expressed per Cmol of biomass [mmol/CmolX/h] and carbon and redox recoveries (in %) of the steady-state aerobic glucose-limited chemostat cultivations of *E. coli*, carried out at a dilution rate $D = 0.1$ h^{-1} in two different chemostat systems

Chemostat Volume	$q_X'^a$	$-q_S$	$-q_{O2}$	q_{CO2}	q_{bp}	Carbon recovery	Redox recovery
4 l	123.8 ± 4.9	38.3 ± 2.9	93.9 ± 3.4	97.1 ± 7.9	20.6 ± 1.7	96.1	97.4
0.5 l	121.9 ± 4.1	39.0 ± 2.2	96.6 ± 3.3	101.5 ± 6.0	19.3 ± 2.5	95.5	96.0

1 Cmol is the amount of compound containing 1 mol of carbon.

[a] $q_X' = q_X + q_{bp}$ (see text).

4.3.2. Separation of cells and supernatant

To obtain a proper procedure for accurate quantification of metabolites in the culture supernatant, three different separation methods for obtaining the filtrate were compared, namely (F_1) quenching of the broth sample with cold stainless steel beads and subsequent filtration (Mashego *et al.* 2003), (F_2) direct filtration of the broth sample without cooling and (F_3) direct centrifugation of the broth (see Materials and Methods). Figure 4.1 presents the results of the measurements of a number of different central metabolites and amino acids in the broth (B) and in the filtrate for the three different filtrate sampling techniques (F_1, F_2, F_3). The data in this figure are averages from four replicate samples taken from two independent chemostat experiments. From these measurements it can be concluded that the amounts of metabolites measured in the filtrate depend on the separation method applied to obtain the filtrate. It was observed that method F_1 (direct filtration after rapid cooling of the broth with cold beads to a temperature close to 0 ^{o}C) in nearly all cases resulted in the highest amounts of measured metabolites in the filtrate. For the cases where indeed significant differences were found, direct filtration without cooling (F_2) resulted in the lowest amounts of measured metabolites. Apparently, rapid cooling of the broth and, to a lesser extent, centrifugation resulted in release of part of the metabolites from the cells. This has been observed previously in *Corynebacterium glutamicum* and attributed to a high sensitivity to cold shock (Wittmann *et al.* 2004). According

to these results, direct filtration of the broth without cooling was chosen as the preferred method to obtain culture supernatant for metabolite quantification.

4.3.3. Metabolite measurements in broth and supernatant

To quantify whether central metabolites of *E. coli* are also present in significant amounts in the culture filtrate during chemostat cultivation, metabolite measurements were carried out in the broth as well as in the filtrate of steady-state chemostat cultures. The measured concentrations of metabolites in the filtrate, the amounts of metabolites in the broth and in the filtrate (both expressed per g dry weight of biomass), and the corresponding percentages of the total amounts of metabolites that are present in the filtrate are shown in Table 4.3. From these results, it can be concluded that most of the measured metabolites are present in significant quantities, if expressed per amount of biomass, in the culture filtrate.

The fractions of metabolites outside the cells appeared to vary between the different metabolites. However, no clear trends could be observed. One of the reasons why most of the measured metabolites are present in the culture supernatant is probably cell lysis. As argued above, the measured TOC content and C/N ratio of the filtrate indicated that the biomass decay rate might have been as high as 1/6 of the growth rate of the culture. If the release of metabolites to the supernatant had been caused by cell destruction alone, and no reconsumption by the living cells would have occurred, the fraction of metabolites in the supernatant would have been approximately 1/6 of the total for each metabolite. The fact that this fraction is significantly higher than 1/6 for more than half of the measured metabolites indicates that there must exist other processes which cause release of metabolites from the cells.

So far, most authors have considered the presence of metabolites of glycolysis, TCA cycle or PPP in the supernatant negligible because the levels have been below the detection limits of their analysis methods (Hiller *et al.* 2007b; Schaub *et al.* 2006). However, this clearly does not agree with the current findings. Due to the sensitivity of the applied LC-ESI-ID-MS/MS analysis method, metabolite concentrations well below 1 µM can be quantified. Due to the fact that the volume of the supernatant is two orders of magnitude larger than the total cell volume, these low extracellular concentrations, which in most cases are between 100 and 1000 times lower than the calculated intracellular concentrations (assuming water content of the cells of 2.5 ml/gDW), represent a significant amount of metabolites. Table 4.3 shows that 0.55 µM Ile still contributes to more than 30 % of the total Ile present. In agreement with our findings, Bolten *et al.* (2007) also detected intermediates from the glycolysis, TCA cycle and PPP in the supernatant for several bacterial species. Even for yeast cells, many intracellular metabolites have been detected in the culture supernatant (Canelas *et al.* 2008a). Apart from cell lysis, other explanations for the presence of metabolites outside the cells are partial permeability of the membrane for certain metabolites (e.g. organic acids in their undissociated form) and the presence of transporters for a large range of compounds. It is known that many bacterial species contain transporters for phosphorylated sugars, including *E. coli*. According to Schwoppe *et al.* (2002; 2003) the G6P transporter protein imports G6P and a number of other phosphorylated sugars via a G6P/Pi

antiport mode of transport. The presence of such a transporter results in a certain ratio between extra- and intracellular G6P, depending on the extracellular phosphate concentration. In our *E. coli* cultures the [G6P(in)]/[G6P(out)] ratio was calculated to be approximately 400.

From the above, it is clear that total broth extraction, as used in several published studies (Chassagnole *et al.* 2002; Schaub *et al.* 2006) cannot be used for proper measurement of intracellular metabolite levels. Therefore, the metabolites present outside the cells have to be eliminated prior to the metabolite extraction procedure.

The usual approach, to avoid the interference of metabolites in the filtrate, is to use the cold methanol quenching method combined with cold centrifugation, with or without a washing step. The advantage of this method is that metabolism is stopped instantaneously and that all compounds that are present outside the cells can be effectively removed. However, according to several studies, quenching with cold aqueous methanol prior to separation might lead to additional leakage of intracellular metabolites from the cells, especially in the case of bacteria. To determine losses of metabolites from the cells when the cold methanol quenching method is applied, we used a rigorous balancing approach whereby the metabolites in all different fractions (broth, filtrate, cell pellet, quenching and washing solutions) were quantified.

4.3.4. Validation of the cold methanol quenching method for chemostat cultivated *E. coli*

Steady-state broth samples were rapidly withdrawn from the chemostat with a dedicated rapid sampling system and directly quenched in 60 % methanol solution at -40 ^{o}C (Lange *et al.* 2001). To quantify metabolite leakage, metabolite measurements were performed in the broth (B), culture filtrate (F), quenching solution (QS), washing solution (WS) and in the cell pellets (IC). This allowed us to verify, from the mass balance for each metabolite, whether metabolite losses could indeed be attributed to leakage because the measured amounts in the different fractions should add up to the amount measured in the broth. The results for a number of representative metabolites from the glycolysis, TCA cycle and PPP are shown in Figure 4.2 and represent averages of four replicate samples taken from two independent steady-state chemostat experiments. It can be seen from this figure that the mass balances close well in most cases (> 95 %). From the metabolite measurements in broth and filtrate, the intracellular amount could be calculated (IC_{cal} in the right columns). For all metabolites, the measured amounts in the cell pellets (IC) were much lower than the calculated amounts (IC_{cal}), indicating that the major part of the intracellular metabolites ended up in the quenching solution (QS) and washing solution (WS). This clearly shows that quenching of *E. coli* cells in cold methanol results in release of the major part of the intracellular metabolites. Subsequently, we investigated whether buffering of the 60 % cold methanol or the addition of salt could reduce the leakage of metabolites during quenching.

Therefore, quenching of the samples was also carried out with (i) 60 % (v/v) aqueous methanol + 70 mM HEPES, (ii) 60 % (v/v) aqueous methanol + 0.9 % NaCl, and (iii) 60 % (v/v) aqueous methanol + 10 mM tricine, all kept at -40 ^{o}C. However, no significantly different results were

obtained for these three alternatives compared with the 60 % cold methanol without any additions (results not shown).
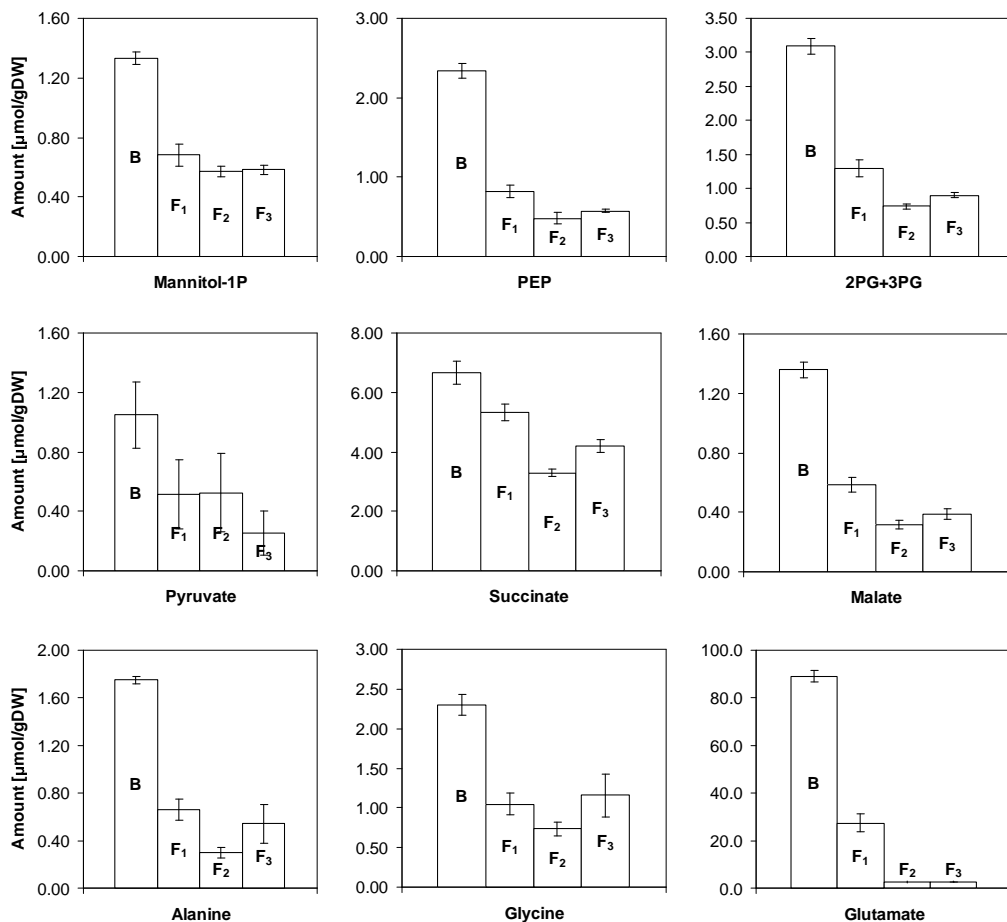
Figure 4.1: Some examples of measured steady-state amounts of metabolites and amino acids in the broth (B) and in the culture filtrates obtained with three different methods: F_1 (quenching of the broth sample with cold stainless steel beads and subsequent filtration), F_2 (direct filtration of the broth sample without cooling), and F_3 (direct centrifugation of the broth). Bars represent the averages with their standard errors of four replicate samples taken from two independent chemostat experiments analyzed in duplicate.

As an alternative to the cold methanol quenching procedure, Villas-Boas and Bruheim (2007) applied cold glycerol-saline as quenching solution for *S. cerevisiae* and *Streptomyces coelicolor*. Although the measured metabolite amounts in the cell pellets were consistently higher than if cold methanol quenching was applied, the authors could not show whether this method completely avoided leakage of metabolites because no metabolite measurements were carried out

Table 4.3: Steady-state concentrations and amounts of some metabolites, amino acids and adenine nucleotides in the filtrate (F_2), in the total broth (B), percentages of metabolites in the filtrate, and intracellular amounts in aerobic glucose-limited chemostat cultures grown at D = 0.1 h^{-1}

	F_2 [µM]	F_2 [µmol/gDW]	B [µmol/gDW]	F_2/Bx100 [%]	IC_{cal} [µmol/gDW]
Central Metabolites					
G6P	1.33	0.13 ± 0.02	1.54 ± 0.05	8.1	1.42 ± 0.06
F6P	1.12	0.11 ± 0.04	0.48 ± 0.01	21.9	0.38 ± 0.04
T6P	0.59	0.055 ± 0.004	0.19 ± 0.01	29.2	0.13 ± 0.01
M6P	0.12	0.011 ± 0.003	0.49 ± 0.01	2.2	0.48 ± 0.01
6PG	4.19	0.39 ± 0.05	0.49 ± 0.01	80.4	0.10 ± 0.05
Mannitol-1P	8.51	0.80 ± 0.08	1.79 ± 0.03	44.8	0.99 ± 0.09
G3P	1.58	0.15 ± 0.02	0.32 ± 0.02	46.7	0.17 ± 0.02
FBP[a]	-	-	0.82 ± 0.04	-	-
F2,6bP	0.68	0.06 ± 0.01	0.41 ± 0.01	15.5	0.35 ± 0.01
2PG+3PG	6.06	0.57 ± 0.04	2.22 ± 0.03	25.7	1.65 ± 0.05
PEP	5.44	0.51 ± 0.04	2.12 ± 0.03	24.1	1.61 ± 0.05
Pyruvate	5.18	0.49 ± 0.06	1.24 ± 0.07	39.3	0.75 ± 0.10
α-ketoglutarate	0.68	0.064 ± 0.005	0.38 ± 0.01	17.0	0.31 ± 0.01
Succinate	20.71	1.95 ± 0.28	4.60 ± 0.14	42.4	2.65 ± 0.31
Fumarate	0.20	0.019 ± 0.002	0.24 ± 0.01	7.9	0.22 ± 0.01
Malate	3.98	0.38 ± 0.02	1.32 ± 0.02	28.5	0.94 ± 0.03
Amino Acids					
Alanine	2.33	0.22 ± 0.01	1.55 ± 0.03	14.1	1.34 ± 0.03
Asparagine	1.04	0.10 ± 0.01	0.68 ± 0.01	14.4	0.58 ± 0.01
Aspartate	2.77	0.26 ± 0.01	2.83 ± 0.03	9.2	2.57 ± 0.03
Glutamate	16.53	1.56 ± 0.09	76.25 ± 0.70	2.0	74.69 ± 0.71
Glutamine	2.30	0.22 ± 0.02	6.36 ± 0.06	3.4	6.14 ± 0.06
Glycine	5.57	0.52 ± 0.03	2.04 ± 0.05	25.7	1.51 ± 0.06
Histidine	1.21	0.11 ± 0.005	0.26 ± 0.01	44.0	0.15 ± 0.01
Isoleucine	0.55	0.05 ± 0.004	0.17 ± 0.01	31.6	0.11 ± 0.01
Leucine	0.72	0.07 ± 0.01	0.43 ± 0.02	15.9	0.36 ± 0.02
Lysine	0.84	0.08 ± 0.01	1.29 ± 0.02	6.1	1.21 ± 0.02
Methionine	0.19	0.02 ± 0.002	0.07 ± 0.002	25.6	0.05 ± 0.003
Phenylalenine	1.91	0.18 ± 0.02	0.31 ± 0.02	58.9	0.13 ± 0.03
Proline	0.90	0.08 ± 0.01	0.74 ± 0.01	11.4	0.66 ± 0.01
Serine	5.54	0.52 ± 0.06	1.05 ± 0.06	49.5	0.53 ± 0.08
Threonine	1.97	0.19 ± 0.01	0.65 ± 0.01	28.4	0.47 ± 0.02
Tryptophan	0.21	0.02 ± 0.002	0.04 ± 0.001	47.8	0.02 ± 0.003
Tyrosine	0.90	0.08 ± 0.004	0.27 ± 0.01	31.4	0.18 ± 0.01
Valine	1.30	0.12 ± 0.01	0.63 ± 0.04	19.5	0.51 ± 0.04
Ornithine	1.84	0.17 ± 0.01	0.66 ± 0.02	26.2	0.49 ± 0.03
Adenine nucleotides					
ATP	≤ 0.01	≤ 9.43E-4	5.95 ± 0.06	0	5.95 ± 0.06
ADP	≤ 2.50E-4	≤ 2.35E-5	2.31 ± 0.01	0	2.31 ± 0.01
AMP	≤ 0.01	≤ 9.43E-4	0.91 ± 0.02	0	0.91 ± 0.02

Note: The indicated errors represent the standard errors of the means.

[a] FBP was quantified in the broth only.

in the broth and in the filtrate. A disadvantage of applying mixtures containing glycerol as quenching liquid is the fact that it cannot be evaporated and, thus, cannot be completely removed from the cell pellet.

Until now, no proper alternative to the cold methanol quenching and washing procedure has been proposed that was demonstrated not to result in leakage of intracellular metabolites. An alternative method for the determination of intracellular metabolites in *E. coli*, whereby metabolite leakage can be circumvented, is the differential method, proposed but not applied by several authors (Bolten *et al.* 2007; Mashego *et al.* 2007a; Schaub *et al.* 2006) that was in fact used above to determine the intracellular metabolite amounts from the metabolite measurements in broth and culture filtrate (IC_{cal}).

4.3.5. Application of the differential method

The differential method was applied for quantification of central metabolites and amino acids in aerobic glucose-limited chemostat cultures run at a dilution rate of 0.1 h^{-1}. After steady-state was reached, broth samples were rapidly withdrawn from the chemostats and directly quenched and filtrate samples were obtained by direct filtration (see Materials and methods). After extraction, metabolites were analyzed in the broth and in the filtrate. The results are shown in Table 4.3. Two different chemostat systems were used, with working volumes of 4 and 0.5 l, and the results of the metabolite measurements appeared to be very similar for both systems. The averages of intracellular metabolite measurements from at least three independent runs are presented in the last column of Table 4.3, which also includes the intracellular ATP, ADP and AMP levels. Remarkably, these metabolites could not be detected in the filtrate because they were below the detection limit of the analysis procedure.

A possible drawback of the proposed differential method would be that in the case of high metabolite concentrations in the filtrate, two relatively large numbers are subtracted from each other resulting in large errors in the calculated intracellular amounts. It can be observed from the results in Table 4.3 that the metabolite with the highest fraction present in the filtrate was 6PG (80 %), all others were much lower (50 % or less). However, due to the accurate LC-ID-MS/MS analysis method and the reproducibility of the replicate chemostat cultivations, the standard errors of the obtained metabolite quantifications appeared to be relatively low (Figure 4.2 and Table 4.3), thereby making the method also applicable to metabolites that occur in significant amounts outside the cells.

An important aspect for meaningful metabolome quantification is that the sampling and quenching of the cells is sufficiently fast to obtain a proper snapshot of the actual metabolite concentrations. Therefore, the time between the withdrawal of the sample and the complete arrest of all metabolic activity by the quenching procedure should be significantly shorter than the turnover times of the intracellular metabolite pools. The residence time of the cells in the applied rapid sampling device, that is the traveling time from the chemostat to the tube containing the quenching solution was estimated to be less than 80 ms (Lange *et al.* 2001). The turnover times

of the intracellular metabolite pools can be estimated from the calculated metabolic fluxes for the applied cultivation conditions and the measured pool sizes of the metabolites. This has been done for intracellular pools of free amino acids of different microorganisms (Bolten and Wittmann 2008; Wittmann *et al.* 2004), resulting in turnover times of tens of seconds to more than 100 min. Due to the higher fluxes through the central metabolic pathways, the turnover times of central metabolites are generally lower. Using published metabolic flux analysis (MFA) results for aerobic glucose-limited chemostat cultures of *E. coli* K12 expressed relative to the glucose consumption rate (Kayser *et al.* 2005), we calculated the flux distributions through the central metabolic pathways for the glucose uptake rate measured in our chemostat cultures (Table 4.2). From the calculated fluxes and the measured pool sizes, the turnover times were calculated (see Table 4.4). It can be seen from Table 4.4 that the turnover times of the intermediates of the central metabolic pathways are in the seconds to subseconds range. It can be concluded from these results that the applied sampling procedure should be fast enough to obtain proper measurements of the intracellular levels of free amino acids as well as the central metabolites.
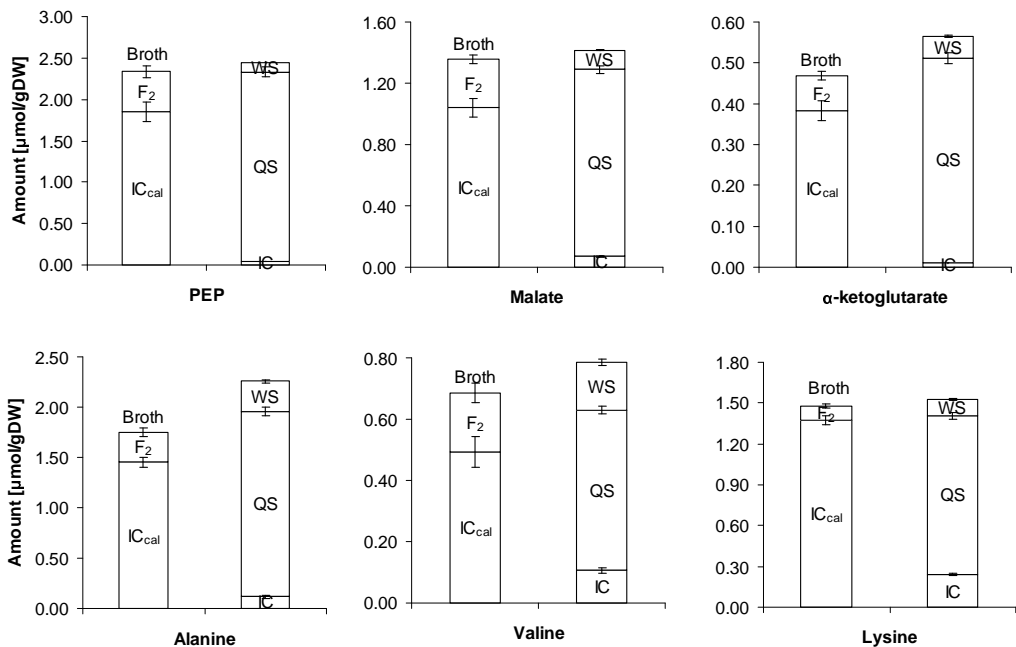
Figure 4.2: Examples of results of the balancing approach for quantification of metabolite leakage during the cold methanol quenching procedure. F_2, amount measured in the filtrate; $IC_{cal} = B - F_2$, calculated amount in the cell pellet; WS, measured amount in the washing solution; QS, measured amount in the quenching solution; IC, measured amount in the biomass pellet. Bars represent the averages, with their standard errors, of four replicate samples taken from two independent chemostat experiments analyzed in duplicate.

Table 4.4: Turnover times (τ) of some central metabolites, calculated from the metabolic flux distributions during growth in aerobic glucose-limited chemostat culture (Kayser *et al.* 2005) at a dilution rate of 0.1 h^{-1} (see text) and the measured pool sizes (Table 4.3)

Central Metabolites	τ [s]
G6P	3.5
F6P	1.6
6PG	0.6
2PG+3PG	2.7
PEP	2.6
Pyruvate	1.5
α-ketoglutarate	1.1
Succinate	10.5
Fumarate	0.9
Malate	3.7

4.3.6. Quality check of the obtained metabolome data

Although the intracellular metabolite levels of *E. coli* K12 during glucose-limited steady-state chemostat cultivation that have been published so far are in most cases of the same order of magnitude, there are big variations. These variations might have been caused by the different sampling/quenching techniques and/or the different analysis procedures applied. Either total broth extractions have been performed or cells have been quenched in cold methanol, resulting in leakage. Furthermore, the limit of detection of the applied analysis methods may have varied significantly, and measurements in the noise level range should be considered with care. The application of ^{13}C internal standards has considerably increased the accuracy of the results. Taking this into account, the metabolite data published so far should be interpreted with caution because they might not represent the real situation.

However, without ending up in complicated thermodynamic considerations (Kummel *et al.* 2006), a few checks can be carried out to examine the quality of metabolome data. First, it is well known that for healthy growing cells the adenylate energy charge (ATP+ADP/2)/(ATP+ADP +AMP) is generally stable at values around 0.8 to 0.9 (Chapman *et al.* 1971). As has been shown previously (Bolten *et al.* 2007), for many published metabolite datasets of *E. coli* the calculated e-charge appears to be far outside this range, and this is indicative of erroneous measurements. From our data, an energy charge of 0.8 can be calculated, and this is in the expected range.

The quality of the metabolome data can be checked further by calculating the mass action ratios (MARs) for reactions which are known to operate close to equilibrium (see (Visser *et al.* 2000) and references therein). For these reactions the calculated MAR should be close to the equilibrium constant (K_{eq}). Using our metabolite data, the MARs of some known near-equilibrium reactions were calculated and compared with the published equilibrium constants (see Table 4.5). It can be seen from this table that the MAR of the reactions catalyzed by

phosphoglucose isomerase (PGI), mannose-6-phosphate isomerase (PMI), adenylate kinase (AK), fumarase (FUM), and phosphoglyceratemutase (PGM) + enolase (ENO) are all very close to K_{eq}. This is a good indication of the thermodynamic feasibility of the metabolome data obtained with the differential method. Calculation of MAR values for near equilibrium reactions from previously published metabolite measurements carried out in similar aerobic chemostat cultures of *E. coli* K12 at the same dilution rate (Buchholz *et al.* 2001; Chassagnole *et al.* 2002) resulted in large deviations from the published equilibrium constants. For example, from the metabolite data published by Chassagnole *et al.* (2002) it can be calculated that the MAR's for PGI and PGM+ENO (with literature values in parentheses) are 0.17 (0.33) and 11.52 (0.80), respectively. From the data of Buchholz *et al.* (2001), the calculated MARs for PGI and AK are 1.14 (0.33) and 4.86 (0.57 – 1.06), respectively. Such large discrepancies are a reason to question the reliability of the so far published data.

Table 4.5: Mass action ratios (MAR) calculated from the measured metabolite levels and published equilibrium constants for some relevant equilibrium reactions

Enzyme	Reaction	MAR	K_{eq}	Reference
PGI	G6P ↔ F6P	0.27 ± 0.03	0.33	(Seeholzer 1993)
PMI	F6P ↔ M6P	1.27 ± 0.14	1.10	(Seeholzer 1993)
PGM+ENO[a]	2+3PG ↔ PEP	0.98 ± 0.04	$K_{PGM}=0.19$	(Grisolia and Carreras
			$K_{ENO}=5.00$	(Wold and Ballou 1957)
AK	2ADP ↔ AMP + ATP	1.01 ± 0.03	0.57-1.06	(Lawson and Veech 1979)
FUM	Malate ↔ Fumarate + H_2O	0.23 ± 0.01	0.23	(Keruchenko *et al.* 1992)

[a] $\dfrac{PEP}{2PG+3PG} = \left(\dfrac{1}{K_{ENO}} + \dfrac{1}{K_{ENO}K_{PGM}} \right)^{-1} = 0.80$

The results of measurements of metabolites participating in NAD^+-dependent oxidation/reduction reactions operating close to equilibrium can also be used to estimate the *in vivo* NAD^+/NADH ratio, which is an important parameter in physiological studies. By assuming that the enzyme mannitol-1-phosphate dehydrogenase operates near to equilibrium and assuming an intracellular pH of 7.0, the NAD^+/NADH ratio was calculated from the measured F6P and Mannitol-1P levels to be equal to 48. By assuming that the enzymes malate dehydrogenase and aspartate transaminase operate close to equilibrium, an NAD^+/NADH ratio of 71 was calculated (details of the calculations are shown in the Appendix 4.5). Remarkably, the estimated cytosolic NAD^+/NADH ratio is close to the value found for *S. cerevisiae* under similar conditions (Canelas *et al.* 2008b).

4.3.7. Can the differential method be applied to dynamic experiments?

To capture the highly dynamic changes in metabolite levels during pulse response experiments, the sample frequency should be sufficiently high. Taking into account the required sample frequency in such experiments carried out with *E. coli*, which is in the order of seconds to sub-seconds (Buziol *et al.* 2002; Schaefer *et al.* 1999), the withdrawal of two samples for each single measurement is not feasible. The question, however, is how fast the expected changes are in the levels of the metabolites that are present in the culture supernatant. It should be realized here that during steady chemostat cultivation the turnover time of all extracellular metabolites is equal to the liquid residence time, which is equal to the working volume of the reactor divided by the feed rate and thus equal to the reciprocal of the dilution rate. In case of a chemostat with a dilution rate $D = 0.1$ h^{-1} the liquid residence time, and thus the turnover time of the pool of extracellular metabolites is 10 h. This implies that within the time span of a pulse response experiment, which is of the order of seconds to minutes, no significant changes are expected to occur if the rate of release of these metabolites remains at the steady-state level during the pulse response experiment. If this is the case, measurement of the steady-state levels of the metabolites of interest in the culture supernatant would be sufficient, and this is something which has to be verified beforehand. Therefore, the application of the differential method for dynamic measurements will probably require only broth sampling.

4.4. Conclusions

In this work, it has been shown from highly sensitive LC-ESI-ID-MS/MS measurements of metabolite levels in the culture supernatant of aerobic glucose-limited chemostat cultivated *E. coli* cells that although the absolute concentrations are low, significant total amounts of metabolites are present outside the cells due to the large supernatant volume. This implies that total broth extraction cannot be carried out to obtain meaningful intracellular metabolite levels and that effective removal of extracellular metabolites is necessary prior to metabolite extraction. The most commonly applied method to remove extracellular compounds is cold methanol quenching and subsequent centrifugation. From our thorough investigation on the fate of central metabolites and amino acids on quenching of *E. coli* cells with this method, it can be concluded that significant leakage of intracellular metabolites into the cold aqueous methanol solution occurs. Therefore, this method cannot be applied. Because appropriate alternative methods to remove the extracellular metabolites before extraction are not available, the only way to obtain reliable results is to apply a differential method, whereby measurements of the metabolites in the total broth are corrected with measurement of the metabolites in the culture supernatant. Due to the large turnover time of the metabolites present in the culture supernatant in case of chemostat cultivation, this method is also applicable to short-term pulse response experiments where metabolite measurements of total broth extracts can be corrected with steady-state measurements in the culture filtrate. However, to be able to apply the differential method, the method for the quantification of metabolites should be highly sensitive and reproducible. The LC-ESI-ID-MS/MS method we used for metabolite analysis has proven to be a powerful tool that minimizes

variations in analysis as a result of partial loss or degradation during the sample processing procedure, the analysis or instrument drift. Figure 4.3 summarizes the proposed procedure as a result of this work. The application of this procedure to steady-state chemostat cultures yielded a reliable metabolome dataset for *E. coli* K12 MG1655 under these conditions. We believe that further application of this method will yield more appropriate data of levels of intracellular metabolites that will offer more realistic integration of metabolome data with other omics data into large-scale mathematical models.
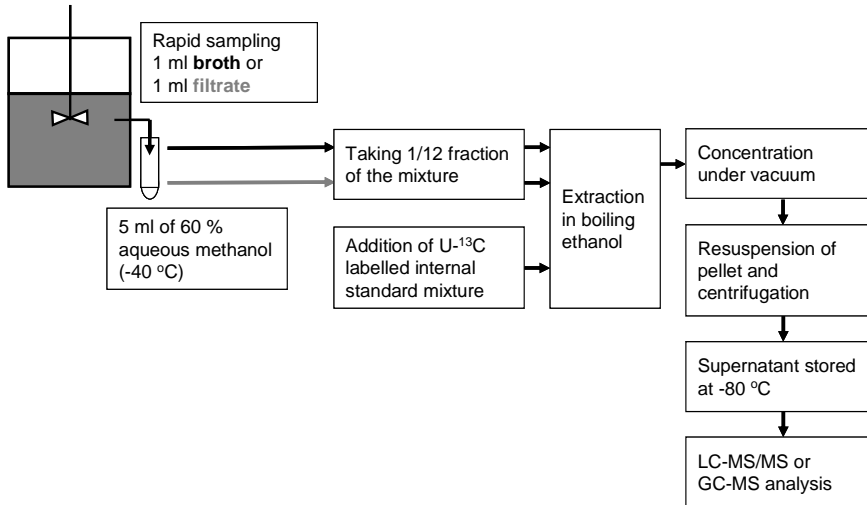
Figure 4.3: Applied differential sampling and analysis procedure for accurate metabolome analysis in *E. coli*.

4.5. Appendix

The NAD$^+$/NADH ratio was calculated in two different ways under the assumption that reactions displayed in Table 4.6 operate close to equilibrium.

The *in vivo* NAD$^+$/NADH ratios were calculated as follows:

$$\frac{\text{NAD}^+}{\text{NADH}} = \frac{\text{F6P}}{\text{Mannitol-1P}} \frac{1}{K_1} = 48.4$$

$$\frac{\text{NAD}^+}{\text{NADH}} = \frac{\text{Asp}}{\text{Glu}} \frac{\alpha\text{KG}}{\text{Mal}} \frac{K_3}{K_2} = 71.3$$

Table 4.6: Reactions operating close to equilibrium used to estimate the *in vivo* $NAD^+/NADH$ ratio

	Reaction	K_{eq}		Reference
1	Mannitol-1P + NAD^+ ↔ F6P + NADH + H^+	K_1	$7.9x\ 10^{-3}$ (pH 7.0)	(Kiser and Niehaus 1981)
2	malate + NAD^+ ↔ oxaloacetate + NADH + H^+	K_2	$2.33x\ 10^{-5}$ (pH 7.0)	(Wilcock and Goldberg 1972)
	aspartate + αKG ↔ oxaloacetate	K_3	0.145	(Kishore *et al.* 1998)

Acknowledgements

Rapid dynamics of *in vivo* flux and metabolite responses

Abstract

Glucose pulse experiments at seconds time scale resolution were performed in aerobic glucose-limited *Escherichia coli* chemostat cultures. The dynamic response of O_2-uptake and growth rate in seconds time resolution was determined using a new method based on the dynamic broth O_2-mass balance and the pseudo-steady-state ATP balance. Significant fold changes in metabolites (10 - 1/10) and fluxes (4 - 1/4) were observed during the short (200 s) period of glucose excess, the subsequent glucose starvation and the return to glucose-limited growth. During glucose excess there was no secretion of by-products, and the accumulated intracellular metabolites served as energy source during the starvation phase. Flux changes of reactions were strongly correlated to the concentrations of involved compounds. Surprisingly the 3 - 4 fold increase in growth rate and hence protein synthesis rate was not matched by a significant increase in amino acid concentrations and suggests the rapid increase of transcripts, which is mediated by changed central metabolites. Accordingly, relations were found between growth rate and FBP concentration, respectively O_2-uptake rate and AMP/ATP ratio.

5.1. Introduction

In metabolic engineering studies kinetic models help in the quantitative understanding of the cellular metabolism and in this way they can be used (by selecting genetic engineering targets) to improve the yield of microorganisms (Stephanopoulos 1994). A kinetic metabolic model consists of mass-balance-based differential equations which require the enzyme level, enzyme kinetics information and extracellular metabolite concentrations. These kinetic models predict the fluxes and intracellular metabolite levels as function of enzyme levels and extracellular concentrations, and therefore allow selecting for the enzymes which for example mostly affect the product rate. Subsequently these selected changes in enzyme levels can be implemented by genetic engineering techniques.

Traditionally kinetic models are set up using published *in vitro* kinetics of enzymes. This approach suffers from several problems: i) For many enzymes, e.g. in product pathways, the *in vitro* kinetics have not been studied, ii) Enzymes which catalyze the same reaction in different organisms do seldom have the same kinetics due to specific mutations, iii) *in vitro* kinetics might not apply to *in vivo* conditions (Teusink *et al.* 2000). These problems can only be avoided by focusing on the *in vivo* kinetics for all enzymes in the organism of interest.

The information on *in vivo* kinetics is usually obtained from stimulus-response experiments in which cells, grown at steady-state, are perturbed by an external stimulus, and dynamic responses of the intracellular metabolites are monitored in a time window of tens to a few hundred seconds. In such a set-up the enzyme levels can be assumed constant and is therefore preferred compared to steady-state perturbations, which require additional measurements of changes in enzyme levels. Such rapid stimulus-response experiments have been applied to *Saccharomyces cerevisiae* and *Penicillium chrysogenum* (Nasution *et al.* 2006; Theobald *et al.* 1997; Visser *et al.* 2004).

Also for *Escherichia coli* these studies were performed, applying a sudden addition of a concentrated glucose solution to a glucose-limited aerobic chemostat culture (Buchholz *et al.* 2002; Chassagnole *et al.* 2002; Hoque *et al.* 2005; Schaefer *et al.* 1999; Schaub and Reuss 2008). In these *E. coli* perturbation experiments only glycolytic intermediates and adenine nucleotides were measured. The measurements were depending on either only broth sampling (Chassagnole *et al.* 2002; Schaub and Reuss 2008) or separation of extracellular metabolites by centrifugation (Buchholz *et al.* 2002; Chassagnole *et al.* 2002; Hoque *et al.* 2005; Schaefer *et al.* 1999). The intracellular metabolites were analyzed using enzyme-based assays and mass spectrometry (MS)-methods without metabolite specific internal standards. However, previously we have shown that these sampling/analysis methods are not satisfying for intracellular metabolite quantification due to leakage problems and the differential method is required for proper intracellular metabolome analysis in *E. coli* (Taymaz-Nikerel *et al.* 2009). Moreover the isotope dilution mass spectrometry (IDMS) method, which makes use of labeled internal standards for each metabolite, effectively decreases errors due to possible variations taking place in the sample processing and analysis (Wu *et al.* 2005). Because accurate information on intracellular metabolite levels is essential to obtain true *in vivo* kinetics, these newly developed sampling and analysis methods need to be applied to *in vivo* kinetic studies with *E. coli*.

A further problem in these previous *in vivo* kinetic studies in *E. coli* is the limited quantification of changes in fluxes after the pulse, such as possible secretion of by-products, possible changes in storage metabolism and especially the change in growth rate. Previous *in vivo* kinetic studies with *S. cerevisiae* (Wu *et al.* 2006) and *P. chrysogenum* (Nasution 2007) have shown that such fluxes can be quantified using the combination of offgas (O_2/CO_2) measurements together with element (carbon and degree of reduction) and ATP balances. In the previous *in vivo* kinetic studies of *E. coli* such an approach was not applied and assumptions were made such as a non-changing growth rate after the perturbation and sometimes the absence of product secretion. Also the ATP balance was not used for lack of knowledge of the ATP-stoichiometric parameters. Recently for *E. coli* these parameters were estimated (Taymaz-Nikerel *et al.* 2010a), allowing use of the ATP balance for this purpose.

Finally, in previous rapid perturbation experiments only the short glucose excess period was studied and no information was given on subsequent glucose starvation and return to the steady-state upon restart of previous steady-state feeding.

The goal of this work is to perform *in vivo* kinetic studies for *E. coli* carrying out rapid pulse experiments using the recently developed validated methods for analysis of a much wider range of intracellular metabolites (glycolysis, TCA cycle, pentose phosphate pathway (PPP), amino acids and nucleotides) and using offgas (O_2/CO_2) and dissolved O_2 (DO) measurements in combination with stoichiometric (carbon, redox, ATP) calculations to quantify growth rate, secreted fluxes and intracellular fluxes during the rapid pulse experiment covering the periods of glucose limitation, -excess, -starvation and return to the initial glucose-limited steady-state. Precautions were taken that no oxygen depletion could occur during the perturbation experiments.

5.2. Materials and Methods

5.2.1. Organism and chemostat conditions

The *E. coli* K12 MG1655 [λ^-, F$^-$, rph^{-1}, (*fnr*$^-$267)del] was cultivated in aerobic glucose-limited chemostat cultures (at 37 ^{o}C, pH 7) with 4 kg working mass in 7 l laboratory fermentors, controlled by weight (Applikon, Schiedam, The Netherlands). The dilution rate (D) was 0.1 h^{-1}. The mineral medium (Taymaz-Nikerel *et al.* 2009) contained 30 g/l glucose.H_2O and allowed a steady-state biomass concentration of about 10.5 gDW/l.

The operating conditions, measurement of offgas (O_2/CO_2), dissolved O_2, medium feeding and steady-state conditions were as described in Taymaz-Nikerel *et al.* (2009). The steady-state was analyzed for biomass, residual glucose, offgas (O_2/CO_2), possible secreted by-products and total organic carbon (TOC) for quantification of biomass lysis (Taymaz-Nikerel *et al.* 2009).

5.2.2. Glucose pulse experiment

To ensure a sufficient oxygen transfer, before the glucose pulse inlet air was blended with pure O_2 in order to have about 39 % O_2 in the incoming gas, as in De Mey *et al.* (2010b). The gas inflow rate was increased from 1.67 l/min air to 1.67 l/min air + 0.5 l/min O_2. Broth and filtrate sampling were carried out to determine the concentration of intracellular metabolites at steady-state before blending (Taymaz-Nikerel *et al.* 2009). When, after blending, the increased DO concentration in the fermentor reached its new steady-state, broth and filtrate sampling for intracellular metabolites was repeated in order to investigate whether the increased dissolved O_2 and decreased CO_2 levels would have an effect on the metabolism. Subsequently feed and outflow pumps were stopped just before the pulse.

The pulse experiment was planned to have an initial bulk glucose concentration of 0.5 g/l. Glucose solution was injected into the reactor (at t = 0) via a sterile syringe, the volume change caused by the added glucose solution being less than 0.5 %. After the pulse was given, the metabolite dynamics were followed by broth sampling from the fermentor during 20 min, using smaller sampling intervals for the first 6 min. Filtrate sampling was performed with cooling to about 1 ^{o}C using cold stainless steel beads, in order to determine concentration of residual glucose and possible secreted by-products, during the initial period of 360 s (Mashego *et al.* 2003). The glucose-medium feeding and broth outflow were restarted 510 s after the pulse. Offgas O_2/CO_2, DO concentration and pH were monitored online during the whole transient. The scheme of the pulse experiment is shown in Figure 5.1.

5.2.3. Rapid sampling

At steady-state: The differential method was used to obtain the amounts of intracellular metabolites (Taymaz-Nikerel *et al.* 2009). The required broth- and filtrate sampling was carried out as in Taymaz-Nikerel *et al.* (2009). Briefly 1 ml broth was, using a special rapid sampling device (Lange *et al.* 2001), withdrawn from the fermentor into tubes containing 5 ml of 60 % aqueous methanol precooled at -40 °C, which were immediately mixed after sampling by vortexing. Filtrate was sampled from the fermentor using syringe filtration (pore size 0.45 μm, cellulose acetate, Whatman GmbH, Germany) at room temperature without cold steel beads. After removal of the cells, the obtained filtrate was immediately mixed with 5 ml of 60 % aqueous methanol precooled at -40 °C in order to process these samples in the same way as the broth samples. The exact amount of samples obtained (for broth and filtrate) was quantified gravimetrically. For every steady-state condition two samples were taken and analyzed in duplicate. The intracellular metabolite amount is then obtained by difference (broth - filtrate) (Taymaz-Nikerel *et al.* 2009) and expressed in μmol/gDW.

During pulse: The differential method was used to obtain the amounts of intracellular metabolites (Taymaz-Nikerel *et al.* 2009) during the perturbation as well as for steady-state. Sampling for broth was performed as described above. The amount of metabolite in the filtrate during the pulse was found (data not shown) not to change (as expected due to the 10 h residence

time of the filtrate), which allows subtraction of filtrate amounts at pre-steady-state from broth amounts during the transient. For each time point one broth sample was taken and analyzed in duplicate. For measurement of extracellular glucose and secreted compounds during the transient, syringe filtration (pore size 0.45 μm, cellulose acetate, Whatman GmbH, Germany) with cold stainless steel beads (Mashego *et al.* 2003) was employed simultaneously with broth sampling using a second rapid sampling port. For each time point one sample was taken and analyzed in triplicate.
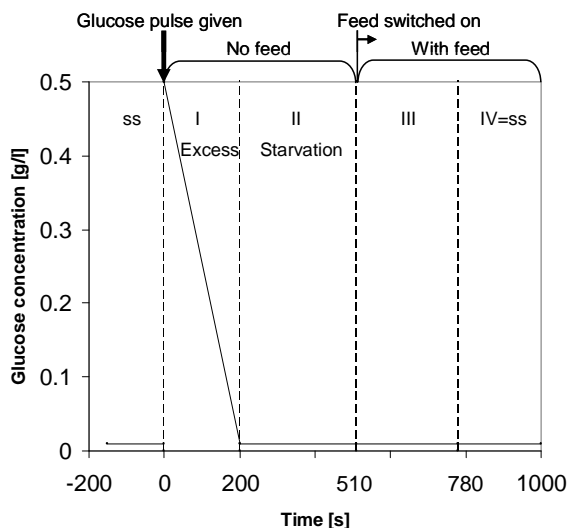
Figure 5.1: Scheme of the glucose pulse experiment.

5.2.4. Metabolite extraction procedure

Metabolites were extracted in 75 % boiling ethanol (3 min, 90 $^{\circ}$C) as described in Taymaz-Nikerel *et al.* (2009). It is noteworthy that before extraction, 100 μl of 100 % U-[13]C- labeled cell extract, obtained from an aerobic yeast culture as explained in Wu *et al.* (2005), was added to every sample as internal standard.

5.2.5. Analytical protocols

The protocols for cell dry weight, residual glucose, offgas (O_2/CO_2) and TOC (for biomass lysis) measurements were as described in Taymaz-Nikerel *et al.* (2009).

Measurement of organic acids and ethanol in the supernatant: The supernatant samples obtained after the glucose pulse were extensively analyzed for possible organic acid and ethanol secretions. Commercial enzymatic kits (Boehringer Mannheim/R-Biopharm, Roche) were used

for the measurement of acetate, lactate and formate concentrations. HPLC (Aminex HPX-87H ion exclusion column, Bio-Rad, CA, USA), LC-MS/MS (van Dam *et al.* 2002) and NMR analysis were performed to check the presence of organic acids such as fumarate, pyruvate, malate, succinate, citrate and α-ketoglutarate. Ethanol presence was checked with gas chromatography (Chrompack CO 9001, Hewlett Packard, Palo Alto, CA) using a flame ionization detector.

Measurement of intracellular metabolite concentrations: Metabolites of the glycolysis, TCA cycle and PPP were quantified with IDMS described by van Dam *et al.* (2002) and Wu *et al.* (2005). Amino acids were quantified with IDMS applying GC-MS as described in Taymaz-Nikerel *et al.* (2009). The concentrations of the nucleotides were also analyzed with IDMS and further details of the applied LC–ESI–MS/MS procedure have been described elsewhere (Seifar *et al.* 2009).

5.2.6. Calculation methods

Biomass-specific rates during steady-state: The biomass-specific glucose consumption rate (-q_S), oxygen consumption rate (-q_{O2}), carbon dioxide production rate (q_{CO2}), the growth rate (μ) and the cell lysis rate (q_{lysis}) were calculated (in units of mmol *i*/h/Cmol X) from the respective mass balances. q_{lysis} is calculated from the difference between measured TOC content in the broth and TOC content in the culture supernatant. The specific growth rate, μ, is then the sum of the dilution rate in the chemostat and q_{lysis} (Taymaz-Nikerel *et al.* 2009).

Biomass-specific rates during the pulse experiment: -q_S was obtained from the measured extracellular glucose concentration and the glucose mass balance. q_i of secreted by-products can be obtained by analyzing these products in filtrate during the pulse, as has been shown before for ethanol production by *S. cerevisiae* (Theobald *et al.* 1997; Wu *et al.* 2006). During the transient μ cannot be reliably obtained from the biomass mass balance because only a very small change in biomass concentration can be expected during the pulse experiment (maximum increase of about 0.25 gDW/l with about 10.5 gDW/l biomass present). This small (2 %) increase cannot be measured reliably using biomass dry weight analysis. Therefore we adopted the use of the ATP balance to calculate μ during the pulse using -q_{O2} during the pulse obtained at a seconds time scale resolution. To obtain this dynamic -q_{O2}, the dynamic dissolved O_2-mass balance is applied using the measured dissolved O_2-profile during the pulse, a validated k_La value and the properly validated measurement of dynamic response of the dissolved O_2 probe (see Appendix 5.5.1 for the full details). The obtained -q_{O2} is used with the available validated stoichiometric ATP model (steady-state (Taymaz-Nikerel *et al.* 2010a)), which leads to the O_2-Herbert-Pirt relation allowing the calculation of the dynamic changing μ from the dynamic changing -q_{O2} (Appendix 5.5.2). For this approach a steady-state of the ATP pool is required, which however also applies as pseudo-steady-state during the pulse due to the very low turnover time of ATP (~ 1 s, see Table 5.4). As an independent check -q_S', which is the substrate used for biomass synthesis, can be calculated from μ as calculated with the substrate Herbert-Pirt relation (Appendix 5.5.2). Subsequently this

calculated $-q_S'$ can be compared to the measured $-q_S$. This calculation depends on accurate values for k_La value as shown by a sensitivity analysis (see Appendix 5.5.5).

Mass Action Ratio (MAR): To calculate the thermodynamic feasibility of the flux direction for near-equilibrium reactions, it is useful to calculate the MAR. For a reversible reaction $aA + bB \leftrightarrow cC + dD$, the corresponding MAR is calculated as $(C^c D^d)/(A^a B^b)$.

Intracellular NAD$^+$/NADH ratio: The reaction catalyzed by mannitol-1-phophate-5-dehydrogenase, known to operate close to equilibrium, with the measured fructose-6-phospate (F6P) and mannitol-1P levels was used to estimate the *in vivo* NAD$^+$/NADH ratio (assuming an intracellular pH of 7.0). This was described before in Taymaz-Nikerel *et al.* (2009).

Adenylate energy charge: Energy charge (EC) was calculated according to

$$EC = \frac{ATP + (ADP/2)}{ATP + ADP + AMP}.$$

E4P concentration: See Appendix 5.5.3.

Intracellular fluxes: The intracellular fluxes were calculated with metabolic flux analysis (MFA) using the metabolic network of *E. coli* for growth on glucose described in Taymaz-Nikerel *et al.* (2010a). In this network the PEP-glyoxylate cycle (PEP carboxykinase (PPCK), isocitrate lyase (ICL), and malate synthase(MALS)), shown to be operating at low growth rates (Fischer and Sauer 2003), was incorporated. The addition of this cycle created a parallel pathway, which requires additional information to perform MFA. The ratios of $Flux_{PPC}/ Flux_{PPCK} = 2$ and $Flux_{ICL} = 0.3 \times Flux_{ACoNT}$ were assumed since these average ratios were observed at dilution rates $0.1 - 0.4 \ h^{-1}$ in glucose-limited continuous cultures of *E. coli* (Nanchen *et al.* 2006).

Turnover times: The turnover times of the intracellular compounds were calculated with the equation, $\tau = c_i /F_i$, where τ [s] is the turnover time, c_i [µmol/gDW] is the steady-state intracellular amount in the pool of compound i and F_i [µmol/gDW/s] is the total incoming flux into the pool i at steady-state (or pseudo-steady-state) obtained using intracellular fluxes (with MFA as above).

5.3. Results and Discussion

To reliably elucidate the *in vivo* dynamics of the intra/extracellular metabolite concentrations and fluxes in response to pulse addition of glucose under aerobic glucose-limiting conditions for *E. coli* K12 MG1655, the stimulus-response experiments were performed in duplicate using two independent chemostat cultures (Chemostat 1, 2).

5.3.1. Steady-state characteristics

Uptake/secretion fluxes: Metabolic steady-state of *E. coli* in the chemostats was achieved by cultivating the cells using a dilution rate of $0.1 \ h^{-1}$, yielding about 10.5 gDW/l cell dry weight as

steady-state biomass concentration. The obtained biomass-specific rates at steady-state in two independent chemostats are given in Table 5.1. The presence of cell lysis was also found previously (Taymaz-Nikerel *et al.* 2010a; Taymaz-Nikerel *et al.* 2009). The recovery of carbon and degree of reduction balances (whereby the biomass composition reported in Taymaz-Nikerel *et al.* (2010a) was used) were close to 100 % (Table 5.1) allowing data reconciliation (χ^2 test used with a null hypothesis of significant measurement deviations at a significance level of 0.1 %). Using the reconciled μ, the rates -q_S, -q_{O2} and q_{CO2} were calculated by means of the previously established stoichiometric model (Taymaz-Nikerel *et al.* 2010a). The last column of Table 5.1 shows a very close agreement between the reconciled rates in Chemostat 1, 2 and the rates obtained via metabolic flux analysis of the stoichiometric network model.

The enrichment of inlet air with pure O_2 was necessary before perturbation experiments, in order to avoid O_2 limitation for cells during the stimulus-response experiments. The blending of air increased the DO concentration from the steady-state value of 78 % (0.178 mmol O_2/l) to a new steady-state of 196 % (0.444 mmol O_2/l). The steady-state specific rates (Table 5.1) were not affected (data not shown) by the change in DO concentration.

Table 5.1: Average cell dry weight concentration [gDW/l], measured, reconciled and expected (from stoichiometric model (Taymaz-Nikerel *et al.* 2010a)) biomass-specific rates (q_i, expressed per Cmol of biomass [mmol/CmolX/h]), carbon (C) and degree of reduction (γ) recoveries [%] of the steady-state aerobic glucose-limited chemostat cultivations of *E. coli* at a dilution rate of 0.1 h^{-1}

	Chemostat 1		Chemostat 2		Expected from stoichiometric model[a]
	Measured	**Reconciled**	**Measured**	**Reconciled**	
C_X	10.72 ± 0.05		10.44 ± 0.15		
μ	120.83 ± 2.43	120.58 ± 2.40	120.16 ± 2.36	120.10 ± 2.37	120.34 ± 2.39
-q_S	33.04 ± 1.20	34.28 ± 0.85	33.32 ± 1.29	34.27 ± 0.88	34.44 ± 1.80
-q_{O2}	79.30 ± 3.05	76.80 ± 2.9	78.34 ± 3.12	77.28 ± 3.1	77.07 ± 10.31
q_{CO2}	84.87 ± 3.26	85.07 ± 3.0	85.15 ± 3.39	85.52 ± 3.2	86.30 ± 10.33
q_{lysis}	16.35 ± 0.67	16.42 ± 0.67	18.23 ± 0.61	18.39 ± 0.59	
C Recovery	103.8 ± 6.8		102.7 ± 6.2		
γ Recovery	105.6 ± 6.1		103.9 ± 5.4		

[a] The average μ was input to the stoichiometric network model for carrying out metabolic flux analysis.

Intracellular metabolite levels: During the steady-state, samples were taken for measurement of intracellular metabolites in central metabolism (glycolysis, TCA cycle, PPP), free amino acids and nucleotides at the two different DO concentration values, to check for a possible effect on the intracellular metabolite amounts from the higher dissolved oxygen and lower carbon dioxide concentrations. In Table 5.2 the steady-state intracellular amounts of metabolites are shown at these two different DO concentrations for the two independent chemostat experiments. The

amount of nucleotides present extracellular were either below the detection limit or not present at all, therefore for nucleotides, amounts in broth samples are presented.

Table 5.2 shows that for each of the chemostat experiments the increase in DO concentration did not affect the metabolite levels significantly. However when we compare the average (DO = 78 and 196 %) metabolite amounts in the two chemostats, some differences can be seen. The amounts of glycolytic metabolites in the two chemostats were highly reproducible. However, not all the intermediates of TCA cycle, amino acids and nucleotides were measured to be the same, with (for some metabolites) a difference of up to a factor 2 - 3. There is no clear answer for the discrepancy in metabolite levels between the two experiments. However, most of the results were very comparable to the previously found values under the same conditions (Taymaz-Nikerel *et al.* 2009).

It is remarkable that most amino acid amounts were rather low (< 0.5 μmol/gDW); only Gln, Lys, Glu, Asp, Pro, Gly and Ala are 1 - 5 μmol/gDW. Clearly Glu (> 60 μmol/gDW) dominated all amino acids, representing 80 % of the total amino acid pool.

The obtained metabolome data were checked in terms of thermodynamic acceptability in relation to the known flux direction. The mass action ratios (MARs), which should be close to or lower than the equilibrium constant (K_{eq}), of some known near-equilibrium reactions were calculated and compared with the published K_{eq} (Table 5.3). In general, the two chemostat experiments depicted similar values with some exceptions that are due to the difference in metabolite measurements in the two cultures (Table 5.2). It can be seen that the MAR of the reactions catalyzed by phosphoglucose isomerase (PGI) in Chemostat 1, mannose-6-phosphate isomerase (PMI), adenylate kinase (AK) in Chemostat 1, fumarase (FUM) in Chemostat 1 are very close to their known K_{eq}. These results are thermodynamically consistent. The steady state *in vivo* MAR of PGM+ENO is close also to the value (~ 1) found in *S. cerevisiae* (Canelas *et al.* 2008b; Mashego *et al.* 2006).

Comparable values (~ 60) for the *in vivo* NAD$^+$/NADH ratio, which is an important parameter in physiological studies, were obtained for two different cultures which are also close to the value (48) of our previous work (Taymaz-Nikerel *et al.* 2009). These results show that nearly all (> 98 %) of NAD(H) is in its oxidized form. These high NAD$^+$/NADH values are required to obtain a negative ΔG_R (2nd law of thermodynamics) of the steps between phosphofructose kinase (PFK) and phosphoglycerate kinase (PGK) in glycolysis (Canelas *et al.* 2008b). In the present work ΔG_R is found to be -0.85 kJ/mol, agreeing with the 2nd law of thermodynamics and showing that this part of glycolysis is close to equilibrium.

The adenylate energy charge was close to 0.90 for Chemostat 2 as expected, since for healthy growing cells it is generally stable at values around 0.8 to 0.9 (Chapman *et al.* 1971). Chemostat 1 showed a much lower value which points to a possible error in the ADP analysis result of this experiment, which is also seen in the deviating MAR for AK.

Table 5.2: Steady-state intracellular amount of intermediates [before (DO = 78 %), after (DO = 196 %) blending of inlet air with O_2 and average of those] and metabolite pool turnover time (τ) in two independent chemosats

	Chemostat 1				Chemostat 2			
	DO = 78 % [µmol/gDW]	DO = 196 % [µmol/gDW]	Average [µmol/gDW]	τ [s]	DO = 78 % [µmol/gDW]	DO = 196 % [µmol/gDW]	Average [µmol/gDW]	τ [s]
Central Metabolites								
G1P	ND	0.14 ± 0.01			ND	0.16 ± 0.19		
G6P	1.41 ± 0.05	1.76 ± 0.06	1.59 ± 0.08	**3.8**	1.05 ± 0.15	1.35 ± 0.03	1.20 ± 0.15	**2.9**
F6P	0.41 ± 0.02	0.42 ± 0.03	0.42 ± 0.04	**1.4**	0.48 ± 0.05	0.59 ± 0.01	0.53 ± 0.05	**1.8**
T6P	0.12 ± 0.01	0.141 ± 0.005	0.13 ± 0.01		0.10 ± 0.02	0.17 ± 0.02	0.14 ± 0.03	
M6P	0.46 ± 0.01	0.52 ± 0.01	0.49 ± 0.02		0.55 ± 0.01	0.559 ± 0.005	0.56 ± 0.01	
6PG	0.20 ± 0.04	0.21 ± 0.03	0.21 ± 0.05	**0.9**	0.17 ± 0.02	0.22 ± 0.02	0.19 ± 0.02	**0.9**
Mannitol-1P	0.91 ± 0.06	1.10 ± 0.06	1.01 ± 0.09		1.14 ± 0.03	1.23 ± 0.02	1.18 ± 0.03	
FBP[a]	0.69 ± 0.11	0.38 ± 0.03	0.53 ± 0.11	**1.8**	0.66 ± 0.06	0.63 ± 0.03	0.65 ± 0.07	**2.1**
G3P	0.24 ± 0.02	0.27 ± 0.01	0.26 ± 0.02	**5.1**	0.43 ± 0.03	0.46 ± 0.03	0.44 ± 0.05	**8.7**
F2,6bP	0.31 ± 0.02	0.40 ± 0.05	0.35 ± 0.05		0.59 ± 0.06	0.69 ± 0.06	0.64 ± 0.08	
2PG/3PG	1.18 ± 0.05	1.52 ± 0.06	1.35 ± 0.08	**2.0**	1.80 ± 0.02	1.90 ± 0.03	1.85 ± 0.04	**2.8**
PEP	1.38 ± 0.05	1.72 ± 0.08	1.55 ± 0.09	**2.6**	1.73 ± 0.02	1.94 ± 0.03	1.84 ± 0.04	**3.1**
Pyruvate	0.62 ± 0.09	0.51 ± 0.01	0.57 ± 0.09	**1.1**	0.37 ± 0.07	0.53 ± 0.08	0.79 ± 0.10	**1.5**
Citrate[a]	10.36 ± 0.17	11.24 ± 0.28	10.80 ± 0.33	**43.3**	3.91 ± 0.12	4.20 ± 0.15	4.05 ± 0.19	**16.3**
α-KG	0.29 ± 0.01	0.32 ± 0.01	0.30 ± 0.01	**0.7**	0.91 ± 0.30	1.21 ± 0.19	1.06 ± 0.36	**2.4**
Succinate	2.22 ± 0.47	1.79 ± 0.19	2.00 ± 0.51	**10.0**	ND	ND		**-**
Fumarate	0.22 ± 0.01	0.25 ± 0.01	0.24 ± 0.01	**1.1**	0.34 ± 0.02	0.39 ± 0.03	0.37 ± 0.03	**1.6**
Malate	0.76 ± 0.03	0.88 ± 0.03	0.82 ± 0.04	**2.8**	1.65 ± 0.15	1.98 ± 0.21	1.81 ± 0.25	**6.1**
Amino Acids								
E4P-derived								
His	0.11 ± 0.02	0.11 ± 0.03	0.11 ± 0.04	**26.1**	0.10 ± 0.03	0.17 ± 0.01	0.13 ± 0.03	**32.9**
Phe	0.08 ± 0.03	0.08 ± 0.10	0.08 ± 0.11	**10.1**	0.25 ± 0.04	0.45 ± 0.05	0.35 ± 0.07	**44.8**
Tyr	0.22 ± 0.05	0.14 ± 0.02	0.18 ± 0.05	**27.9**	0.19 ± 0.01	0.24 ± 0.02	0.21 ± 0.02	**33.3**
3PG-derived								
Gly	1.15 ± 0.15	1.41 ± 0.25	1.28 ± 0.29	**26.7**	3.02 ± 0.17	2.89 ± 0.10	2.96 ± 0.19	**61.7**
Trp	0.03 ± 0.01	0.02 ± 0.01	0.02 ± 0.01	**9.4**	0.029 ± 0.002	0.028 ± 0.002	0.028 ± 0.003	**11.1**
Ser	0.23 ± 0.21	0.40 ± 0.23	0.32 ± 0.31	**3.7**	0.85 ± 0.23	0.30 ± 0.30	0.57 ± 0.38	**6.8**
Pyr-derived								
Ala	1.17 ± 0.12	1.14 ± 0.09	1.16 ± 0.15	**44.7**	2.33 ± 0.07	2.31 ± 0.02	2.32 ± 0.07	**89.7**
Val	0.67 ± 0.22	0.32 ± 0.03	0.50 ± 0.22	**29.6**	0.59 ± 0.02	0.54 ± 0.14	0.56 ± 0.14	**33.6**
Leu	0.41 ± 0.08	0.27 ± 0.01	0.34 ± 0.08	**28.1**	0.47 ± 0.02	0.48 ± 0.02	0.48 ± 0.03	**39.6**
αKG-derived								
Glu	58.88 ± 1.71	67.92 ± 1.17	63.40 ± 2.08	**179.7**	83.73 ± 0.94	87.80 ± 1.21	85.76 ± 1.53	**243.1**
Gln	8.64 ± 0.19	10.05 ± 0.19	9.34 ± 0.27	**181.6**	4.55 ± 0.09	4.50 ± 0.30	4.52 ± 0.31	**87.9**
Lys	1.14 ± 0.08	1.17 ± 0.05	1.15 ± 0.09	**85.6**	2.10 ± 0.02	2.24 ± 0.02	2.17 ± 0.03	**160.9**
Pro	0.61 ± 0.04	0.61 ± 0.03	0.61 ± 0.05	**65.8**	1.33 ± 0.02	1.29 ± 0.02	1.31 ± 0.03	**140.9**
Orn	0.33 ± 0.08	0.37 ± 0.08	0.35 ± 0.12	**27.2**	0.75 ± 0.08	0.85 ± 0.05	0.80 ± 0.10	**62.6**
Oaa-derived								
Asp	2.07 ± 0.09	2.26 ± 0.09	2.16 ± 0.13	**30.7**	4.01 ± 0.08	4.01 ± 0.07	4.01 ± 0.10	**57.0**
Asn	0.55 ± 0.03	0.59 ± 0.02	0.57 ± 0.03	**48.1**	0.60 ± 0.03	0.67 ± 0.02	0.63 ± 0.03	**53.3**
Thr	0.39 ± 0.05	0.39 ± 0.05	0.39 ± 0.07	**16.8**	0.79 ± 0.03	0.85 ± 0.02	0.82 ± 0.03	**35.4**
Ile	0.19 ± 0.07	0.06 ± 0.01	0.13 ± 0.07	**11.4**	0.08 ± 0.01	0.15 ± 0.05	0.11 ± 0.05	**10.3**
Cys	0.15 ± 0.08	0.35 ± 0.09	0.25 ± 0.12	**25.6**	0.06 ± 0.02	0.11 ± 0.03	0.09 ± 0.04	**8.9**

Table 5.2 continued

Met	0.05 ± 0.01	0.03 ± 0.01	0.04 ± 0.01	**6.4**	0.107 ± 0.003	0.11 ± 0.01	0.11 ± 0.01	**18.1**
Nucleotides								
AMP	1.03 ± 0.11	0.99 ± 0.10	1.01 ± 0.15	**7.4**	0.24 ± 0.13	0.48 ± 0.15	0.36 ± 0.20	**2.6**
ADP	3.22 ± 0.05	3.23 ± 0.08	3.22 ± 0.10	**0.9**	0.91 ± 0.04	0.89 ± 0.04	0.90 ± 0.06	**0.3**
ATP	4.99 ± 0.16	6.42 ± 0.22	5.71 ± 0.27	**1.7**	4.74 ± 0.13	4.73 ± 0.18	4.74 ± 0.22	**1.4**
CMP	ND	ND			ND	ND		
CDP	0.13 ± 0.02	0.16 ± 0.02	0.14 ± 0.02		0.27 ± 0.01	0.30 ± 0.02	0.28 ± 0.03	
CTP	ND	ND			ND	ND		
UMP	0.16 ± 0.03	0.28 ± 0.05	$0.22 \quad 0.03$		ND	ND		
UDP	0.69 ± 0.03	0.77 ± 0.04	0.73 ± 0.05		0.48 ± 0.06	0.48 ± 0.05	0.48 ± 0.07	
UTP	1.80 ± 0.09	2.24 ± 0.13	2.02 ± 0.16		2.84 ± 0.07	2.77 ± 0.06	2.80 ± 0.09	
GMP	ND	ND			ND	ND		
GDP	0.70 ± 0.01	0.74 ± 0.03	0.72 ± 0.03		0.34 ± 0.04	0.30 ± 0.02	0.32 ± 0.04	
GTP	1.23 ± 0.06	1.41 ± 0.07	1.32 ± 0.09		1.99 ± 0.28	1.74 ± 0.15	1.87 ± 0.32	
IMP	ND	ND			ND	ND		
IDP	0.36 ± 0.02	0.33 ± 0.02	0.35 ± 0.03		ND	ND		
ITP	0.47 ± 0.02	0.51 ± 0.02	0.49 ± 0.02		ND	ND		

[a] Amount in the broth samples.

Intracellular Fluxes: The steady-state intracellular fluxes of the central metabolism in *E. coli* (see Figure 5.6) were calculated with the known inputs (Table 5.1, reconciled rates) of steady-state $-q_S$, $-q_{O2}$ and μ and the set flux ratios (see Materials and Methods). In this network it is seen that 55 % of the substrate uptake enters in PPP and 45 % goes to glycolysis. The higher ratio towards PPP is a result of the assumed presence of the glyoxylate pathway (Fischer and Sauer 2003; Nanchen *et al.* 2006), which decreases the flux of isocitrate dehydrogenase (ICDH) that is NADPH dependent. The lower production of NADPH via ICDH is then compensated with higher NADPH production in the PPP.

Table 5.3: Steady-state mass action ratios (MAR), NAD$^+$/NADH ratio and energy charge calculated from the measured metabolite levels and range of published equilibrium constants (Goldberg *et al.* 2004) for some relevant equilibrium reactions

	Reaction	MAR or Metabolite ratio		K_{eq}
		Chemostat 1	Chemostat 2	
PGI	G6P $\leftrightarrow$ F6P	0.26 ± 0.01	0.44 ± 0.04	0.19 - 0.67
PMI	F6P $\leftrightarrow$ M6P	1.18 ± 0.06	1.04 ± 0.05	0.99 - 1.80
PGM+ENO	2+3PG $\leftrightarrow$ PEP	1.15 ± 0.05	0.99 ± 0.02	0.10 - 1.79
AK	2ADP $\leftrightarrow$ AMP + ATP	0.56 ± 0.04	2.11 ± 0.59	0.20 - 1.45
FUM	Fumarate + H_2O $\leftrightarrow$ Malate	3.48 ± 0.12	4.89 ± 0.43	2.10 - 9.49
PEP/Pyruvate		2.74 ± 0.24	2.34 ± 0.15	
NAD$^+$/NADH		52.5 ± 3.36	56.8 ± 3.00	
Energy charge		0.74 ± 0.03	0.87 ± 0.04	

Turnover times: The availability of intracellular flux data with the intracellular metabolite concentration data allows calculating the turnover times (τ) of metabolite pools. For the steady-state, results are shown in Table 5.2, depicting that the central metabolites and adenine nucleotides have a much lower turnover time (1 - 10 s) compared to most of the amino acids (5 - 50 s). Remarkably, some of the amino acids, i.e. Ile, Ser, Trp and Cys, have τ values comparable to central metabolites, which is of course due to the very low amino acid levels. Most amino acids have a τ value in the range of 10 - 60 s and Glu has the highest τ (180 - 240 s). This means that changes can be expected also in the amounts of intracellular amino acids during the pulse experiment, which has a time frame of about 200 s.

5.3.2. Dynamic response characteristics

General observations

The above characterized steady-states of two aerobic glucose-limited chemostat cultures were subjected to a glucose pulse via increasing the glucose concentration in the culture from its limiting value of 14 mg/l to 500 mg/l (see Figure 5.1). Figure 5.2 shows the online extracellular concentration measurements (DO, O_2/CO_2 in the offgas and pH) and Figure 5.3 shows the residual concentration of glucose as function of time in two independent chemostats. These results indicate that the pulse experiment is very reproducible in the two different chemostats with respect to four phases that can be distinguished after the pulse (Figure 5.2). In phase I (0 - 200 s), called glucose excess, the added extra glucose was rapidly consumed leading to decreased DO concentration, decreased offgas O_2 concentration, increased offgas CO_2 concentration and a pH dip. This clearly shows that the increased glucose uptake is accompanied by increased O_2 consumption and CO_2 production. In phase II (200 - 510 s), called glucose starvation, despite the lack of external substrate supply, there was still O_2 consumption and CO_2 production albeit at much decreased levels. In phase III (510 - 800 s) there was a restart of feed and outflow, leading to a constant glucose supply rate equal to its previous steady-state value. In this period O_2 consumption and CO_2 production slowly increased. In phase IV (> 800 s) the previous steady-state was recovered as observed from online measurements. It is satisfactory to see that all online concentration measurements return to their previous steady-state values.

Dynamics of uptake/secretion rates after the glucose pulse

Specific uptake rate of glucose: The glucose concentration after the pulse decreased nearly linear and glucose was consumed in about 200 s (Figure 5.3). The substrate uptake rate ($-q_S$) was found to be 121.10 and 111.11 mmol/CmolX/h for Chemostat 1 and for Chemostat 2, respectively, which is on average a 3.4 fold increase compared to the reference steady-state. The average $-q_S$ (116.1 mmol/CmolX/h) is lower than the maximal glucose uptake rate observed in batch which is about 276 mmol/CmolX /h (not shown) and is also lower than the reported maximum glucose uptake rate for *E. coli* MG1655 (11mmol/g/h = 255.2 mmol/CmolX/h, (Fischer *et al.* 2004)). As
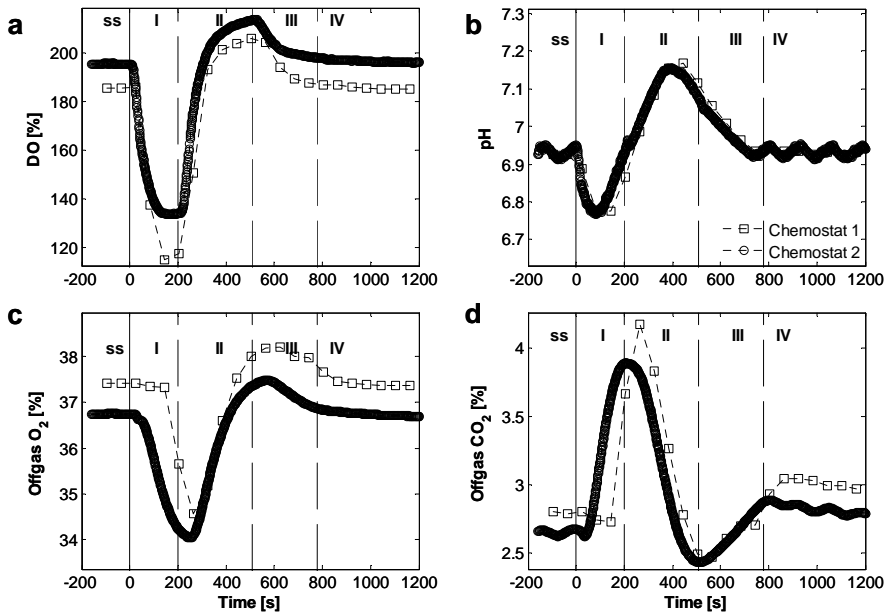
Figure 5.2: Measurements of (a) Dissolved oxygen (DO) [%], (b) pH, (c) offgas O$_2$ [%] and (d) offgas CO$_2$ [%] in the time-frame of pulse. Pulse was given at time 0.

can be expected, *E. coli* cultured at $\mu = 0.12$ h^{-1} (Table 5.1) has indeed a significantly lower maximal glucose uptake capacity than cells cultured in batch ($\mu^{max} \sim 0.7$ h^{-1}) (116 versus 276 mmol glucose/CmolX/h).

Fluxes of secreted by-products: It can be expected that certain compounds (acids or alcohols) are secreted after the glucose pulse, i.e. pyruvate and acetate are well known products for *E. coli*. Therefore filtrate samples, taken at the end of the glucose consumption period (~ 200 s), were analyzed (for ethanol, acetate, lactate, formate, fumarate, pyruvate, malate, succinate, citrate, α-ketoglutarate) using various techniques (GC, HPLC, enzyme-based, NMR and LC-MS/MS). The measured metabolite concentration results (see Appendix 5.5.4, Table 5.5) lead to the conclusion that there were hardly any compounds secreted during the pulse. In the work of Lara *et al.* (2009), using a different *E. coli* strain, extracellular acetate and formate accumulation was reported after a glucose pulse to a glucose-limited culture where the pulse was given outside the reactor, using the BioScope. In that work -q$_S$ was increased 10 fold but even then the secreted concentrations were very low which supports the present findings. Also Link *et al.* (2010) tested the response of *E. coli* after excess supplement of glucose by transferring the fed-batch grown cells to batch reactors. In contrast to our results, they have observed acetate and formate excretion after the glucose pulse. The production of these by-products might be due to the much higher concentration of glucose given (~ 8 g/l against 0.5 g/l glucose in our experiment) or due to possible oxygen depletion/limitation during the pulse and as a result of possible anaerobiosis.

The observed pH-dip, in the absence of secreted organic acids, after the pulse (Figure 5.2) is readily explained by the increased CO$_2$ concentration in the offgas, leading to increased dissolved

CO_2, which dissociates rapidly into HCO_3^- and H^+. The pH increase after 100 s was due to the pH control which was in operation throughout the whole experiment. After depletion of glucose (> 200 s, phase II), an increase in pH was observed (see Figure 5.2), which correlates with the decreased CO_2 production and hence decreased broth CO_2 concentration, leading to conversion of dissolved HCO_3^- into CO_2 and OH^-.
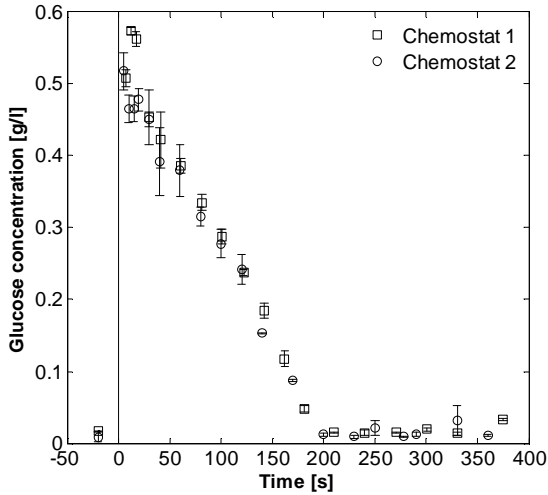
Figure 5.3: Residual glucose concentration [g/l] with time [s]. Pulse was given at time 0.

Specific oxygen uptake rate: The measured O_2/CO_2 offgas data alone was not informative enough to calculate, using dynamic gas phase balances, $-q_{O2}$ and q_{CO2} as function of time (at seconds time scale) due to the fermentor parameters such as large dead volumes (headspace and tubing) which cause gas mixing effects and time delay and the bicarbonate buffering of broth which severely adds to offgas CO_2 dynamics. Furthermore dynamics in the measured O_2/CO_2 mole fraction is influenced by offgas sensor dynamics and process and measurement noises (Wu *et al.* 2003). Therefore online dissolved O_2 concentration data were used to calculate $-q_{O2}$ from the dynamic dissolved O_2 mass balance while taking into account the dynamics of the DO-sensor (see Appendix 5.5.1). Figure 5.4a presents the results, which clearly shows the time varying O_2 consumption rate ($-q_{O2}(t)$) at seconds time resolution in the four phases mentioned above.

In phase I the 3.4 fold-increased $-q_S$ caused a 3.2 fold increase in $-q_{O2}$ within 10 s (-77.3 to -250 mmol O_2/Cmol X/h). A new steady-state in $-q_{O2}$ was reached after about 50 s (Figure 5.4a). These rapid dynamics can be understood given the very low turnover time of metabolites in glycolysis, TCA cycle and ATP (Table 5.2). In phase II the oxygen consumption steeply decreased in several tens of seconds to a very low value of about 35 mmol O_2/Cmol X/h (Figure 5.4a), which was 2.2 fold lower than the steady-state value and close to the maintenance O_2-consumption rate of 21.54 mmol O_2/Cmol X/h (Appendix 5.5.2 and Taymaz-Nikerel *et al.* (2010a)). This consumed O_2
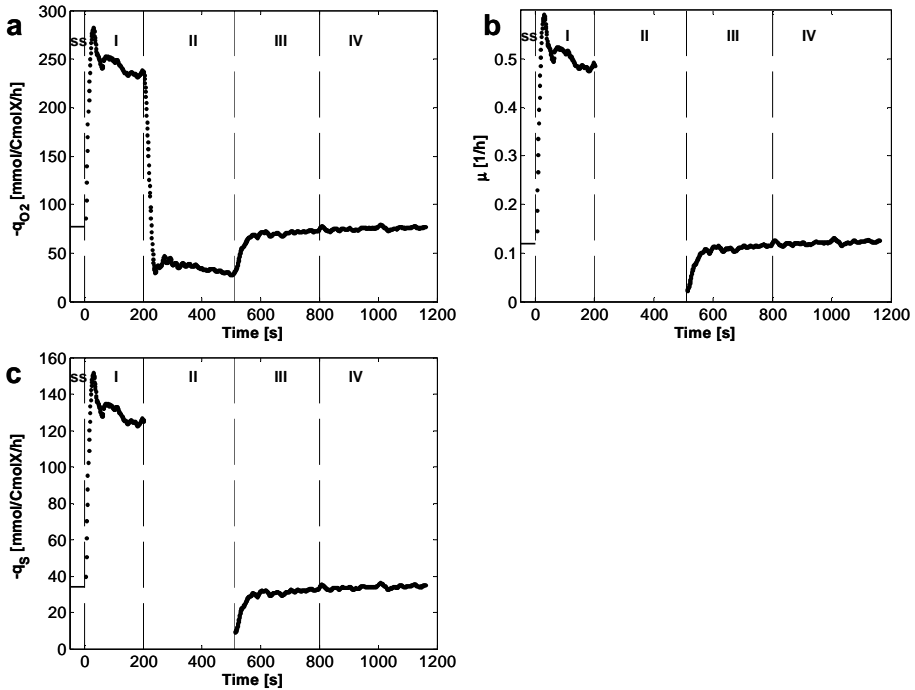
Figure 5.4: (a) Calculated $-q_{O2}$ from the dissolved O_2 mass balance, (b) Calculated μ from Herbert-Pirt relation and (c) $-q_S$ calculated from Herbert-Pirt relation for Chemostat 2. Pulse was given at time 0.

requires electron donor, which cannot be taken up from the supernatant because glucose and secreted products were absent. Therefore the consumed electrons must be supplied from intracellular metabolites which have accumulated in phase I and are consumed in phase II (see below). In phase III/IV $-q_{O2}$ quickly returned to its original steady-state level due to the glucose feeding.

Specific growth rate: In phase I growth rate, μ(t), was calculated from the obtained $-q_{O2}$(t) and the Herbert-Pirt relation, which gives $-q_{O2}$ as function of μ (Appendix 5.5.2) (Taymaz-Nikerel *et al.* 2010a). This calculation is essentially based on the ATP-balance and the pseudo-state property of the ATP pool during the transient because the turnover time of the ATP pool is ≤ 1 s (see calculation methods section in Materials and methods). The results (Figure 5.4b) show that, following the glucose pulse, the growth rate μ increased very rapidly (in several tens of seconds) from its steady-state value of 0.12 h^{-1} to 0.48 h^{-1}. This shoot-up is reasonable since $μ^{max}$, measured during the batch, was 0.7 h^{-1} (data not shown). The change in the stoichiometry (decreased ratio of q_{O2}/q_S) can be fully explained by the increased μ and is due to a lower impact of maintenance at high μ. This well known phenomenon was also observed before in our previous steady-state chemostat conditions: cultures run at high growth rates yield lower q_{O2}/q_S ratios due to less impact of maintenance (Taymaz-Nikerel *et al.* 2010a).

109

Having the information of $\mu(t)$, the Herbert-Pirt relation for substrate uptake allows calculating the substrate uptake rate $-q_S'(t)$ required to synthesize biomass (see Materials and methods). In phase I the calculated pseudo-steady-state $-q_S'$ was about 128 mmol/CmolX/h (Figure 5.4c), which is about 10 % higher than the measured $-q_S$ (116 mmol/CmolX/h). The $-q_S'(t)$ result in phase I can be used to construct the $C_S'(t)$ curve showing the amount of substrate used for growth. The expectation would be that $C_S'(t) > C_S(t)$, where the difference would be the amount of intracellularly accumulated changed metabolite levels to accommodate the increased fluxes in phase I. However C_S' was slightly lower than the C_S (Figure 5.5). The small discrepancy is probably due to small errors in the measurement for DO and the calculated k_La value (see Appendix 5.5.1) which leads to errors in $-q_{O2}(t)$ and the $-q_S'$ (t). For example, a 10 % lower k_La value brings the measured and calculated values for q_S and C_S much closer (see Appendix 5.5.5, Figure 5.14). This calculation shows that in phase I, also during the transient, O_2-consumption and glucose consumption are in close agreement with the established steady-state stoichiometry where glucose is used for growth and maintenance only. This is completely due to the pseudo-steady-state property of the ATP pool during the transient.
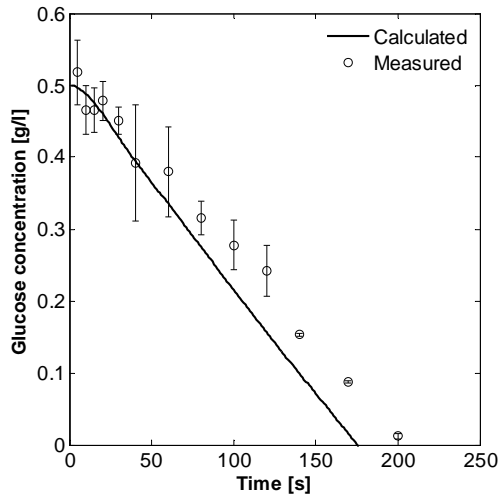
Figure 5.5: Comparison of the residual glucose concentration calculated from Herbert-Pirt relation to the measured concentration (Chemostat 2).

In phase II the glucose-based Herbert-Pirt relation cannot be used to obtain μ from $-q_{O2}$ because the electron donor is not glucose but most likely a mixture of intracellular metabolites which were accumulated in phase I (see below). In phase III glucose is again the electron donor and we can again obtain $\mu(t)$ from $-q_{O2}(t)$ as before. It is observed that $\mu(t)$ rapidly (in tens of seconds) increased from a very low value (~ 0.02 h^{-1}) to the previous steady-state value of 0.12 h^{-1}. The calculated $-q_S'$ (from Herbert-Pirt) increased rapidly to the previous steady-state value as well. It was found that in the first part of phase III, $-q_S'(t)$ was smaller than the $-q_S$, the difference being

used to rebuild the intracellular metabolite levels from their low phase II-levels to the steady-state levels (phase III, IV).

Intracellular fluxes during glucose excess

Figure 5.6 shows the flux distribution through central carbon metabolism in the pseudo-steady-state of phase I as fold changes relative to the fluxes at steady-state before perturbation. It is seen that the 3.4 fold increase of the substrate uptake rate, 2.8 fold increase of the oxygen consumption rate and 3.7 fold increase of the growth rate causes the glycolytic fluxes to increase ~ 3.2 fold and TCA cycle fluxes ~ 2.5 fold (Figure 5.6). The flux (within central metabolism) that increased less (1.3 fold) is the pyruvate kinase reaction. The most increased flux is the PEP carboxylase (8.1 fold) (and hence PEP carboxykinase since the ratio between those reactions were set to be constant at 2 according to Nanchen *et al.* (2006)) and glucose-6-phosphate-1-dehydrogenase (G6PDH) (4.2 fold), which is due to the nearly 4 fold increased growth rate requiring more anaplerosis and NADPH. The higher fold changes in anabolic rates compared to catabolic rates are due to the lower value of the q_{O2}/q_S ratio at higher growth rate because of less impact of maintenance.

The intracellular fluxes in phase II cannot be calculated because there are multiple intracellular pools (from phase I) that are used as carbon and energy source (see below). In phase III the metabolism reaches back to the initial steady-state, thus the intracellular fluxes at the pseudo-steady-state of phase III are same as steady-state (and thus in phase IV) (not shown).

Metabolite dynamics

General observations: During the stimulus-response experiments levels of the extracellular present metabolites of glycolysis, TCA cycle and amino acids do remain the same as at steady-state (data not shown). This is as expected, due to the large time constant (10 h) of the extracellular concentration pools. This result allows us to use the differential method to obtain the intracellular metabolite levels by subtracting the steady-state amount of metabolite in the filtrate from the amount in the broth during the transient. The analytical approach obtained high sensitivity and specificity via MS/MS while minimizing systematic error by including isotope-labeled internal standards throughout.

The metabolite changes are shown in fold changes relative to the steady-state values (as presented in Table 5.2) in two time frames (0 - 30 s and 0 - 1200 s, Figures 5.8 - 5.11 and Appendix 5.5.6 Figures 5.15 - 5.19). The two independent chemostat pulse experiments show the same dynamic pattern for all metabolites, and the fold changes showed differences for only some metabolites, demonstrating the reproducibility of our pulse experiments. The four phases in the transient observed for fluxes and extracellular concentrations (offgas O_2/CO_2 and pH) were also clearly distinguishable for intracellular metabolites in both experiments. For nearly all metabolites, as expected, the previous steady-state levels were recovered (fold change back to 1) at the end of

phase III and during phase IV. Exceptions were pyruvate (Figure 5.9) and succinate (Figure 5.10).
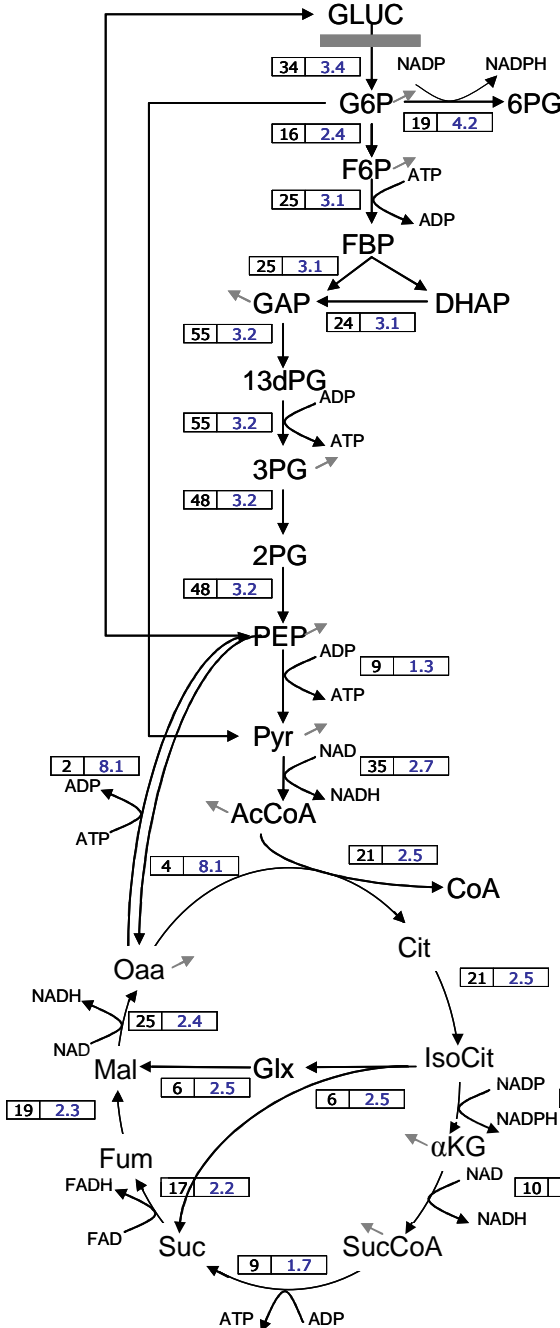
Table 5.4: Fold change of metabolite levels at pseudo-steady-state in phase I relative to the steady-state and turnover times [s] at pseudo-steady-state in phase I (Chemostat 2)

		Concentration fold change	τ
G6P		4.8	4.2
T6P		1.0	-
M6P		2.2	-
6PG		9.5	2.0
E4P		4.3	0.7
	His	1.6	13.9
	Tyr	1.0	8.9
Mannitol1P		2.0	-
FBP		8.2	5.6
G3P		1.1	2.6
F2,6bP		5.8	-
2PG+3PG		0.3	0.3
	Gly	1.2	19.7
	Trp	0.8	2.4
PEP		0.1	0.1
Pyruvate		1.3	0.6
	Ala	1.4	34.7
	Val	1.3	12.0
	Leu	2.1	22.8
Cit+IsoCit		1.3	8.7
α-KG		1.5	1.1
	Glu	1.1	71.5
	Gln	2.0	48.0
	Lys	1.2	51.6
	Pro	1.4	55.0
	Orn	1.6	26.7
Succinate[*]		3.6	16.5
Fumarate		1.8	1.2
Malate		1.5	3.9
	Asp	0.8	13.0
	Asn	0.8	12.2
	Thr	1.1	10.6
	Ile[*]	0.2	0.5
	Cys	2.2	5.3
	Met	0.6	3.0
ADP		1.1	0.1
ATP		1.0	0.5

[a] Metabolite measurement from Chemostat 1.

Figure 5.6: The steady-state intracellular fluxes [mmol/CmolX/h] and the relative flux fold changes at pseudo-steady-state in phase I (0-200 s) in the central metabolism (glycolysis, TCA cycle), shown respectively in the boxes (left and right) next to the corresponding enzymatic reaction (Chemostat 2).

The dynamic metabolite profiles (Figures 5.8 - 5.11 and Appendix 5.5.6) and the dynamic -q_S and -q_{O2} uptake rate profiles (Figure 5.4) both showed that after exposure to glucose excess (phase I) the central metabolism reached a pseudo-steady-state within approximately 30 - 50 s after the glucose pulse. This experimentally observed time for the transient is in very good agreement with the turnover times of the metabolite pools (Table 5.2). The metabolite levels during the pseudo-steady-state of phase I (in fold changes relative to the steady-state) are shown in Table 5.4. When this fold change of each metabolite (Table 5.4) is plotted as function of steady-state turnover time (Table 5.2), it is clearly seen (Figure 5.7a) that the metabolites that have the lowest turnover times show the highest fold change, as can be expected. The exceptions are ATP, ADP, pyruvate, fumarate and α-ketoglutarate that do not exert much dynamics although they have low turnover times. For ATP and ADP this can be explained by their conserved moiety property (cyclically phosphorylation/dephosphorylation) while pyruvate, α-ketoglutarate and fumarate are generally known (*P. chrysogenum* (Nasution *et al.* 2006) and *S. cerevisiae* (Wu *et al.* 2006)) to be involved in near-equilibrium transaminase reactions, involving the large C_3, C_5 and C_4 pools of Ala, Glu and Asp, leading to relatively high turnover times of the combined pools.

The accumulated carbon, relative to the steady-state, from all measured intracellular metabolites inside the cell (during phase I) was 2.6 mmol carbon per liter broth (see Figure 5.7b) which represents 16 % of the added glucose amount (16.7 mM carbon). This accumulated carbon is then consumed in phase II.

The calculated cumulative consumption of oxygen in phase II was 1.31 mmol O_2/l broth (Figure 5.4a), although there was no external substrate available during this phase. The electrons (degree of reduction) available in the 2.6 mmol carbon of cumulative intracellular metabolites at the end of phase I was 10.0 mmol electrons/l broth (Figure 5.7c) which is equivalent to a maximal O_2 consumption of 2.5 mmol O_2/l broth. This shows that about 50 % of the consumed metabolites in phase II are catabolised. These intermediates, representing about 10 mg glucose equivalents per gDW, are clearly sufficient to act as electron donor and substrate in phase II, the most abundant one being Glu representing ~ 1/3 of the electrons accumulated at the end of phase I. It therefore appears that *E. coli* cells can accumulate in periods of substrate excess (at time scale of several tens of seconds) a relevant amount of carbon as intracellular metabolites. Clearly such accumulation phenomena are of major relevance for large-scale glucose-limited fed-batch cultivations, where *E. coli* is exposed to glucose gradients (alternating excess to starvation) at time scales of fermentor mixing times 30 - 300 s (Vrabel *et al.* 2000).

Phase I (glucose excess): Highly dynamic changes occurred in the intracellular metabolite levels in phase I. *Glycolysis and PPP:* The hexose phosphates G6P, M6P directly increased about 3 - 5 fold and then reached a pseudo-steady-state already after about 20 - 30 s (Figure 5.8). FBP, F2,6bP and the PPP intermediate 6PG (see Figures 5.8 and 5.9) showed a much higher fold increase (10 - 15 fold). The concentrations of lower glycolytic metabolites 2PG+3PG and PEP dropped immediately nearly 10 fold and remained low (Figure 5.9). The increase in G6P and decrease in PEP agree very well with the activity of phosphotransferase system (PTS), which consumes PEP and produces G6P.

The accumulation of phosphorylated C_6 metabolites and decrease of phosphorylated C_3 metabolites (2PG+3PG and PEP) are related to the 3.4 fold increase in $-q_S$. This glycolytic metabolite- flux pattern was also observed by others in *E. coli* under similar conditions (Buchholz *et al.* 2002; Chassagnole *et al.* 2002; De Mey *et al.* 2010b; Hoque *et al.* 2005; Schaefer *et al.* 1999) and was also observed in *P. chrysogenum* (Nasution *et al.* 2006) and *S. cerevisiae* (Mashego *et al.* 2006; Visser *et al.* 2004; Wu *et al.* 2006). The 3.1 fold flux increase through the enzyme PFK (Figure 5.6) is driven by the increase of the hexose phosphate levels, but also by the increase in the concentration of AMP (Figure 5.11), which is a potent activator of PFK (Keseler *et al.* 2009).

The increase of 6PG (also observed by (Chassagnole *et al.* 2002)) is due to the 4.2 fold increased flux through G6PDH, stimulated by the 5 - 10 fold increase in G6P, to provide the NADPH for the steeply 3.7 fold increased rate of biomass formation.
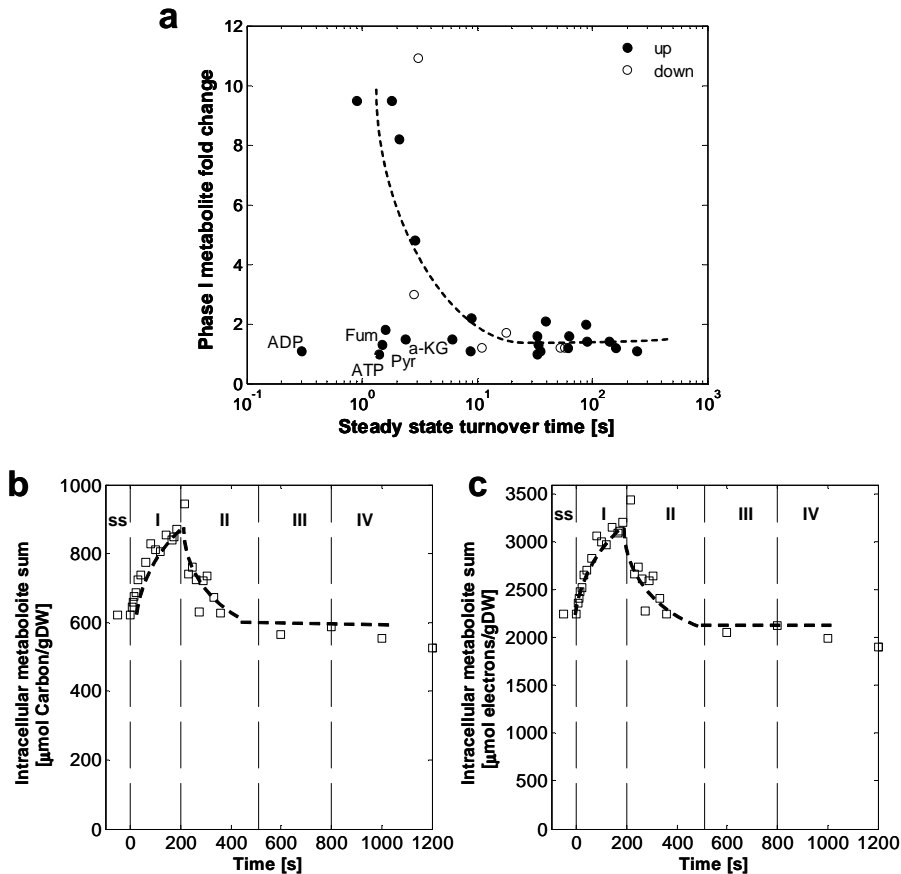
Figure 5.7: (a) Fold changes in metabolite levels (pss, phase I) relative to their steady-state as function of the corresponding steady-state turnover times, (b) Total amount of intracellular metabolite-associated carbon [µmol Carbon/gDW] and (c) electrons [µmol electrons/gDW] calculated from the measured intermediates (Figures 5.8-5.10, 5.15-5.19) at each time point.
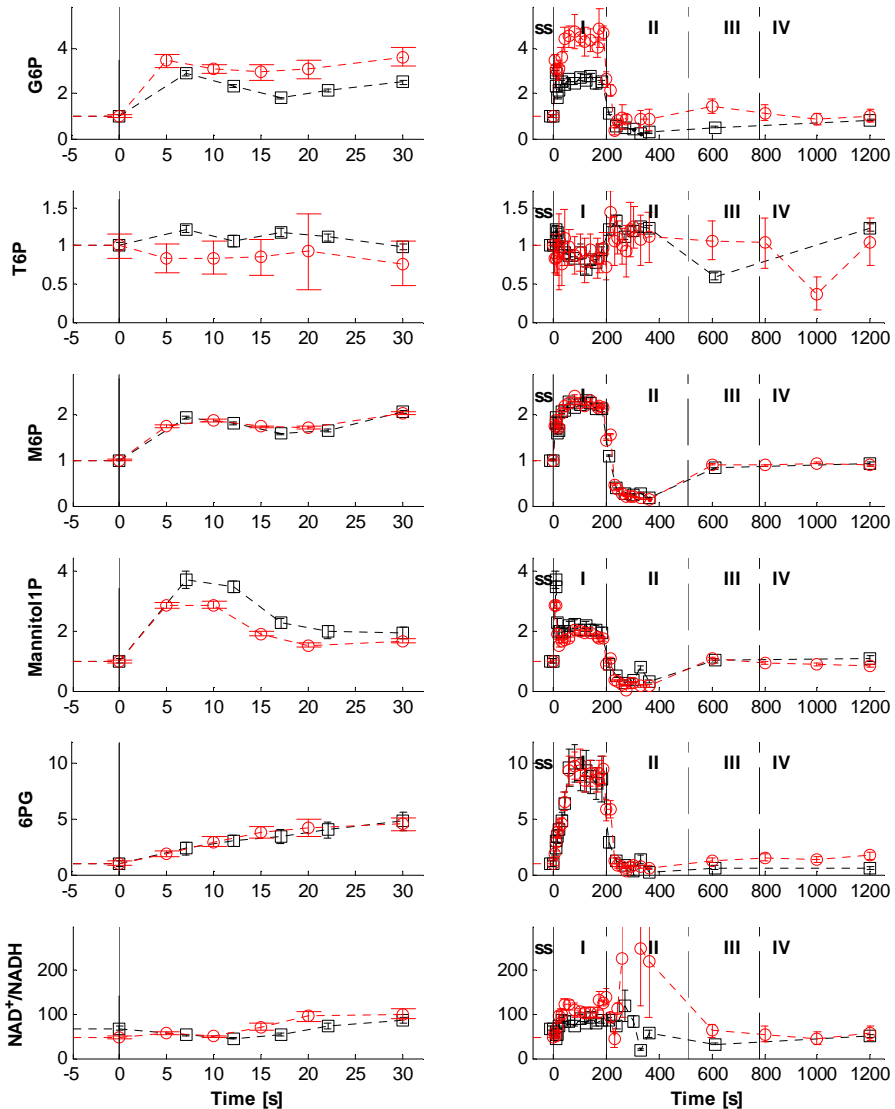
Figure 5.8: Intracellular levels of upper glycolytic metabolites, 6PG and Mannitol-1P as fold changes relative to their steady-state levels and NAD$^+$/NADH ratio in two time frames (left: 0-30 s, right: 0-1200 s), squares: Chemostat 1, circles: Chemostat 2.

Remarkably the pyruvate concentration did not increase significantly, which agrees with the absence of secreted by-products. The strongly 3.4 fold increased pyruvate synthesis rate is apparently more than matched by its increased consumption for growth (anaplerosis) and for catabolism (TCA cycle and O_2 consumption).

TCA cycle and glyoxylate route: For most of the TCA cycle intermediates only moderate (up to 1.5 fold, Table 5.4) increases in metabolite levels are seen (citrate, α-ketoglutarate, fumarate and

malate), which is in agreement with previous findings (De Mey *et al.* 2010b). These small fold changes of the TCA cycle metabolite concentrations have to be judged against a 2.5 fold increase in TCA cycle fluxes to provide the electrons for the increased O_2 consumption, which indicates the presence of other kinetically relevant metabolites. Only succinate increases about 10 fold towards the end of phase I, which might point to a kinetic limitation of succinate dehydrogenase. In fact, Link *et al.* (2010) showed that this enzyme enters a saturation state in similar perturbation experiments.

The fluxes of the glyoxylate shunt increased 2.5 fold following the fold changes of the TCA cycle reactions aconitase and isocitrate dehydrogenase. The fold change was the same because the ratio of the glyoxylate cycle to TCA cycle was set to 3/7 according to Nanchen *et al.* (2006) (see Materials and Methods).

Nucleotides: During phase I ATP slightly decreased, AMP strongly increased and ADP increased very slightly (Figure 5.11), but the sum of the adenine nucleotides did not change significantly, whereas the EC-value remained high (Figure 5.11). This is due to a balance between the steeply increased ATP demand (for growth) which is rapidly matched by the increased ATP supply from steeply increased oxygen consumption. This indicates that the electron transport chain has a very high capacity.

Mass action ratios and metabolite ratios: To investigate the thermodynamic feasibility of the metabolome response in relation to flux direction, the near-equilibrium reactions were examined. It was seen that the MAR of reactions between PFK and PGK (MAR of FBP to 3PG, Figure 5.9) and enolase reaction (PEP/2PG+3PG, Figure 5.9) sharply decreased after the glucose pulse to accommodate the 3.4 fold increase in flux, as can be expected from a thermodynamic point of view. The MAR of the fumarase reaction (Figure 5.10) also significantly decreased in response to the 2.3 fold flux increase. This indicates that the kinetic capacity of this near equilibrium reaction is not excessive. In contrast to the present findings in *E. coli*, the *in vivo* MAR of fumarase, in *S. cerevisiae* (Mashego *et al.* 2006) and *P. chrysogenum* (Nasution *et al.* 2006) under comparable glucose pulse experiments remained close (< 15 %) to their steady-state value but MAR of enolase decreased, as observed here.

Following Canelas *et al.* (2008b) and Taymaz-Nikerel *et al.* (2009) it is possible to calculate the cytosolic $NAD^+/NADH$ ratio (Figure 5.8) from concentrations of Mannitol-1P and F6P. Because in this experiment reliable F6P results could not be obtained, measured G6P along with the known equilibrium constant of PGI (Seeholzer 1993) was used for this calculation. In phase I the $NAD^+/NADH$ ratio steeply increased (from 60 to 100), which indicates a surprising increased oxidation level of the NAD(H) pool. This is in strong contrast to the observations in *S. cerevisiae* (Wu *et al.* 2006) and *P. chrysogenum* (Nasution *et al.* 2006) where the $NAD^+/NADH$ ratio decreased, in similar glucose pulse experiments. The difference might be explained by the much higher increase in oxygen uptake rate in *E. coli*, which leads to a very fast rate of consumption of the produced NADH, possibly leading to a higher oxidation level of the $NAD^+/NADH$ couple. The resulting lower NADH value, leading to less inhibition of TCA cycle dehydrogenases, can potentially also explain the faster rate (2.5 fold) of the TCA cycle, where most of the TCA cycle intermediates only changed about 1.5 fold.

The turnover times of intermediates during the pseudo-steady-state in phase I are shown in Table 5.4, in comparison to their steady-state values. The biggest change occurs in the 2PG+3PG pool, where the turnover time decreases 9 fold, showing the extreme dynamics of this pool under the studied conditions.

Comparison to eukaryotes: When the short-term dynamics of (glycolysis/TCA cycle) metabolome in aerobic chemostat grown *E. coli* is compared to a glucose pulse with *S. cerevisiae* (Mashego *et al.* 2006; Wu *et al.* 2006) and *P. chrysogenum* (Nasution *et al.* 2006), it is seen that most of the observations are similar, such as rapid increase in the phosphorylated C_6 metabolites, rapid decrease in the 2PG+3PG and PEP, moderate increase in the TCA cycle intermediates and rapid achievement of a new pseudo-steady-state. Differences in the response of the different organisms is reflected in secreted ethanol (*S. cerevisiae*) and increased storage material (*P. chrysogenum*), none of which occurs in *E. coli*. Also, the pseudo-steady-state is achieved in a much shorter time period (~ 30 s) in *E. coli* compared to these eukaryotes (~ 100 s). Furthermore, *E. coli* has a much larger capacity to oxidize NADH (steep increase in O_2 consumption) and generate ATP. The measured maximal O_2-uptake rate (in mmol O_2/h/Cmol X) after a glucose pulse given to the organisms, initially cultivated at 0.1 h^{-1}, was 250 for *E. coli* (this work) and 113 for *S. cerevisiae* (AB Canelas, personal communication, 2010). In *E. coli* this leads to a more oxidized NAD^+/NADH couple (in contrast to the more reduced levels in *S. cerevisiae* and *P. chrysogenum*). *E. coli* maintains its ATP level and a high EC, as opposed to *S. cerevisiae* and *P. chrysogenum*, where these values strongly decrease.

Amino acids: One of the important findings of the present study is that most amino acids (see Appendix 5.5.6) revealed moderate (up to 1 - 2 fold) changes in their concentration already in the initial 50 s of phase I. This would not be expected due to the relatively higher steady-state turnover times of the free amino acids (Table 5.2). However the projection of steady-state turnover time to infer pulse dynamics should always be treated with caution as indicated in this case. In the pseudo-steady-state (in phase I) turnover times of all amino acids (see Table 5.4) strongly decrease (due to increased growth rate) and then match globally with the observed response time of amino acids.

In vivo kinetic relations: In general the amino acid concentrations followed the dynamic response of their corresponding precursor metabolite in central metabolism as can be seen (Appendix 5.5.6) for the E4P-, pyruvate- and α-ketoglutarate-derived amino acids. 3PG- and oxaloacetate-derived amino acid levels did not follow one trend, but some increased with decreased precursor level or vice versa. Most of the oxaloacetate-derived amino acids did not change significantly while Cys slightly increased. In general the 1 - 2 fold changes in amino acid levels are much more modest than their steep 3 - 4 fold flux changes (due to 3.7 fold flux change in growth rate). The 3.7 fold increase in amino acid synthesis flux appears to be mainly driven by significant (5 - 10 fold) increases in most of their precursor metabolite concentrations (i.e. E4P, oxaloacetate (malate) and α-ketoglutarate).

The 3.7 fold increase in growth rate (Figure 5.4b) requires the same fold change in protein biosynthesis rate, which requires a 3.7 fold increased ribosome activity. This high increase in ribosome activity must be due to increased mRNA levels because there is hardly any fold change
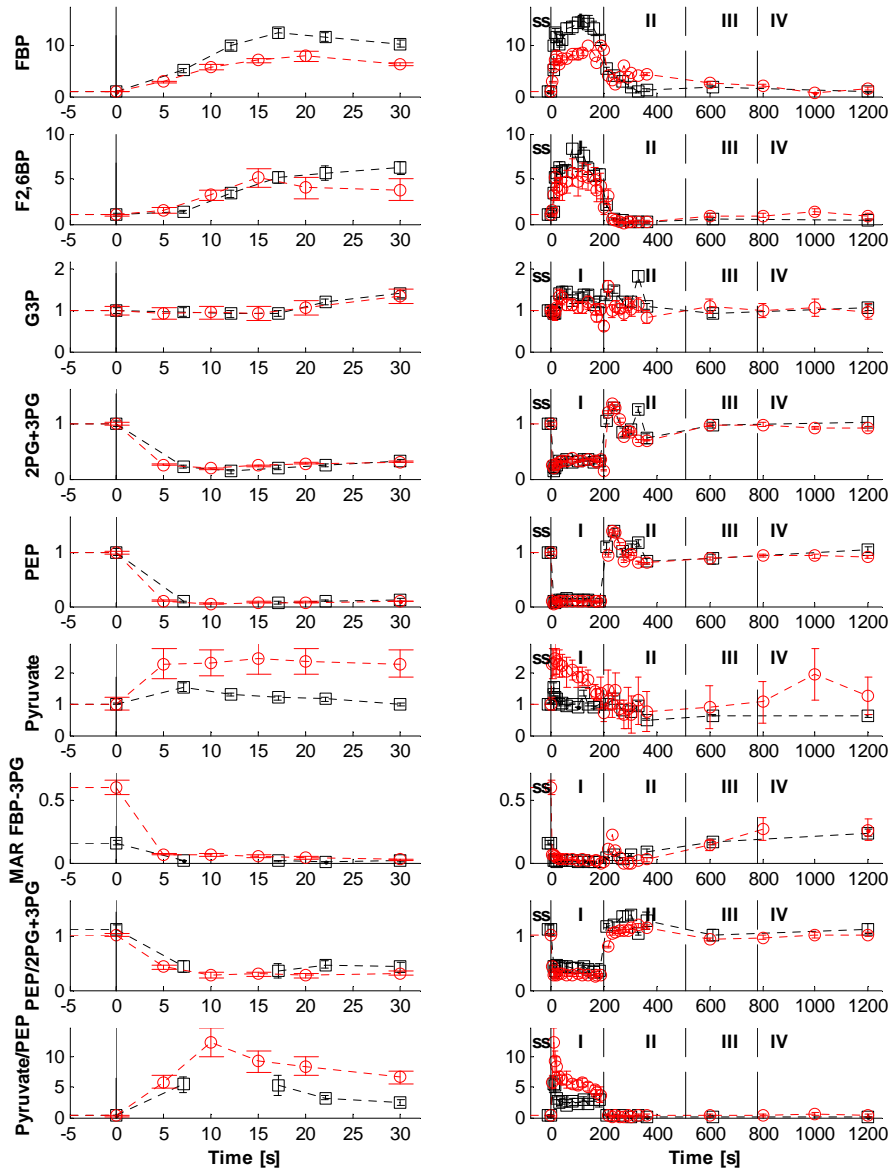
Figure 5.9: Intracellular levels of lower glycolytic metabolites as fold changes relative to their steady-state levels and mass action ratio (MAR) of FBP-3PG, PEP/(2PG+3PG), Pyruvate/PEP in two time frames (left: 0-30 s, right: 0-1200 s), squares: Chemostat 1, circles: Chemostat 2.

in ATP and amino acid levels. It is therefore hypothesized that the transcription rate of many proteins is increased within seconds due to increased mRNA levels in response to changed levels of metabolites which bind to a global transcription factor. In *E. coli* the global transcription factor Cra is known to be inactivated by F1P and FBP. Hardiman *et al.* (2009) demonstrated the impact

of changes in FBP concentration in relation to Cra on the transcription of central carbon metabolism genes and the effect of these changes on the metabolic fluxes. Our finding of a more than 10 fold increase (within 15 s) in the concentration of FBP can therefore be expected to lead to high transcript levels, creating a high ribosomal protein production rate, explaining the 3 - 4 fold increase in μ. In support of this hypothesis, our data shows a strong positive correlation between FBP concentration and growth rate (Figure 5.12a), in agreement with the findings (in *E. coli* chemostat cultures) of Schaub and Reuss (2008). The difference in the absolute amount of
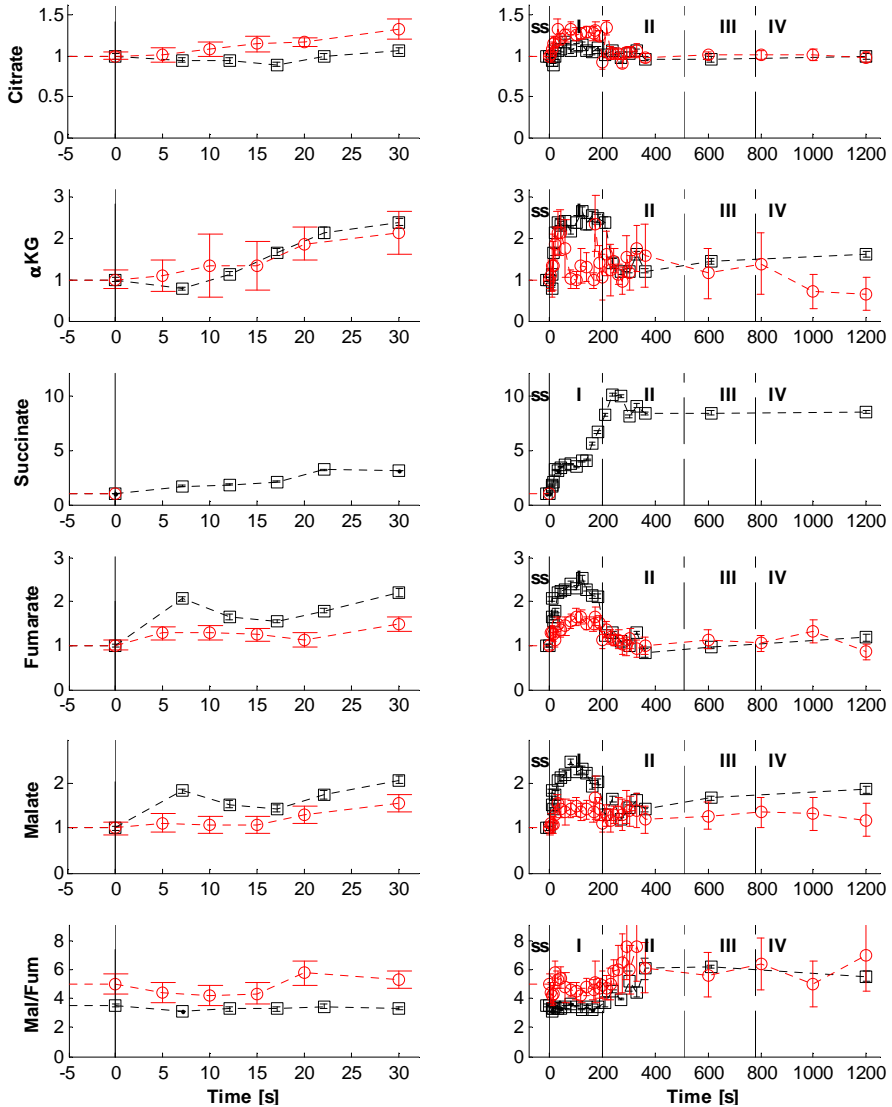
Figure 5.10: Intracellular levels of TCA cycle metabolites as fold changes relative to their steady-state levels and mass action ratio (MAR) of fumarase in two time frames (left: 0-30 s, right: 0-1200 s), squares: Chemostat 1, circles: Chemostat 2.
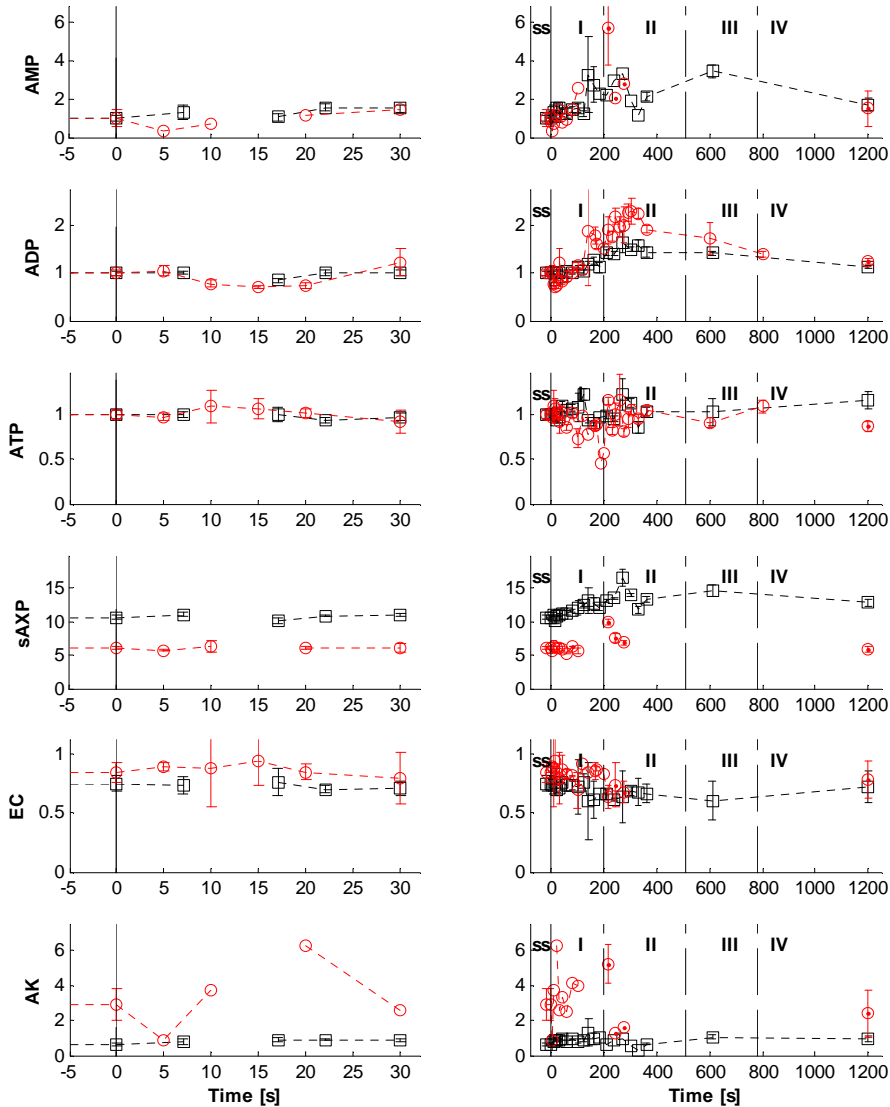
Figure 5.11: Intracellular levels of adenine nucleotides as fold changes relative to their steady-state levels and sum of adenine nucleotides (sAXP=AMP+ADP+ATP), energy charge (EC), mass action ratio (MAR) for adenylate kinase (AK) in two time frames (left: 0-30 s, right: 0-1200 s), squares: Chemostat 1, circles: Chemostat 2.

FBP between the two studies is probably due to the different sampling methods used. Schaub and Reuss (2008) used total broth sampling, whereby applying combined quenching/extraction with a helical coil heat exchanger, and this might have caused overestimation of metabolite levels, depending on the amount of the metabolite present extracellularly.

The fast increase of the oxygen consumption rate after the glucose pulse (Figure 5.4a) is a consequence of the speeding up of the activity of electron transport phosphorylation (ETC

coupled to H^+-ATPase, abbreviated as ETP). This change in the ETP activity might be due to high substrate (NADH) supply and/or less product (adenine nucleotides ATP, AMP and ADP) inhibition. The first hypothesis does not hold in our case because the NAD^+/NADH ratio increases after the pulse (Figure 5.8), leading to a lower NADH concentration as substrate for the ETC. On the other hand, AMP shows a strong increase and ATP slightly decreases, which is readily explained by the 3.7 fold increased protein synthesis rate (discussed above) at the ribosomes (which produces massive AMP). We hypothesize that an increased AMP/ATP ratio is an emergency signal for energy shortage that stimulates the ETP mechanism, leading to rapid increase of oxygen consumption rate. Figure 5.12b shows a direct relation between the AMP/ATP ratio and the oxygen consumption rate occurring in the first 50 s of phase I.
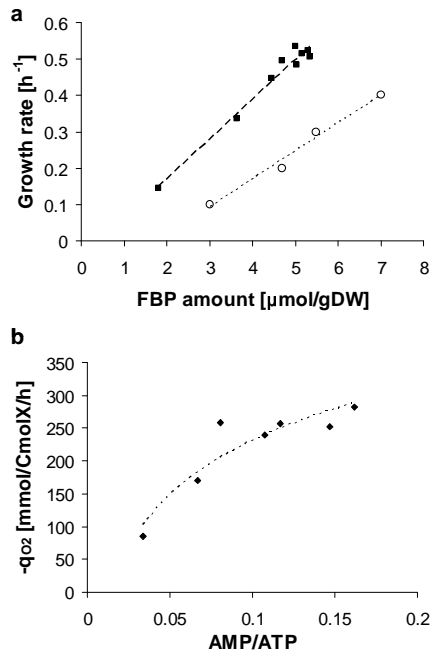
Figure 5.12: (a) Specific growth rate plotted as a function of the intracellular FBP amount, this work (squares) and from Schaub and Reuss, 2008 (circles), (b) Specific oxygen uptake rate as a function of the AMP/ATP ratio.

Phase II (starvation): During this phase there is no glucose uptake, which results in the collapse of the amounts of hexose phosphates (G6P, M6P), 6PG, Mannitol-1P, FBP and F2,6bP along with the sharp increase of 2PG+3PG and PEP that is due to the absence of PTS activity and the much lower glycolytic flux.

Mass action ratios and metabolite ratios: To check the thermodynamic feasibility of the dynamic metabolite response, the MAR of near-equilibrium reactions was investigated again (as in phase I). In general it was observed that MAR increased as expected due to the lower flux. The MAR of

the FBP to 3PG increased at the beginning of phase II and reached to values as occurred before the pulse. The MAR of enolase (PEP/2PG+3PG) returned to a value slightly above the steady-state value indicating a possible presence of gluconeogenesis during phase II (see Figure 5.9). The PEP/pyruvate ratio sharply increased due to absence of flux through the PTS. The MAR of fumarase also returned to the steady-state value. The redox state NAD^+/NADH ratio sharply dropped to a value lower than its initial value, also indicating gluconeogenesis which is driven by a high NADH level.

TCA cycle: The concentrations of the TCA cycle intermediates citrate, α-ketoglutarate, succinate, fumarate and malate remained rather constant during this phase. Despite conversion of TCA cycle intermediates (there is O_2-consumption), there is no depletion of metabolites as occurs in the upper glycolysis. This agrees with the very low anaplerosis rate due to the very low growth rate, which causes a conserved moiety property of all TCA cycle intermediates.

Nucleotides: During phase II ATP did not change as much as in phase I, but there was a slight decrease of EC, probably due to the steep decrease in O_2-consumption and the associated ATP production.

Amino acids: The amino acids generally followed the pattern of their corresponding precursor metabolite, as in phase I, e.g. E4P-derived Tyr decreased, 3PG-derived Gly and Trp increased, Ala and Leu decreased following their precursor pyruvate, and α-ketoglutarate-derived Glu, Gln, Pro and Orn decreased. Also the oxaloacetate-derived amino acids Asn, Thr and Ile increased.

Phase III/IV: With the restart of the glucose feed (at the beginning of phase III), in general most of the measured intermediates, such as the upper and lower glycolytic metabolites, PPP intermediates, TCA cycle organic acids as well as most of the amino acids, quickly returned to their steady-state values. Exceptions are pyruvate, that had a lower value than its initial value at the end of phase IV, malate was higher (2 fold) and the most striking difference was for succinate which was 8 fold higher compared to its steady-state value. These exceptions cannot be explained.

5.4. Conclusions

The glucose pulse experiment carried out by perturbing the reference steady-state was dynamically and quantitatively fully described in this work, in terms of *in vivo* rates and *in vivo* metabolites both extracellularly and intracellularly. The obtained flux and metabolite concentration-time patterns i) agree with the metabolite turnover times, ii) were highly corresponding, iii) their values returned to their previous steady-state and iv) did show mirror image responses in glucose excess and starvation phases.

As expected, the strongly increased rates were accompanied by respectively increased/decreased metabolite concentration in upper/lower glycolysis, by decreased MARs in near equilibrium reactions in glycolysis, and by increased precursor concentration for most amino acid synthesis pathways, and pentose phosphate pathway. Surprisingly, considering the 3 - 4 fold increase in

amino acid synthesis rate, due to such fold increase in growth rate, the amino acid concentrations only marginally changed (1 - 2 fold), which points to a fast and strong transcription response to explain the increased protein production rate from the ribosomes. Here the known Cra (global transcription factor)-based impact of FBP (increased) on transcription (increased) is considered of major importance, suggesting a direct link between the metabolites of the central metabolism and transcription.

Another surprising result is that the energy charge and ATP level hardly decreased during the massive increase in ATP requirement (~ 4 fold) in the transient, pointing to a matching strong increase in ATP production rate from the electron transport chain phosphorylation. Here a strong correlation is found between $-q_{O_2}$ and the AMP/ATP ratio showing that the ETP is inhibited by ATP and stimulated by AMP.

Furthermore, the proposed method for online dynamic calculation of $-q_{O_2}(t)$ and hence $\mu(t)$ at seconds time scale will be beneficial for future dynamic model studies because calculated network fluxes depend clearly on a correct μ value. Moreover, the presented approach on assessment of pseudo-steady-state turnover times (rather than steady-state turnover times) will be more realistic in time-scale-analysis-based model reduction techniques (Nikerel *et al.* 2009).

5.5. Appendix

5.5.1. Calculation of $-q_{O_2}$ during the transient from mass balance of dissolved O_2

The DO-probe used to measure DO concentration consists of a membrane through which O_2 has to diffuse and reach to the actual electrode. These response dynamics of the DO-probe can be approximated well by a first-order model (Lee and Tsao 1979).

The response dynamics is different for different probes, furthermore the same probe can show different response dynamics under different conditions, and depends on the age of the probe. For these reasons, in order to reveal the dynamics of the probe applicable to the pulse experiment, just before the pulse experiment the steady-state culture was perturbed by adding pure O_2 and DO measurements were recorded (see Figure 5.13). The DO-readings reached a new steady-state as indicated.

In Figure 5.13 C_p is the probe measurement, C_L is the unknown real DO-concentration that is calculated by the dissolved O_2 mass balance:

$$\frac{dC_L}{dt} = \frac{\varphi_L}{V_L}(C_{L,in} - C_L) + k_L a(C_L^* - C_L) + q_{O_2} C_X \tag{5.1}$$

where C_L is the oxygen concentration in the liquid phase, Φ_L is the liquid flow rate, V_L is the volume of the liquid phase, $k_L a$ is the volumetric mass transfer coefficient for oxygen, C_L^* is the saturation value of the oxygen concentration in the liquid bulk in equilibrium with the oxygen

content of the gas bulk, C_X is the biomass concentration and q_{O2} is the specific O_2 consumption rate.
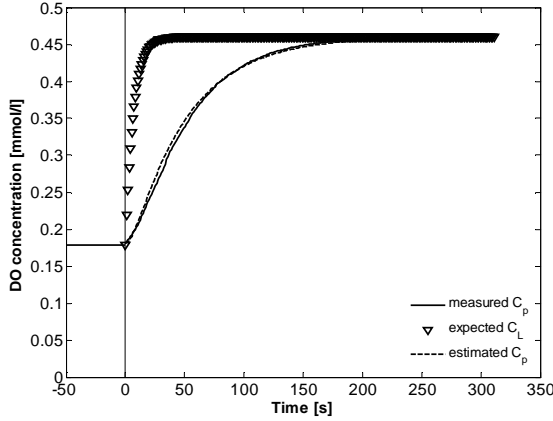
Figure 5.13: Dissolved oxygen (DO) concentration [mmol/l] as a function of time: line: DO-probe readings during addition of O_2 to air, triangles: real DO concentration after correction for DO-probe dynamics, dashed line: calculated DO-probe signal using the real DO concentration and the probe dynamics.

During the transient of DO due to adding pure O_2-gas, C_X and q_{O2} do not change because the feeding rate and metabolism do not change. The term $\frac{\varphi_L}{V_L}(C_{L,in}-C_L)$ is neglected since both dissolved O_2 concentration and the liquid flow rate are very small. Then,

$$\frac{dC_L}{dt}=k_L a(C_L^*-C_L)+q_{O_2}C_X \tag{5.2}$$

Solving the above equation with constant $k_L a$ (504 h^{-1}, obtained from the new steady-state DO concentration), C_L^* (0.513 mmol/l), q_{O2} (77.28 mmol/CmolX/h) and C_X (10.44 gDW/l) yields:

$$C_L(t)=\frac{q_{O_2}C_X+k_L aC^*}{k_L a}\left[1-e^{-k_L a\,t}\right]+C_L^{ss}e^{-k_L a\,t} \tag{5.3}$$

in which the known new steady-state C_L^* and $k_L a$ will be implemented. The DO-probe first-order kinetic parameter k is then calculated with

$$\frac{dC_p}{dt}=k\,(C_L-C_p) \tag{5.4}$$

by minimizing the squared error between $C_{p,estimated}$ and $C_{p,measured}$ at each time point. This optimization solution yielded k = 0.0211 s^{-1}. To show the nice fit, $C_{p,estimated}$ is also plotted (Figure 5.13). This shows that the DO-probe has a time constant of about 50 s.

Then the differential equations Eq. 5.2 and Eq. 5.4 are solved to calculate $-q_{O_2}$ during the glucose pulse using the calculated C_L after the glucose pulse with Savitzky-Golay smoothing filters (MATLAB, The MathWorks Inc., Natick, MA, USA).

5.5.2. Herbert-Pirt relations

For the stoichiometric metabolic network model described in Taymaz-Nikerel *et al.* (2010a), all the steady-state fluxes in the network can be written as a function of $-q_S$ and μ. When the intracellular fluxes in the ATP balance equation are replaced with their expressions as a function of $-q_S$ and μ, the Herbert-Pirt relations are derived. The derived Herbert-Pirt relation (Taymaz-Nikerel *et al.* 2010a) describing $-q_{O_2}$ as a function of μ is $-q_{O_2}=0.44\mu+21.54$. After calculating $\mu(t)$, $-q_S(t)$ was calculated with $-q_S=0.25\mu+3.59$ (Taymaz-Nikerel *et al.* 2010a).

5.5.3. Calculation of E4P concentration

The intracellular concentration of E4P was calculated with the assumption that the following seven reactions operate at equilibrium.

FBP $\leftrightarrow$ GAP + DHAP (aldolase, $K_1 = 0.086$ mM (Connett 1985))
DHAP $\leftrightarrow$ GAP (triosphosphate isomerase, $K_2 = 0.045$ (Veech *et al.* 1969))
GAP + S7P $\leftrightarrow$ E4P + F6P (transaldolase, $K_3 = 1.05$ (Vaseghi *et al.* 1999))
GAP + S7P $\leftrightarrow$ R5P + X5P (transketolase 1, $K_4 = 0.83$ (Vaseghi *et al.* 1999))
E4P + X5P $\leftrightarrow$ F6P + GAP (transketolase 2, $K_5 = 10$ (Vaseghi *et al.* 1999))
Ru5P $\leftrightarrow$ X5P (phosphoribulose epimerase, $K_6 = 1.4$ (Vaseghi *et al.* 1999))
R5P $\leftrightarrow$ Ru5P (phosphopentose isomerase, $K_7 = 025$ (Vaseghi *et al.* 1999))

Among the metabolites mentioned in the above reactions, the concentrations of F6P and FBP are available. Therefore E4P was written as a function of equilibrium constants, F6P and FBP. The relation is: $E4P=\left(\dfrac{K_1\ K_2\ K_3\ F6P\ FBP}{K_4\ K_5{}^2K_6\ K_7}\right)^{1/3}$.

Specific cell volume of 1.77 ml/gDW (Chassagnole *et al.* 2002) was considered for converting the amount of metabolites into concentrations.

5.5.4. Measurements in the supernatant sample

Table 5.5: The analysis results of the supernatant samples taken ~ 200 s after the glucose pulse

Compound	Experiment number	Concentration [mg/l]	Measurement Method
Formic acid	Chemostat1	3.6 ± 0.2	Enzymatic
	Chemostat2	6.77 ± 0.04	Enzymatic
	Chemostat2	54.7	NMR
Fumaric acid	Chemostat1	ND	LC-MS/MS
	Chemostat2	0.06 ± 0.03	LC-MS/MS
Pyruvic acid	Chemostat1	ND	LC-MS/MS
	Chemostat2	0.5 ± 0.4	LC-MS/MS
	Chemostat2	0.0	NMR
Malic acid	Chemostat1	0.58 ± 0.01	LC-MS/MS
	Chemostat2	0.5 ± 0.1	LC-MS/MS
Succinic acid	Chemostat1	4.7 ± 0.2	LC-MS/MS
	Chemostat2	3.9 ± 0.5	LC-MS/MS
Citric acid	Chemostat1	6.644 ± 0.004	LC-MS/MS
	Chemostat2	6.4 ± 0.2	LC-MS/MS
	Chemostat2	0.0	NMR
α-ketoglutaric acid	Chemostat1	0.55 ± 0.01	LC-MS/MS
	Chemostat2	0.4 ± 0.2	LC-MS/MS
Acetic acid	Chemostat1	3.41 ± 0.2	Enzymatic
	Chemostat2	4.0 ± 0.1	Enzymatic
	Chemostat2	12.0	NMR
D-lactic acid	Chemostat1		Enzymatic
	Chemostat2	2.6 ± 1.7	Enzymatic
	Chemostat2	0.0	NMR
Ethanol	Chemostat1	ND	GC
	Chemostat2	ND	GC

ND: not detected
NMR analysis was performed for the pooled samples of t = 140, 170 and 200 s in Chemostat 2. Enzymatic analysis was performed in triplicate and LC-MS/MS measurements were done in duplicate.

5.5.5. Effect of $k_L a$ value on the fluxes and calculated glucose concentration

In order to study the effect of $k_L a$ value on the determined $-q_{O2}$ (and hence μ, $-q_S$ and C_S), the used $k_L a$ value was varied ± 10 %. The results are shown in Figure 5.14, showing that the value has indeed an effect on the results.
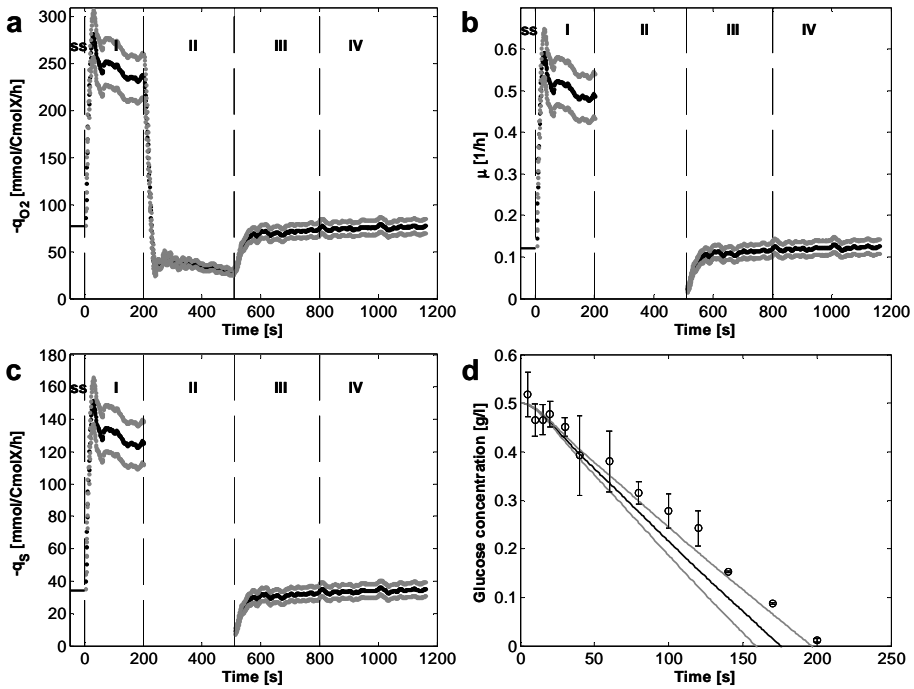
Figure 5.14: ± 10 % $k_L a$ incorporated (shown in gray) in Figures 5.4 and 5.5 in the text.

5.5.6. Patterns of intracellular amino acids throughout the glucose pulse in relation to their precursor
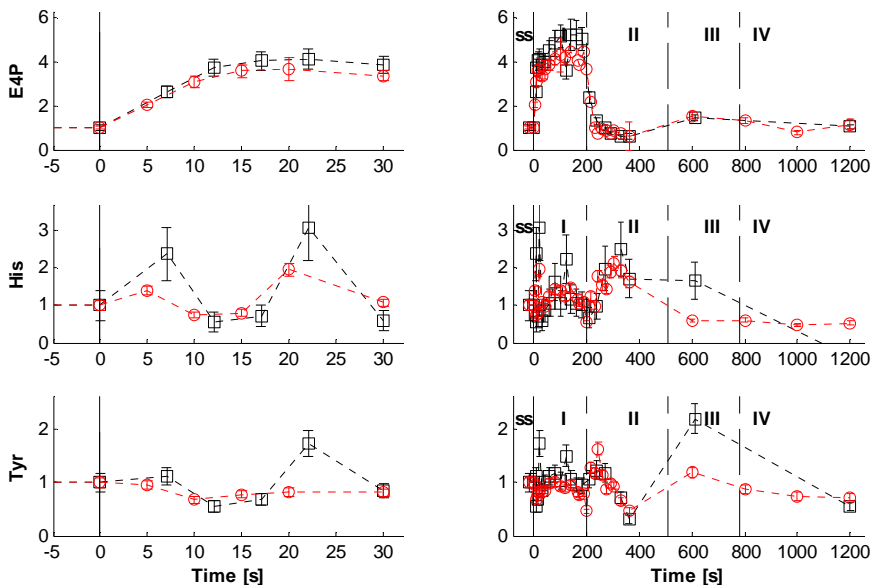
Figure 5.15: Intracellular levels of (aromatic) amino acids derived from E4P as fold changes relative to their steady-state levels (squares: Chemostat 1, circles: Chemostat 2).
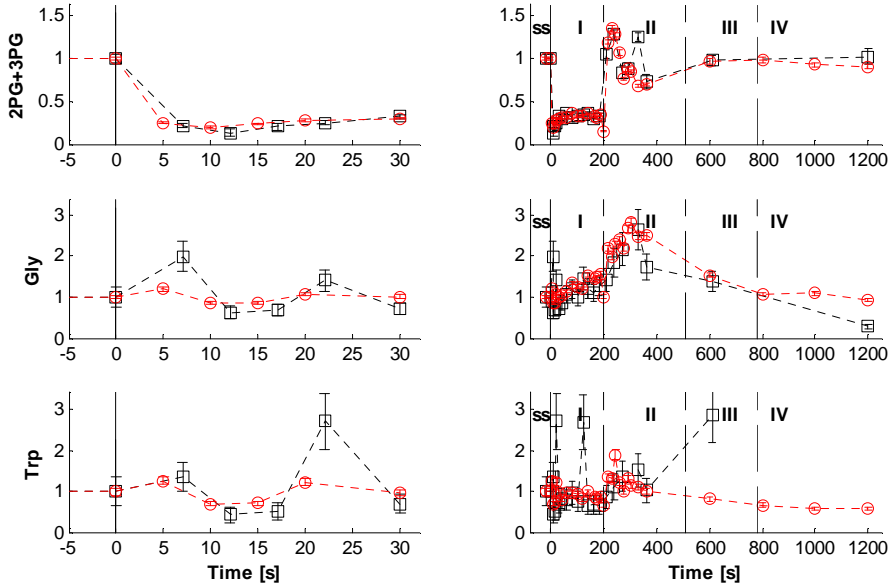
Figure 5.16: Intracellular levels of (aromatic) amino acids derived from 3PG as fold changes relative to their steady-state levels (squares: Chemostat 1, circles: Chemostat 2).
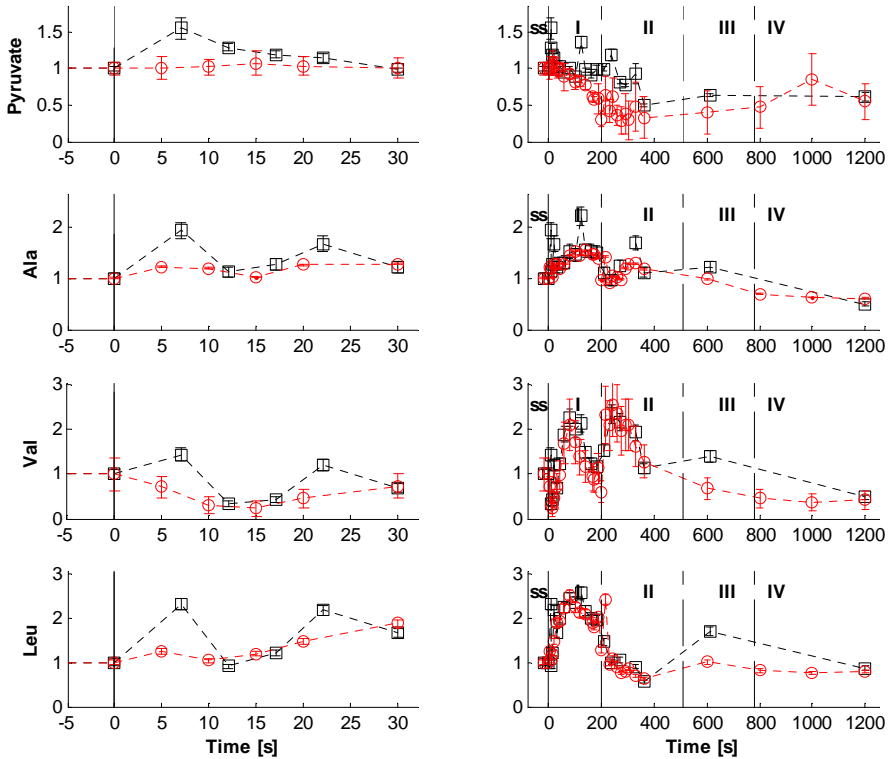
Figure 5.17: Intracellular levels of amino acids derived from Pyruvate as fold changes relative to their steady-state levels (squares: Chemostat 1, circles: Chemostat 2).
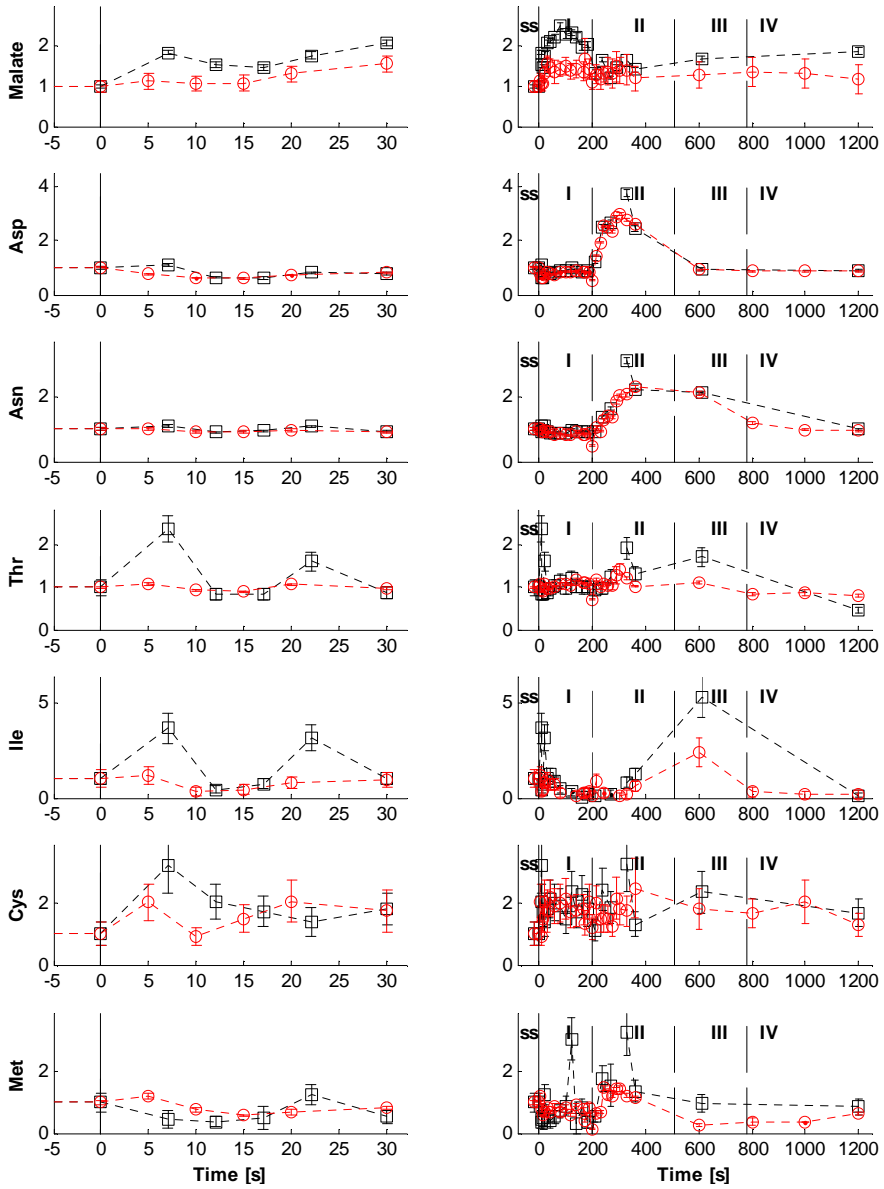
Figure 5.18: Intracellular levels of amino acids derived from Oaa as fold changes relative to their steady-state levels (squares: Chemostat 1, circles: Chemostat 2).
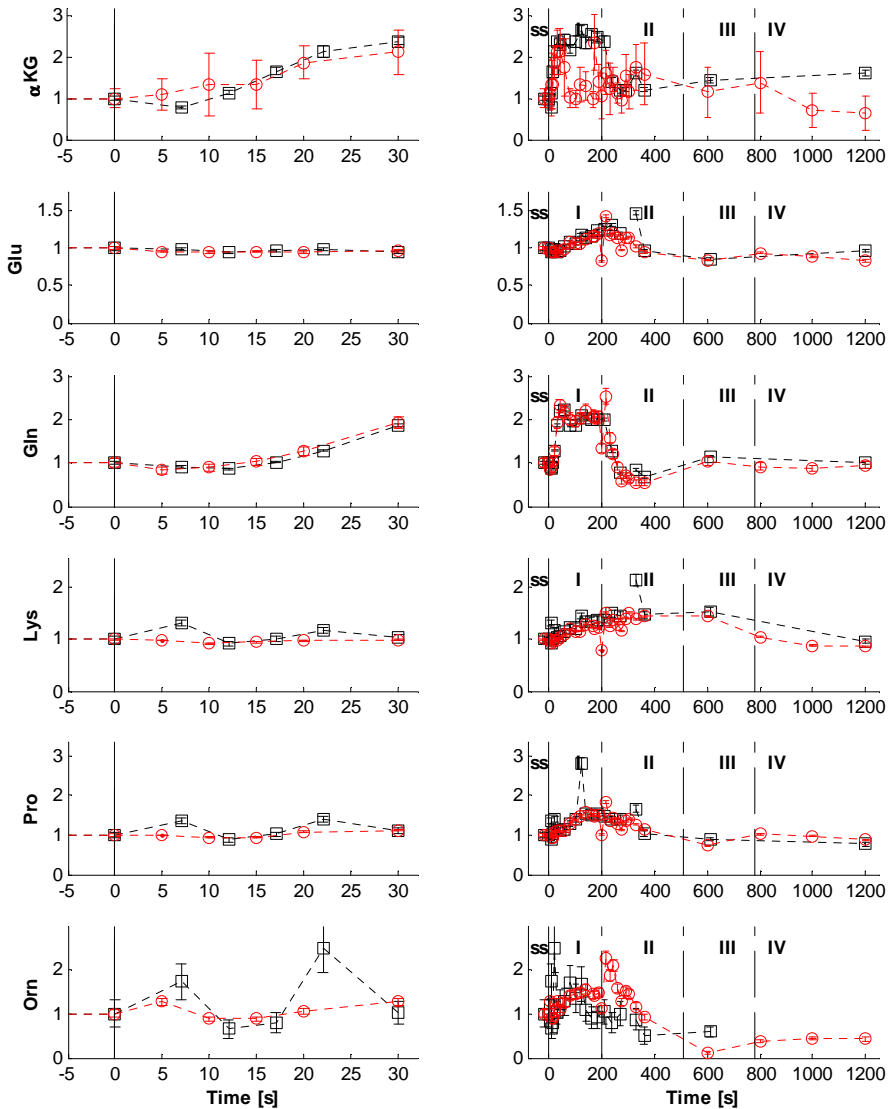
Figure 5.19: Intracellular levels of amino acids derived from α-KG as fold changes relative to their steady-state levels (squares: Chemostat 1, circles: Chemostat 2).

Acknowledgments

Chapter 6

Catching prompt metabolite dynamics with the BioScope

Abstract

The design and application of a BioScope, a mini plug-flow reactor for carrying out pulse response experiments, specifically designed for *Escherichia coli* is presented. Main differences with the previous design are an increased volume specific membrane surface for oxygen transfer and significantly decreased sampling intervals. The characteristics of the new device (pressure drop, residence time distribution, plug-flow characteristics and O_2 mass transfer) were determined and evaluated. Subsequently, 2.8 mM glucose perturbation experiments on glucose-limited aerobic *E. coli* chemostat cultures were carried out directly in the chemostat as well as in the BioScope (for two time frames: 8 and 40 s). It was ensured that fully aerobic conditions were maintained during the perturbation experiments. To avoid metabolite leakage during quenching, metabolite quantification (glycolytic and TCA cycle intermediates and nucleotides) was carried out with a differential method, whereby the amounts measured in the filtrate were subtracted from the amounts measured in total broth. The dynamic metabolite profiles obtained from the BioScope perturbations were very comparable with the profiles obtained from the chemostat perturbation. This agreement demonstrates that the BioScope is a promising device for studying *in vivo* kinetics in *E. coli* that shows much faster response (< 10 s) in comparison with eukaryotes.

6.1. Introduction

Metabolic engineering, the modification of specific biochemical reactions of an organism and/or the introduction of new ones with the use of recombinant DNA-technology, can be applied for the directed improvement of product formation in industrial microorganisms (Stephanopoulos 1999). Hereby it should be realized that the product pathway to be engineered is always part of a larger metabolic network, designed to serve the benefit of the organism and controlled by the latter through a hierarchy of regulatory interactions. Generally the product pathway withdraws carbon precursors, metabolic energy (ATP) and reducing equivalents, in the form of NADPH, from central metabolism and produces NADH. The main factors which determine the flux through the product pathway are (1) the enzyme levels in the pathway, (2) the concentrations of cofactors (ATP, NADPH, NADH) and (3) the concentrations of the relevant intermediates of central metabolism.

To fully and quantitatively understand the relation between a product pathway and connected central metabolism, mathematical models are indispensible (Krömer *et al.* 2006; Wiechert 2002). To allow the quantitative evaluation of the effect of genetic interventions (changing enzyme levels and/or their kinetic properties) on cellular behaviour and productivity, dynamic models, based on the kinetic properties of the individual enzymes, are required (Chou and Voit 2009; Nikerel *et al.* 2009).

It is common practice to determine enzyme kinetic properties from *in vitro* experiments with isolated enzymes, thereby using optimal conditions for each individual enzyme. However, these conditions rarely resemble the natural environment of enzymes inside the living cell. It has been shown that applying enzyme kinetic properties obtained under *in vitro* conditions for kinetic modeling of the *in vivo* behaviour of yeast might lead to erroneous predictions (Teusink *et al.* 2000). Therefore, there is an urgent need for accurate enzyme kinetic data which are valid under *in vivo* conditions. These can be obtained from perturbations of well defined steady-state conditions of whole cells and requires to measure enzyme levels, fluxes and metabolite levels. If perturbation experiments are carried out in a sufficiently short time frame (seconds to several minutes), the enzyme levels can be assumed not to change and hence only intra- and extracellular metabolite concentrations as a function of time are required to obtain the rates from the mass balances.

The rapid perturbation technique was pioneered by Theobald *et al.* (1993) with the aim to elucidate the *in vivo* kinetic properties of yeast glycolysis. They developed a rapid sampling technique which allowed taking samples from a bench scale bioreactor each 4 - 5 s. Schaefer *et al.* (1999) further improved sampling from a stirred tank bioreactor, using an automated rapid sampling device capable of sampling in time intervals of 0.22 s. Hoque *et al.* (2005) also developed a rapid sampling device enabling to take samples from the reactor within a second. However, a drawback of these approaches is the disturbance of the steady-state condition when carrying out a perturbation experiment. Therefore, only one perturbation experiment can be performed per chemostat. Additionally, the number of different kinds of samples that can be taken is limited, e.g. the samples required for metabolome analysis in the broth and in the

supernatant, for transcriptome analysis, for enzyme activity measurements and proteome measurements might be treated differently, which would require repetition of the perturbation and thus multiple steady-state chemostat cultures.

To avoid these disadvantages, Visser *et al.* (2002) and Buziol *et al.* (2002) proposed sampling and perturbation devices, which allow performing the perturbations outside the reactor (instead of perturbing the whole culture), based on a stopped-flow technique that was originally used in the work of de Koning and van Dam (1992). The disadvantage of the sampling device of Buziol *et al.* (2002) is that the maximum time window of sampling is about 20 s for aerobic perturbations because their system does not allow continuous supply of oxygen in the sampling / perturbation device.

An improved stopped-flow technique, allowing oxygenation and thus longer perturbation times, was prototyped by Visser *et al.* (2002), who introduced the acronym "BioScope" for the device. The system was further improved by Mashego *et al.* (2006). The BioScope is a mini plug-flow reactor coupled to a steady-state chemostat and has a gas and a broth channel separated by a silicone membrane for oxygen and carbon dioxide exchange. It is important to emphasize that with the BioScope the amount of sample obtained is, in principle, unlimited and different sampling/quenching protocols can be applied in the same perturbation experiment (e.g. for the measurement of metabolites in total broth and supernatant).

The BioScope device has been successfully used for perturbation experiments in yeast (Kresnowati *et al.* 2008; Mashego *et al.* 2007b) and filamentous fungi (Nasution *et al.* 2006). Although the performance of the BioScope in its present configuration has been successful, much shorter sampling time intervals are required for *Escherichia coli* perturbation experiments due to the expected faster reaction dynamics of the *E. coli* central metabolism (Buchholz *et al.* 2002; Chassagnole *et al.* 2002; Hoque *et al.* 2005; Schaefer *et al.* 1999).

This contribution describes the characterization of a BioScope II device, redesigned for *E. coli* perturbation experiments on a time scale of seconds. The performance of the new device is demonstrated by comparing the results of glucose perturbations carried out in the redesigned BioScope, coupled to a steady-state chemostat culture of *E. coli* with results of similar perturbations carried out directly in the chemostat. Precautions were taken that no oxygen depletion could occur during these perturbation experiments. For metabolite quantification, a differential method was used (Taymaz-Nikerel *et al.* 2009) whereby the intracellular metabolite levels were obtained from measurements in total broth and filtrate samples.

6.2. Materials and Methods

6.2.1. BioScope design

The design of the BioScope (Figure 6.1) adapted for *E. coli* perturbation experiments was based on the 2nd generation BioScope (BioScope II) developed for perturbation experiments in yeast

(Mashego *et al.* 2006). Modification of BioScope II to fulfil the requirements for *E. coli* perturbation experiments was aimed at meeting relevant criteria as:

- Sufficient oxygen transfer capacity and plug-flow characteristics.
- A high sampling frequency, with a time interval of maximally 1 s between samples, is required for the first 4 subsequent sampling ports to catch the expected fast initial reaction dynamics of *E. coli* (Buchholz *et al.* 2002; Chassagnole *et al.* 2002; Hoque *et al.* 2005; Schaefer *et al.* 1999).
- No disturbance of the steady-state conditions of the chemostat. Therefore the inflow rate of the BioScope should not exceed the outflow rate of the chemostat culture.
- The pressure drop over the total channel should be less than 1 bar to prevent possible damage to the channel. Additionally, the cassette used in the pump-head is not recommended to be operated at differential pressures above 1 bar (ISMATEC, Glattbrugg, Switzerland).

To decrease the residence time in the BioScope without significantly increasing the through flow rate, the working volume was decreased. This was accomplished by reducing the internal diameter of the BioScope II channel from 1.2 mm to 0.8 mm and the channel length from 6.51 m to 4.00 m. This resulted in a decrease of the volume of the BioScope from the original 3.5 ml to 1.005 ml.

A LabVIEW (National Instruments Corporation, Austin, TX, USA) script was used to control a series of magnetic pinch valves for withdrawal of samples at different channel positions. The sampling ports were situated at the following channel volumes relative to the substrate addition point: 0.010; 0.022; 0.034; 0.056; 0.101; 0.165; 0.297; 0.461; 0.678 and 1.005 ml corresponding to sampling ports 1–10, respectively, as indicated in Figure 6.1. The corresponding residence times for the different sampling ports depends on the applied through flow rate, whereby increasing the through flow rate leads to decreased residence times and vice versa. This design would shorten the maximal observation time window for 10 samples, e.g. to 30.2 s at 2 ml/min, and hence if it is desired to have a shorter observation window, a faster flow rate should be used.

6.2.2. Pressure drop, residence time distribution (RTD) and oxygen transfer

Oxygenation of and CO_2 removal from the broth in the BioScope channel was achieved via the silicone membrane separating the liquid and the gas channels. The pressure drop over the liquid channel was measured at each sample port for different broth flow rates.

The residence time distribution for the different sample ports was measured by a tracer response experiment as described previously (Mashego *et al.* 2006; Visser *et al.* 2002). First, the BioScope channel was flushed with deionized water, then at t = 0 the water flow was changed to a 1.0 N KCl solution and the response at every port was measured with a conductivity meter (Dionex, Sunnyvale, USA). RTD measurements were carried out for flow rates of 2 and 4 ml/min in fivefold. The RTD of the flow cell was measured separately, using the same method. All data

were monitored using an in-house made program in LabVIEW (National Instruments Corporation, Austin, TX, USA). Afterwards the raw time and conductivity data were used as an input for a home-made computer program that calculates the mean residence time of every port and its variance by first computing the E and F-curves on the basis of the raw data (Perry and Green 1997) while correcting for the residence time of the conductivity meter. Subsequently for every port, the Peclet number, which is a characteristic for the plug-flow behaviour of the reactor, was calculated based on the normalized variance of the residence time (Fogler 1991).
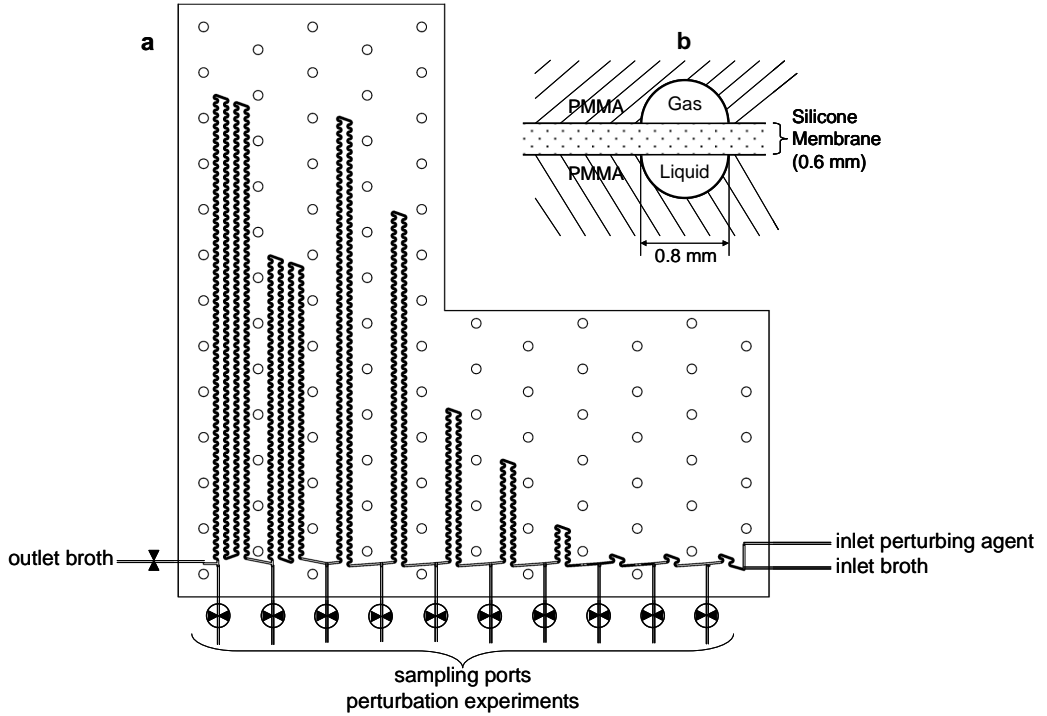
Figure 6.1: (a) 2D serpentine channel geometry of the BioScope. (b) Cross-section of the BioScope channel.

The determination of the oxygen overall mass transfer coefficient $k_{overall}$ of the BioScope was performed as described previously (Mashego *et al.* 2006; Visser *et al.* 2002). Water was flushed with nitrogen gas to remove all dissolved oxygen. The deoxygenated water (37 °C) was fed to the BioScope at a flow rate of 0.5, 1 and 2 ml/min, respectively. The dissolved oxygen (DO) concentration of the stream was measured at the different sampling ports using a flow cell in which a DO probe was mounted. The parameter $k_{overall}$ was estimated from the measured DO profiles by a least sum-of-squares fit using MATLAB (The MathWorks Inc., Natick, MA, USA) as described by Mashego *et al.* (2006).

6.2.3. Strain and preculture conditions

Escherichia coli K12 MG1655 [λ⁻, F⁻, rph⁻¹] was obtained from The Netherlands Culture Collection of Bacteria (NCCB). Cells were grown to stationary phase in shake-flasks on LB medium. Culture aliquots containing 50 % (v/v) glycerol were kept at -80 °C until they were used as inoculum of the precultures for chemostat experiments.

Precultures were grown on minimal medium with the following composition per liter: 5.0 g $(NH_4)_2SO_4$, 2.0 g KH_2PO_4, 0.5 g $MgSO_4.7H_2O$, 0.5 g NaCl, 2.0 g NH_4Cl, 5.5 g glucose.$1H_2O$, 0.001 g thiamine-HCl, 1 ml of trace elements solution as described by Verduyn *et al.* (1992) and 40 mM MOPS. The pH of the medium was adjusted to 7.0 with 1 M K_2HPO_4 before filter sterilization (pore size 0.2 μm, cellulose acetate, Whatman GmbH, Germany).

6.2.4. Chemostat cultivation

Aerobic glucose-limited chemostat cultures were carried out on minimal medium at a dilution rate (D) of 0.1 h⁻¹ in a 7 l laboratory bioreactor with a working volume of 4 l, controlled by weight (Applikon, Schiedam, The Netherlands). The medium composition was adapted from a previously published medium (Taymaz-Nikerel *et al.* 2009) to obtain a decreased chloride concentration, because too high Cl⁻ concentrations were found to interfere with the LC part of the LC-MS analysis. The composition of the low Cl⁻ minimal medium was, per liter: 1.25 g $(NH_4)_2SO_4$, 1.15 g KH_2PO_4, 0.5 g $MgSO_4.7H_2O$, 0.5 g NaCl, 30 g glucose.$1H_2O$, 0.001 g thiamine-HCl, 2 ml of trace elements solution and 0.2 ml silicone-based antifoaming agent (BDH, Poole, UK). The composition of the trace elements solution was described in Verduyn *et al.* (1992). This low Cl⁻ medium allowed a steady-state biomass concentration of about 8 gDW/l. The medium was filter sterilized (pore size 0.2 μm, polyethersulfone, Sartorius, Goettingen, Germany) without pH adjustment, the final pH of the medium was around 5.

The operating conditions, measurement of offgas (O_2/CO_2), medium feeding and steady-state conditions were as described in Taymaz-Nikerel *et al.* (2009). The steady-state was analyzed for cell dry weight, residual glucose and total organic carbon (TOC) for biomass lysis as described in Taymaz-Nikerel *et al.* (2009).

6.2.5. Rapid sampling and metabolite quantification

Quantification of intracellular metabolites was carried out with a differential method, as described previously (Taymaz-Nikerel *et al.* 2009), whereby the intracellular metabolite levels were obtained from measurements in total broth and filtrate samples. Before the perturbation experiments, that is when the culture was at steady-state, broth and filtrate sampling were carried out as described in Taymaz-Nikerel *et al.* (2009). For intracellular metabolite quantification during the perturbation experiments (in the reactor as well as in the BioScope) only broth sampling was carried out because the metabolite concentrations in the filtrate did not change

significantly during such experiments (not shown). Time patterns of intracellular metabolite levels during perturbation experiments were therefore obtained by subtraction of the measured amounts in the filtrate during steady-state conditions shortly before the perturbation, from the measured total broth amounts during transient conditions.

In brief, the procedure was as follows: fast sampling was carried out as described previously (Lange *et al.* 2001) whereby 1 ml of broth was rapidly withdrawn from the bioreactor and instantaneously quenched in tubes containing 5 ml of 60 % aqueous methanol, precooled at -40 °C, which were immediately mixed after sampling by vortexing. For filtrate sampling, syringe filtration (pore size 0.45 µm, MILLEX-HV, Millipore, Carrigtwohill, Co. Cork, Ireland) at room temperature was employed as described in Taymaz-Nikerel *et al.* (2009). The obtained 1 ml filtrate was immediately mixed with 5 ml of 60 % aqueous methanol, precooled at -40 °C, in order to process these samples in the same way as the broth samples. The exact amounts of sample obtained (for broth and filtrate) were quantified gravimetrically. For every steady-state condition two samples were taken and analyzed in duplicate. During perturbation experiments, one sample was taken and analyzed in duplicate for each time point.

For measurement of glucose and produced organic acids, syringe filtration (pore size 0.45 µm, MILLEX-HV, Millipore, Carrigtwohill, Co. Cork, Ireland) with cold stainless steel beads was employed (Mashego *et al.* 2003). For the perturbation experiments carried out directly in the chemostat, this was done simultaneously with rapid broth sampling using a second sample port. For the perturbation experiments carried out in the BioScope, each perturbation experiment was carried out twice, one for filtrate sampling and one for broth sampling. Each sample was analyzed in triplicate.

6.2.6. Perturbation experiments

In the chemostat: A moderate glucose pulse, whereby the extracellular glucose concentration was instantaneously increased from the steady-state level of 14 mg/l to 500 mg/l was applied. To achieve this, 20 ml glucose pulse solution was directly injected into the reactor with a sterile syringe. At the same time the glucose solution was injected, the feed pump was stopped. The pump was restarted 510 s after the start of the perturbation experiment.

One hour before the perturbation, the air stream for aeration of the reactor was mixed with a stream of 1.34 mol/h of pure oxygen (total gassing rate 5.80 mol/h) which resulted in an increase of the oxygen concentration of the aeration gas to 39 % (v/v). This was done to prevent the occurrence of oxygen limitation during the perturbation experiments.

In the BioScope: Short-term perturbation experiments were carried out using the BioScope designed for *E. coli* experiments, described above. In brief, broth was withdrawn from the chemostat at a flow rate of either 1.8 ml/min or 3.6 ml/min (depending on the time scale of observation), using a peristaltic pump (ISMATEC, Glattbrugg, Switzerland). The broth was mixed with a concentrated pulse solution (0.2 or 0.4 ml/min for broth flow rates of 1.8 and 3.6

ml/min, respectively) and pumped through the serpentine-shaped BioScope channel. The perturbation solution contained 27.8 mM glucose which resulted in the same initial bulk glucose concentration as for the perturbation carried out directly in the chemostat. The gas channel of the BioScope was continuously flushed with enriched air (63 % O_2) at a flow rate of 0.3 mol/h. For each time point one sample was taken and analyzed in duplicate.

Also for the BioScope experiments quantification of intracellular metabolites was carried out with the differential method, as described above. A sample tube (polystyrene, diameter of 17 mm) containing 5 ml of 60 % aqueous methanol (-40 °C) was placed under each port of the BioScope in the cryostat (Lauda RP 1845, Lauda-Köningshofen, Germany). For each sample point 1 ml of broth was withdrawn by adjusting the opening time of the valve correspondingly, i.e. 30 s for a flow rate of 2 ml/min and 15 s for a flow rate of 4 ml/min. The broth was sampled directly into the cold methanol solution. The total sampling time was 300 and 105 s for a flow rate of 2 ml/min (all ports used) and 4 ml/min (7 ports used), respectively. The sample processing procedure was the same as described in Taymaz-Nikerel *et al.* (2009).

For the measurement of the residual glucose concentration as well as organic acid production, filtrate sampling was carried out. Therefore sample tubes (polystyrene, diameter of 17 mm) filled with 32 g stainless steel beads each were placed in a cryostat and cooled down to 0 °C. From each sample port of the BioScope 3 ml of broth was withdrawn into each sample tube whereby the opening time of the valve was set at 90 s for a flow rate of 2 ml/min and 45 s for a flow rate of 4 ml/min. After sampling of the whole series, the content of each tube (steel beads with quenched broth of ~ 0 °C) was transferred to a pre-cooled syringe and directly filtered into Eppendorf tubes which were stored at -20 °C until further analysis.

After each pulse experiment, the BioScope was flushed with water, ethanol and air to clean the serpentine channels and tubings. It was not needed to sterilize the BioScope before use, because the flow of broth from the bioreactor through the BioScope is one way and does not enter the reactor anymore.

6.2.7. Metabolite extraction procedure

Metabolites were extracted in 75 % boiling ethanol (3 min, 90 °C) as described in Taymaz-Nikerel *et al.* (2009). Before extraction, 100 μl of 100 % U-^{13}C- labelled cell extract was added as internal standard.

6.2.8. Measurement of intracellular metabolite concentrations

Metabolites of the glycolysis, TCA cycle and PPP were quantified with Isotope Dilution Mass Spectrometry (IDMS) as described by van Dam *et al.* (2002) and Wu *et al.* (2005). The concentrations of the nucleotides were also analyzed with IDMS. Further details of the applied LC–ESI–MS/MS procedure have been described elsewhere (Seifar *et al.* 2009).

6.2.9. Calculation procedures

Biomass-specific rates: The biomass-specific glucose consumption rate (q_S), oxygen consumption rate (q_{O2}), carbon dioxide production rate (q_{CO2}) and the cell lysis rate (q_{lysis}) were calculated for each chemostat cultivation from the steady-state mass balances. q_{lysis} was calculated from the difference between the measured TOC content in the broth and in the supernatant as described in Taymaz-Nikerel *et al.* (2009). The specific growth rate, μ, in the chemostat was calculated as the sum of the dilution rate and q_{lysis}. The reconciled rates were calculated by standard data reconciliation techniques (Verheijen 2010).

Mass Action Ratio (MAR): For a reaction aA + bB ↔ cC + dD, the corresponding mass action ratio is calculated as $(C^c D^d)/(A^a B^b)$. Hereby a, b, c and d are the stoichiometric coefficients of the reactants/products of A, B, C and D, respectively.

6.3. Results and Discussion

6.3.1. BioScope characteristics

Pressure drop over the liquid channel of the BioScope

The observation time window of the BioScope is dependent on the total flow rate (sum of the flow rates of the perturbation agent and the culture broth) that is fed to the system and the liquid volume of the serpentine channel. An important prerequisite is not to exceed the maximum allowable liquid pressure, in order to ensure a stable flow rate and to prevent possible damage. A too high pressure drop over the liquid channel will also lead to bulging of the silicon membrane into the gas channel and result in an increase of the liquid volume which will change the residence time distribution.

The pressure drop over the liquid channel of the BioScope was measured at each sample port for flow rates between 1 and 4 ml/min. As expected, the pressure drop increases with increasing liquid flow rate and linearly increases with the channel length (not shown). At a flow rate of 2.5 ml/min and higher the measured pressure drop at some sample ports towards the end of the channel was higher than 1 bar, which we considered as the upper limit because for the peristaltic pump used a stable flow rate was not guaranteed for differential pressures above 1 bar (see materials and methods). To avoid excessive membrane bulging and variances in the set flow rates, the pressure drop over the liquid channel was kept below 1 bar by using only a part of the liquid channel in case of flow rates exceeding 2.5 ml/min. As an example, for experiments carried out at a flow rate of 4 ml/min, sample port 8 was used as waste outlet and thus the part of the channel after port 8 was not used.

Residence time distribution and plug-flow characteristics

The residence time distributions for flow rates of 2 and 4 ml/min were measured fivefold and the results obtained are depicted in Figure 6.2a. It was found that the residence times calculated for the first 3 to 4 sampling ports contained high inaccuracies (not shown). This is due to the fact that the correction made for the contribution of the conductivity cell to the measured residence time was relatively high for these first ports, because of the small volume of the corresponding part of the channel. Therefore, we used linear regression on the RTD data obtained for the ports further downstream of the channel to determine the residence times for the first sampling ports. A total flow rate of 2 ml/min enabled to sample from all 10 ports, representing periods of exposure from 1.66 to 40.10 s. A total flow rate of 4 ml/min allowed to sample from 7 ports, representing periods of exposure from 1.06 to 8.02 s. It should be noted that the measured residence times were higher than the ones obtained from the design, e.g. at 2 ml/min the residence time for the last sample port was 40.10 s instead of the designed value of 30.2 s. The most probable reason for this is that the pressure in the liquid channel resulted in bulging of the silicone membrane into the gas channel, thus increasing the volume of the liquid channel. This shows the importance of carrying out RTD measurements instead of relying on the design parameters only.
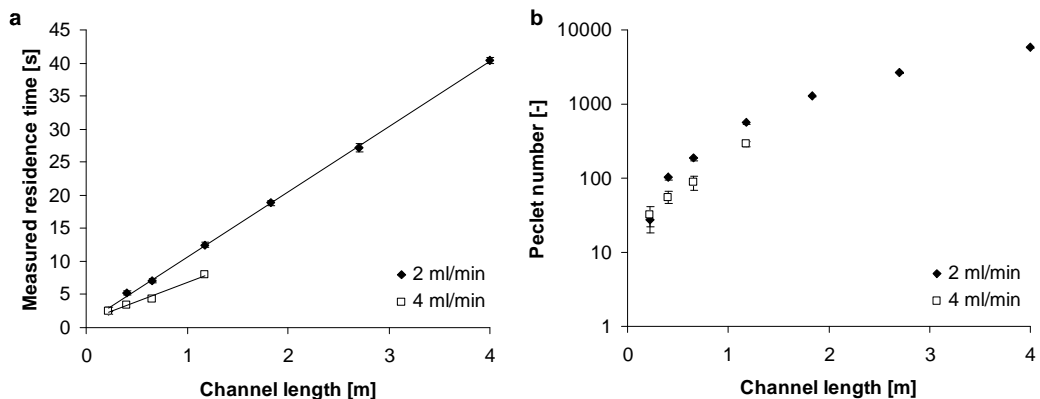
Figure 6.2: BioScope characteristics. (a) Measured residence times [s] as a function of the channel length L [m] at a flow rate of 2 ml/min (diamonds) and 4 ml/min (squares). (b) Calculated Peclet number as a function of the channel length L [m] at a flow rate of 2 ml/min (diamonds) and 4 ml/min (squares).

Figure 6.2b depicts the corresponding calculated Peclet numbers, which could not be calculated for the first 3 and 4 ports at flow rate 2 and 4 ml/min, respectively, for the reason outlined above, i.e. the large contribution of the volume of the conductivity cell used. It is known that when Pe > 30 dispersion effects can be considered negligible (Visser *et al.* 2002). As can be seen from Figure 6.2b the calculated Peclet numbers were all close to or higher than 30 and thus proper plug-flow characteristics were obtained.

Oxygen Transfer

The oxygen transfer characteristics of the BioScope were measured by introducing a flow of deoxygenated water into the liquid channel of the BioScope, which was subsequently oxygenated via the silicone membrane by flushing air through the opposite gas channel. The DO concentration of the stream was measured at the different sampling ports of the BioScope using a flow cell in which a DO probe was mounted. The obtained DO profiles for the different flow rates applied (0.5, 1 and 2 ml/min) are shown in Figure 6.3a. It can be seen from this figure that the steepness of the increase of the DO vs the channel length is inversely proportional to the liquid flow rate, due to the increased liquid residence time, and thus increased time for oxygen transfer, at lower flow rates. From the obtained DO concentration profiles the overall mass transfer coefficients for oxygen ($k_{overall}$) for the different flow rates were estimated, the results are depicted in Figure 6.3b. It can be seen from this figure that $k_{overall}$ increases with increasing liquid flow rate, and seems to level off at higher flow rates. This is most probably the result of a decrease of the liquid boundary layer at higher flow rates. The value of $k_{overall}$ for a flow rate of 2 ml/min was estimated to be $3.2 \ 10^{-5}$ m/s. This value is significantly higher than the value of $1.8 \ 10^{-5}$ m/s estimated for BioScope II (Mashego *et al.* 2006), which was designed for pulse response experiments with *Saccharomyces cerevisiae* and comparable to the estimated $k_{overall}$ for the first-generation BioScope ($3.0 \ 10^{-5}$ m/s) (Visser *et al.* 2002).
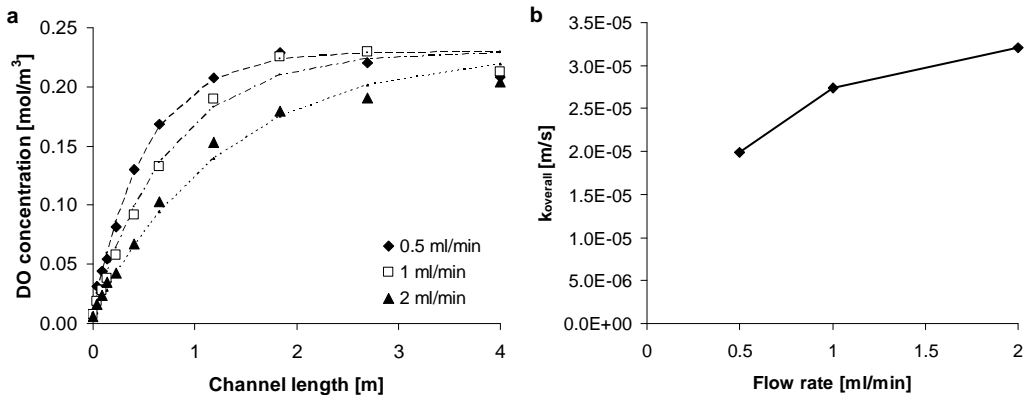
Figure 6.3: (a) Measured dissolved oxygen (DO) concentration profiles with the fitted patterns that belong to the estimated $k_{overall}$, (b) Estimated $k_{overall}$ as function of different flow rates.

Considering the specific surface area for gas exchange of 3183 m^2/m^3 for a semicircular channel with a diameter of 0.8 mm, the $k_L a$ for oxygen transfer can be calculated to equal 367 h^{-1}. This is lower (albeit sufficient enough) than the $k_L a$ of the chemostat which was approx. 500 h^{-1}, as was calculated from the oxygen uptake rate and dissolved oxygen tension during steady-state chemostat cultivation of *E. coli*. From this it was concluded that the oxygen transfer capacity of

the BioScope would be high enough to carry out the glucose pulse experiments while maintaining fully aerobic conditions.

6.3.2. Characteristics of the *E. coli* steady-state

In this study two aerobic glucose-limited steady-state chemostat cultivations on minimal medium at a dilution rate of 0.1 h^{-1} were carried out. The raw and reconciled biomass-specific rates of glucose consumption, biomass decay, biomass growth, oxygen consumption and carbon dioxide production for the two steady-state cultures are given in Table 6.1. The results show that the cultures were reproducible and that there were no significant differences between the reconciled and measured q-rates, indicating that during aerobic steady-state chemostat growth of *E. coli,* glucose was converted to biomass without significant amounts of by-product formation, except cell lysis products.

Table 6.1: Measured and reconciled data for aerobic glucose-limited *E. coli* chemostat cultures at D = 0.1 h^{-1}, with their standard errors

	Experiment 1		Experiment 2	
	Measured	**Reconciled**	**Measured**	**Reconciled**
C_X **[gDW/l]**	8.40 ± 0.12	8.36 ± 0.12	8.02 ± 0.12	8.02 ± 0.12
D [h^{-1}]	0.101		0.105	
μ [mmol/Cmol X.h]	129.5 ± 2.7	129.2 ± 2.7	136.6 ± 2.7	136.6 ± 2.6
-q$_S$ [mmol/Cmol X.h]	40.78 ± 1.6	42.3 ± 1.2	44.61 ± 1.8	44.5 ± 1.3
-q$_{O2}$ [mmol/Cmol X.h]	120.3 ± 5.9	115.7 ± 4.7	125.4 ± 8.3	121.1 ± 5.8
q$_{CO2}$ [mmol/Cmol X.h]	124.4 ± 6.1	124.6 ± 4.9	130.2 ± 8.7	130.5 ± 6.0
q$_{lysis}$ [mmol/Cmol X.h]	28.9 ± 1.6	28.9 ± 1.6	31.4 ± 1.2	31.3 ± 1.2
Carbon Recovery [%]	103.8 ± 6.1		99.7 ± 5.3	
Redox Recovery [%]	106.1 ± 5.5		101.8 ± 4.3	

Intracellular metabolite levels were obtained from measurements in total broth and culture filtrate according to Taymaz-Nikerel *et al.* (2009). Table 6.2 gives an overview of the intracellular levels of the glycolytic and TCA cycle intermediates and nucleic acids during steady-state chemostat growth for the two experiments. Most of the measured metabolite levels in the filtrate were comparable (results not shown) with previous findings (Taymaz-Nikerel *et al.* 2009). Also in these experiments no nucleotides were detected in the filtrate. The intracellular metabolite levels in the two independent cultures appeared very similar for most of the compounds measured, which indicates the reproducibility of our measurements/cultivations.

Table 6.2: Average intracellular levels of glycolytic and TCA cycle intermediates, and adenine, guanine and uridine nucleotides, measured during steady-state chemostat growth [µmol/gDW]

Metabolite	Experiment 1	Experiment 2
G6P	1.22 ± 0.04	1.22 ± 0.02
F6P	0.27 ± 0.01	0.28 ± 0.01
M6P	0.40 ± 0.01	0.44 ±0.01
Mannitol-1P	0.42 ± 0.03	0.75 ± 0.09
6PG	0.27 ± 0.01	0.22 ± 0.02
FBP	0.67 ± 0.02	0.55 ± 0.07
2PG+3PG	1.24 ± 0.04	1.38 ± 0.03
PEP	1.19 ± 0.05	1.22 ± 0.03
Pyruvate	0.43 ± 0.02	0.30 ± 0.04
Citrate[a]	1.64 ± 0.06	1.12 ± 0.02
Succinate[a]	16.55 ± 0.54	22.41 ± 0.43
Fumarate[a]	0.41 ± 0.07	0.38 ± 0.01
Malate[a]	1.35 ± 0.04	1.57 ± 0.04
ADP	1.30 ± 0.04	1.41 ± 0.05
ATP	5.30 ± 0.16	5.30 ± 0.29
GDP	0.37 ± 0.03	0.31 ± 0.03
GTP	1.42 ± 0.12	1.53 ± 0.07
UDP	0.65 ± 0.05	0.64 ± 0.05
UTP	1.00 ± 0.06	1.54 ± 0.11

[a] Amount in the broth.

6.3.3. Perturbation experiments: comparison of reactor to BioScope

Glucose perturbation experiments were carried out directly in the chemostat (Experiment 1, time window of 40 s) and outside the chemostat by using the BioScope (Experiment 2) at two different flow rates: 2 and 4 ml/min providing observation time windows of 8 and 40 s, respectively. The dissolved oxygen concentration in the chemostat before the glucose pulse carried out in the chemostat (Experiment 1) was about 0.42 mol/m^3 (note that 100 % of air saturation at 37 ^{o}C and 1 bar corresponds with a dissolved oxygen concentration of 0.23 mol/m^3) because oxygen enriched air was used for aeration to prevent oxygen limitation during the pulse experiment (see materials and methods). During the glucose pulse experiment carried out in the chemostat the dissolved oxygen concentration decreased to approx. 0.35 mol/m^3 (in 40 s). For the glucose pulse carried out in the BioScope (Experiment 2), the dissolved oxygen concentration in the chemostat was 0.15 mol/m^3 because normal air was used for aeration. During the glucose pulse carried out in the BioScope the dissolved oxygen concentration never dropped below 0.14 mol/m^3 (DO measured at the last sampling port of the BioScope). These results confirm that there was no

oxygen limitation during the glucose perturbation experiments both in the chemostat and in the BioScope.

Because the pH in the BioScope was not controlled, it was verified whether a significant change in the pH occurred during the glucose pulse experiment. The pH of the broth measured at the end of the serpentine channel (waste outlet) of the BioScope was 6.8, showing that the pH decreased only slightly (from pH 6.9 in the reactor to pH 6.8 at the end port of the BioScope) during the glucose pulse.

The measured dynamic patterns of the intracellular levels of the glycolytic and TCA cycle intermediates and nucleic acids during the glucose pulse experiments carried out in the chemostat and the BioScope are shown in Figures 6.4 - 6.7. Figure 6.8 presents some derived quantities (mass action and relevant metabolite ratios).

It can be seen from the results shown in Figures 6.4 - 6.7 that the sudden increase of the external glucose concentration from about 14 mg/l to 500 mg/l led to a fast response of the intracellular metabolite concentrations. The BioScope data obtained at the two different flow rates corresponded well with each other, indicating that these pulses were well reproducible. Moreover, the dynamic metabolite patterns obtained from the BioScope pulse experiments were in most cases very similar to the patterns obtained from the pulse experiments carried out directly in the chemostat.

For the majority of the measured metabolites most of the dynamics occurs during the first 5 - 10 s after the pulse. This implies that to properly catch these dynamics in prokaryotes, intensive sampling at a resolution of seconds to subseconds is required, indicating once again the usefulness and necessity of the BioScope and/or similar devices. Clearly the frequency of the manual sampling carried out during the pulse experiment in the chemostat, which was approx. one sample per 5 s, was not sufficient to catch the dynamics of *E. coli*.

It can be observed from the metabolite patterns shown that after a period of about 20 s a metabolic pseudo-steady-state (pss) was reached. Also, the metabolic pss in *E. coli* was reached much faster than observed for yeast or filamentous fungi in similar glucose pulse experiments, for which this took several minutes (Mashego *et al.* 2006; Nasution *et al.* 2006; Wu *et al.* 2006). As can be seen from the results shown in Figures 6.4 - 6.7 the measured metabolite levels during this pss appeared very similar in the BioScope and chemostat pulse experiments.

6.3.4. Perturbation experiments: metabolite responses

The metabolites belonging to different pathways clearly showed different dynamics (Figures 6.4 - 6.7). Hereby the glycolytic intermediates showed the fastest dynamic behaviour (see Figures 6.4 and 6.5), while the changes in the levels of the TCA cycle intermediates occurred slower (see Figure 6.6). Little dynamics was observed for the adenosine, guanosine and uridine nucleotides throughout the perturbation (see Figure 6.7).

The most rapidly responding metabolites were PEP, pyruvate, 2PG+3PG and G6P (see Figures 6.4 and 6.5). The rapid decrease of PEP and corresponding increase of pyruvate clearly shows the fast response of the phosphotransferase system (PTS) through which one mol PEP is utilized for glucose translocation and phosphorylation, producing one mol of pyruvate. This resulted in a very large increase of the pyruvate/PEP ratio, one of the indicators of the phosphorylation state of PTS, until after about 10 s a pss was reached (see Figure 6.8). The fast decrease of the PEP level corresponded with a comparable fast decrease of the level of 2PG+3PG (Figure 6.5). The mass action ratio PEP/(2PG+3PG) also shows a fast decrease until after a few seconds a pss is reached.

The fast response of the PTS system is also reflected in the fast change of the G6P level, which increased with a factor three within a second after the pulse. Remarkably, the F6P level increased much slower. This results in a very fast and steep decrease of the mass action ratio of PGI from
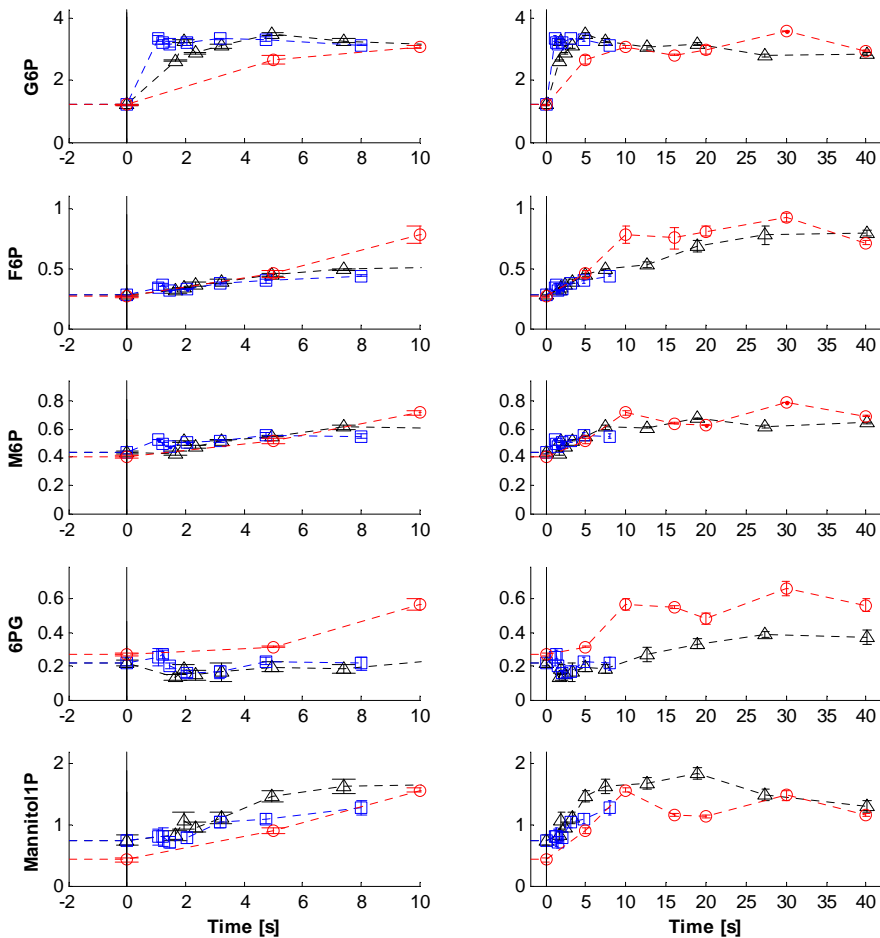
Figure 6.4: Measured dynamic patterns [μmol/gDW] of glycolytic metabolites, 6PG and Mannitol-1P during the glucose pulse in the reactor (Experiment 1, circles) and in the BioScope (Experiment 2, triangles: flow rate 2 ml/min, total perturbation period 40.1 s and squares: flow rate 4 ml/min, total perturbation period 8.0 s).

0.23, which is close to the equilibrium value of 0.32±0.08 (Goldberg *et al.* 2004), to 0.1, followed by a slow recovery to a pss value that is close to the initial value (see Figure 6.8). This suggests that the extremely fast increase of G6P induces a rapid but temporary displacement from equilibrium of PGI.
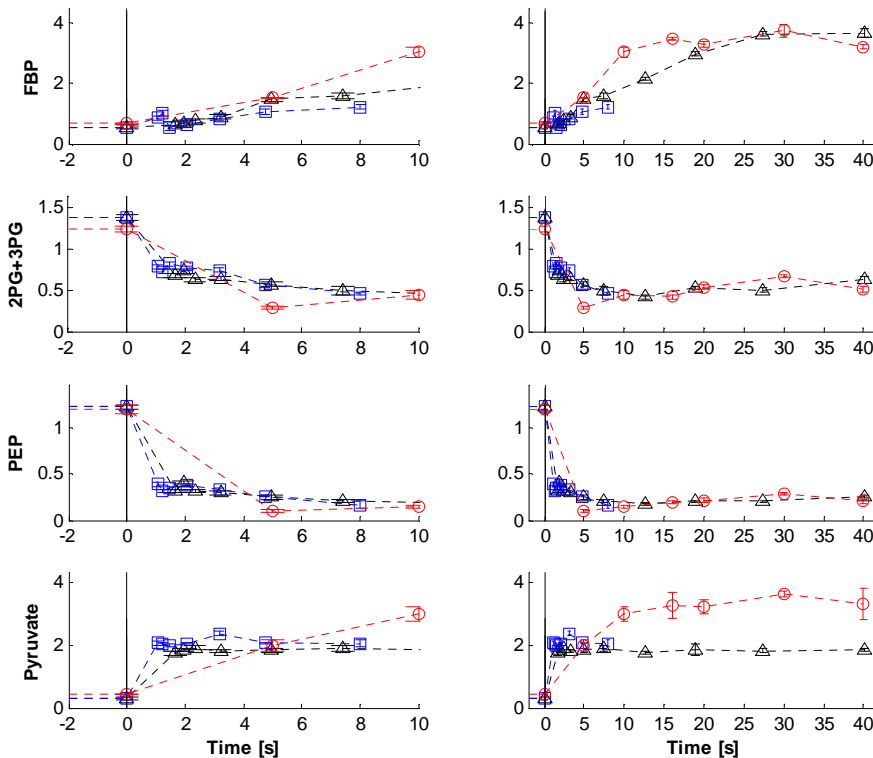
Figure 6.5: Measured dynamic patterns [µmol/gDW] of lower glycolytic metabolites during the glucose pulse in the reactor (Experiment 1, circles) and in the BioScope (Experiment 2, triangles: flow rate 2 ml/min, total perturbation period 40.1 s and squares: flow rate 4 ml/min, total perturbation period 8.0 s).

The levels of the measured hexose-phosphates G6P, F6P and M6P increased to reach a pss with values of respectively 3-, 3- and 2-fold their initial value. However, the dynamics during the increase of the metabolites were very different, as is reflected in the mass action ratios. Compared to the F6P/G6P ratio the M6P/F6P ratio shows a relatively slow decrease to a pss value which is about 2/3 of the initial value (Figure 6.8), which might be due to an increased anabolic demand.

The fact that the intracellular levels of the nucleotides do not change significantly during the perturbation experiments shows the robustness of the energy system of *E. coli* (Figure 6.7). Similar results for nucleotides were obtained in replicate perturbation experiments (data not shown).
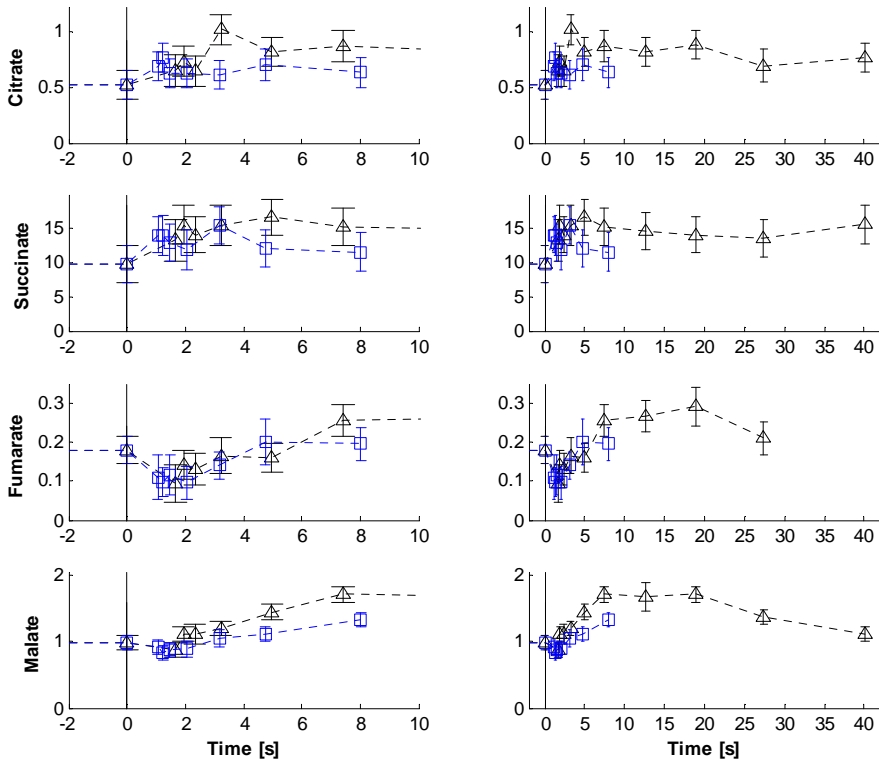
Figure 6.6: Measured dynamic patterns [µmol/gDW] of TCA cycle metabolites during the glucose pulse in the BioScope (Experiment 2, triangles: flow rate 2 ml/min, total perturbation period 40.1 s and squares: flow rate 4 ml/min, total perturbation period 8.0 s).

Several authors have reported the fast metabolic response of different strains of *E. coli* K12 to glucose perturbations in aerobic glucose-limited chemostats at a dilution rate of 0.1 h^{-1} (Buchholz *et al.* 2002; Chassagnole *et al.* 2002; Hoque *et al.* 2005; Schaefer *et al.* 1999; Schaub and Reuss 2008). The initial glucose concentration obtained after injection of the pulse solution was either 0.3 g/l (Chassagnole *et al.* 2002; Schaub and Reuss 2008) or 3 g/l (Buchholz *et al.* 2002; Hoque *et al.* 2005; Schaefer *et al.* 1999).

The sudden injection of a glucose solution into a glucose-limited chemostat results in the sudden relief of carbon-limited conditions and thus in a sharp increase of the oxygen uptake rate. However, in none of the previous studies it was reported whether special precautions were taken to prevent oxygen limitation. Furthermore no results of dissolved oxygen measurements were presented to show that oxygen non-limited conditions were maintained during the glucose perturbation.

Although the published glucose pulse experiments were carried out in a similar way, different methods for sampling, quenching, and metabolite extraction were used. Schaefer *et al.* (1999) and Buccholz *et al.* (2002) used an automated rapid sampling device whereby the sample was sprayed into a cold methanol solution (60 % v/v, -50 $^{\circ}$C). After cold centrifugation, the cell pellet was

extracted in cold perchloric acid. Hoque *et al.* (2005) also applied cold methanol quenching (60 % v/v, -80 °C), cold centrifugation and cold perchloric acid extraction. The advantage of the cold methanol procedure is that it allows removal of the extracellular metabolites, but has the disadvantage that part of the intracellular metabolites is lost by leakage from the cells into the cold methanol solution (Bolten *et al.* 2007; Taymaz-Nikerel *et al.* 2009). Both Chassagnole *et al.* (2002) and Schaub and Reuss (2008) used total broth sampling, whereby Chassagnole *et al.*
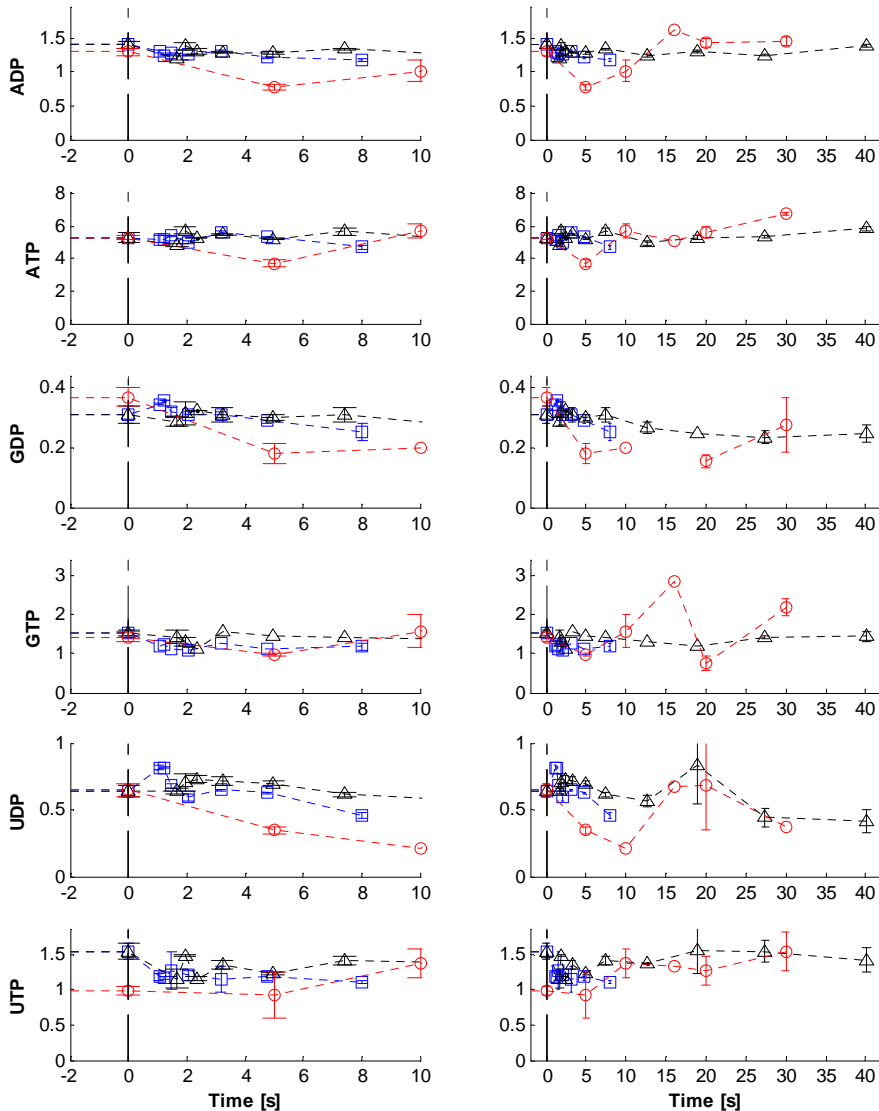
Figure 6.7: Measured dynamic patterns [μmol/gDW] of nucleotides during the glucose pulse in the reactor (Experiment 1, circles) and in the BioScope (Experiment 2, triangles: flow rate 2 ml/min, total perturbation period 40.1 s and squares: flow rate 4 ml/min, total perturbation period 8.0 s).

(2002), sampled either into liquid nitrogen (for measurement of acid labile metabolites) or in cold perchloric acid. Schaub and Reuss (2008) applied combined quenching and extraction of the broth with a helical coil heat exchanger. It should be noted that total broth extraction may lead to overestimation of metabolite levels, depending on the amount present in the intracellular medium. It has been shown that in *E. coli* this is indeed the case for many metabolites (Taymaz-Nikerel *et al.* 2009).
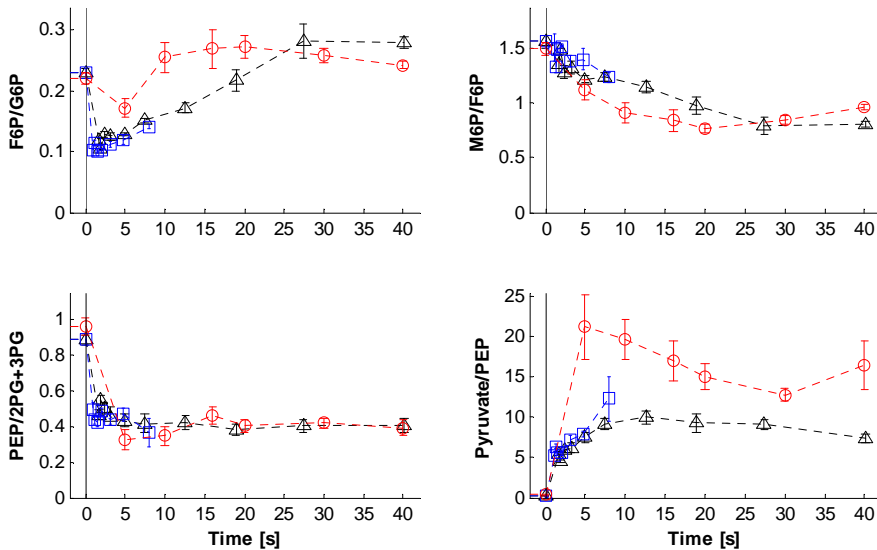
Figure 6.8: Calculated mass action ratios (MAR) for phosphoglucose isomerase (PGI), mannose-6P isomerase (PMI), combined enolase (ENO), phosphoglyceratemutase (PGM) and Pyr/PEP ratio during the glucose pulse in the reactor (Experiment 1, circles) and in the BioScope (Experiment 2, triangles: flow rate 2 ml/min, total perturbation period 40.1 s and squares: flow rate 4 ml/min, total perturbation period 8.0 s).

For several metabolites the reported response to a glucose pulse was similar to what has been measured in the present study, although the absolute levels were sometimes different, e.g. a very rapid increase (within one second) of the G6P level and corresponding decrease of PEP due to the sudden increase of glucose translocation and phosphorylation by the PTS (Buchholz *et al.* 2002; Schaefer *et al.* 1999). However, Schaefer *et al.* (1999) and Hoque *et al.* (2005) reported a decrease for both PEP and pyruvate after the glucose pulse, which is not expected when glucose uptake is mediated by the PTS. Another example to differences from our results is that both Schaefer *et al.* (1999) and Buchholz *et al.* (2002) reported a rapid decline followed by an increase of PEP. Moreover, the metabolite profiles reported by both authors showed an oscillatory behaviour, which was not observed in our experiments. Hoque *et al.* (2005) and Schaub and Reuss (2008) observed similar trends in the responses of 2PG+3PG and PEP after the glucose pulse, but the responses were much less fast and pronounced as observed in our experiments.

Remarkably, the reported steep decline of the intracellular ATP level after subjecting the *E. coli* chemostat culture to a glucose pulse (Chassagnole *et al.* 2002; Hoque *et al.* 2005) was not observed in our experiments.

Compared to eukaryotes (*S. cerevisiae* and *Penicillium chrysogenum*) the dynamics in *E. coli* are much faster (about factor 7) but similar profiles of metabolites can be observed (Mashego *et al.* 2007b; Nasution *et al.* 2006). For pyruvate, a different profile in yeast was observed due to the fact that yeast does not have the PTS. Another difference we observed is that the intracellular nucleotide levels do not change much during a glucose pulse in *E. coli*, whereas a sharp decrease in the ATP level was observed in eukaryotes (Mashego *et al.* 2007b; Nasution *et al.* 2006).

6.4. Conclusions

Metabolic responses of *E. coli* to glucose pulses were efficiently determined within a short time period (40 s) in an adapted BioScope system. Metabolite responses were shown to differ with respect to relative concentration changes and dynamic behavior. The good agreement between the dynamic patterns of several glycolytic, TCA cycle intermediates and nucleotides in *E. coli* after a glucose pulse carried out directly in the chemostat and in the BioScope demonstrates that the BioScope is a promising device for studying *in vivo* kinetics. Additionally, the BioScope system has the advantage that it allows withdrawal of sufficient sample volume for extensive metabolite analysis. An important aspect which has often been neglected is to maintain aerobic conditions during rapid perturbation experiments. It was shown that oxygen transfer in the BioScope is sufficient to achieve this.

Kinetic metabolic models appear necessary in order to fully exploit the information on the complex *in vivo* regulation of metabolic networks. The analysis of metabolome data after a glucose pulse can be complemented by investigations aiming at performing different perturbation experiments to obtain richer kinetic data that would increase our understanding quantitatively.

Acknowledgments

Flux and metabolite flexibility in central metabolism

Abstract

A kinetic experimental approach to provide *in vivo* information on the flux capacity of the central metabolism can be based on the *in vivo* dynamic response of fluxes and intracellular metabolites, at a time scale of 40 s, to glycolytic (glucose) and gluconeogenic (pyruvate, succinate) substrate pulses in *Escherichia coli*. To achieve this, two independent glucose-limited aerobic chemostat experiments were performed under identical conditions (D = 0.1 h^{-1}). One chemostat was used to provide the biomass for BioScope pulse experiments with three different substrates to obtain the information on dynamic metabolite response (< 40 s). The other chemostat was used to perform the same pulse experiments in the chemostat to obtain the dynamic flux response. The dynamic biomass-specific O$_2$ consumption rate, q$_{O2}$(t), was determined with the dynamic dissolved O$_2$ mass balance using the dissolved O$_2$-probe response characteristics and the measured dissolved O$_2$-profile during the pulses. μ(t) is calculated either from q$_{O2}$(t) and the degree of reduction balance (pseudo-steady-state (pss) conditions) or from the yield of produced biomass on consumed O$_2$ (dynamic conditions). Interestingly after each added different substrate, within 40 s the growth rate increased from its steady-state value of 0.13 h^{-1} to 0.3 h^{-1}, indicating a capacity limit in e.g. ribosomes. The three different substrates achieved pss in about 30 - 40 s and a huge O$_2$ uptake capacity of the cells was observed. Most importantly, during the 40 s transient the pss approximation was valid due to metabolite turnover times of seconds, allowing simple intracellular flux calculations during the transient. The observed dynamic responses of intermediates for the three different substrates show massive reorganization and enormous flexibility (up to 12 - 100 fold change) of intracellular fluxes (most important being the occurrence of gluconeogenesis after the pyruvate and succinate pulses), which matches with the steep changes in metabolite levels leading to dynamic shifts in mass action ratio's of pseudo/near equilibrium reactions. From the dynamic intracellular metabolite and flux information, the *in vivo* kinetics was studied based on a simplified thermodynamic approach. It was found that several enzymes showed simple near-equilibrium kinetics as found before in baker's yeast (Q-linear kinetics, (Canales *et al.* 2010)).

7.1. Introduction

It is generally expected that improvement of microorganisms, towards a higher product rate/ yield, can benefit from genome-scale kinetic models in which all major metabolic fluxes can be calculated as function of enzyme levels and enzyme kinetic properties. This allows the identification of premium gene targets for metabolic pathway engineering, thus avoiding the labor intensive trial-and-error genetic engineering and strain testing (Nielsen 2001; Stephanopoulos 1994).

In vivo kinetic modeling of metabolism requires experimental information on fluxes, enzyme levels and metabolite concentrations under a number of different conditions which can be obtained from perturbations of controlled steady-state cultures (Nikerel *et al.* 2006; Oldiges and Takors 2005; Theobald *et al.* 1997; Visser *et al.* 2002). In rapid short-term perturbation experiments the enzyme levels can be assumed constant and only measurements of concentrations of extra- and intracellular metabolites are required for kinetic modeling purposes. The measured extracellular concentrations allow mass-balance-based calculation of the associated uptake/secretion fluxes, leading to all reaction fluxes in the network (Taymaz-Nikerel *et al.* 2010c). The combination of changed fluxes and changed intracellular metabolite concentrations provides the required information to deduce the *in vivo* kinetic properties of the enzymes.

For *Escherichia coli* it was recently demonstrated that these rapid perturbation experiments can be performed in the BioScope (De Mey *et al.* 2010b) and it was found that metabolite dynamics in *E. coli* are indeed very fast (< 1 s), requiring perturbation experiments within a time frame of 20 - 40 s.

In these stimulus-response experiments the perturbing agent is generally chosen to be glucose because it ensures an immediate response of the pathways in central metabolism. However, it should be realized that perturbing the system in an alternative way, e.g. using a different substrate, will yield different responses, which gives richer information to capture the *in vivo* kinetics.

The advantage of information richness in these rapid perturbation experiments (e.g. carried out in the BioScope) comes with a disadvantage. The limitation of a rapid perturbation experiment is that the change in the extracellular concentration of the pulsed substrate cannot be quantified accurately in the short time period (20 - 40 s) of the pulse experiment, because this change is small. Hence the uptake rate of substrate is difficult to quantify. For this purpose samples should be taken during a longer period of time, which cannot be achieved in the BioScope but which is possible in the bioreactor. More importantly, applying pulses in the bioreactor also does permit monitoring the changes in the offgas O_2/CO_2 and dissolved O_2 concentration, thus allowing the time (at seconds time scale) resolved quantification of O_2 uptake rate (Taymaz-Nikerel *et al.* 2010c; Wu *et al.* 2006). O_2 and substrate consumption rates are essential to construct carbon and redox balances (Nasution 2007; Wu *et al.* 2006) allowing the quantification of changes in growth

rate at seconds time scale, which is needed to calculate the *in vivo* fluxes during the rapid pulse experiment.

In succinate production from glucose both glycolytic and gluconeogenic pathways such as the glyoxylate pathway and PEP carboxykinase (PPCK) are important. Therefore the main aim of this work is to apply a kinetic experimental approach to study in *E. coli* the *in vivo* kinetic response to glycolytic and gluconeogenic substrate pulses to provide *in vivo* information on flux capacity of e.g. the glyoxylate and PPCK path. The pulse substrates were glycolytic (glucose) and gluconeogenic (pyruvate, succinate). A wide range of metabolites (glycolysis, pentose phosphate pathway (PPP), tricarboxylic acid (TCA) cycle, nucleotides and amino acids) were monitored in each experiment.

7.2. Materials and Methods

7.2.1. Strain and fermentation conditions

The *E. coli* K12 MG1655 [λ^-, F$^-$, rph^{-1}] strain was cultivated (temperature 37 ^{o}C, pH 7) in aerobic glucose-limited chemostat cultures with minimal medium at a dilution rate (D) of 0.1 h^{-1} in 7 l laboratory bioreactors with a working mass of 4 kg, controlled by weight (Applikon, Schiedam, The Netherlands). The preculture conditions, medium composition, fermentor conditions (temperature control, pH control, overpressure, aeration rate, stirrer speed, dissolved oxygen and offgas measurements) were as stated in De Mey *et al.* (2010b). It is noteworthy that the here used nutrient medium was designed with much lower Cl$^-$ and K$^+$ concentrations, because too high Cl$^-$ concentrations were found to interfere with the LC part of the LC-MS analysis of intracellular metabolites.

7.2.2. Rapid perturbation experiments

Rapid perturbation experiments in the bioreactor and in the BioScope were carried out as described before (De Mey *et al.* 2010b; Taymaz-Nikerel *et al.* 2010c). To be able to calculate, in the bioreactor perturbation experiment, the O$_2$-uptake rate from the dynamic dissolved O$_2$ mass balance, it is necessary to obtain the dynamics of the DO-probe before the perturbation. In brief, before starting the perturbation experiment, the air inlet to the reactor was blended with pure O$_2$ in order to obtain about 39 % O$_2$ in the incoming gas (the gas inflow rate was increased from 1.67 l/min air to 1.67 l/min air + 0.5 l/min O$_2$). The measured DO profile in this transient was used to obtain the DO-probe dynamics (see Appendix 7.5.1). The feed pump and broth outflow were stopped at the start of the perturbation experiment and restarted at 510 s after the pulse. Perturbation to the reactor was performed with a 20 ml pulse solution, directly injected in the reactor by means of a sterile syringe.

Perturbation in the BioScope was studied for two different flow rates (at 1.8 ml/min broth + 0.2 ml/min pulse and 3.6ml/min broth + 0.4 ml/min pulse) to cover two time frames (8 and 40 s) of the perturbation experiment.

The pulse solution was either 27.8 mM glucose, 55.5 mM pyruvate or 41.6 mM succinate. This resulted in a substrate concentration of 16.7 mCmol/l carbon of each substrate at the start of each pulse (both in the bioreactor and the BioScope).

7.2.3. Rapid sampling for intracellular metabolites

The differential method (Taymaz-Nikerel *et al.* 2009) was applied to obtain the amounts of intracellular metabolites at steady-state as well as during the transient state. The required broth sampling and filtrate sampling was carried out as described in Taymaz-Nikerel *et al.* (2009). Every steady-state before perturbation was sampled twice and each sample was analyzed in duplicate. For intracellular metabolite determination during the perturbation experiment, only sampling for broth was performed (De Mey *et al.* 2010b; Taymaz-Nikerel *et al.* 2010c) at each time point and analyzed in duplicate.

For measurement of glucose and possible secreted by-products (organic acids, alcohols) the filtrate sampling was performed in the reactor and in the BioScope as described in De Mey *et al.* (2010b).

7.2.4. Metabolite extraction procedure

Metabolites were extracted in 75 % boiling ethanol (3 min, 90 $^{\circ}$C) as described in Taymaz-Nikerel *et al.* (2009). Before extraction, 100 μl of 100 % U-^{13}C- labeled cell extract was added to each sample as internal standard for isotope dilution mass spectrometry (IDMS)-based metabolite quantification (Wu *et al.* 2005).

7.2.5. Analytical protocols

Measurement of offgas (O_2 and CO_2), cell dry weight, residual glucose, total organic carbon and intracellular metabolite concentrations were carried out as described before (De Mey *et al.* 2010b; Taymaz-Nikerel *et al.* 2009). Supernatant (filtrate) samples for extracellular pyruvate determination during the pyruvate pulse were kept in the fridge (about 4 $^{\circ}$C) about a few days until analysis. Pyruvate concentration was measured with HPLC (Aminex HPX-87H ion exclusion column, Bio-Rad, CA, USA) with a refractive index detector (Waters 2414) and UV detector at 210 nm. The column was eluted with phosphoric acid (15 mmol/l) at a column temperature of 59 $^{\circ}$C and a flow rate of 0.6 ml/min. The extracellular succinate concentration

during the succinate pulse was analyzed enzymatically (Boehringer Mannheim/R-Biopharm, Roche).

The supernatant samples obtained after the pulses were extensively analyzed for possible by-product secretions. HPLC (Aminex HPX-87H ion exclusion column, Bio-Rad, CA, USA; the column was eluted with 1.5 mmol/l phosphoric acid except for pyruvate quantification) and LC-MS/MS (van Dam *et al.* 2002) analysis were performed to check the presence of ethanol, acetaldehyde, glyoxylate, acetate, formate, lactate, fumarate, pyruvate, oxaloacetate, malate, succinate, citrate and α-ketoglutarate.

Metabolites of the glycolysis, TCA cycle, PPP, adenine nucleotides and free amino acids were quantified with IDMS, which mainly includes using uniformly ^{13}C-labeled metabolites as internal standards in the metabolite extraction procedure (see above) and the subsequent analysis, as described by Wu *et al.* (2005). The concentrations of the metabolites of the glycolysis, TCA cycle and PPP were analyzed by LC-MS/MS (van Dam *et al.* 2002; Wu *et al.* 2005), the concentrations of the nucleotides were analyzed with LC–ESI–MS/MS (Seifar *et al.* 2009) and amino acids were analyzed by GC-MS (Taymaz-Nikerel *et al.* 2009).

7.2.6. Calculation methods

Biomass-specific rates during steady-state: The mass-balance-based and reconciled (conservation of elements) biomass-specific glucose consumption rate ($-q_S$), oxygen consumption rate ($-q_{O2}$), carbon dioxide production rate (q_{CO2}), growth rate (μ) and cell lysis rate (q_{lysis}) were calculated as described before (De Mey *et al.* 2010b; Taymaz-Nikerel *et al.* 2009).

Biomass-specific uptake/secretion rates during the pulse experiment: $-q_S$, q_i of secreted by-products and $-q_{O2}$ during the pulses were obtained from experimental data as described in Taymaz-Nikerel *et al.* (2010c). To obtain the dynamic $-q_{O2}(t)$, the dynamic dissolved O_2 (DO) mass balance is applied using the measured DO-profile during the pulse, a validated k_La value and the properly validated measurement of dynamic response of the DO probe (see Appendix 7.5.1 for the full details). $\mu(t)$ is then calculated as follows. In pseudo-steady-state at $t > 30 - 40$ s μ follows from the degree of reduction balance, $\gamma_S(-q_S) = \gamma_X\mu + \gamma_{O2}(-q_{O2})$, where absence of secreted products is assumed, ($\gamma_S = 24$ for glucose, 10 for pyruvate and 14 for succinate, $\gamma_X = 4.3$ (Taymaz-Nikerel *et al.* 2010a), $\gamma_{O2} = -4$) using the experimentally obtained $-q_{O2}(t)$ and $q_S(t)$. During the transient ($t < 30$-40 s), large changes in metabolite concentrations prevent the use of the simple γ-balance. The dynamic pattern of μ during the transient ($t < 30 - 40$ s) then follows from $-q_{O2}(t)$ and the assumption that the yield of produced biomass on consumed O_2 (μ/q_{O2}) is constant during the transient. Appendix 7.5.2 shows that this is indeed true for the range of growth rates (0.13 - 0.3 h^{-1}) occurring in the pulse experiment.

Intracellular fluxes and turnover times: The intracellular fluxes in steady-state and transient state were calculated with metabolic flux analysis using the appropriate metabolic network of *E. coli* (Taymaz-Nikerel *et al.* 2010c) with the available $q_S(t)$, $q_{O2}(t)$ and $\mu(t)$ as input. This assumes,

in the period before metabolite steady sate (< 40 s), applicability of metabolite pseudo-steady-state, which holds due to the observed very short turnover time of nearly all metabolites (< 1 s).

The metabolic network for growth on glucose is as described in Taymaz- Nikerel *et al.* (2010a) with the addition of the PEP-glyoxylate route (Nanchen *et al.* 2006), leading to the final network as in Taymaz-Nikerel *et al.* (2010c). The addition of the PEP-glyoxylate route created a parallel pathway, which requires additional information to perform MFA. Ratios of $Flux_{PPC}/Flux_{PPCK} = 2$ and $Flux_{ICL} = 0.2 \times Flux_{ACoNT}$ were assumed since these average ratios were observed (Nanchen *et al.* 2006) at dilution rates $0.1 - 0.4$ h^{-1} in glucose-limited continuous cultures of the same *E. coli* strain as used in the present work.

For the pyruvate network, the phosphofructokinase (PFK) reaction was replaced with the fructose-1,6-bisphosphatase (FBP) reaction. Additionally the oxidative PPP and PEP carboxylase reactions were set to 0. In the succinate network, again PFK was replaced by FBP and again the oxidative PPP, and PEP carboxylase reactions were set to 0. These choices will be discussed in the appropriate result section. The turnover times of the intracellular pools were calculated as described in Taymaz-Nikerel *et al.* (2010c).

Mass Action Ratio (MAR), Intracellular NAD$^+$/NADH ratio, energy charge: Thermodynamic feasibility of the direction of fluxes was judged by calculating mass action ratios of intracellular pseudo- and near-equilibrium reactions. Intracellular MARs, NAD$^+$/NADH ratio and energy charge were calculated as described before (De Mey *et al.* 2010b; Taymaz-Nikerel *et al.* 2009). For the NAD$^+$/NADH ratio calculation, the concentration of F6P (not successfully analyzed in the transient) was calculated from G6P and the equilibrium constant of the reaction phosphoglucose isomerase (PGI) under assumption of PGI equilibrium.

Concentration of unmeasured intermediates: The intracellular concentration of E4P was calculated through the non-oxidative PPP reactions that were assumed to operate near equilibrium, as described in Taymaz-Nikerel *et al.* (2010c). The intracellular concentration of oxaloacetate was calculated from the near-equilibrium reaction, malate dehydrogenase (Malate + NAD$^+$ $\leftrightarrow$ oxaloacetate + NADH + H$^+$, $K = 2.33 \times 10^{-5}$ at pH 7.0) using the information of NAD$^+$/NADH ratio and malate concentration.

7.3. Results and Discussion

7.3.1. Steady-state: reproducibility and recovery after perturbation

E. coli was grown in two independent aerobic glucose-limited chemostats on an adapted low Cl$^-$ defined minimal medium at a dilution rate of 0.1 h^{-1} until steady-state was achieved (as observed from biomass, DO, offgas O$_2$ and CO$_2$ concentrations). The average steady-state values for biomass concentration and uptake/secretion rates in these cultures showed no significant differences (Table 7.1). There was no by-product formation and the presence of cell lysis was again observed (Taymaz-Nikerel *et al.* 2009; Taymaz-Nikerel *et al.* 2010c). However, on the here used low Cl$^-$ medium there is significantly more biomass lysis ($q_{lysis} = 0.030$ Cmol/CmolX/h) than

in the previous experiments (q_{lysis} = 0.018 Cmol/CmolX/h) (Taymaz-Nikerel *et al.* 2009; Taymaz-Nikerel *et al.* 2010c). Another difference is observed in batch cultivation with μ^{max} = 0.63 h^{-1} in the present and 0.7 h^{-1} in the previous experiments. These differences (μ^{max} and q_{lysis}) can be caused by the different medium and/or by the strain used. The differences in supernatant composition (due to the different medium used) are shown in Appendix 7.5.3 and clearly in the present experiments concentrations of K$^+$ and Cl$^-$ are much lower compared to the previous experiments (Taymaz-Nikerel *et al.* 2009; Taymaz-Nikerel *et al.* 2010c), leading to a much lower osmotic strength. This suggests that the lower osmotic strength has caused the increased cell lysis. An important other difference is in the obtained q_S, q_{O2} and q_{CO2}, which are much higher (about 30 %) than previously found (Table 7.1), showing much more catabolism. Although both strains are wild type K12 MG1655, the previous strain [λ$^-$, F$^-$, rph^{-1}, (*fnr*$^-$ 267)del] (Taymaz-Nikerel *et al.* 2009; Taymaz-Nikerel *et al.* 2010c) additionally carries a deletion around the *fnr* (fumarate-nitrate respiration) regulatory gene, resulting in a strain that is unable to grow by anaerobic respiration (Soupene *et al.* 2003). The strain in the present experiments does not carry this deletion and therefore, these two strains are expected to behave identical under aerobic conditions. Our present results indicate that somehow our present strain, without the mentioned deletion, needs more catabolism at low K$^+$ and Cl$^-$ concentrations.

Table 7.1: Steady-state cell dry weight, C_X [gDW/l], reconciled biomass-specific fluxes [mmol/CmolX/h] and expected rates [mmol/CmolX/h] from the stoichiometric model (Taymaz-Nikerel *et al.* 2010a) using μ as input in aerobic glucose-limited *E. coli* chemostat cultures at D = 0.1 h^{-1}

	Experiment 1		Experiment 2	
	Reconciled	**Expected from stoichiometric model**	**Reconciled**	**Expected from stoichiometric model**
C_X	8.36 ± 0.12		8.02 ± 0.12	
μ	129.2 ± 2.7		136.6 ± 2.6	
$-q_S$	42.3 ± 1.2	36.7 ± 1.9	44.5 ± 1.3	38.6 ± 2.0
$-q_{O2}$	115.7 ± 4.7	81.2 ± 10.9	121.1 ± 5.8	84.6 ± 11.5
q_{CO2}	124.6 ± 4.9	91.1 ± 11.0	130.5 ± 6.0	95.1 ± 11.5
q_{lysis}	28.9 ± 1.6		31.3 ± 1.2	

In experiment 1 the chemostat steady-state was perturbed by sequential addition of three different substrates and surprisingly it was observed that within about 15 min after each substrate pulse the steady-state fluxes were recovered. In experiment 2, another similar independent chemostat was perturbed outside the biorector, in the BioScope, with the same three substrates.

In experiment 1 steady-state intracellular metabolites were analyzed at 6 time points (before and after each of the three substrate pulses added to the reactor) by taking 2 samples, each analyzed in duplicate. In experiment 2 the steady-state was analyzed before and after each BioScope experiment (Appendix 7.5.4). Comparing exp 1 and exp 2, before the perturbation experiments (49.8 and 50.6 h which represent about 7 residence times after start of feeding) shows very good

reproducibility for most metabolites which demonstrates the reliability of our IDMS-based MS/MS protocol for metabolite analysis and also reproducibility of the chemostat experiments. Very interesting is that in exp 1 the flux and metabolite steady-state is recovered after each different substrate pulse. The fact that the same flux and metabolite steady-state are recovered strongly indicates that a possible change of enzyme levels in central metabolism due to genetic regulation can be neglected in the total time frame of the perturbation experiment (~ 900 s).

Moreover exp 1 shows that over a period of 50 - 100 h of chemostat cultivation, covering 7 - 14 residence times or 10 - 20 generations, the metabolite levels do not significantly change (see Appendix 7.5.4). This is different from *Saccharomyces cerevisiae* (Mashego *et al.* 2005) where intracellular metabolite levels significantly changed within 15 - 20 generations of chemostat cultivation. Given these observations it is allowed to average all metabolite measurements shown in Appendix 7.5.4.

These average intracellular amounts of metabolites, the corresponding percentages of the total amounts of metabolites that are present in the filtrate and turnover times of the pools for exp 1 and exp 2 are shown in Table 7.2. From these results, it is seen that in the present *E. coli* cultures most of the measured metabolites are present in significant quantities in the culture filtrate, as was shown elsewhere for the other strain and standard salt medium (Taymaz-Nikerel *et al.* 2009). Most metabolite results presented in Table 7.2 are very well in agreement with the results of Taymaz-Nikerel *et al.* (2009), where a standard medium and the (*fnr*⁻ 267)del strain was used. The metabolite that shows the biggest difference is Glu, being about 5 times higher in the previous work. This is most probably due to the higher osmolarity (higher Cl^- and K^+) in the previous standard medium because it is known that in gram-negative bacteria increased osmolarity can lead to increases in the level of free intracellular Glu (Tempest *et al.* 1970).

The thermodynamic feasibility of the obtained steady-state metabolome data was checked by comparing the mass action ratios (Table 7.3) of several known near-equilibrium reactions, i.e. PGI and fumarase (FUM). The values were not much different from our previous findings and from the published equilibrium constants confirming their near equilibrium status. The MAR does agree with the flux direction.

The steady-state intracellular fluxes of the central metabolism were calculated with the known inputs (Table 7.1, reconciled rates) of steady-state $-q_S$, $-q_{O2}$ and μ (see Figure 7.2). When compared with the previous work (Taymaz-Nikerel *et al.* 2010c), it is seen that the glycolytic and TCA cycle fluxes are higher and the oxidative PPP flux is lower, which is caused by the already mentioned increased catabolism. The flux through the glyoxylate pathway and a gluconeogenic flux from Oaa to PEP set to ratios of $Flux_{ICL} = 0.2 \times Flux_{ACoNT}$ and $Flux_{PPC}/ Flux_{PPCK} = 2$ based on the findings of Nanchen *et al.* (2006), as explained in "Calculation methods".

The very low turnover times (0.2 - 2 s) of nearly all intracellular metabolites of glycolysis, TCA cycle and nucleotides (Table 7.2) confirm once more the necessity of the rapid sampling, made possible in the BioScope. Usually it is believed that amino acids have much higher turnover times compared to central carbon metabolism, which is not observed here. In agreement with our

Table 7.2: Steady-state intracellular (IC) amounts [µmol/gDW] of glycolysis, TCA cycle intermediates, amino acids and adenine nucleotides, percentages of metabolites outside the cells compared to total amount, and turnover times [s] calculated via MFA

	Experiment 1			Experiment 2		
	Average IC amount	**% outside the cells**	**Turnover time [s]**	**Average IC amount**	**% outside the cells**	**Turnover time [s]**
Central Metabolites						
G6P	1.22±0.04[a]	0	2.4	1.22±0.02	5.0	2.4
F6P	0.27±0.01[a]	0	0.6	0.28±0.01[a]	0	0.6
M6P	0.40±0.01[a]	0	NA	0.44±0.01[a]	0	NA
6PG	0.27±0.01[a]	0	2.3	0.22±0.02	25.5	1.9
Mannitol-1P	0.42±0.03	57.9	NA	0.75±0.09	35.7	NA
G3P	0.33±0.02[a]		6.0	0.38±0.01[a]		6.9
FBP	0.67±0.02[a]	0	1.6	0.55±0.07	14.2	1.3
2PG+3PG	1.24±0.04	10.1	1.4	1.38±0.03	7.0	1.6
PEP	1.19±0.05	8.3	1.5	1.22±0.03	3.9	1.5
Pyruvate	0.43±0.02[a]	0	0.7	0.30±0.04	23.2	0.4
Citric Acid	1.64±0.06[a]			0.52±0.13		1.2
α-KG	0.16±0.01[a]	0	0.2	0.19±0.02[a]		
Succinate	16.55±0.54[a]			22.41±0.43[a]		
Fumarate	0.45±0.08[a]			0.18±0.04		0.4
Malate	1.35±0.04[a]			0.98±0.11	37.3	2.4
Amino Acids						
Alanine	1.65±0.06	14.5	59.4	1.46±0.05	12.3	52.5
Asparagine	0.53±0.02	17.4	41.6	0.60±0.02	15.1	47.3
Aspartate	2.14±0.09	26.7	28.2	1.89±0.07	15.1	25.0
Cysteine	-			0.12±0.03	26.4	11.9
Glutamate	18.75±0.40	2.0	49.4	23.36±0.22	2.2	61.6
Glutamine	5.21±0.14	6.8	94.1	3.55±0.20	4.4	64.1
Glycine	0.78±0.09	58.1	15.2	1.49±0.12	29.7	29.0
Histidine	0.14±0.02	46.2	31.8	0.22±0.02	4.3	49.7
Isoleucine	0.09±0.01	39.5	7.5	0.07±0.01	20.7	6.2
Leucine	0.16±0.02	47.8	12.2	0.20±0.01	10.7	15.5
Lysine	1.87±0.06	6.9	129.2	1.47±0.01	2.7	101.4
Methionine	-			0.025±0.005	25.8	3.8
Phenylalenine	0.55±0.02[a]		65.5	0.25±0.01[a]		29.8
Proline	0.36±0.02	25.8	35.6	0.37±0.01	8.7	36.7
Serine	-			0.39±0.15	47.9	4.3
Threonine	0.70±0.06	18.0	28.0	0.57±0.02	5.7	23.1
Tryptophan	0.014±0.003	52.6	5.0	0.033±0.002	6.7	12.2
Tyrosine	0.09±0.01	57.1	13.2	0.13±0.01	18.3	18.8
Valine	0.42±0.04	21.2	23.3	0.45±0.05	4.9	24.8
Ornithine	0.29±0.04	46.1	21.2	0.30±0.03	21.7	21.5
Adenine Nucleotides						
ATP	5.30±0.16	0	0.8	5.30±0.29	0	0.8
ADP	1.30±0.04	0	0.2	1.41±0.05	0	0.2
AMP	-			0.58±0.04	0	3.9
Calculated Metabolites						
E4P	0.035±0.001			0.034±0.004		
GAP	0.068±0.002			0.06±0.01		
DHAP	1.51±0.04			1.37±0.17		
Oaa	0.003±0.0002			0.001±0.0002		

[a] Amount in the broth. In the filtrate G6P, F6P, M6P, 6PG, FBP, pyruvate was not detected (Exp 1). For citrate, succinate, fumarate and malate the analysis in the filtrate was not reproducible, therefore only broth results are presented (Exp 1 and succinate in Exp 2). NA: Results not available because those metabolites are not present in the stoichiometric model used.

previous findings (Taymaz-Nikerel et al. 2010c), it is found that the amino acids Ser, Ile, Met and Trp have turnover times comparable to those of central metabolites (< 10 s) and furthermore many amino acids have turnover times of about 50 s. The turnover times for most of the metabolite pools when compared to our previous experiments (Taymaz-Nikerel *et al.* 2009; Taymaz-Nikerel *et al.* 2010c) are lower in the present work, which is due to higher (~ 25 - 30 %) uptake/secretion fluxes (Table 7.1). The exception is 6PG that has a two times higher turnover time, which can be explained partially by the low growth yield of this strain, leading to a decreased need of NADPH and hence a decreased PPP flux.

Table 7.3: Steady-state mass action ratios (MAR), NAD$^+$/NADH ratio and energy charge calculated from the measured metabolite levels and range of published equilibrium constants for some relevant equilibrium reactions

	Reaction	This study	(Taymaz-Nikerel *et al.* 2010c)	K$_{eq}$ range
PGI	G6P ↔ F6P	0.22 ± 0.01	0.35 ± 0.04	0.19 - 0.67
PMI	F6P ↔ M6P	1.53 ± 0.08	1.11 ± 0.08	0.99 - 1.80
PGM+ENO	2+3PG ↔ PEP	0.92 ± 0.06	1.07 ± 0.05	0.10 - 1.79
AK	2ADP ↔ AMP + ATP	1.55 ± 0.15[a]	1.33 ± 0.59	0.20 - 1.45
FUM	Fumarate + H$_2$O ↔ Malate	4.22 ± 1.36	4.22 ± 0.45	2.10 - 9.49
Pyruvate/PEP		0.30 ± 0.04	0.40 ± 0.04	
NAD$^+$/NADH		93.8 ± 13.1	54.7 ± 4.5	
Energy charge		0.82 ± 0.08[a]	0.80 ± 0.05	

[a] Only Experiment 2 (AMP measurement was not available from Experiment 1).

7.3.2. Stimulus-response experiments

Time-resolved uptake/secretion fluxes obtained from chemostat pulse experiments

Quantification of *in vivo* enzyme kinetics requires information on the uptake/secretion fluxes such as -q$_S$, -q$_{O2}$, μ and secretion rate of by-products, as input for the dynamic intracellular reaction rate calculations during the pulse. Offgas and DO during the dynamic experiments cannot be measured in the BioScope. Additionally the very short time window of samples taken from the BioScope does not allow accurate calculation of -q$_S$ from extracellular substrate concentration, which hardly decreases in the 8 - 40 s BioScope time window. To obtain the dynamic -q$_S$ and -q$_{O2}$, pulse experiments were repeated in the bioreactor whereby online measurements were followed in a longer time frame (~ 900 s) than the pulses in the BioScope (40 s). The continuously monitored DO, pH (controlled at 7) and offgas online measurements after the pulse addition of glucose, pyruvate and succinate to a glucose-limited continuous culture (exp 1) are shown in Figure 7.19, 7.20 and 7.21, respectively in Appendix 7.5.5. The pulse experiments were successful in the sense that different substrates resulted in very different dynamic responses as observed from the online measurements. Surprisingly the analysis of

culture supernatant did not reveal any significant by-product formation during any of the pulse experiments. Also surprisingly after the pulses (~ 900 s) the original steady-state was recovered with respect to DO and O_2/CO_2 in the offgas, showing that $-q_S$, $-q_{O2}$, q_{CO2} and hence all other fluxes did recover to their previous steady-state, which is in agreement with the above mentioned recovery of the intracellular metabolite levels after each pulse.

Glucose pulse: Figure 7.19 in Appendix 7.5.5 shows the dynamics of the online measurements after the glucose pulse. In the glucose excess phase (0 - 275 s) a steep decrease of DO (which still remained far from zero) and offgas O_2 was observed, clearly showing a steep increase in O_2-consumption due to increased glucose consumption. Also an increase in offgas CO_2 was observed. However given the observed ΔO_2 of 2.5 %, a ΔCO_2 of about 3 % was expected (RQ ~ 1.1, (Taymaz-Nikerel *et al.* 2009)), where only ΔCO_2 = 1.0 % was observed. This clearly indicates (as found before (Taymaz-Nikerel *et al.* 2010c)) that the missing gaseous CO_2 remains in the broth as HCO_3^- leading to significant H^+ release, as evidenced from the decrease in pH. This decrease is not due to secreted organic acids which were, despite extensive analytical analysis efforts, not observed. After glucose depletion, the period of glucose starvation (275 - 510 s) shows the expected opposite behavior of the online measurements. This starvation response supports the absence of possible secreted by-products. Finally after restart of chemostat feeding and broth outflow (> 510 s) all online measurements returned to their previous steady-state values.

The added glucose, following a linear decrease, was depleted after 275 s (Figure 7.1a), leading to a glucose uptake rate of 96.4 mmol/CmolX/h (Figure 7.1b), which is 2.3 fold of the steady-state value (Table 7.1). The oxygen uptake rate reached a pseudo-steady-state value of about 280 mmol/CmolX/h (also about 2.3 fold of the reference state) within 40 s after the addition of glucose, and stayed at that value during the whole further glucose excess period, 40 - 275 s (Figure 7.1c). Figure 7.1d shows that during glucose excess the calculated growth rate rapidly (within 40 s) increased to a pss value of about 0.28 h^{-1} (~ 2.2 fold increase).

Pyruvate pulse: The added pyruvate led to a steeply decreased DO concentration, decreased offgas O_2 and increased offgas CO_2 concentration (Appendix 7.5.5, Figure 7.20), indicating steeply increased O_2 consumption and CO_2 production due to pyruvate uptake. After the pyruvate addition, the pyruvate uptake did not increase the pH, which points either to a possible acid by-product formation or to bicarbonate production that balances the H^+ amount in the culture. In the former case possible secreted organic acid would have the same number of protons as pyruvate (-1), e.g. acetate and/or formate. However, analysis of the supernatant revealed that there were no such compounds. There is a substantial discrepancy (Figure 7.20) between ΔO_2 (2.5 %) and ΔCO_2 (1.7 %), which points to a very substantial accumulation of HCO_3^-, which explains the pH behavior. HCO_3^- accumulation can indeed explain the CO_2 and pH findings (see Appendix 7.5.6). After pyruvate was depleted a starvation phase sets in where O_2 consumption and CO_2 production decreased and pH increased (due to CO_2-stripping). With the restart of feed and outflow (leading

to a constant glucose supply rate equal to the previous steady-state value) O_2 consumption and CO_2 production increased and the pH returned to the set point value. It is satisfactory to see that all online measurements returned to their previous steady-state values. The added pyruvate was utilized immediately showing a linear decrease in concentration and was depleted already after
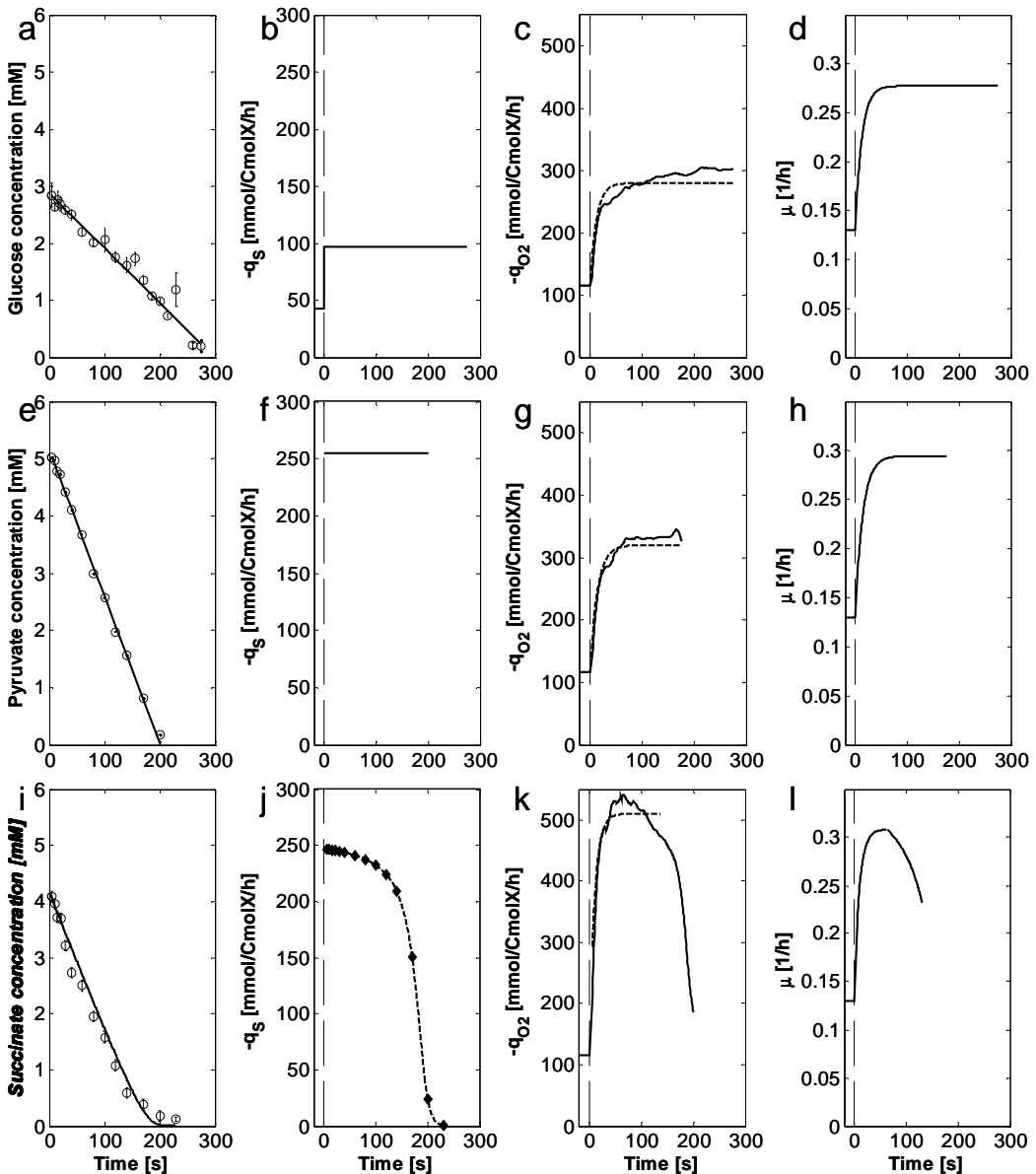
Figure 7.1: Glucose (top row), pyruvate (middle row) and succinate (bottom row) pulses given in the bioreactor. a, e, i. Measured residual substrate concentration / b, f, j. Mass balance-derived substrate uptake rate (-q_S) / c, g, k. Mass balance-derived oxygen uptake rate (-q_{O2}), dashed line: estimated / d, h, l. Growth rate (μ).

200 s (Figure 7.1e). The pyruvate uptake rate was found to be 254.6 mmol/CmolX/h (Figure 7.1f). In *E. coli* pyruvate is transported by a specific active transport system that is an energy-dependent process (Lang *et al.* 1987). Although the exact mechanism is unknown, it is evident that the required transporters were available in the biomass cultivated under aerobic glucose-limited conditions. The oxygen uptake rate tremendously increased to 320 mmol/CmolX/h already 40 s after the addition of pyruvate (Figure 7.1g) and it was found that again μ increases very rapidly (< 40 s) from its steady-state value of 0.13 h^{-1} to 0.29 h^{-1} (Figure 7.1h).

Succinate pulse: In the case of succinate addition, a very steep and large decrease in DO and offgas O_2 was observed, indicating a very high O_2 consumption. The sudden increase of the culture pH after the added succinate (Figure 7.21) is due to the uptake of succinate as it was added as Suc^{-2} salt (at pH ~ 7). The produced bicarbonate (as evidenced from the discrepancy between offgas ΔO_2 of 3.8 % and ΔCO_2 of 1.2 %) would also be high as in the pyruvate case, but because succinic acid is a dicarboxylic acid (2 protons taken up), the pH now increases. The measurements in the supernatant (after the pulse) revealed that again there were no secreted compounds. After succinate was depleted (starvation-phase), O_2 consumption and CO_2 production decreased and the pH increased further (due to CO_2-stripping). With the restart of the chemostat feed and outflow (leading to a constant glucose supply equal to the previous steady-state value) O_2 consumption and CO_2 production increased, pH dropped and all online measurements returned to their previous steady-state values.

The extracellular succinate concentration after the given pulse is shown in Figure 7.1i. It was observed that succinate depleted after 220 s, which is faster than the depletion of glucose. In contrast to glucose and pyruvate, a non-linear decrease in concentration was observed. Hyperbolic uptake kinetics ($-q_S = \dfrac{-q_S^{max} \, C_S}{K_S + C_S}$) was assumed. Fitted parameters were $K_S = 0.20 \pm 0.03$ mM succinate, $q_S^{max} = 259 \pm 29$ mmol succinate/CmolX/h and the results were statistically acceptable. Under aerobic conditions C_4-dicarboxylates are reported to be taken up by *E. coli* using the Dct system that has an apparent K_m of 10 to 20 μM for C_4-dicarboxylates and is driven by the electrochemical proton gradient (Gutowski and Rosenberg 1975). Our results reveal that a succinate uptake system with high capacity is present in the glucose-limited *E. coli*, but the uptake rate decreases with a decreasing concentration of succinate (Figure 7.1j) due to a moderate affinity; our affinity constant is about 10 times higher than reported by Gutowski and Rosenberg (1975).

The oxygen uptake rate tremendously increased (to 510 mmol/CmolX/h), which is 4.4 fold of its steady-state value, already 40 s after the addition of succinate (Figure 7.1k) and remained there until around 100 s. Thereafter q_{O2} decreased due to decreasing succinate uptake rate (q_S) following the decreasing succinate concentration. During the succinate pulse, the calculated growth rate increased up to 0.31 h^{-1} within 40 s and decreased after about 70 s due to the decline in the q_S and q_{O2} (Figure 7.1l).

Interestingly, after each added different substrate, the growth rate increased (from 0.13 h^{-1}) to a similar value of 0.3 h^{-1}. This growth rate capacity is less than the μ = 0.5 h^{-1} observed in a glucose pulse in our previous research (using medium with more Cl$^-$ and with the deletion strain, (Taymaz-Nikerel *et al.* 2010c)). The fact that three different substrates lead to the same maximal μ indicates a capacity limit in e.g. ribosomes. It is known that rRNA level has a direct relation with μ; at higher μ rRNA is higher (Dennis and Bremer 1974). This explains why the *E. coli* cells cultured at μ = 0.13 h^{-1} cannot achieve the batch μ^{max}. Also of interest is that the three substrates achieve pseudo-steady-state in about 30 - 40 s. Another important observation is the huge oxygen uptake capacity of the cells. The oxygen uptake rate after the glucose pulse is comparable (250 mmol/CmolX/h) to the previous strain/medium (Taymaz-Nikerel *et al.* 2010c). In the present experiment the glucose and pyruvate pulses give similar q$_{O2}$ in pseudo-steady-state (Figures 7.1c and 7.1g). For the succinate pulse oxygen was consumed at a much faster rate (~ 500 mmol O$_2$/CmolX/h). This high q$_{O2}$ agrees with the maximal oxygen uptake rate observed for the present strain (~ 500 mmol/CmolX/h at batch conditions with μ^{max} ~ 0.6 h^{-1}) and the elsewhere reported maximal q$_{O2}$ for *E. coli* of 20 mmol O$_2$/gDW/h (~ 500 mmol O$_2$/CmolX/h) (Carlson and Srienc 2004). This maximal O$_2$ uptake rate, that indicates the capacity limit of the electron transport chain, appears to be independent of growth rate at which *E. coli* is cultivated, being similar at μ = 0.13 h^{-1} (chemostat) and μ = 0.6 h^{-1} (batch).

(Pseudo-steady-state) intracellular fluxes

With the information of the pseudo-steady-state (pss) values for -q$_S$, -q$_{O2}$ and μ (obtained after 40 s), the pss intracellular fluxes were calculated after pulses of glucose, pyruvate and succinate (Figure 7.2, 7.3, 7.4). After the *glucose pulse*, with the 2.3 fold increase in -q$_S$, the glycolytic fluxes increased about 2.3 fold and the TCA cycle fluxes about 2.5 fold (Figure 7.2). When compared to the previous strain (Taymaz-Nikerel *et al.* 2009; Taymaz-Nikerel *et al.* 2010c), the increase in the glycolysis (previous 3.2 fold) is lower whereas similar fold change was observed in the TCA cycle. The higher flux increase in the TCA cycle (compared to glycolysis) is consistent with the higher O$_2$ consumption rate of the present experiment. The flux entering the PPP increased only 1.8 fold, showing that the NADPH required for biosynthesis is supplied from both the highly increased isocitrate dehydrogenase (ICDH) and the less increased PPP. The decrease in the small flux through PEP carboxylase, PPC, (and hence PPCK) can be explained by the increase in the glyoxylate route. Clearly the glyoxylate route is the major anaplerotic route compared to PPCK. The glyoxylate route is very important in succinate production, and it reveals here a capacity of at least 18 mmol/CmolX/h.

The *pyruvate pulse* (Figure 7.3) results in gluconeogenesis, evident from the reversed (negative) direction of fluxes through the glycolytic enzymes above pyruvate. The flux through oxidative PPP is set to zero (because 6PG is very low, see below). Gluconeogenesis is therefore only needed to supply carbon precursors for growth, which increases about 2 - 3 fold. This gluconeogenesis is partially possible due to PEP/glyoxylate path (Nanchen *et al.* 2006) and shows its importance. There is a strong flux increase into the glyoxylate route, being 25 mmol/CmolX/h, which is higher than for the glucose pulse. The activity of the PPC reaction

(PEP→Oaa) is assumed to be absent in the pyruvate network because the PEP concentration is very low (see below). Most remarkable the direction of pyruvate kinase (PYK) reversed, creating most of the gluconeogenic flux. This reversal is possible by the combination of a very low PEP concentration and requires a high intracellular pyruvate concentration. The flux through pyruvate dehydrogenase (PDH) reaches a level of about 200 mmol/h/CmolX, which is much higher than for the glucose pulse (125 mmol/h/CmolX), also indicating a steeply increased intracellular

Metabolite	Concn fold change	τ
G6P	2.4	2.6
F6P	2.7	0.8
M6P	1.5	-
6PG	1.7	1.2
E4P	2.6	1.1
His	0.5	11.7
Phe	1.3	6.5
Tyr	0.6	5.4
Mannitol1P	2.1	-
FBP	6.2	3.5
2PG/3PG	0.4	0.3
Gly	0.6	8.7
Trp	0.5	3.0
Ser	-	-
PEP	0.2	0.1
Pyruvate	6.2	1.1
Ala	1.0	24.4
Val	0.8	9.0
Leu	1.1	8.2
Cit/Icit	1.5	0.7
Glu	1.0	27.7
Gln	0.7	22.2
Lys	1.0	46.6
Pro	0.9	16.0
Orn	1.0	9.6
Succinate	1.5	15.3
Fumarate	3.6	0.7
Malate	1.4	1.2
Asp	0.6	7.3
Asn	0.9	19.7
Thr	0.9	9.6
Ile	0.7	2.1
Cys	2.0	11.1
Met	1.3	2.3
AMP	1.5	2.7
ADP	0.9	0.1
ATP	1.0	0.4

Figure 7.2: Metabolic reaction network and fluxes for steady-state growth on glucose and glucose pulse. *Left:* The intracellular fluxes [mmol/CmolX/h] at steady-state (glucose-limited, left box) and at pseudo-steady-state after the glucose pulse (right box). The gray arrows indicate fluxes going to biomass. *Right:* Fold change of metabolite levels at glucose pseudo-steady-state relative to the steady-state and metabolite turnover times (τ in seconds) at glucose pseudo-steady-state.

Figure 7.3: Metabolic reaction network and fluxes for pyruvate pulse. *Left:* **The intracellular fluxes [mmol/CmolX/h] at steady-state (glucose-limited, left box) and at pseudo-steady-state after the pyruvate pulse (right box). The gray arrows indicate fluxes going to biomass.** *Right:* **Fold change of metabolite levels at pyruvate pseudo-steady-state relative to the steady-state and metabolite turnover times (τ in seconds) at pyruvate pseudo-steady-state.**

Metabolite		Concn fold change	τ
G6P		0.3	89.6
F6P		0.2	35.2
M6P		0.3	-
6PG		0.05	-
E4P		0.1	0.2
	His	0.7	15.2
	Phe	0.3	1.6
	Tyr	0.5	4.3
Mannitol1P		0.5	-
FBP		0.01	0.03
2PG/3PG		0.1	0.8
	Gly	0.8	9.7
	Trp	0.8	4.5
	Ser	0.2	0.3
PEP		0.2	2.7
Pyruvate		Pulse	-
	Ala	2.1	48.7
	Val	1.4	15.4
	Leu	1.7	11.5
Cit/Icit		2.0	0.6
	Glu	0.8	20.4
	Gln	0.8	22.5
	Lys	0.9	41.1
	Pro	0.9	14.3
	Orn	1.0	9.8
Succinate		1.0	5.5
Fumarate		1.2	0.1
Malate		1.3	0.5
	Asp	0.4	4.7
	Asn	0.8	16.4
	Thr	0.8	8.5
	Ile	0.9	2.5
	Cys	0.5	2.7
	Met	1.1	1.8
AMP		1.0	1.3
ADP		0.9	0.1
ATP		0.9	0.4

pyruvate concentration. The TCA cycle flux reaches a level of about 150 mmol/h/CmolX, compared to 100 for glucose. The TCA cycle flux is partially higher due to the much higher ICDH (~ 120 compared to 70), which compensates the absence of NADPH production from the oxidative PPP.

The *succinate pulse* (as the pyruvate pulse) also gave rise to gluconeogenesis (Figure 7.4), thanks to the PEP/glyoxylate route. The absolute gluconeogenic flux values were similar in both cases,

which is due to the fact that the achieved μ was the same and the oxidative PPP was assumed absent. The supply of succinate caused TCA cycle fluxes (from succinate to oxaloacetate) to increase 12 fold (from 35 in steady-state to around 380 mmol/h/CmolX). The TCA cycle fluxes from citrate to succinate increased 4 - 5 fold. Most remarkable is the extreme increase (140 fold!) in the reverse flux through PPCK (PPC was assumed to be absent; low PEP concentration, see below). This high flux increase is associated with the very high metabolite concentration of C_4 acids and low metabolite concentration of PEP (see below). The glyoxylate route was found to
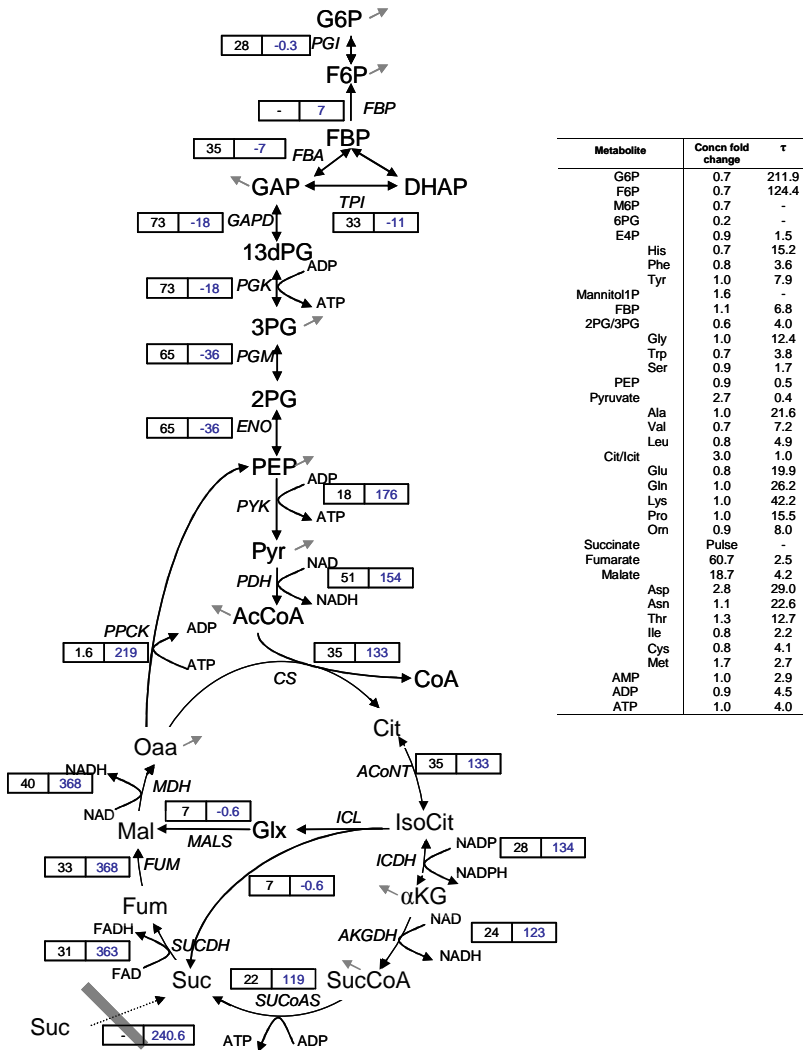
Figure 7.4: Metabolic reaction network and fluxes for succinate pulse. *Left:* **The intracellular fluxes [mmol/CmolX/h] at steady-state (glucose-limited, left box) and at pseudo-steady-state after the succinate pulse (right box). The gray arrows indicate fluxes going to biomass.** *Right:* **Fold change of metabolite levels at succinate pseudo-steady-state relative to the steady-state and metabolite turnover times (τ in seconds) at succinate pseudo-steady-state.**

have a negligible flux (all anaplerosis is now mediated by PPCK), which may be related to the high concentrations of intracellular succinate and malate (see below). This much higher concentration of a product (succinate and malate) is expected respectively to inhibit the kinetics of the isocitrate lyase (ICL) and malate synthase (MALS) reactions. In this pulse pyruvate kinase did not show inverted flux, but its flux was highly increased, in accordance with PPCK, to supply the increased TCA cycle flux.

Remarkably pyruvate and succinate (added as perturbing substrates to the system) were immediately utilized by the cells, and a pss was reached within 20 - 30 s. This points to the presence of their transporters in *E. coli* cultivated on glucose at 0.1 h^{-1}.

Different flux values observed after each pulse give insight about the behaviour of metabolites under different conditions, most important being the immediate occurrence of gluconeogenesis after the pyruvate and succinate pulses due to reversible reactions. It is evident that the glycolytic glucose pulse would trigger the pathway in a different way, as observed in the increased flux of glycolysis. Although the pyruvate and succinate led to same gluconeogenic flux and absence of oxidative PPP flux due to the same increase in μ, there are also major differences between the two networks. Most significant are the reversed direction of PYK during the pyruvate pulse, the extreme increase in TCA cycle reactions between succinate and Oaa and the extreme flux increase of PPCK during the succinate pulse. Now these very large flux changes need to be linked to the changes in measured concentrations for the intracellular metabolites for which we need to discuss first the metabolite transients.

Intracellular metabolites during the transients from BioScope experiments

General observations: By measuring the intracellular metabolite concentrations, we investigated the metabolite responses following pulse additions of glucose, pyruvate and succinate outside the bioreactor (in the BioScope) of biomass obtained from aerobic glucose-limited *E. coli* cultures. The dynamics of the metabolite levels was followed in two time regimes in the BioScope: 0 - 8 s (4 ml/min) and 0 - 42 s (2 ml/min). The comparison of metabolite changes after the glucose, pyruvate and succinate pulses are shown in Figures 7.6 - 7.14. The two different flow rates performed in the BioScope lead to matching results with each other which was already observed before for a glucose pulse (De Mey *et al.* 2010b), showing the reproducibility of BioScope pulse experiments.

Dynamic metabolite responses were created by performing pulses of different substrates, which in case of glycolytic and gluconeogenic substrates resulted in opposite metabolite fold changes. The central carbon metabolism of *E. coli* showed much faster metabolite dynamics (within 10 s) compared to our studies on eukaryotes (~ 100 s) *S. cerevisiae* (Kresnowati *et al.* 2006; Mashego *et al.* 2006; Wu *et al.* 2006) and *Penicillium chrysogenum* (Nasution *et al.* 2006).

Fluxes and metabolites changed dynamically in the same time frame as expected. The intracellular metabolites accumulated inside the cell after each pulse, which also explains the fast increase in the growth rate after each pulse. At the end of glucose depletion (275 s) the

accumulated carbon represents about 20 % of the added glucose amount (see Appendix 7.5.7), which is very well in agreement with our previous glucose pulse findings (Taymaz-Nikerel *et al.* 2010c). For the pyruvate and succinate pulses, the correct amount cannot be presented because the quantification of intracellular pyruvate and succinate, which have a profound contribution, could not be performed with the current sampling/quenching methods. Still estimations can be made by assuming that transport equilibrium of pyruvate is very rapidly achieved with symport of pyruvate and 1 H$^+$, succinate with 2 H$^+$ and intracellular pH is the same as extracellular pH (7).
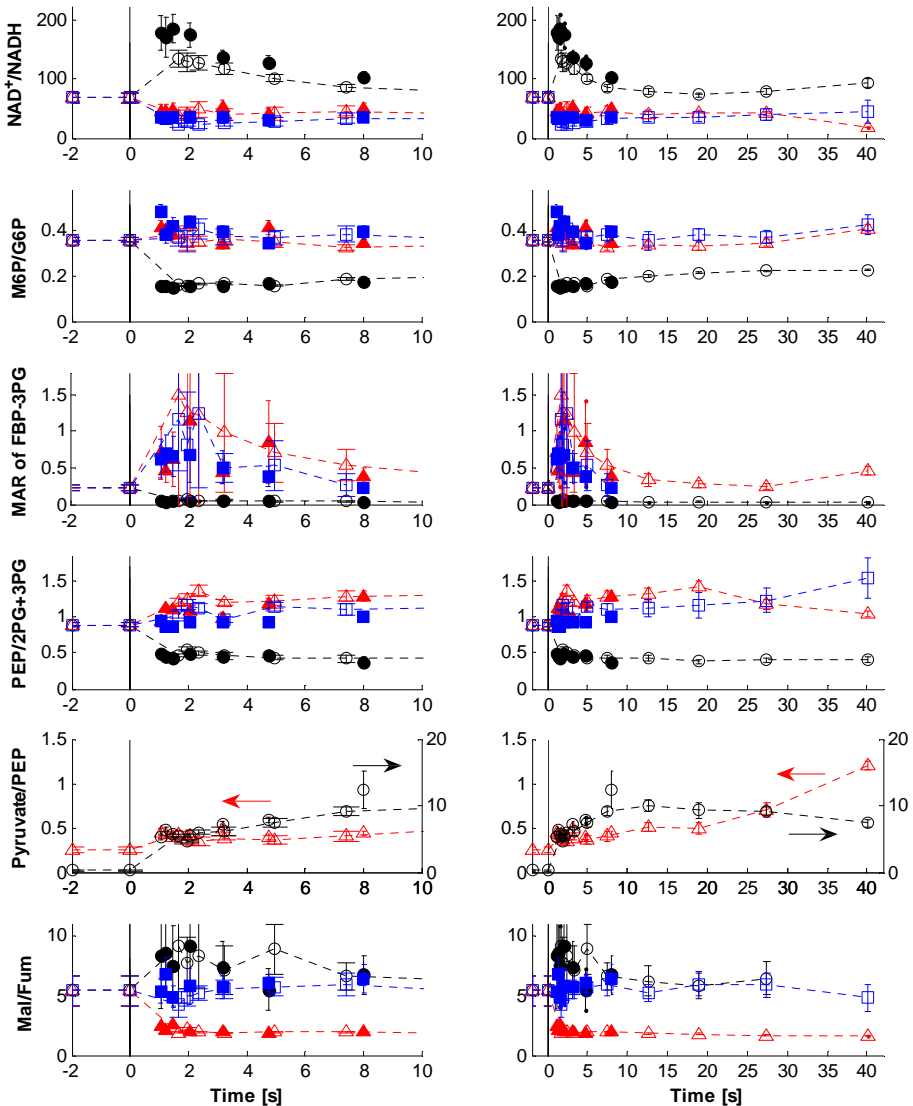
Figure 7.5: Some relevant metabolite ratios and mass action ratios during the glucose (circles), pyruvate (squares) and succinate (triangles) pulse. Open symbols are at flow rate = 2 ml/min, closed symbols are at flow rate = 4 ml/min.

169

Results indicate that a considerable amount (~ 3 % of added pyruvate for pyruvate pulse and ~ 7 % of added succinate for succinate pulse in 40 s) of metabolites also accumulated under these conditions and served as carbon and electron source in the starvation phase after depletion of the pulsed substrate.

The fold changes in metabolite pss concentrations relative to the steady-state are given in the right panels of Figures 7.2, 7.3 and 7.4, with the turnover times of the pss pools. The presented
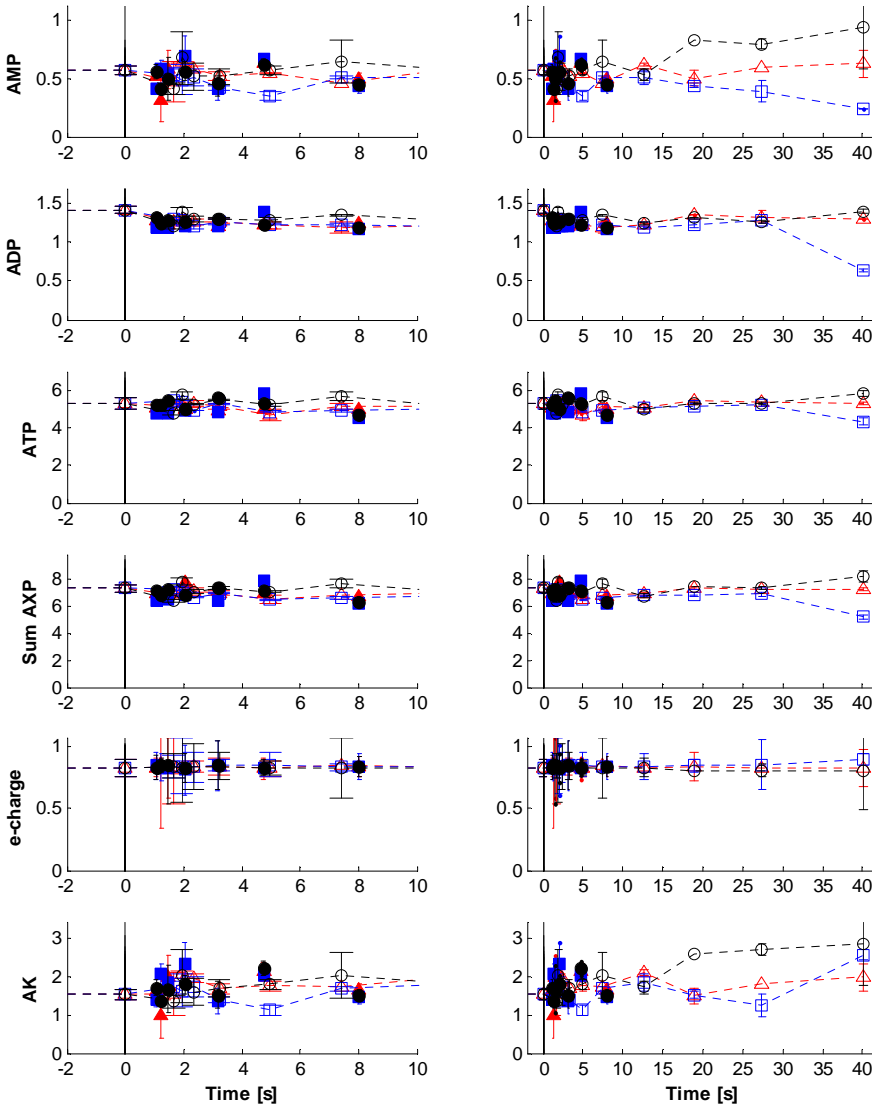
Figure 7.6: Measured adenine nucleotides [µmol/gDW], sum of AXP [µmol/gDW], energy charge (-) and MAR of AK [2ADP ↔ AMP + ATP] (-) during the glucose (circles), pyruvate (squares) and succinate (triangles) pulse. Open symbols are at flow rate = 2 ml/min, closed symbols are at flow rate = 4 ml/min.
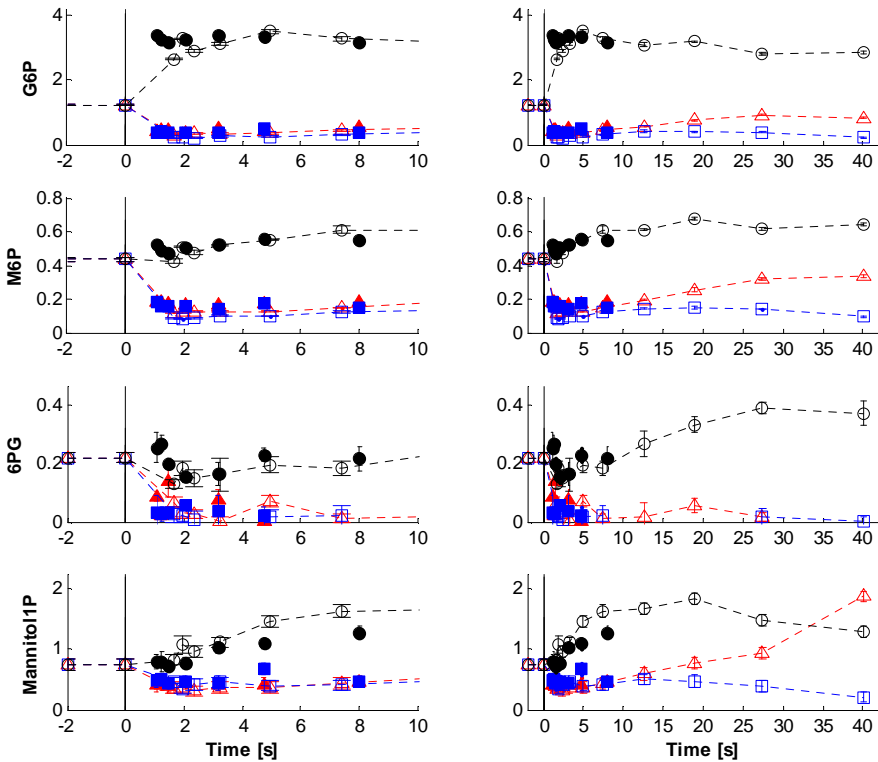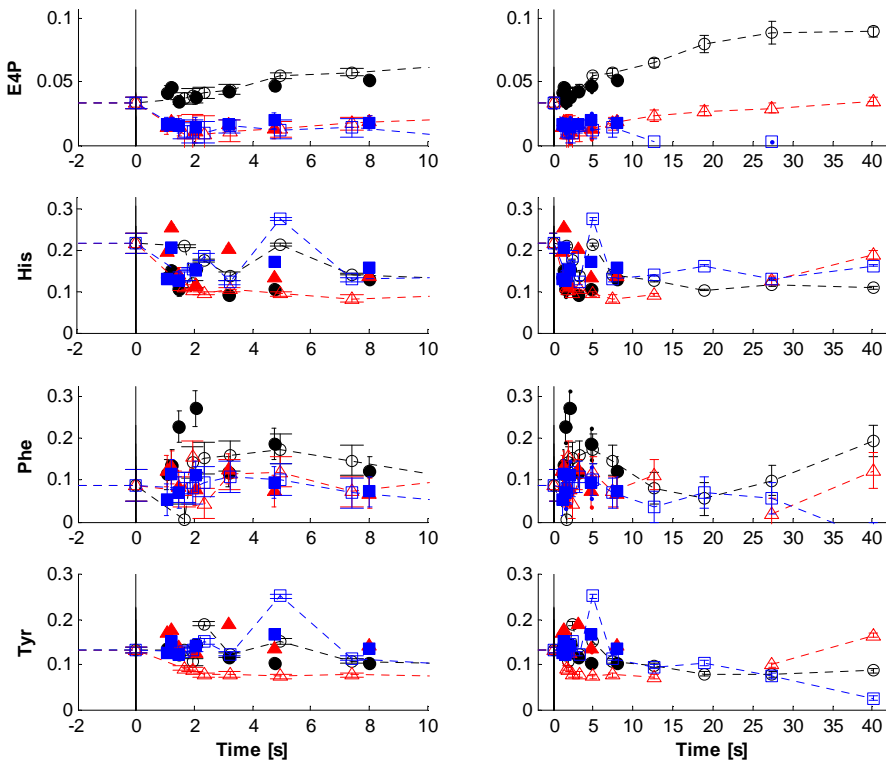
Figure 7.7: Measured amounts of upper glycolytic metabolites, 6PG and Mannitol-1P [µmol/gDW] during the glucose (circles), pyruvate (squares) and succinate (triangles) pulse. Open symbols are at flow rate = 2 ml/min, closed symbols are at flow rate = 4 ml/min.

approach on assessment of turnover times in pseudo-steady-state (rather than in steady-state) is more realistic in time-scale-analysis-based model reduction techniques (Nikerel *et al.* 2009), because it is seen that the turnover times in pss are mostly much lower than at steady-state. This shows that using steady-state turnover times might lead to less model reduction (Nikerel *et al.* 2009) than possible. Most important is that for many metabolites the turnover time is in the order of seconds, which shows that, even in the transient period of 40 s, the system can be approximated as pseudo-steady-state, allowing a simple pseudo-steady-state flux calculation during the transient.

Glycolytic and gluconeogenic substrates trigger a tremendous flux flexibility in central metabolism: The metabolite dynamic patterns after the glycolytic glucose pulse, as was partly discussed in De Mey *et al.* (2010b), were similar to our previous work (Taymaz-Nikerel *et al.* 2010c). The intracellular levels of adenine nucleotides and thus adenylate energy charge of the cells are high and do not change significantly after any given pulse (Figure 7.6), also in agreement with the results of Link *et al.* (2010). This shows, considering the very large changes in O_2-uptake rates (up to factor 5 in 40 s), the extreme robustness of the energy system in *E. coli.*

Only the AMP level increases after the glucose pulse, which was discussed in Taymaz-Nikerel *et al.* (2010c), in relation to the increased ETC rate (O_2-uptake rate) (see below).

Upper glycolytic metabolites and Mannitol-1P increased after the glycolytic glucose pulse whereas they decreased after the gluconeogenic succinate and pyruvate pulses (Figure 7.7). The increase in the glycolytic flux (2.3 fold increase in -q_S) obtained after the glucose pulse is an explanation for the observed increase in upper glycolytic metabolites (2 - 6 fold). For succinate and pyruvate pulses, the upper glycolytic metabolites decreased (Figures 7.7 - 7.8) due to the absence of glucose flux and gluconeogenic flux reversal. The steep decrease of G6P, F6P concentration during the pyruvate/succinate pulses was accompanied by a near collapse of the 6PG pool, strongly suggesting absence of the oxidative PPP (as assumed for the flux calculations in Figures 7.3, 7.4). For NADPH this was compensated by a strongly increased flux of ICDH in the TCA cycle. Due to the absence of activity of the phosphotransferase system (PTS), PEP increased, which facilitates the gluconeogenesis. It is well known (Lowry *et al.* 1971) that when *E. coli* cells are grown on succinate, phosphoenolpyruvate carboxykinase (Ppck) converts oxaloacetate to PEP, which then diverges to gluconeogenesis and to the formation of pyruvate as
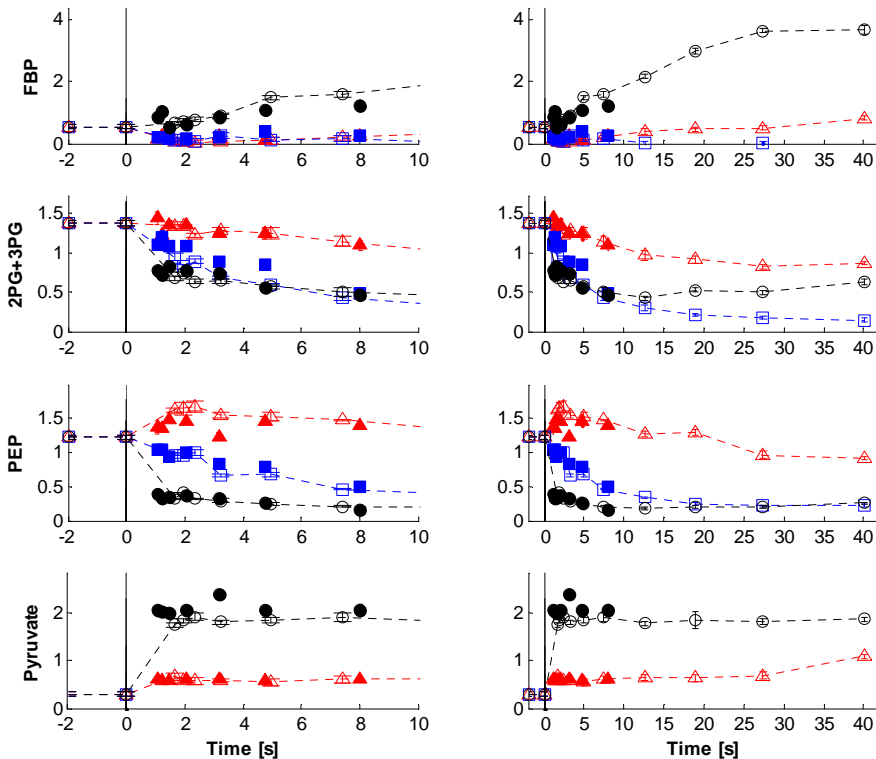
Figure 7.8: Measured amount of lower glycolytic metabolites [µmol/gDW] during the glucose (circles), pyruvate (squares) and succinate (triangles) pulse. Open symbols are at flow rate = 2 ml/min, closed symbols are at flow rate = 4 ml/min.
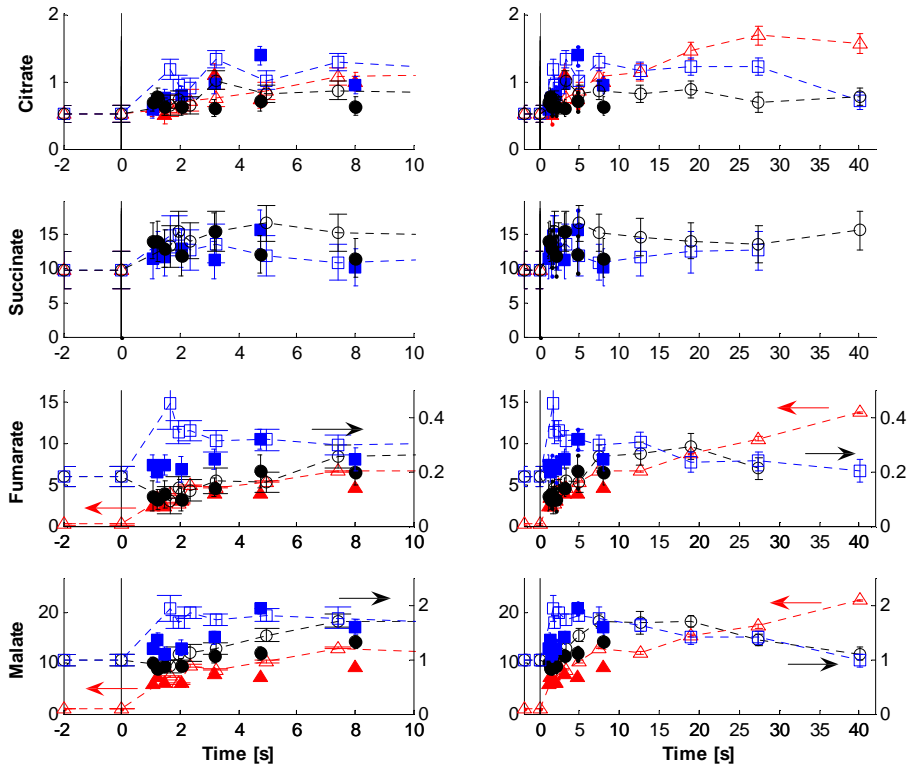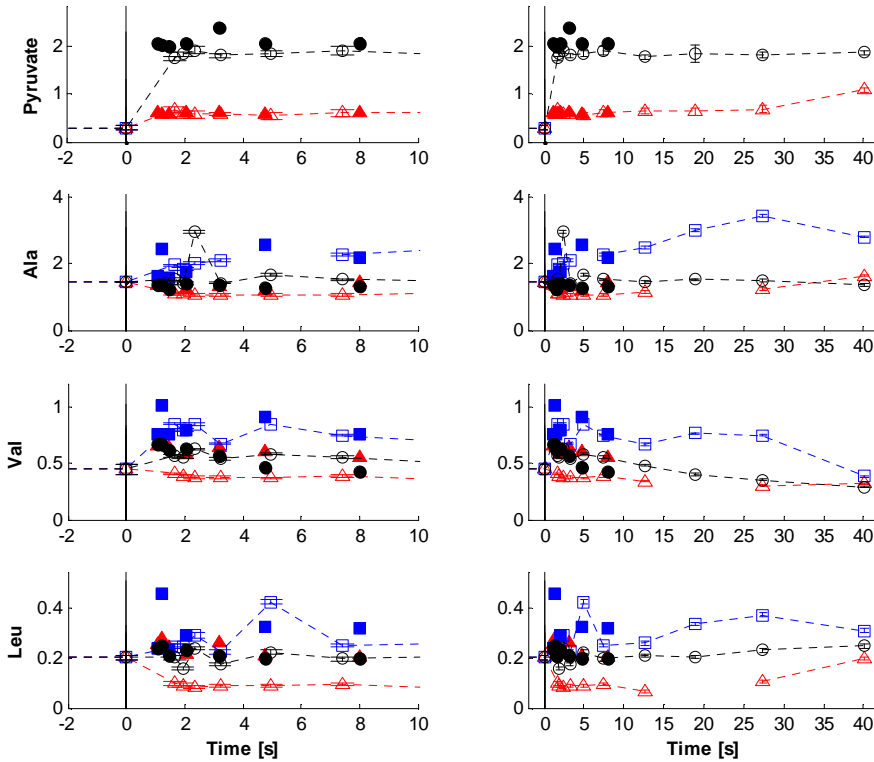
Figure 7.9: Measured amount of TCA cycle metabolites [µmol/gDW] during the glucose (circles), pyruvate (squares) and succinate (triangles) pulse. Open symbols are at flow rate = 2 ml/min, closed symbols are at flow rate = 4 ml/min.

indicated in our flux pattern (Figure 7.4). After the succinate pulse, the huge flux increase in PPCK (140 fold) is also due to very high levels of C_4 acids and low levels of PEP, which created a thermodynamic driving force in the other direction and which stimulated PPCK. The increase in pyruvate level after the succinate pulse (Figure 7.8) is in agreement with the extreme activity of Ppck enzyme, with a high flux (Figure 7.4). This increase in pyruvate was less compared to the glucose pulse (2.7 and 6.2 fold, respectively), most probably due to the absence of PTS activity during the succinate pulse. Our observation of 80 % decrease in PEP after the pyruvate pulse matches well with the calculated reversed flux direction of PYK, since pyruvate concentration is at utmost high level and PEP is low.

During the succinate pulse the TCA cycle is pushed far from equilibrium (especially between succinate and Oaa), which is facilitated by a collapse in the MAR of fumarase as shown from the intracellular fumarate and malate levels (Figure 7.5). This decreased MAR creates the thermodynamic driving force for the 12 fold increase in flux.

Also Link *et al.* (2010) tested the response of *E. coli* after addition of excess glucose, succinate, pyruvate and acetate, by transferring aerobic glucose-limited fed-batch ($\mu = 0.1$ h^{-1}) grown cells

to batch reactors. Comparable results were observed in terms of uptake of added different substrates and observed metabolite changes although their measurements only started after 120 s and they presented only four pss intracellular pools. In contrast to our results, they have observed acetate and formate excretion after glucose and pyruvate pulses and fumarate and α-ketoglutarate secretions after the succinate pulse. The production of these by-products might be due to the much higher concentration of substrates given (e.g. ~ 8 g/l glucose against ~ 0.5 g/l of the present work).

The intracellular amino acids showed also fast dynamic responses with moderate fold changes in agreement with our recent work (Taymaz-Nikerel *et al.* 2010c). Mostly the amino acid levels followed their precursors. Examples are the increase in pyruvate-derived amino acids such as Ala (2.1 fold), Leu (1.7 fold) and Val (1.4 fold) following the increase in pyruvate (Figure 7.11). Another example for this precursor related response of amino acid levels is the decrease in Leu and Val (20 and 30 %) after the succinate pulse with a much more delayed response compared to the glucose pulse (Figure 7.12). Asp level was increased 2.8 fold after the succinate pulse (Figure

Figure 7.10: Measured amount of E4P-derived amino acids [µmol/gDW] during the glucose (circles), pyruvate (squares) and succinate (triangles) pulse. Open symbols are at flow rate 2 ml/min, closed symbols are at flow rate 4 ml/min. *E4P was calculated, not measured.*
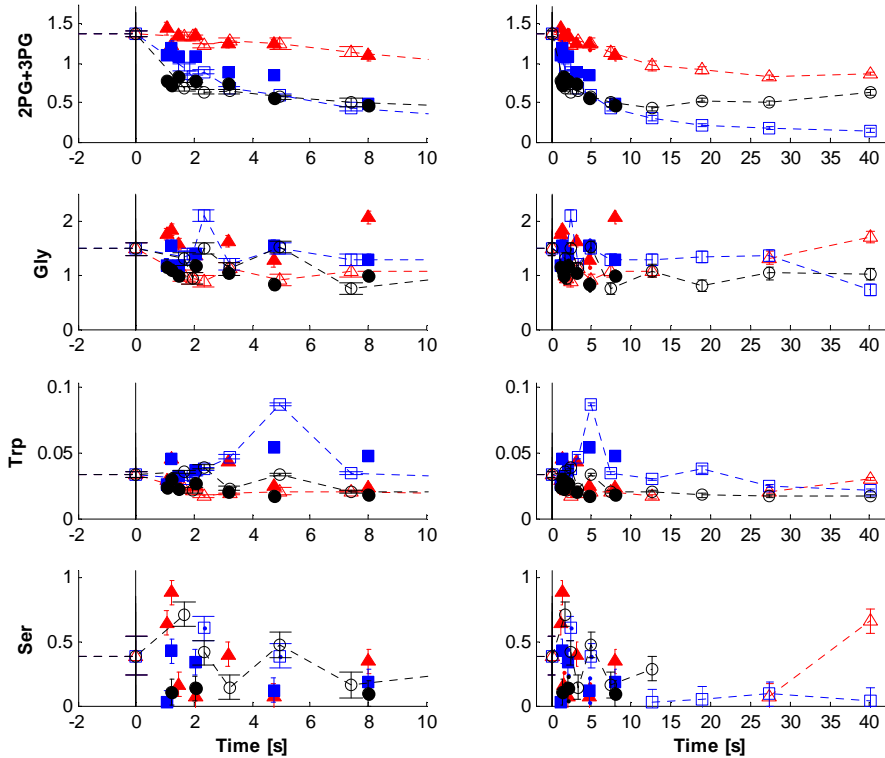
Figure 7.11: Measured amount of 3PG-derived amino-acids [µmol/gDW] during the glucose (circles), pyruvate (squares) and succinate (triangles) pulse. Open symbols are at flow rate 2 ml/min, closed symbols are at flow rate 4 ml/min.

7.14) most probably due to the tremendous increase of C_4 acid metabolites (malate: ~ 19 fold, fumarate: ~ 61 fold). These examples of fast response in amino acid metabolism are surprising because the usually assumed high turnover times for amino acids would lead to hardly any expected response in our 40 s time frame. Indeed the calculated turnover times of amino acids in the current study are much lower compared to the previous literature. However even the faster amino acid turnover times are not in line with the fast amino acid response observed (< 10 s), which is probably due to the boost in the growth rate (2 - 3 fold). This leads to fast increase in the amino acid consumption rate and hence, a fast increase in the flux of amino acid synthesis pathways and shorter turnover times in the pseudo-steady-state. Clearly the fast behaviour of amino acid pools supports the previous discussed fast 2 - 3 fold increase in growth rate.

Dynamics in mass action ratios and flux (directions): The mass action ratio is directly related to the Gibbs free energy of reaction, thus thermodynamic driving force. Information on changes in mass action ratio (as a function of time) gives insight in the direction of the reactions in the cell. This is of importance because then two independent measurements, metabolites and fluxes, can be compared.

Figure 7.12: Measured amount of pyruvate-derived amino acids [µmol/gDW] during the glucose (circles), pyruvate (squares) and succinate (triangles) pulse. Open symbols are at flow rate 2 ml/min, closed symbols are at flow rate 4 ml/min.

Pyruvate and succinate pulses led to the inversion of the MAR of the following glycolytic reactions (see Figure 7.5) M6P/G6P, MAR of FBP to 3PG, PEP/(2PG+3PG), which increased immediately above their equilibrium constant, implying the flux reversal needed for the occurrence of gluconeogenesis.

The MAR of fumarase decreases remarkably in the succinate pulse (Figure 7.5), providing driving force for more than 12 fold increased TCA flux from succinate to Oaa (Figure 7.4). The disequilibrium of TCA cycle was also visible in the O_2 consumption rate, which increased tremendously after the succinate pulse.

The redox potential $NAD^+/NADH$ ratio increased after the glucose pulse, as was observed before (Taymaz-Nikerel *et al.* 2010c), and reached back to the steady-state value in 20 s (Figure 7.5). However, in contrast to the glucose pulse, $NAD^+/NADH$ decreased in the succinate and pyruvate pulses (Figure 7.5). This decrease is in agreement with the occurrence of gluconeogenesis, which consumes NADH. Also from a MAR-point of view the decreased $NAD^+/NADH$ provides the increased driving force for gluconeogenesis around GAP dehydrogenase (GAPDH).
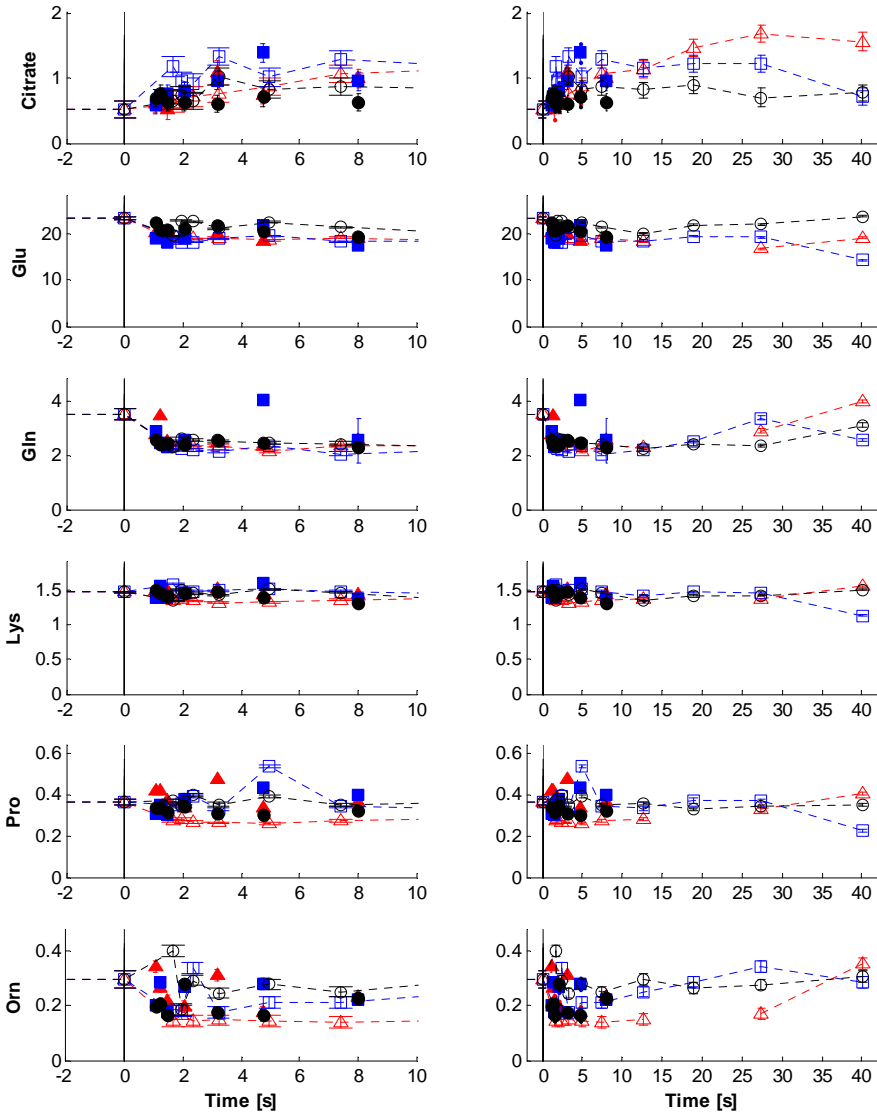
Figure 7.13: Measured amount of α-ketoglutarate-derived amino acids [μmol/gDW] during the glucose (circles), pyruvate (squares) and succinate (triangles) pulse. Open symbols are at flow rate 2 ml/min, closed symbols are at flow rate 4 ml/min.

7.3.3. *In vivo* kinetics

It has been shown that central metabolism, upon different substrate pulses, has tremendous flux flexibility with enormous (reverse) fold changes. These changes seem qualitatively related to large changes in metabolite concentrations leading to changes in MARs of all near reversible reactions. An interesting question is therefore whether there exists a quantitative relation between
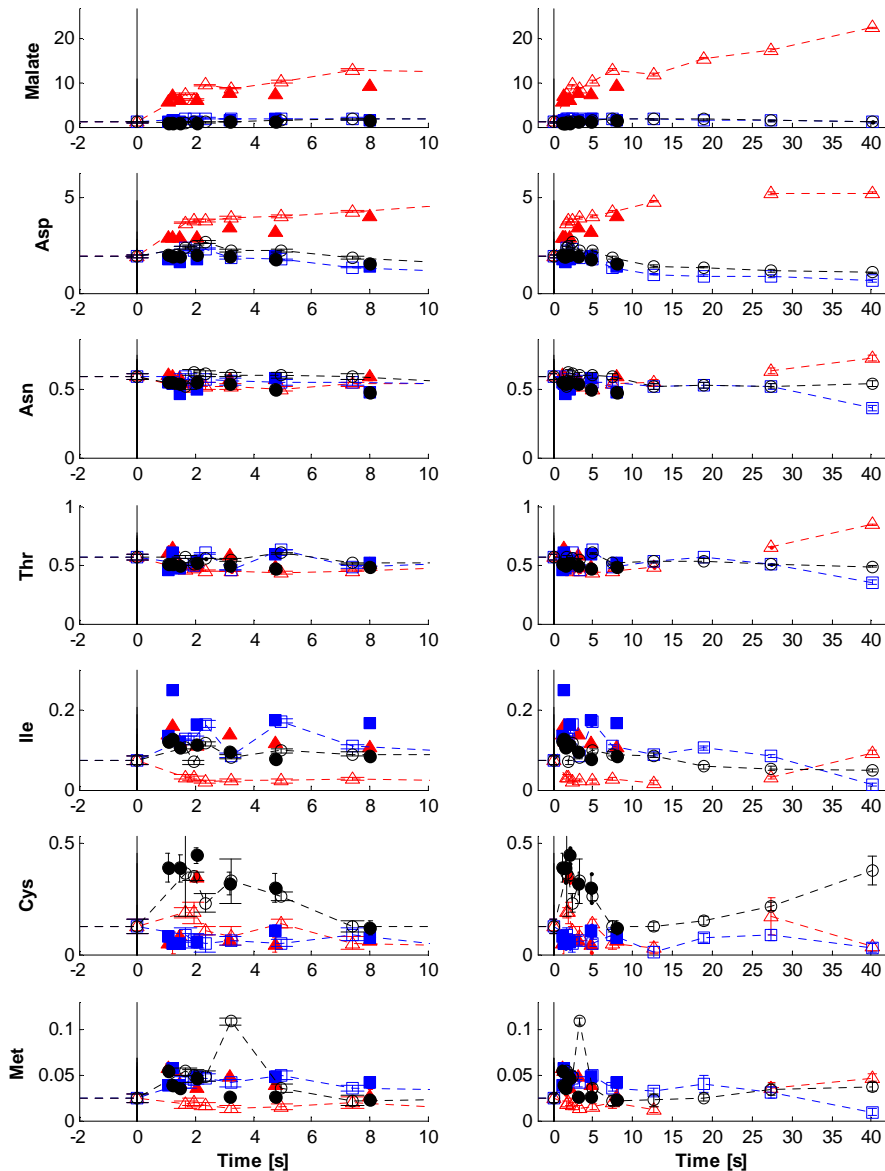
Figure 7.14: Measured amount of oxaloacetate-derived amino acids [µmol/gDW] during the glucose (circles), pyruvate (squares) and succinate (triangles) pulse. Open symbols are at flow rate 2 ml/min, closed symbols are at flow rate 4 ml/min.

reaction rate and MAR. Here we applied a recently introduced kinetic concept (Canelas *et al.* 2010) where for a reaction the Q-value (= MAR) of the reaction (e.g. for A↔B+C, Q = [B] x [C] / [A]) against the reaction rate (v) is plotted. When the measured Q is of the same order of magnitude as the K_{eq} value of the reaction, the reaction can be classified as pseudo-equilibrium or near-equilibrium. When the measured Q is several orders of magnitude lower than K_{eq}, the reaction is classified as far-from equilibrium. Many reactions in central metabolism of *S.*

cerevisiae behaved as pseudo/near equilibrium and a linear Q(v) plot has been observed (Canelas *et al.* 2010), where Q decreases with v.
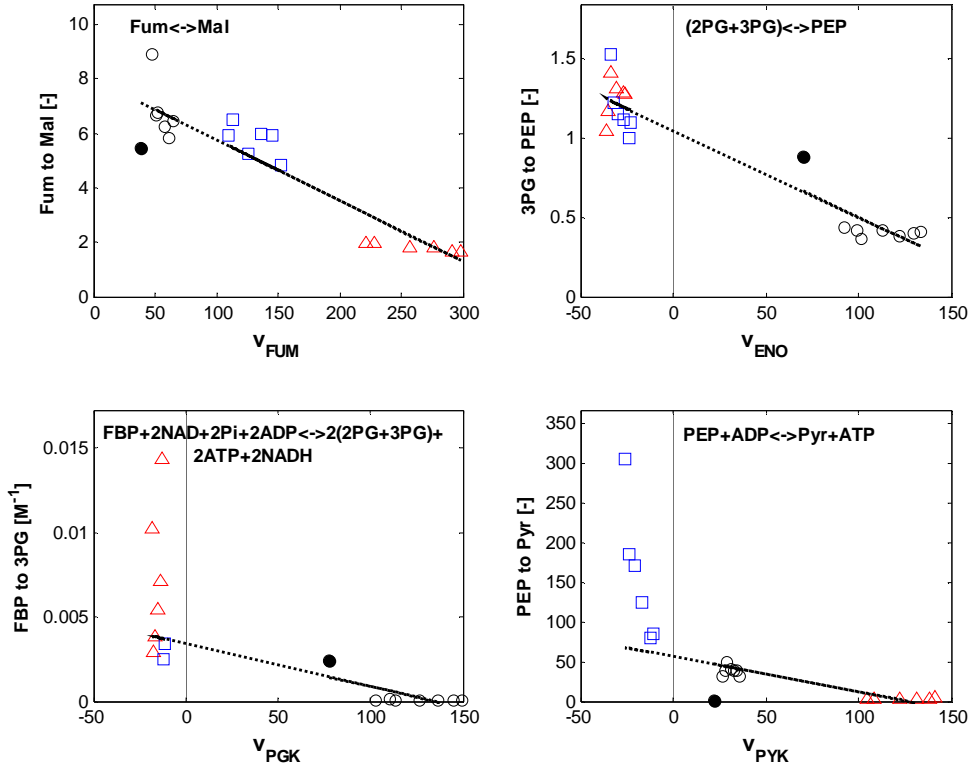
Figure 7.15: Q(= MAR) vs flux (v in mmol/CmolX/h) plots (near-equilibrium reactions) during the glucose (circles), pyruvate (squares) and succinate (triangles) pulse. Closed circle is the perturbed steady-state.

From the dynamic flux and metabolite data set obtained from the 40 s transient for three different substrates, we can establish Q(v) plots for several near-equilibrium reactions, most of which are involved in gluconeogenesis. In our *E. coli* pulse experiments the reactions catalyzed by fumarase, enolase, the lumped reaction from FBP to 3PG and pyruvate kinase show a negative linear dependency of Q versus flux of the enzyme catalyzed reaction (see Figure 7.15). It should be noted that the sign of v changes in several Q(v) plots (gluconeogenesis). These reactions show therefore near equilibrium behaviour. The reactions from FBP to 3PG, enolase and fumarase were also classified as near-equilibrium under *in vivo* conditions in *S. cerevisiae* (Canales *et al.* 2010).

The y-intercept of the MAR vs. flux plot gives the *in vivo* equilibrium constant of the reaction (Canelas *et al.* 2010). The observed K_{eq} for fumarase is 8.00 (Table 7.4), which is higher than the value of 5.18 observed in *S. cerevisiae* (Canelas *et al.* 2010), still lying in the range of published

in vitro data (Table 7.4). For the lumped PGK and ENO reaction a comparison to *in vivo* data from *S. cerevisiae* can be made. In the work of Canelas *et al.* (2010), K_{ENO} x $K_{GPM} = 0.46$ which is lower than our value of 1.05 (Figure 7.15), but which is higher than the range of published *in vitro* data (Table 7.4) at pH 7. For the lumped reaction from FBP to 3PG, literature K_{eq} data shows a very broad range with several orders of magnitude (Table 7.4). K_{eq} in our case is close to the lower end of the range (Table 7.4) as in *S. cerevisiae*, again suggesting that this part of glycolysis is also in near-equilibrium. Importantly, the assumed concentration of inorganic phosphate (Pi) has a big effect on the final K_{eq}. Here 50 mM of Pi concentration is assumed, however if actual Pi is 10 times lower, K_{eq} increases a factor of 100, still being in the published range.

Table 7.4: Comparison of y-intercept of Q(v) plots in *E. coli* to literature K_{eq} range and *in vivo* derived K_{eq} in *S. cerevisiae* (Canelas *et al.* 2010)

Enzyme	Literature K_{eq} range pH ~ 7	*in vivo* K_{eq} (*S. cerevisiae*)	This study y-intercept
FUM	2.10 - 8.40	5.18 ± 0.14	8.00
PGM+ENO	0.24 - 0.83	0.46 ± 0.01	1.05
FBA+TPI+GAPD+PGK, $[M^{-1}]$	0.002 - 100.9	0.0052 ± 0.0005	0.0034
PYK	6451.6	-	56.3
PTS		-	6.45
PGI+PFK	49.5 - 1215	-	-
FBP+PGI, [M]	387 - 688	-	0.084

Pyruvate kinase was classified as far-from-equilibrium by Canales *et al.* (2010). However, it is known to be a reversible reaction (Keseler *et al.* 2009) and indeed in our study this reaction reverses in the pyruvate pulse pseudo-steady-state conditions (gluconeogenesis). Presently K_{eq} is found to be 56.3, which is two orders of magnitude lower than a published ratio of about 6400 (Table 7.4), indicating a possible difference between *in vivo* and *in vitro* conditions.

For the fumarase catalyzed reaction, the gluconeogenic substrates pyruvate and succinate showed a lower MAR with higher flux. The x-intercept of the MAR vs. flux plot for this reaction gives the maximum *in vivo* forward reaction rate of that enzyme (Canales *et al.* 2010). Accordingly the *in vivo* v^{max} of fumarase is found to be ~ 360 mmol/CmolX/h, which is remarkably close to the found flux 368 mmol/CmolX/h at succinate excess pseudo-steady-state conditions (see Figure 7.4). This shows that the cells are at their maximal TCA cycle capacity after the succinate pulse, as was also observed for O_2 uptake rate.

We also investigated the Q(v) relation of far-from-equilibrium reactions such as PTS and the reactions from G6P to FBP and FBP to G6P (Figure 7.16). The lumped reaction of PGI+PFK (G6P to FBP) shows that v increases at increasing MAR, indicating the presence of allestoric effectors for this enzyme. Indeed the found MAR values (Figure 7.16) are orders of magnitude

lower than the *in vitro* K_{eq} (Table 7.4), showing its far-from equilibrium property. The lumped reaction from FBP to G6P (observed under gluconeogenesis) shows a constant MAR-value, orders of magnitude lower than the published K_{eq} (Table 7.4), and is therefore also considered far-from equilibrium. The PTS transport system favors a constant MAR of 6.45 (Figure 7.16). Although there is substantial information in literature on the kinetics of this enzyme complex, the overall K_{eq} is not known. The steady-state glucose concentration could be calculated from the constant MAR of 6.45 and found to be 4.7 mg/l which is in agreement with literature values for residual glucose concentrations at low dilution rates (Chassagnole *et al.* 2002).
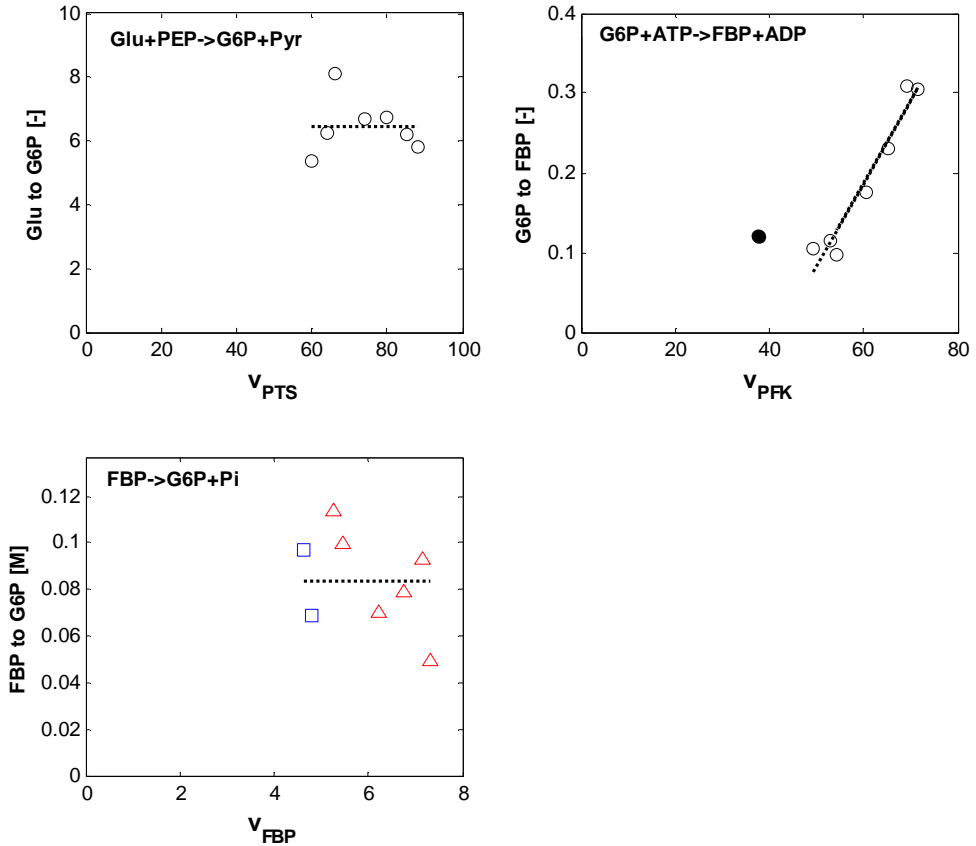
Figure 7.16: Q(= MAR) vs flux (v in mmol/CmolX/h) plots (far-from-equilibrium reactions) during the glucose (circles), pyruvate (squares) and succinate (triangles) pulse. Closed circle is the perturbed steady-state.

7.4. Conclusions

This work allows some remarkable observations on metabolically perturbed *E. coli* cultures: i) applying multiple pulses to the same culture is possible due to the quick return of flux and metabolite values to the initial steady-state, ii) energy charge is strongly homeostatic, whereas the redox status (NAD^+/NADH) is not, iii) both pyruvate and succinate are immediately taken up

with maximal capacity, showing the presence of their transporters in aerobic glucose-limited *E. coli* culture, iv) rapid (< 40 s) achievement of both flux and metabolite pseudo-steady-state for different substrate pulses, v) all metabolites (glycolysis, TCA cycle), but also amino acids show strong dynamics within 40 s, in agreement with low (< order of seconds) metabolite turnover times, vi) the three different substrates show the same rapid 2 - 3 fold increase in growth rate towards $\mu = 0.3$ h^{-1}, which is apparently limited by ribosome capacity. The highest O_2 uptake rate is achieved on succinate and appeared to be the ETC limited O_2 capacity of 20 mmol O_2/g/h. vii) The different substrates expose a tremendous flexibility of central metabolic fluxes. Most impressive are the flux inversion of glycolysis for gluconeogenic substrates, the more than 12 fold rate increase in TCA cycle between succinate and Oaa, the near 140 fold increase in conversion of Oaa to PEP for the succinate pulse and the inversion of pyruvate kinase for the pyruvate pulse. Remarkably most of these flux changes/inversions could be related to changes in thermodynamic driving force as quantified in the MARs. Also for several reactions linear relations appear to exist between rate and MAR (fumarase, enolase).

7.5. Appendix

7.5.1. Calculation of transient -q_{O_2} from liquid phase O_2 mass balance

The procedure followed was similar to described in Taymaz-Nikerel *et al.* (2010c). Differently in the present work, in order to reveal the dynamics of the probe used in the experiment, after the pulse experiment the steady-state culture was perturbed by removing pure O_2 and DO measurements were recorded (see Figure 7.17). The DO-readings reached a new steady-state as indicated.
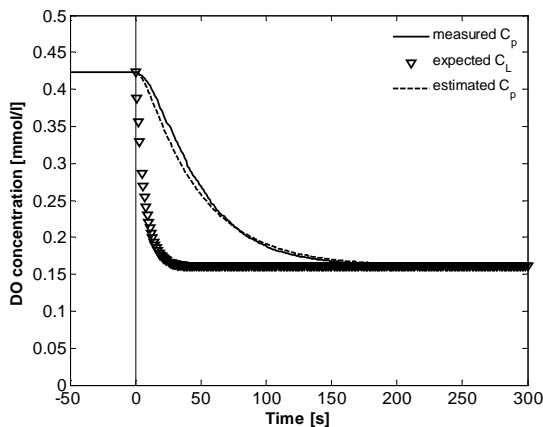
Figure 7.17: Dissolved oxygen (DO) concentration [mmol/l] as a function of time: line: DO probe readings during removal of O_2 from enriched air, circles: expected DO concentration, dashed line: fitting of the data.

The procedure described in Taymaz-Nikerel *et al.* (2010c) was followed, which yielded a DO-probe time constant of 43.1 s that is almost identical to the value of previous work (47.4 s) (Taymaz-Nikerel *et al.* 2010c). To show the nice fit, $C_{p,estimated}$ is also plotted (Figure 7.17).

With this time constant of the probe, the measured DO was back calculated to C_L and the transient $-q_{O2}$ during the glucose, succinate and pyruvate pulses was calculated using the calculated C_L and from C_L^* and k_La with the dynamic broth O_2-mass balance using Savitzky-Golay smoothing filters (MATLAB, The MathWorks Inc., Natick, MA, USA) (Taymaz-Nikerel *et al.* 2010c).

7.5.2. Yield of biomass on O_2 (Y_{OX}) during transient for different substrates

The stoichiometry of the present strain [λ^-, F$^-$, rph^{-1}] and the previous strain [λ^-, F$^-$, rph^{-1}, (*fnr*$^-$ 267)del] are different (discussed in the text). Therefore the ATP stoichiometry determined for the previous strain (Taymaz-Nikerel *et al.* 2010a) does not apply to the present strain, as indicated from the flux results shown in Table 7.1.

We calculated the appropriate P/O ratio that best approximates the four flux cases under study: glucose steady-state, glucose pseudo-steady-state, pyruvate pseudo-steady-state and succinate pseudo-steady-state. P/O of 0.8 was sufficient to simultaneously describe the four cases. With this parameter and K_X and m_{ATP} being same as in Taymaz-Nikerel *et al.* (2010a), Y_{OX} of each network is calculated as a function of growth rate and shown in Figure 7.18.

Figure 7.18 clearly shows that Y_{OX} at 0.13 - 0.3 h^{-1}, which is the range we are interested, does not change significantly. This allows us calculating μ at the transient (just after each pulse) from q_{O2} and a fixed Y_{OX}.
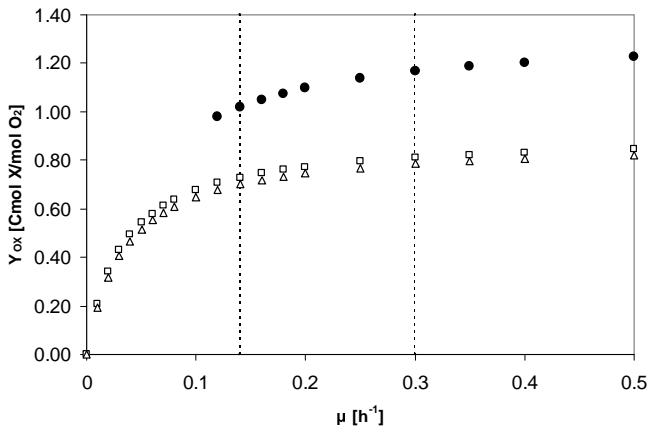
Figure 7.18: Yield of biomass on O_2, Y_{OX} [Cmol X/mol O_2] as a function of growth rate, μ [h^{-1}] for glucose (circles), pyruvate (squares) and succinate (triangles).

7.5.3. Cation/anion composition of the *E. coli* cultures

Table 7.5: Residual concentrations [mM] of some medium constituents

	Previous culture	**Present culture**
NH_4	28.8 ± 0.9	25.9 ± 0.8
PO_4	1.4 ± 0.1	1.9 ± 0.2
SO_4	8.3 ± 0.7	10.8
Cl^{-a}	135	8.6
K^{+a}	150	8.5

[a] Concentration in the feed medium.

7.5.4. Amount of intermediates at different steady-state conditions

Table 7.6: Steady-state intracellular amounts [µmol/gDW] of metabolites in glycolysis, TCA cycle, amino acids and adenine nucleotides at different running times [h] before and after the pulse experiments in two independent experiments. The running time indicates the time passed from the start of medium feeding (continuous phase). At 50.2, 73.6 and 97.6 glucose, succinate and pyruvate pulses were given, respectively

Experiment	Experiment 1						Experiment 2	
Running time [h]	49.8	50.6	73.5	75.2	97.5	99.1	50.3	58.3
Central Metabolites								
G6P	1.40±0.05[a]	1.21±0.04[a]	1.36±0.07[a]	0.97±0.01[a]	1.14±0.07[a]	1.22±0.08[a]	1.16±0.01	1.27±0.02
F6P	0.30±0.01[a]	0.28±0.01[a]	0.30±0.01[a]	0.21±0.01[a]	0.24±0.01[a]	0.27±0.01[a]	0.26±0.01[a]	0.30±0.01[a]
M6P	0.46±0.01[a]	0.39±0.02[a]	0.46±0.01[a]	0.36±0.01[a]	0.37±0.02[a]	0.38±0.01[a]	0.414±0.003[a]	0.46±0.01[a]
6PG	0.30±0.01[a]	0.258±0.004[a]	0.31±0.01[a]	0.26±0.01[a]	0.25±0.01[a]	0.24±0.01[a]	0.18±0.02	0.26±0.02
Mannitol-1P	0.52±0.06	0.40±0.05	0.57±0.03	0.24±0.02	0.44±0.06	0.41±0.03	0.47±0.05	1.02±0.04
G3P	0.42±0.01[a]	0.29±0.01[a]	0.36±0.01[a]	0.210±0.004[a]	0.31±0.05[a]	0.39±0.01[a]	0.37±0.01[a]	0.39±0.02[a]
FBP	0.72±0.01[a]	0.68±0.03[a]	0.75±0.01[a]	0.54±0.02[a]	0.64±0.04[a]	0.70±0.03[a]	0.52±0.11	0.60±0.05
F2,6bP	11.19±0.60[a]	11.21±0.48[a]	9.68±0.18[a]	7.82±0.32[a]	9.54±0.88[a]	10.59±0.32[a]	0.03±0.01[a]	0.06±0.03[a]
2PG+3PG	1.32±0.05	1.22±0.06	1.39±0.04	0.92±0.06	1.28±0.06	1.28±0.02	1.28±0.02	1.47±0.05
PEP	1.28± 0.03	1.18±0.04	1.40±0.05	0.76±0.05	1.18±0.11	1.38±0.05	1.22±0.03	1.24±0.04
Pyruvate	0.52±0.01[a]	0.46±0.02[a]	0.50±0.01[a]	0.31±0.01[a]	0.40±0.03[a]	0.40±0.02[a]	0.25±0.05	0.35±0.04
Citrate	1.62±0.02[a]	1.50±0.02[a]	1.62±0.05[a]	1.33±0.02[a]	1.58±0.12[a]	2.17±0.04[a]	0.17±0.06	0.86±0.05
α-ketoglutarate	0.13±0.02[a]	0.11±0.01[a]	0.16±0.01[a]	0.145±0.004[a]	0.20±0.01[a]	0.22±0.01[a]	0.16±0.02[a]	0.21±0.02[a]
Succinate	19.86±1.07[a]	17.16±1.11[a]	18.53±0.71[a]	14.08±0.44[a]	15.16±0.84[a]	14.53±0.49[a]	21.65±0.31[a]	23.16±0.60[a]
Fumarate	0.48±0.08[a]	0.29±0.03[a]	0.34±0.01[a]	0.20±0.03[a]	1.06±0.30[a]	0.33±0.02[a]	0.09±0.03	0.27±0.01
Malate	1.52±0.05[a]	1.44±0.06[a]	1.48±0.03[a]	1.06±0.03[a]	1.25±0.08[a]	1.35±0.04[a]	0.62±0.05	1.34±0.02
Amino Acids								
Alanine	1.89±0.03	1.64±0.07	1.92±0.07	1.24±0.02	1.66±0.07	1.59±0.03	1.39±0.04	1.53±0.08
Asparagine	0.56±0.04	0.51±0.03	0.63±0.01	0.40±0.01	0.53±0.03	0.55±0.01	0.532±0.004	0.67±0.01
Aspartate	2.52±0.21	2.50±0.12	2.22±0.13	1.56±0.04	2.19±0.16	2.19±0.10	1.76±0.04	2.03±0.04
Cysteine	NA	NA	NA	NA	NA	NA	0.11±0.05	0.16±0.04
Glutamate	20.35±0.09	18.64±0.59[a]	20.57±0.10	17.01±0.22	18.33±0.83[a]	18.77±0.39[a]	23.11±0.14	23.62±0.37
Glutamine	5.88±0.16	5.22±0.13	5.93	4.52±0.17	5.11±0.30[a]	4.90±0.35	3.54±0.24	3.72±0.35
Glycine	1.25±0.17	0.68±0.09	1.23±0.12	0.48±0.31	0.12±0.10	0.70±0.08	1.24±0.10	1.74±0.13
Histidine	0.12±0.03	0.09±0.01	0.30±0.05	0.18±0.003[a]	0.17±0.02	0.17±0.005	0.17±0.01	0.27±0.02
Isoleucine	0.12±0.03	0.06±0.01	0.11±0.02	0.01±0.04	0.06±0.01	0.17±0.04	0.048±0.004	0.09±0.02
Leucine	0.24±0.03	0.13±0.01	0.22±0.03	0.05±0.05	0.15±0.01	0.17±0.01	0.176±0.004	0.22±0.01
Lysine	2.02±0.02	1.91±0.06	2.20±0.10	1.42±0.04	1.86±0.09	1.85±0.01	1.44±0.02	1.50±0.02
Methionine	NA	NA	NA	NA	NA	NA	0.02±0.01	0.033±0.003
Phenylalenine	0.66±0.04[a]	0.46±0.03[a]	0.67±0.03[a]	0.39±0.01[a]	0.54±0.03[a]	0.57±0.02[a]	0.24±0.01[a]	0.27±0.01[a]
Proline	0.45±0.04	0.29±0.02	0.46±0.02	0.24±0.04	0.24±0.04	0.41±0.01	0.34±0.01	0.39±0.01
Serine	NA	NA	NA	NA	NA	NA	0.27±0.19	0.56±0.20
Threonine	0.98±0.11[a]	0.84±0.04	0.90±0.06[a]	0.26±0.05	0.80±0.03[a]	0.93±0.03[a]	0.54±0.02	0.61±0.03
Tryptophan	0.025±0.004	0.003±0.002	0.023±0.002	0.0205±0.0002[a]	0.017±0.002	0.019±0.001	0.030±0.002	0.037±0.003
Tyrosine	0.13±0.02	0.07±0.01	0.14±0.02	0.003±0.041	0.09±0.01	0.12±0.01	0.11±0.01	0.15±0.01
Valine	0.60±0.10	0.27±0.01	0.43±0.04	0.22±0.07	0.48±0.05	0.55±0.11	0.37±0.01	0.52±0.08
Ornithine	0.41±0.08	0.14±0.03	0.34±0.06	0.15±0.07	0.30±0.04	0.41±0.04	0.29±0.06	0.30±0.02
Adenine Nucleotides								
ATP	5.34±0.34	5.58±0.39	6.02±0.25	4.45±0.28	5.15±0.53	5.29±0.19	4.96±0.46	5.65±0.32
ADP	1.36±0.07	1.48±0.10	1.39±0.06	0.98±0.04	1.21±0.09	1.37±0.07	1.35±0.07	1.47±0.07
AMP	NA	NA	NA	NA	NA	NA	0.55±0.02	0.59±0.06

[a] Amount in the broth. In the filtrate G6P, F6P, M6P, 6PG, FBP, pyruvate was not detected (Exp 1). For citrate, succinate, fumarate and malate the analysis in the filtrate was not reproducible, therefore only broth results are presented (Exp 1 and succinate in Exp 2).

NA: Results not available or not detected.

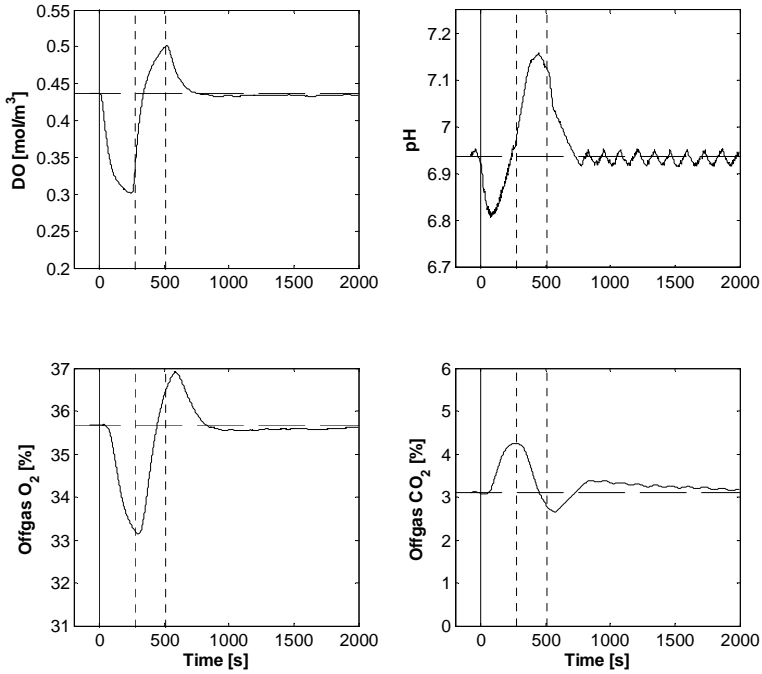**7.5.5. Online measurements during perturbation experiments**

Figure 7.19: Glucose pulse: DO [%], pH, offgas O_2 and CO_2 [%] measurements vs time [s] (t = 0 is the time of glucose addition).
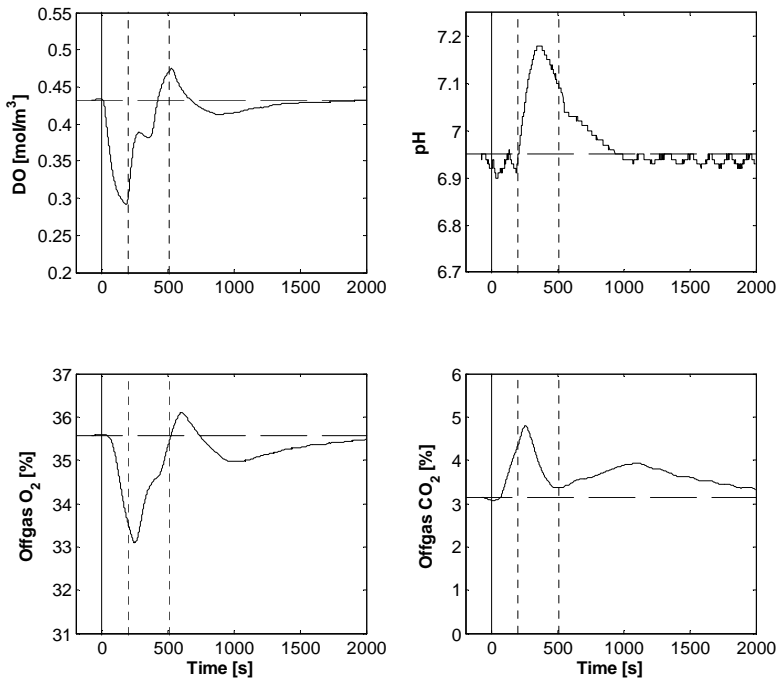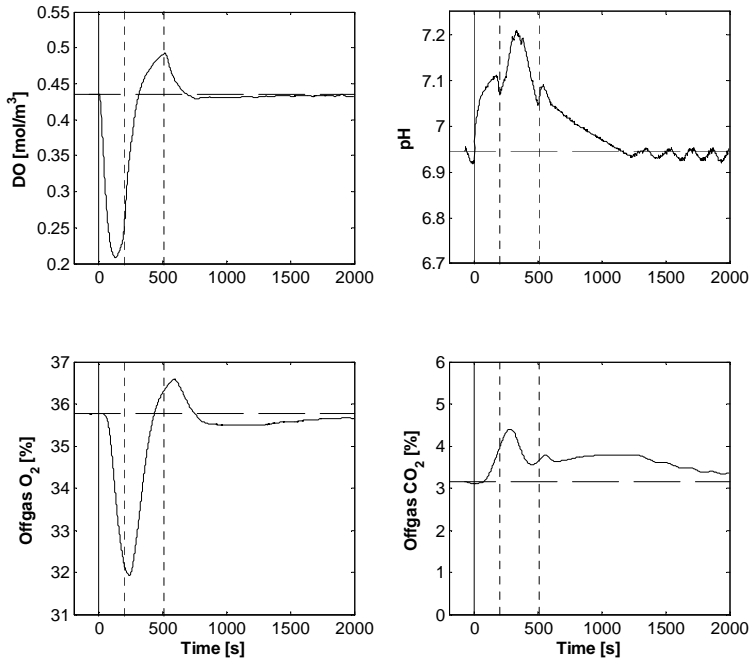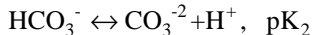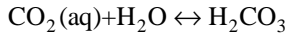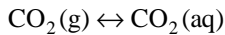

Figure 7.20: Pyruvate pulse: DO [%], pH, offgas O_2 and CO_2 [%], measurements vs time [s] (t = 0 is the time of pyruvate addition).

Figure 7.21: Succinate pulse: DO [%], pH, offgas O_2 and CO_2 [%] measurements vs time [s] (t = 0 is the time of succinate addition).

7.5.6. Bicarbonate concentration during the pyruvate pulse

In general, the concentration of the various molecular species of CO_2 in the liquid phase can be described according to the following association/dissociation reactions:

$$CO_2(g) \leftrightarrow CO_2(aq)$$
$$CO_2(aq) + H_2O \leftrightarrow H_2CO_3$$
$$H_2CO_3 \leftrightarrow HCO_3^- + H^+, \ pK_1$$
$$HCO_3^- \leftrightarrow CO_3^{-2} + H^+, \ \ pK_2$$

H_2CO_3: carbonic acid, HCO_3^-: bicarbonate, CO_3^{-2}: carbonate

Then, at pH = 7 we can write

$$CO_2(aq) + H_2O \leftrightarrow HCO_3^- + H^+.$$
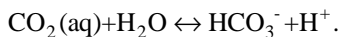
The concentration of dissolved CO_2 can be calculated by Henry's Law:
$[CO_2(aq)] = H \ p_{CO2}$,

where p_{CO2} is the partial pressure (atm) of the dissolved CO_2 and H is Henry's law constant (H depends on temperature, at 37 ^{o}C = 24.90 mM/atm, (Sander 2010)).

The Henderson–Hasselbalch equation for CO_2 is:

$$pH = pK_1 + \log \frac{[HCO_3^-]}{[CO_2(aq)]}.$$

At pH 7 and 37 ^{o}C (pK$_1$ = 6.116 at 37 ^{o}C) (Rispens *et al.* 1968)),

$$[HCO_3^-] = 7.66 \, [CO_2(aq)].$$

At steady-state offgas CO_2 = 3.15 %, $[CO_2(aq)]$ = 1.006 mM, $[HCO_3^-]$ = 7.70 mM.

When the pH behavior after the pyruvate pulse is attributed to bicarbonate concentration (charge balance: $-q_{pyr} - q_{NH_4^+} - q_{HCO_3^-} = 0$), q_{HCO3-} = 325.9 mmol/CmolX/h, equivalent to $\Delta[HCO_3^-]$ of 6.40 mM in 200 s. The reached $[HCO_3^-]$ is 14.10 mM, equivalent to $[CO_2(aq)]$ = 1.84 mM, that is equivalent to offgas CO_2 = 5.77 %, which is not far from the offgas measurements (Figure 7.20).

7.5.7. Accumulated carbon and electrons during the glucose pulse

The total amount of intracellular carbon and electrons after the glucose pulse were calculated from the measured metabolites at each time point and shown in Figure 7.22.
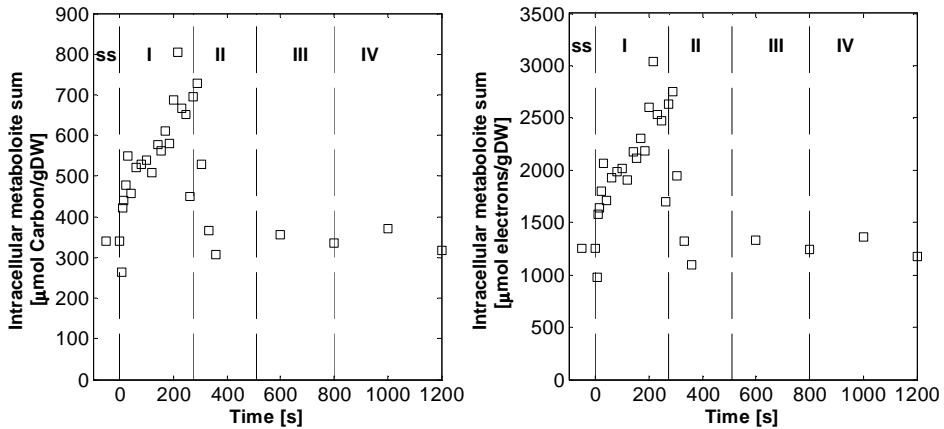
Figure 7.22: Total amount of intracellular metabolite-associated carbon [µmol Carbon/gDW] and electrons [µmol electrons/gDW] calculated from the measured metabolites at each time point.

Acknowledgements

Chapter 8

Comparative fluxome and metabolome analysis for overproduction of succinate

Abstract

A comparative (to the wild type) study on the quantitative fluxes/metabolomics during steady-state and dynamic conditions is performed for a succinate producing aerobic *Escherichia coli* mutant. The mutant had four functional mutations: increased succinate exporter, a deleted succinate importer, deletion of succinate dehydrogenase (SUCDH) and a PEP carboxylase (PPC) with increased capacity due to a point mutation. The steady-state and dynamic pattern of the metabolite concentration levels and fluxes in response to perturbation with different substrates for wild type and mutant strain is used to locate the quantitative changes in the physiology/metabolism of the mutant strain. Unexpectedly the mutant had a higher energy efficiency indicated by a much lower q_{O2} (under glucose-limited conditions) caused by the deletion of the transcription factors IclR and ArcA. The mutant had a much lower uptake capacity for glucose (2.5 fold), pyruvate (5 fold), succinate (26 fold) and O_2 (17 fold under succinate excess) compared to the wild type strain. 28 mM succinate was produced at chemostat, showing that the deletion of the succinate importer and overexpression of succinate exporter was a successful strategy. Deletion of SUCDH and a point mutation in PPC created multiple delocalized large changes in metabolite levels (FBP, pyruvate, 6PG, $NAD^+/NADH$ ratio, α-ketogluarate) corresponding to large changes in fluxes. Compared to the wild type a considerable flux shift occurred from TCA cycle to oxidative pentose phosphate pathway, including inversion of pyruvate kinase. The mutant responded very differently to excess of different substrates, most remarkably the possible reversal of TCA cycle under succinate excess. The mutant and the wild type both showed homeostatic behaviour for energy charge in the pulses. In contrast, large changes in redox level $NAD^+/NADH$ occurred where the mutant showed even larger changes. This large redox change can be associated to reversal of flux direction. The observed huge flexibility in central metabolism following genetic (deletions) and environmental (substrate pulses) perturbations of the mutant strain strongly points to introducing a more powerful succinate exporter in future studies to obtain higher succinate production rate.

8.1. Introduction

Microbial biotechnology has gained considerable interest for sustainable production based on renewable biological resources in response to concerns on the increasing oil prices, depletion of fossil resources and on the environmental aspects. The United States Department of Energy (DOE) has identified the top twelve sugar-based building blocks (US Department of Energy, 2004), which have multiple functional groups that possess the potential to be applied in the production of other useful chemicals. Succinate is one of these building blocks and one of the most attractive green chemicals currently available and much attention is given to developing a bio-based industrial production of succinic acid (McKinlay *et al.* 2007).

Mostly production yields, titers and secretion rates with measured extracellular concentrations of relevant metabolites are studied and compared to either the wild type or high-producer strains (Jantama *et al.* 2008; Otero and Nielsen 2010; Zelle *et al.* 2008). However, rarely information is obtained to characterize/understand the effect of the mutation(s) on the metabolism. This information can be obtained by studying the changed metabolite levels and fluxes under steady-state and dynamic conditions. Such experiments are mostly performed to analyze central metabolism including glycolysis, pentose phosphate pathway (PPP) and TCA cycle, although the production pathways are of outstanding commercial interest and thus in the focus of metabolic engineering. Some examples, which include product pathways, are the glucose pulses presented to *Escherichia coli*-based strains related with the aromatic biosynthesis pathway (Oldiges *et al.* 2004; Schmitz *et al.* 2002) and perturbations to *Penicillium chrysogenum* strains (Nasution *et al.* 2006) to study the penicillin production pathway.

In the present work, we intend to provide a comparative steady-state and dynamic quantitative metabolomics study for a succinate producing aerobic *E. coli* mutant and its wild type. The steady-state and dynamic pattern of the metabolite concentration levels and fluxes in response to perturbation with different substrates for the wild type and a mutant strain will be used to map the quantitative changes in the physiology/metabolism of the mutant strain.

8.2. Materials and Methods

8.2.1. Strains

In this research, the *E. coli* K12 MG1655 [λ^-, F$^-$, rph^{-1}] and a derived mutant *E. coli* K12 MG1655 [λ^-, F$^-$, rph^{-1}, Δ*ackA-pta*, Δ*poxB*, Δ*iclR*, Δ*sdhAB,* Δ*arcA*, Δ*dctA*, Δ*edd*, Δ*eda*, Δ*citDEF*, ppc*(L620S), Δ*FNR-pro37-dcuC*)] were used. The knock-outs and point mutation were created using the method of Datsenko and Wanner (2000). The replacement of the endogenous *dcuC* promoter by an artificial promoter pro37 (De Mey *et al.* 2007) was done as described in De Mey *et al.* (2010a).

8.2.2. Chemostat conditions

Both strains were cultivated in independent aerobic glucose-limited chemostat cultures (pH 7, temperature 37 ^{o}C) with minimal medium at a dilution rate (D) of 0.1 h^{-1} in 7 l laboratory fermentors with a working mass of 4 kg, controlled by a balance (Applikon, Schiedam, The Netherlands). The preculture conditions, medium composition, fermentor conditions (temperature control, pH control, overpressure, aeration rate, stirrer speed, offgas and dissolved oxygen measurements) were as stated in De Mey *et al.* (2010b).

8.2.3. Rapid sampling for intracellular metabolites

The differential method is used for the calculation of the amounts of intracellular metabolites (Taymaz-Nikerel *et al.* 2009) at steady-state as well as during the transient state. Broth sampling and filtrate sampling was carried out as in Taymaz-Nikerel *et al.* (2009). For each steady-state condition two samples were taken and analyzed in duplicate. For intracellular metabolite determination during perturbation, only sampling for broth was performed (De Mey *et al.* 2010b; Taymaz-Nikerel *et al.* 2010b; Taymaz-Nikerel *et al.* 2010c), for each time point one broth sample was taken and analyzed in duplicate.

8.2.4. Short-term perturbation experiments

Short-term perturbation experiments in the BioScope were carried out as described before (Taymaz-Nikerel *et al.* 2010b). In brief, before starting the perturbation experiment, air inlet to the reactor was blended with pure O$_2$ in order to have about 39 % O$_2$ in the incoming gas (the gas inflow rate was increased from 1.67 l/min air to 1.67 l/min air + 0.5 l/min O$_2$). Perturbation experiments were performed in the BioScope, unless stated otherwise, for two different flow rates (at 1.8 ml/min broth + 0.2 ml/min pulse and 3.6ml/min broth + 0.4 ml/min pulse). For the wild type strain, the pulse solution was either 27.8 mM glucose, 55.5 mM pyruvate or 41.6 mM succinate. Each of them resulted in a pulse of 16.7 mmol carbon/l. For the succinate producing mutant strain, the same glucose and pyruvate pulses were applied and instead of succinate, deionized water was given (glucose feed stopped), because a large amount of extracellular succinate was already present in the culture.

8.2.5. Perturbation experiments in the bioreactor

To obtain uptake/secretion flux capacities, the required flux information cannot be obtained from the BioScope experiments and therefore pulse experiments were performed in the steady-state chemostat. For the wild type these experiments have been presented already for glucose, pyruvate and succinate pulses (Taymaz-Nikerel *et al.* 2010b). For the mutant the glucose excess experiment in batch on glucose was available, the pyruvate excess experiment (initial broth

concentration of 5.5 mM) was performed in the chemostat, in the presence of steady-state glucose flux. A succinate pulse to the succinate producing mutant at steady-state (where the steady-state already contained 28 mM succinate) was not meaningful. Therefore glucose feed was switched off and the resulting succinate uptake was monitored.

8.2.6. Metabolite extraction procedure

Metabolites were extracted in 75 % boiling ethanol (3 min, 90 ^{o}C) as described in Taymaz-Nikerel *et al.* (2009). Before extraction, 100 µl of 100 % U-^{13}C- labeled cell extract was added to each sample as internal standard for isotope dilution mass spectrometry (IDMS)-based metabolite quantification (Wu *et al.* 2005).

8.2.7. Analytical procedures

Measurement of offgas, cell dry weight, residual glucose, total organic carbon and intracellular metabolite concentrations were carried out as described before (De Mey *et al.* 2010b; Taymaz-Nikerel *et al.* 2009). The succinate concentration was analyzed enzymatically (Boehringer Mannheim/R-Biopharm, Roche) and with HPLC (Aminex HPX-87H ion exclusion column, Bio-Rad, CA, USA).

8.2.8. Calculation procedures

The biomass-specific rates, mass action ratios, intracellular NAD^{+}/NADH ratio, energy charge, concentration of E4P were calculated as described before (De Mey *et al.* 2010b; Taymaz-Nikerel *et al.* 2009).

Intracellular fluxes in steady-state were calculated with metabolic flux analysis using the appropriate metabolic network of *E. coli* with the reconciled uptake/secretion rates as input. The metabolic network for growth of the wild type strain on glucose is as described in Taymaz-Nikerel *et al.* (2010a) with the addition of the PEP-glyoxylate route (Nanchen *et al.* 2006), leading to the final network as in Taymaz-Nikerel *et al.* (2010c). The addition of PEP-glyoxylate route created a parallel pathway, which requires additional information to perform MFA. Ratios of Flux$_{PPC}$/ Flux$_{PPCK}$ = 2 and Flux$_{ICL}$ = 0.2 x Flux$_{ACoNT}$ were assumed since these average ratios were observed at dilution rates 0.1 - 0.4 h^{-1} in glucose-limited continuous cultures of *E. coli* (Nanchen *et al.* 2006).

For the growth of the mutant strain on glucose, where catabolism of glucose (not possible in the "cut"-TCA cycle) is performed in the oxidative PPP leading to NADPH production, NAD(P) transhydrogenase reaction was added, while the reactions PEP carboxykinase (PPCK), SucCoA

synthetase (SUCoAS) and succinate dehydrogenase (SUCDH) were set to 0. For the network with succinate consumption under succinate excess conditions, SUCoAS was freed.

8.3. Results and Discussion

8.3.1. Mutations in the producer strain

The mutant in this work is *E. coli* K12 MG1655 [λ⁻, F⁻, rph⁻¹, Δ*ackA-pta*, Δ*poxB*, Δ*iclR*, Δ*sdhAB,* Δ*arcA*, Δ*dctA*, Δ*edd*, Δ*eda*, Δ*citDEF*, ppc*(L620S), Δ*FNR-pro37-dcuC*)], which is extensively described in Beauprez (2010). In brief, the wild type strain produces acetate under aerobic batch conditions, therefore the routes (phosphate acyltransferase-acetate kinase: Δ*ackA-pta*, pyruvate oxidase: Δ*poxB*) that are known to be active in acetate formation were deleted. Also, increasing the flux from pyruvate to TCA cycle intermediates through activation of glyoxylate route by deletion of the transcription factors (Δ*iclR*, Δ*arcA*) leads to less acetate production in batch. For the same purpose (decrease of acetate formation), the genes *cit*D, *cit*E and *cit*F that code for citrate lyase, which converts citrate into oxaloacetate and acetate under anaerobic conditions, were knocked out (Δ*citDEF*). The genes that code for the enzymes of Entner-Doudoroff (ED) pathway were eliminated (Δ*edd*, Δ*eda*) to overcome a possible NADH limitation problem, and thus increasing the succinate formation. However the ED pathway was reported to be inactive for *E. coli* cells grown on glucose (Fischer and Sauer 2003). All these mentioned deletions are not relevant under aerobic glucose-limited chemostat conditions as applied here.

The mutations relevant to this study related to increased succinate production: Improved succinate production was pursued by deletion of succinate dehydrogenase (Δ*sdhAB)*, which is essential for aerobic succinate production because it prevents conversion of succinate to fumarate. The additional strategy was increasing succinate export and decreasing succinate import: DctA is known to be responsible for the aerobic dicarboxylate uptake system, thus it was deleted (Δ*dctA*) and succinate exporter DcuC was overexpressed (Δ*FNR-pro37-dcuC*). A second strategy was to improve flux capacity from PEP to Oaa (PEP carboxylase: PPC) to boost the rate of citrate, and therefrom succinate, formation. PEP carboxylase is inhibited by accumulation of malate, succinate and aspartate, which are expected to increase when succinate is produced. This can be overcome by point mutations introduced at the amino acid residues responsible for allosteric binding. The allosteric inhibition sites of PPC are located at lys491, lys620, lys650, and lys773. Among those, only the lys620 to serine mutant enzyme, as applied in our mutant (ppc*(L620S)), maintained the wild type catalytic properties with a significant desensitization to take mentioned feedback inhibition (Yano and Izui 1997).

Summarizing, the mutations that are expected to have an effect under our culture conditions are deletion of succinate dehydrogenase (Δ*sdhAB*), deletion of succinate importer (Δ*dctA*), overexpression of succinate exporter (Δ*FNR-pro37-dcuC*) and introduction of a point mutation in PPC (ppc*(L620S)).

8.3.2. Uptake/secretion rates

Both wild type and mutant were characterized for their uptake/secretion rates under steady-state and dynamic conditions (reactor perturbations).

Steady-state: The steady-state features of wild type strain and mutant strain are compared to characterize the producer mutant strain. The cell dry weight, mass-balance-based biomass-specific rates, the corresponding carbon and degree of reduction recoveries and the reconciled biomass-specific rates for both strains are shown in Table 8.1. Reconciliation was acceptable considering χ^2 test with a null hypothesis of significant measurement deviations at a significance level of 0.1 %. The mutant strain produces about 8 mmol/CmolX/h succinate and there is cell lysis of $\mu_{lysis} = 0.014 h^{-1}$, which is less than found in the wild type ($\mu_{lysis} = 0.031 h^{-1}$).

Table 8.1 shows that q_{O2} and q_{CO2} are much lower in the mutant. This corresponds to the lower glucose uptake rate, despite a significant succinate production. This means that in the mutant the energy metabolism is much more efficient. Recently the same effect was observed in a non succinate-producing *E. coli* as a result of the synergetic effect of the deleted transcriptional regulators IclR and ArcA (Beauprez 2010). The molecular basis of this important effect is not known, but is clearly confirmed in our succinate producing mutant, which also has these deletions.

Clearly the mutant produces succinate, which shows that the implemented exporter is functioning and can export the succinate, which cannot be converted to fumarate anymore (*ΔsdhAB).*

Fermentor perturbation studies: Under batch glucose excess the mutant showed 2.5 times lower glucose uptake rate and 2.5 fold lower O_2 uptake rate (Table 8.2). With addition of pyruvate excess (while glucose feeding continued, see Appendix 8.6.1) the mutant showed maximal rates

Table 8.1: Steady-state data in aerobic glucose-limited *E. coli* chemostat cultures, D = 0.1 h^{-1}

	Wild type		Mutant strain	
	Measured	**Reconciled**	**Measured**	**Reconciled**
C_{Suc}[mM]	0		28 ± 1.4	27.8 ± 1.4
C_X[gDW/l]	8.02 ± 0.12	8.02 ± 0.12	8.71 ± 0.07	8.70 ± 0.07
D[h^{-1}]	0.105		0.107	
μ[mmol/Cmol X.h]	136.6 ± 2.6	136.6 ± 2.6	121.5 ± 3.6	120.9 ± 3.5
$-q_S$[mmol/Cmol X.h]	44.61 ± 1.8	44.5 ± 1.3	41.09 ± 1.5	41.56 ± 1.2
$-q_{O2}$[mmol/Cmol X.h]	125.4 ± 8.3	121.1 ± 5.8	97.45 ± 9.5	92.35 ± 3.9
q_{CO2}[mmol/Cmol X.h]	130.2 ± 8.7	130.5 ± 6.0	96.67 ± 9.5	96.67 ± 3.9
q_{lysis}[mmol/Cmol X.h]	31.4 ± 1.2	31.3 ± 1.2	14.8 ± 2.7	14.3 ± 2.6
$q_{Succinate}$[mmol/Cmol X.h]	-	-	7.96 ± 0.47	7.94 ± 0.47
Carbon Recovery [%]	99.7 ± 5.3		101.4 ± 22	
Redox Recovery [%]	101.8 ± 4.3		103.9 ± 23	

of q_{pyr} and q_{O2} of 53 and 131 mmol/CmolX/h, which are 5 and 2.4 fold lower than for the wild type (Table 8.2). Under succinate excess (its uptake was monitored by stopping glucose feed in the mutant culture), the mutant clearly consumed the succinate which was produced before (see Appendix 8.6.2), but the calculated consumption rates were q_{Suc} = 9.3 mmol/CmolX/h with q_{O2} = 31 mmol/CmolX/h, q_{CO2} = 36 mmol/CmolX/h and µ = 0, which are about 20 - 30 times lower than in the wild type (see Table 8.2), showing that the intended knockout of the succinate importer was very successful, but that there is still low capacity succinate importer present.

In conclusion these steady-state/dynamic experiments show that the mutant has much lower uptake capacities for glucose (2.5 fold), pyruvate (5 fold), succinate (26 fold) and O_2 (17 fold under succinate excess). Also it is found that the knockout of the importer and overexpression of the exporter were very successful.

Table 8.2: Uptake/secretion rates of mutant and wild type at excess conditions for glucose, pyruvate and succinate (q rates in mmol/CmolX/h, µ in h^{-1})
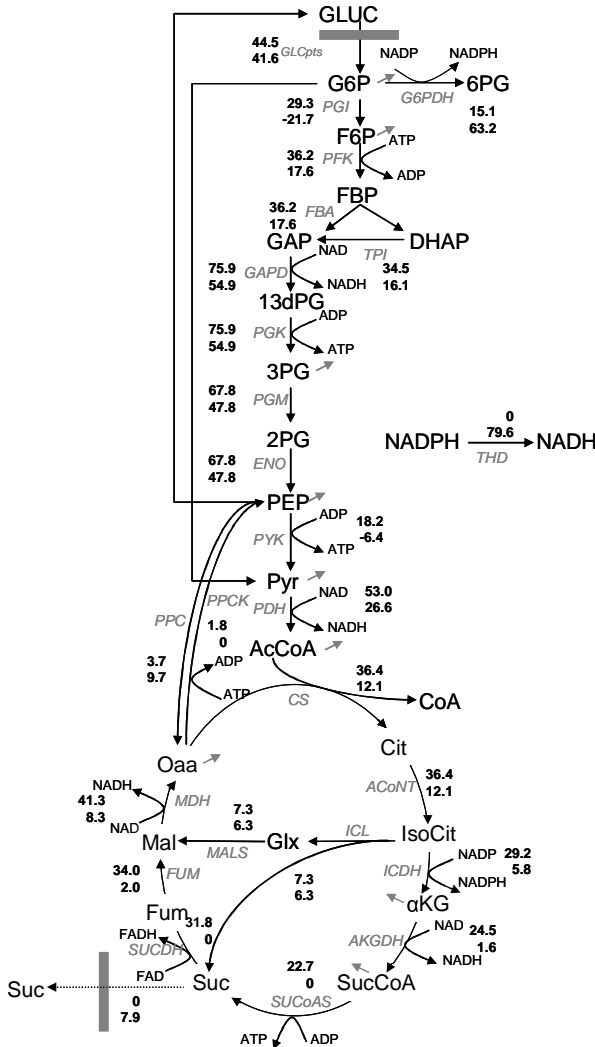
	Mutant strain				Wild type			
	glucose batch	glucose pulse	pyruvate pulse	succinate excess	glucose batch	glucose pulse	pyruvate pulse	succinate pulse
-q$_{glu}$	113	-	-	-	276	96	-	-
-q$_{pyr}$	-	-	53.3	-	-	-	255	-
-q$_{suc}$	-	-	-	9.3	-	-	-	240
-q$_{O2}$	213	-	131.5	30.8	500	280	320	510
µ	0.43	-	-	0	0.63	0.28	0.29	0.31

8.3.3. Intracellular fluxes on glucose

For the mutant grown on glucose the steady-state intracellular flux calculations show that the PPP has a much higher flux (see Figure 8.1). The PPP has to provide all NADH (obtained from NADPH through transhydrogenase) because the TCA cycle is cut through and cannot provide NADH. As a consequence, the glycolytic flux and the TCA cycle flux are much lower in the mutant. The flux from PEP to Oaa was 3 times higher in the mutant, showing that the point mutation (ppc*(L620S)) was successful, indicating the importance of this flux for succinate overproduction. The importance of increasing flux towards Oaa was already noticed and studied by others either by overexpressing *E. coli* PEP carboxylase (Millard *et al.* 1996), or introducing pyruvate carboxylase (Sanchez *et al.* 2005a; Vemuri *et al.* 2002b), or by overexpressing *E. coli* malate deyhdrogenase (Hong and Lee 2001; Stols and Donnelly 1997).

Most remarkable is that the pyruvate kinase reaction reverses in the mutant strain, which is consistent with the very high intracellular pyruvate concentration in the mutant (see below). This flux reversal is necessary because the large G6P diversion to PPP leads to a low glycolytic flux which produces too little PEP for the phosphotransferase system (PTS). The reversal of this

reaction was also observed under pyruvate pulse conditions for the wild type (Taymaz-Nikerel *et al.* 2010b).

Figure 8.1: Metabolic flux patterns of central carbon metabolism for aerobic growth of wild type (μ = 0.137 h^{-1}) and mutant *E. coli* (μ = 0.121 h^{-1}) on glucose. All fluxes are given in mmol/CmolX/h. First values represent wild type strain, second values represent mutant strain. Gray arrows indicate the fluxes to biomass synthesis.

8.3.4. Steady-state metabolite levels on glucose

In order to see the effects of the two network-related mutations (Δ*sdhAB* and ppc*(L620S)) on the metabolome of the mutant strain grown on glucose, the extracellular and intracellular

metabolite amounts are compared with that of wild type strain (see Table 8.3). The thermodynamic feasibility of the metabolome data of the mutant strain is checked by assessing the mass action ratios (Table 8.4). MAR of PGI, PMI, PGM+ENO and FUM catalyzed reactions are in the range of the reported K_{eq} for both strains, showing the thermodynamic feasibility. The MAR of fumarase is ~ 2 times lower compared to the wild type strain, though still thermodynamically feasible, but the flux is very low (2 mmol/CmolX/h, Figure 8.1). MAR of AK is higher than the reported K_{eq} for both strains, indicating that the *in vivo* and *in vitro* conditions can be different.

Although there are several large differences in the amounts of intermediates, the nucleotide levels and the energy charge (Table 8.4) of the two strains are almost the same (a satisfying value of ~ 0.8), showing once again the robustness/homeostasis of the energy system in *E. coli* despite very different oxygen consumption rates of the two strains (Table 8.1).

When the metabolite levels are compared, it is seen that in the mutant strain the amounts of metabolites outside the cell is most of the time much higher, especially the organic acids pyruvate, citrate, fumarate and malate, in general agreeing with their higher intracellular levels.

Main metabolite concentration differences in the mutant are in pyruvate (5 fold up), FBP (1.5 fold down), 6PG (10 fold down), NAD^+/NADH redox ratio (1.5 fold more reduced), C_4 acids (1.5 - 3 fold higher) and α-ketoglutarate (10 fold up). The 10 fold lower 6PG level occurs with a 4 fold increase in the oxidative PPP flux (Figure 8.1), indicating that the mutant has acquired a large capacity in this pathway, which generates the electrons for aerobic respiration.

Table 8.3: Steady-state amount of extracellular and intracellular metabolites [µmol/gDW]

	Wild type strain		Mutant strain	
	Extracellular	**Intracellular**	**Extracellular**	**Intracellular**
Central Metabolites				
G6P	0.06±0.02	1.22 ± 0.02	0.08±0.01	1.03 ± 0.03
F6P	-	0.28 ± 0.01	0.03±0.01	0.19 ± 0.01
M6P	-	0.44 ± 0.01	0.01±0.00	0.33 ± 0.01
Mannitol-1P	0.41±0.09	0.75 ± 0.09	0.31±0.01	0.76 ± 0.02
6PG	0.08±0.02	0.22 ± 0.02	0.04±0.00	0.02 ± 0.01
FBP	0.09±0.06	0.55 ± 0.07	0.004±0.002	0.36 ± 0.03
2PG+3PG	0.10±0.02	1.38 ± 0.03	0.96±0.02	1.11 ± 0.05
PEP	0.05±0.01	1.22 ± 0.03	1.16±0.02	1.11 ± 0.06
Pyruvate	0.09±0.03	0.30 ± 0.04	3.72±0.10	1.49 ± 0.12
Citrate	0.60±0.13	0.52 ± 0.13	2.13±0.06	0.52 ± 0.08
α-KG	0.17±0.05	0.02 ± 0.05	0.11±0.06	0.19 ± 0.07
Succinate	12.72±2.69	9.69 ± 2.72	-	-
Fumarate	0.19±0.04	0.18 ± 0.04	3.77±0.11	0.51 ± 0.15
Malate	0.59±0.11	0.98 ± 0.11	3.42±0.14	1.47 ± 0.19
Nucleotides				
AMP	<	0.58 ± 0.04	<	0.54 ± 0.05
ADP	<	1.41 ± 0.05	<	1.33 ± 0.03
ATP	<	5.30 ± 0.29	<	5.47 ± 0.05

The 5 fold higher pyruvate level is a result of the need to convert pyruvate to PEP (inversion of PYK) to provide enough PEP for the PTS, because the glycolytic flux to PEP is insufficient due to the large G6P diversion into the oxidative PPP. This low glycolytic flux is also supported by the lower FBP concentration and the consistently lower concentrations for the other glycolytic intermediates.

Interestingly the $NAD^+/NADH$ ratio strongly decreased in the mutant, showing a more reduced cytosol. This more reduced $NAD^+/NADH$ couple also corresponds to the higher C_4 acid level (due to malate dehydrogenase). The higher C_4 acid pool and the 3 fold increase of flux between PEP and the C_4-pool is a strong indication of a large increase in capacity of the PPC rate in the mutant strain, indicating that the point mutation was successful.

For the mutant the TCA cycle shows a 10 fold increase in α-ketoglutarate, whereas citrate is not changed and the ACoNT flux is 3 times lower. This could point to product inhibition by α-ketoglutarate on the ICDH reaction.

Table 8.4: Steady-state mass action ratios (MAR), $NAD^+/NADH$ ratio and energy charge calculated from the measured metabolite levels and range of published equilibrium constants for some relevant equilibrium reactions

	Wild type	Mutant strain	K_{eq}
PGI: G6P ↔ F6P	0.23±0.01	0.19±0.01	0.19 - 0.67
PMI: F6P ↔ M6P	1.57±0.06	1.71±0.10	0.99 - 1.80
PGM+ENO: 2+3PG ↔ PEP	0.89±0.03	0.99±0.07	0.10 - 1.79
FUM: Fumarate + H_2O ↔ Malate	5.43±1.26	2.90±0.93	2.10 - 9.49
AK: 2ADP ↔ AMP + ATP	1.54±0.14	1.66±0.16	0.20 - 1.45
Pyruvate/PEP	0.24±0.03	1.35±0.13	
$NAD^+/NADH$:	47.2±5.99	31.9±1.92	
Energy charge	0.82±0.07	0.84±0.08	

Summarizing, it seems that the observed metabolite changes in the mutant (Table 8.3) support the proposed flux scheme (Figure 8.1), especially the large increase in oxidative PPP, the resulting low glycolytic flux, the inversion of PYK and an increased capacity for PPC.

More important we find that the SUCDH deletion creates large changes in many metabolites (pyruvate, FBP, 6PG, $NAD^+/NADH$, C_4 acids and α-ketoglutarate) far away from the deleted reaction. This shows that not only the metabolites in close proximity (C_4 acids and α-ketoglutarate) are changed, but also distant metabolites (pyruvate, FBP, 6PG, glycolytic intermediates, $NAD^+/NADH$) are clearly changed, which is to be expected due to all metabolic interactions.

### 8.3.5. Response of metabolites in pulses

The measured metabolite concentrations, during the pulse experiments applied in the BioScope, showed that the different substrate pulses lead to very different metabolite responses. The same glucose and pyruvate pulses were applied both the wild type and the mutant, whereas succinate pulse was applied only to the wild type. For the mutant, broth was mixed with water to create a condition for succinate uptake, as there is already 28 mM succinate present. The pulse experiments for glucose, pyruvate and succinate in the wild type were assessed in our previous work (Taymaz-Nikerel *et al.* 2010b), here we will show and discuss the difference in metabolite responses to these pulses observed for the wild type and mutant strains.

General observations: The energy charge (Figure 8.2) was maintained for both the wild type and mutant for the three pulses (glucose, pyruvate, succinate), showing the robustness of the energy system. The redox ratio $NAD^+/NADH$ for the wild type and the mutant (Figure 8.5) was the same for the glucose pulse (increase and then decrease) as observed before. For the pyruvate and succinate pulses, the mutant shows that this couple becomes much more reduced than in the wild type. A more reduced couple (compared to glucose pulse) is needed to create a driving force for gluconeogenesis, which occurs on pyruvate and succinate. The mutant is more reduced than the wild type, which for succinate can be explained by a possible reversal of the TCA cycle (see below).

Glucose pulse: The mutant shows much less increase in FBP, which points to a lower PFK flux due to a large diversion of G6P to the oxidative PPP. In addition, the glucose uptake rate during the glucose pulse is most likely lower in the mutant (Table 8.2), which also contributes to decrease of the PFK flux. Lower 2PG+3PG, PEP and much higher pyruvate levels are observed in the mutant, which supports the occurrence of flux reversal (pyruvate to PEP) to provide enough PEP for the PTS, as discussed from flux calculations. The higher fumarate and lower citrate, malate levels in the mutant cannot be explained, but are possibly related to the much lower fluxes of the TCA cycle.

Pyruvate pulse: During the pyruvate pulse in the BioScope, glucose was absent. The mutant is known to have 5 times lower pyruvate uptake rate and 2 times lower O_2 uptake rate than the wild type (Table 8.2). These lower uptake rates cause that the upward (gluconeogenic) fluxes in the mutant are much smaller, leading to far lower metabolite levels for G6P, M6P, FBP, 2PG+3PG and PEP (Figure 8.3). In order to favor gluconeogenesis under these conditions the $NAD^+/NADH$ ratio (Figure 8.5) in the mutant is 4 fold lower (4 fold more reduced couple). The higher NADH and the lower malate levels (Figure 8.4) suggest a very low Oaa level, which agrees with the observed very low citrate level (Figure 8.4).

Summarizing, during the pyruvate pulse in the mutant, compared to the wild type, all rates are much lower resulting in much lower metabolite levels, but the system is much more reduced to promote gluconeogenesis.
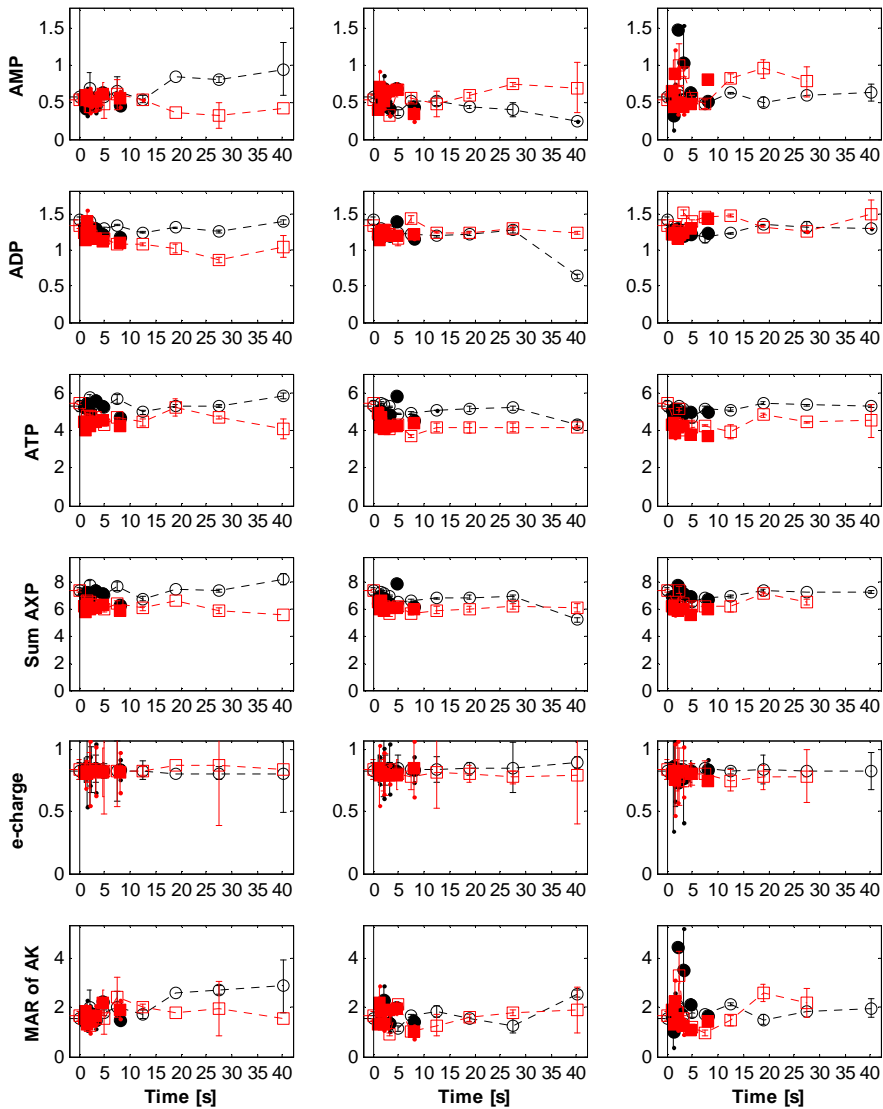
Figure 8.2: Adenine nucleotides, sum of adenine nucleotides [µmol/gDW], e-charge and MAR of AK in the wild type (circles) and in the mutant (squares) after the glucose pulse (left), pyruvate pulse (middle) and succinate/no pulse (right) in the BioScope. Closed symbols are at flow rate of 4 ml/min.

Succinate pulse: The succinate uptake rate of the mutant is 26 fold lower than in the wild type (Table 8.2). In addition it follows that the succinate uptake is just fast enough to provide energy for maintenance, where growth is absent. Hence succinate is completely catabolized. The flux calculation (Figure 8.6) shows that succinate can only be fully catabolized using a reverse TCA cycle. This remarkable result is supported by the very low $NAD^+/NADH$ ratio; hence NADH is high in combination with the very low citrate level (Figure 8.4), which points towards the
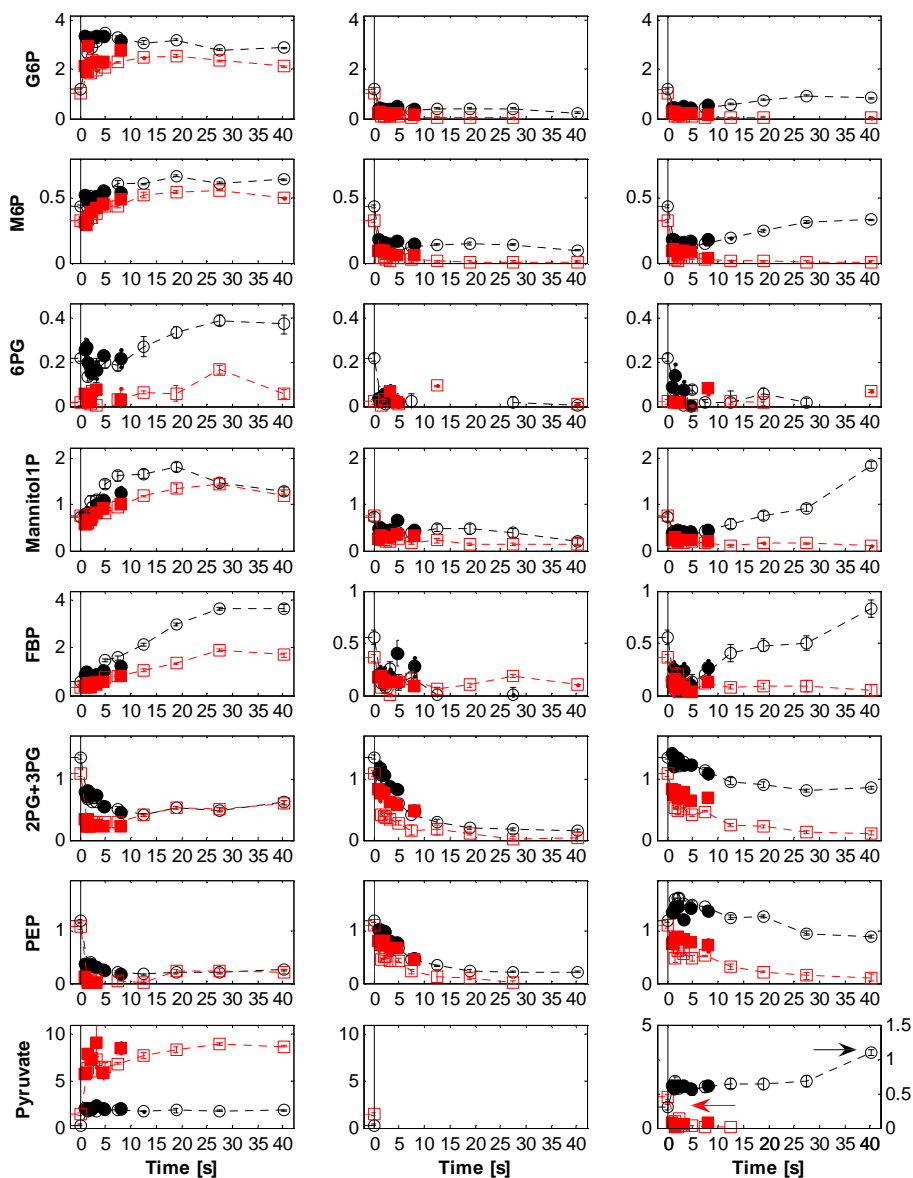
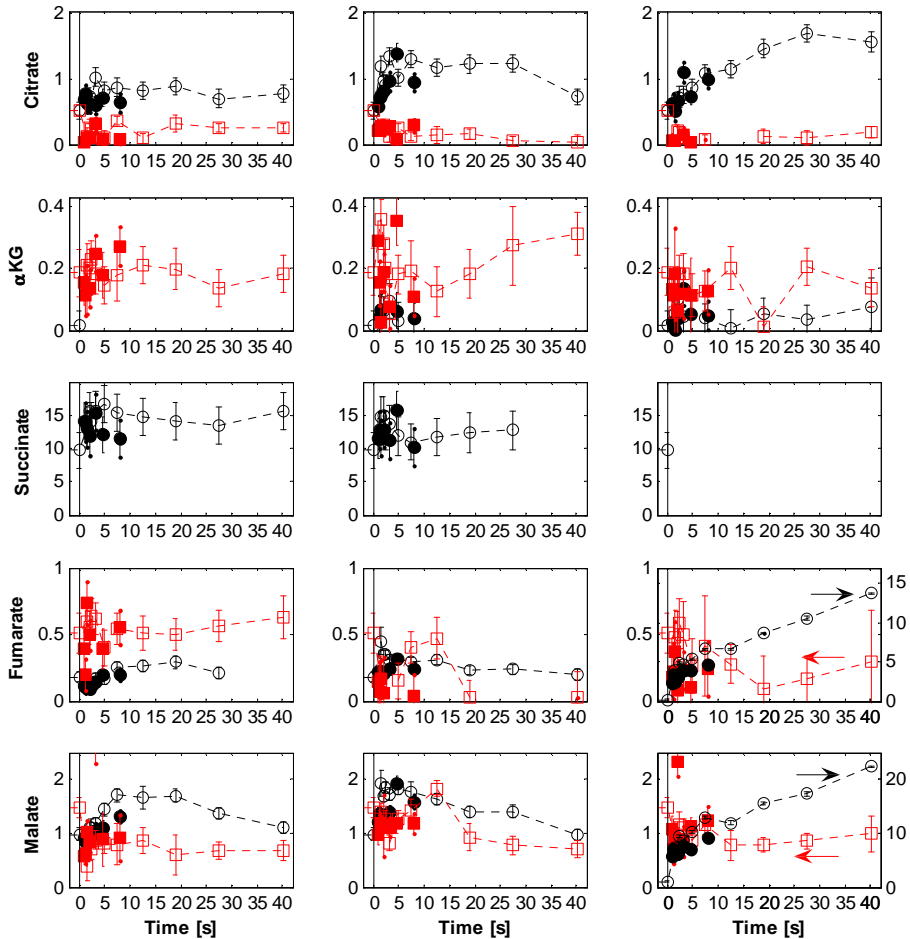**Figure 8.3: Glycolitic metabolites [µmol/gDW] in the wild type (circles) and in the mutant (squares) after the glucose pulse (left), pyruvate pulse (middle) and succinate/no pulse (right) in the BioScope. Closed symbols are at flow rate of 4 ml/min.**

possible conversion of succinate to citrate. The glyoxylate path then creates malate and/or fumarate, which are also much (10 fold) lower in the mutant, following the very low citrate level (Figure 8.4). Gluconeogenesis is then needed to bring the succinate carbon source to the oxidative PPP (to generate electrons for oxidative phosphorylation) at very low rate. This glycolysis rate (Figure 8.6) is ~ 2 times lower in the mutant compared to the wild type (Taymaz-

Nikerel *et al.* 2010b) and explains the very low concentrations of glycolytic intermediates (Figure 8.3).

Furthermore it is seen that the fluxes of PYK and PDH are zero. These two fluxes are very sensitive to the maintenance term, which is 75 ± 15 mmol/CmolX/h (Taymaz-Nikerel *et al.* 2010a). Within the error margin of the m_{ATP}, it is seen that these reactions do not occur.
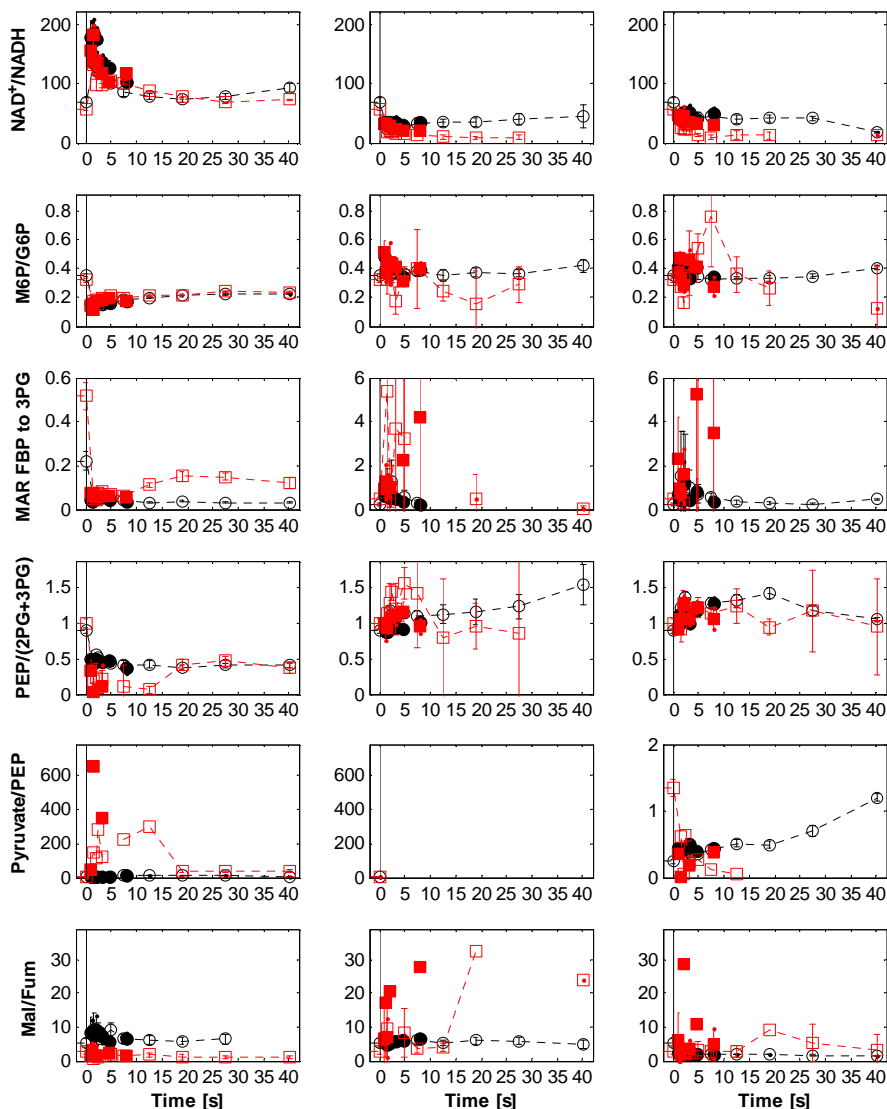

Figure 8.4: TCA cycle intermediates [µmol/gDW] in the wild type (circles) and in the mutant (squares) after the glucose pulse (left), pyruvate pulse (middle) and succinate/no pulse (right) in the BioScope. Closed symbols are at flow rate of 4 ml/min.

8.4. New targets to improve succinate production

One of the significant findings of this study is the flexibility of the central metabolism in *E. coli*, which we have shown before also for the wild type strain (Taymaz-Nikerel *et al.* 2010b). The

mutant strain is also flexible in terms of reorganizing the fluxes such as the reversal of TCA cycle under succinate excess conditions, reversal of PYK and high PPP flux. The observed flexibility under excess carbon conditions can also be expected when much higher amount of carbon is withdrawn from the cell, such as succinate secretion. There comes the importance of a more efficient product exporter. Therefore a powerful succinate exporter and elimination of remaining succinate importer should be the first new targets, because it has been shown that central metabolism is flexible enough to accommodate these large changed fluxes.

Figure 8.5: NAD$^+$/NADH ratio and some mass action ratios in the wild type (circles) and in the mutant (squares) after the glucose pulse (left), pyruvate pulse (middle) and succinate/no pulse (right) in the BioScope. Closed symbols are at flow rate of 4 ml/min.
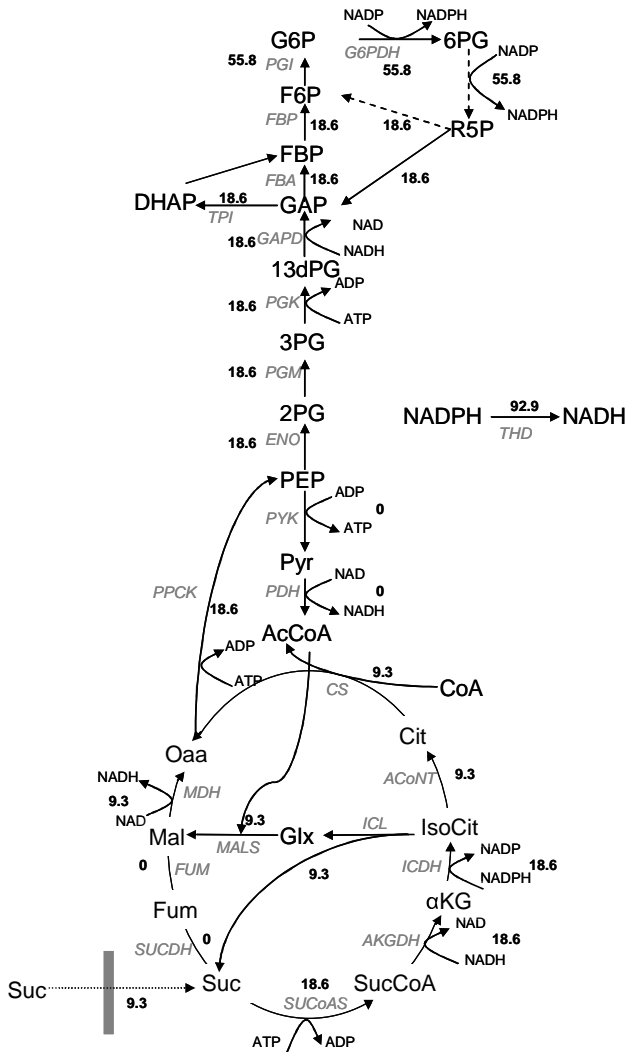
Figure 8.6: Metabolic flux pattern of central carbon metabolism of *E. coli* mutant during succinate excess (q_{Suc} = 9.3, q_{O2} = 32.5, μ = 0, m_{ATP} = 71). All fluxes are given in mmol/CmolX/h.

8.5. Conclusions

The characterization of the succinate producing *E. coli* mutant revealed that the deletion of the transcription factors IclR and ArcA caused strong decrease in q_{O2}, indicating a much higher energy efficiency of the mutant. Second, the uptake capacity for carbon sources of the mutant was much less, indicated by the lower maximal rates of q_{glu}, q_{pyr}, q_{suc} and q_{O2}. Thirdly, the production of succinate in the mutant showed that the deletion of the succinate importer and overexpression of succinate exporter were successful. In addition to these findings, it is found that the deletion of SUCDH creates on glucose multiple delocalized changes in metabolite levels,

which can be connected to specific large flux changes in central metabolism. Further, it is observed that the mutant responds very different to excess of different substrates, even reversal of TCA cycle is strongly indicated. These changes indicate the extreme flexibility of the central metabolic network following substrate pulses. This suggests that only a more powerful succinate exporter (product pull) will be successful to increase succinate production yields.

Present work is an example of application of rapid pulse experiments to compare a producer strain and its wild type to understand the impact of the applied gene deletions and to monitor the flexibility of central metabolism.

8.6. Appendix

8.6.1. Pyruvate uptake of the mutant strain

The capability of the mutant to take up pyruvate was studied in the chemostat. The same concentration of the pyruvate pulse given in the BioScope was also given to the bioreactor (without stopping the glucose feed) to observe the behavior of the mutant culture. Figure 8.7, the online measurements, shows that the mutant cells could take up pyruvate.
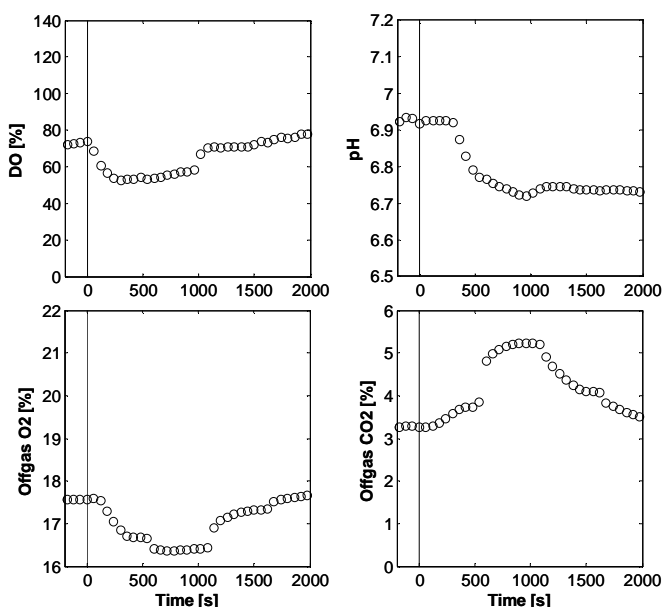
Figure 8.7: DO [%], pH, offgas O_2 and CO_2 [%] measurements vs time [s] after the pyruvate pulse for the succinate producing strain.

It was observed that DO drops with the supply of pyruvate and returns back to initial steady-state at about 1000 s. This shows that the added pyruvate (5.55 mM) was consumed in about 1000 s,

leading to q_{pyr} of 53.3 mmol/CmolX/h. New q_{O2} was calculated from the DO-profile and offgas O_2-profile (with the proper mass balances), both independent calculations leading to the same value of 131 mmol/CmolX/h (Table 8.2).

8.6.2. Succinate uptake of the mutant strain

The mutant strain produced 28 mM succinate at steady-state. The capability of the mutant to take up succinate was checked in the chemostat. After the culture was back at steady-state (after pyruvate pulse), the feeding was stopped to observe if the cells would take up succinate which was already present (28 mM). Figure 8.8 shows the online measurements, which imply that the mutant cells could take succinate very slowly, consuming the available succinate in 8 h.

In the absence of glucose in the mutant culture, it was observed that DO increases in the first 100 s and stays at that new state for about 8 h. The decreased q_{O2} is also indicated by the change in the offgas O_2. Both calculations from DO-profile and offgas O_2 led to the same q_{O2} of about 31 mmol/CmolX/h. The decrease in the oxygen consumption rate corresponds to the succinate uptake. It is seen that in about 8 h succinate was depleted with q_{suc} of 9.3 mmol/CmolX/h. From the degree of reduction balance, it was found that $\mu = 0$ during the succinate uptake (Table 8.2).
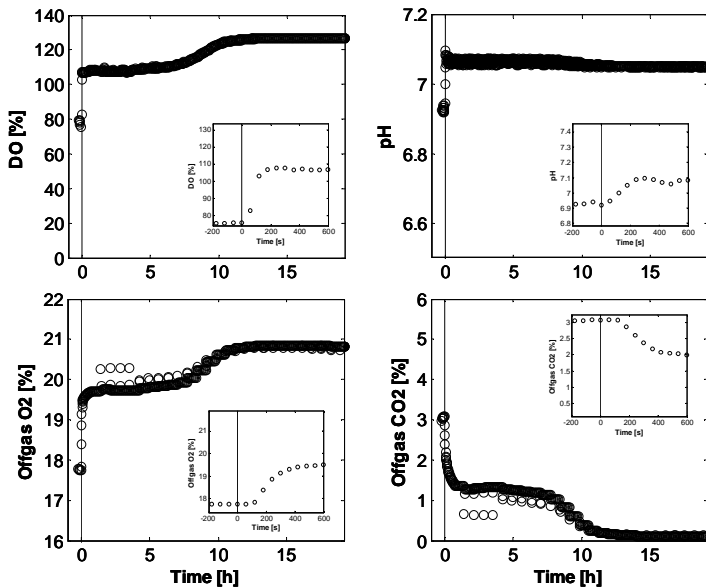
Figure 8.8: DO [%], pH, offgas O_2 and CO_2 [%] measurements vs time after the feeding was stopped for the succinate producing strain.

Acknowledgements

Fast dynamic response of the fermentative metabolism to aerobic and anaerobic glucose pulses

Abstract

The response of *Escherichia coli* cells to transient exposure (step increase) in substrate concentration and anaerobiosis leading to mixed-acid fermentation metabolism was studied in a two-compartment bioreactor system consisting of a stirred tank reactor (STR) connected to a mini plug-flow reactor (PFR: BioScope, 3.5 ml volume). Such a system can mimic the situation often encountered in large-scale, fed-batch bioreactors. The STR represented the zones of a large-scale bioreactor that are far from the point of substrate addition and that can be considered as glucose-limited, whereas the PFR simulated the region close to the point of substrate addition, where glucose concentration is much higher than in the rest of the bioreactor. In addition, oxygen-poor and glucose-rich regions can occur in large-scale bioreactors. The response of *E. coli* to these large-scale conditions was simulated by continuously pumping *E. coli* cells from a well stirred, glucose- limited, aerated chemostat ($D = 0.1$ h^{-1}) into the mini-PFR. A glucose pulse was added at the entrance of the PFR. In the PFR, a total of 11 samples were taken in a time frame of 92 s. In one case aerobicity in the PFR was maintained in order to evaluate the effects of glucose overflow independently of oxygen limitation. Accumulation of acetate and formate was detected after *E. coli* cells had been exposed for only 2 s to the glucose-rich (aerobic) region in the PFR. In the other case, the glucose pulse was also combined with anaerobiosis in the PFR. Glucose overflow combined with anaerobiosis caused the accumulation of formate, acetate, lactate, ethanol and succinate, which were also detected as soon as 2 s after of exposure of *E. coli* cells to the glucose and O_2 gradients. This approach (STR- mini-PFR) is useful for a better understanding of the fast dynamic phenomena occurring in large-scale bioreactors and for the design of modified strains with an improved behavior under large-scale conditions.

9.1. Introduction

Imperfect mixing in large-scale bioreactors leads to the emergence of spatial gradients. In the case of large-scale fed-batch cultures, substrate gradients are commonly encountered (Enfors *et al.* 2001; Lara *et al.* 2006a; Schmalzriedt *et al.* 2003), and can cause significant effects in cell physiology (Lara *et al.* 2006a). Cells can travel from glucose-limited conditions in the bulk of the bioreactor, to zones of high glucose concentrations at the substrate feeding point. This in turn, may create an anaerobic region, as the respiration rate of the cells is importantly increased during exposure to glucose-concentrated regions (Enfors *et al.* 2001; Lara *et al.* 2006a; Schmalzriedt *et al.* 2003). This is particularly important in high-cell density cultures. The presence of glucose or dissolved oxygen gradients can have a negative impact on cells, decreasing their productivity. It has also been reported to be a main source of failure during the scale-up of cultures (Bylund *et al.* 2000; Bylund *et al.* 1999). The accumulation of by-products like acetate and formate due to glucose/oxygen gradients is strongly undesirable as it represents a waste of carbon, triggers transcriptional regulation processes and causes loss of productivity.

The effects of environmental gradients and their exposure time on cells can be studied at the laboratory scale using scale-down experimental approaches (Lara *et al.* 2006a; Palomares *et al.* 2010; Sweere *et al.* 1987). From the various experimental scale-down configurations, the most commonly used approach to simulate substrate gradients is a two-compartment system in which a stirred tank reactor (STR) is connected to a plug-flow reactor (PFR) (Lara *et al.* 2006a; Palomares *et al.* 2010). Cells exiting the STR are passed through a PFR where a concentrated glucose solution is injected to simulate the substrate-feeding zone of a large-scale bioreactor. Oxygen depletion can also occur in the PFR if mass transfer is not enough to sustain aerobic conditions. Several reports exist on the study of glucose gradients and the concomitant oxygen-limiting conditions in fed-batch cultures of *Escherichia coli* (Bylund *et al.* 1998; Lin and Neubauer 2000; Xu *et al.* 1999). In such studies, the residence time in the PFR was 56 s and the first sample was taken 14 s after cells entered the PFR. A drawback from such studies is that the effects of glucose gradients are not completely decoupled from those of dissolved oxygen tension (DOT), which is of particular importance to better understand the effect of each variable on cell physiology. Moreover, only a limited analysis on cell responses can be derived from the studies mentioned above. Although Neubauer *et al.* (1995) measured the DOT at the exit of the PFR for an *E. coli* scale-down study, no DOT profiles were shown in the glucose-rich region and only four to five sample points over a period of 56 s were available in the PFR. In the present study, we employed the second generation BioScope (Mashego *et al.* 2006) as the PFR compartment to evaluate the dynamic response of fermentative metabolism of *E. coli* cells cultured aerobically and under glucose limitation, and subjected to a glucose gradient either under fully aerobic or fully anaerobic conditions. An important difference between the experimental settings of this work and the previously mentioned reports is that in the present study the cells have a steady-state background immediately prior to their exposure to the pulses. This enables the study of *E. coli* response to a single perturbation after a completely defined physiological state, in comparison to other studies in which it has been demonstrated that the age of a culture (for instance, during a fed-batch process) also influences the response of the cells to cyclic environmental oscillations

(Enfors *et al.* 2001). Using the BioScope, 11 samples were taken during a relative short time frame, 92 s (of which 5 samples were taken during the first 20 s), to monitor the extracellular accumulation of mixed-acid fermentation metabolites during exposure to a glucose gradient. This time frame is wider than in other studies using rapid sampling devices (Buziol *et al.* 2002), but narrower than previous scale-down studies. This generated short time-resolved (in the range of seconds) useful biological information about the characteristic response times of fermentative metabolism during exposure to glucose and oxygen gradients. This information helps to explain the metabolic deviation at different scales of cultivation.

9.2. Materials and Methods

9.2.1. Bacterial strain and Culture Medium

E. coli K12 derivative W3110 (ATCC 27325) was used and cultured in a mineral medium containing the following components (in g/l): Glucose monohydrate, 7.5; $(NH_4)_2SO_4$, 5.0, KH_2PO_4, 2.0; $MgSO_4.7H_2O$, 0.5; NaCl, 0.5; NH_4Cl, 2.0; Thiamine, 0.001. A trace elements solution (Verduyn *et al.* 1992) was added at a proportion of 2 ml/l of medium.

9.2.2. Chemostat Culture

E. coli was cultured in a glucose-limited chemostat at a dilution rate of 0.1 h^{-1} in a 7 l bioreactor with a working volume of 3 l (Applikon, Schiedam, The Netherlands) under aerobic conditions. The bioreactor was operated at an aeration rate of 0.5 vvm and an agitation rate of 500 rpm and overpressure of 0.3 bar. The pH and temperature were controlled at 7.0 and 37 °C, respectively. DOT was measured (Mettler-Toledo, Greifensee, Switzerland), but not controlled, only to verify that aerobic conditions were maintained at all times in the chemostat (> 80 % air saturation). The content of O_2 and CO_2 in the inlet and outlet gases was analyzed by an exhaust gas analyzer (NGA 200, Rosemount Analytics, Hasselroth, Germany).

9.2.3. Two-compartment bioreactor system

Simulation of glucose gradients

Exposure of cells to glucose gradients in large-scale bioreactors was simulated by means of a two-compartment system, shown in Figure 9.1, which consisted of a mini PFR connected to a stirred tank bioreactor (glucose-limited chemostat). A broth flow of 1.8 ml/min was derived from the liquid effluent of the chemostat and connected to the PFR. At the entrance of the PFR, the broth was mixed with a concentrated glucose solution of 166.7 mM (30 g/l) flowing at 0.2 ml/min. After mixing with the broth, the concentration of glucose in the liquid entering the PFR

was 16.7 mM (3 g/l). In this system, cells experienced a substrate gradient while moving from a glucose-limited (chemostat) to glucose-rich (PFR) regions.

The PFR consisted of a mini-bioreactor called BioScope, designed for continuous perturbation experiments, and that has been described in detail previously (Mashego *et al.* 2006). Briefly, it consists of two hemispherical channels with a two-dimensional serpentine geometry, milled in a Perspex block, and separated by a silicone membrane permeable to O_2 and CO_2. One of the hemispherical channels was used for liquid flow, while the other was used for exchange of gases by countercurrent gas flow. The total volume of the PFR was 3.5 ml and the total length was 6.51 m. The mini-bioreactor was equipped with 11 ports for computer-controlled sampling at different distances from the inlet point, corresponding to increasing residence times of the cells in the PFR under high glucose concentrations. The first port allowed sampling shortly before the addition of the glucose-concentrated solution. The PFR was placed in a chamber at a controlled temperature of 37 °C, equal to the STR temperature. Samples were taken from the PFR and instantaneously cooled in a cryostat kept at 0 °C (Lauda RK 20 KS, Lauda-Köningshofen, Germany). Shortly after sampling (which took around 15 min), the biomass was removed by filtering through 0.45 μm (Millex-HV, Millipore, Cork, Ireland) using pre-cooled syringes (T = -20 °C). The supernatants were stored at -80 °C for further analysis.
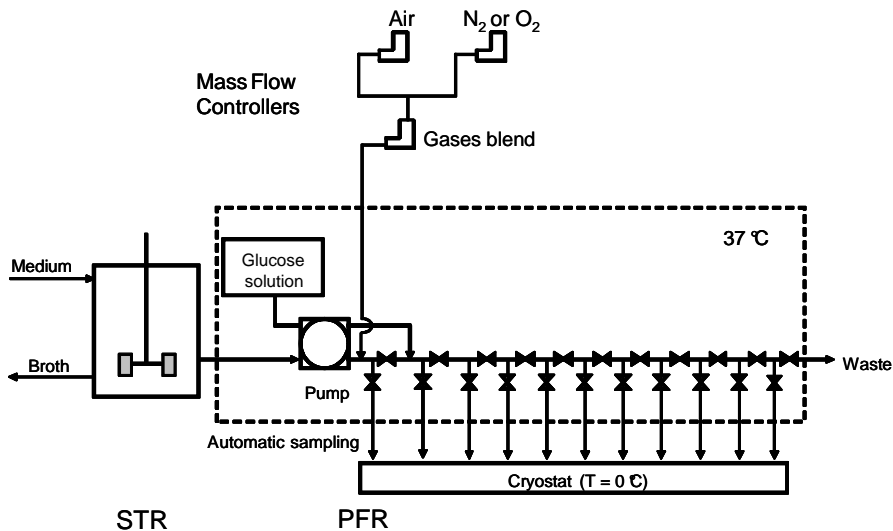
Figure 9.1: Simplified diagram of the experimental bioreactors and sampling system used to simulate spatial gradients of glucose and dissolved oxygen.

Simulation of dissolved oxygen gradients

To study the effects of a sudden up-shift of the glucose concentration without oxygen limitation, the gas channel of the BioScope was continuously flushed with a blend of air/oxygen at 100 ml/min that was controlled with mass flow controllers (Brooks Instruments, Ede, The

Netherlands). To assess the effects of an increase in glucose concentration under anaerobic conditions, the gas channel was flushed with pure nitrogen. In this case, a blend of air/nitrogen was sparged in the chemostat to lower its DOT to 15 % (ca. 0.03 mmol/l) and thereby shorten the transition to fully anaerobic conditions after the glucose pulse. Such a DOT is considered high enough to maintain aerobic conditions in *E. coli* cultures (Lara *et al.* 2006b; Sandoval-Basurto *et al.* 2005). This was confirmed because the concentration of CO_2 in the exhaust gases and the biomass concentration in the broth did not change after the DOT decrease, which indicated that the steady-state in the chemostat was not altered (data not shown). During the glucose pulse experiments, the DOT in the BioScope was measured using a single polarographic dissolved O_2 probe (Mettler-Toledo GmbH) mounted onto a flow cell that was consecutively switched to each of the 11 sampling ports. Glucose pulses under aerobic and anaerobic conditions were carried out twice. The data shown are an average of two values, and the differences between both values are also reported.

9.2.4. Analytical techniques and calculation methods

Biomass concentration was determined as dry cell weight of washed pellet samples dried in Falcon tubes at 70 °C for at least 24 h. Glucose, lactate, succinate and formate were analyzed by enzymatic assays (R-Biopharm, Boehringer Mannheim, Darmstadt, Germany). Acetate and ethanol were quantified by gas chromatography (Chrompack CO 9001, Hewlett Packard, Palo Alto, CA) using a flame ionization detector. The reported values of yields and specific rates were calculated with the proper mass balances over the time periods involved.

9.3. Results

9.3.1. Characteristics of the steady-state

The chemostat was operated at a dilution rate of 0.1 h^{-1}. Steady-state was confirmed by a constant composition of the offgases and a stable biomass concentration (2.79 ± 0.03 g/l). The residual glucose concentration was 0.14 ± 0.01 mM. The biomass yield on glucose was 0.41 g/g at steady-state. The specific uptake rates of glucose and oxygen (q_S and q_{O2}) were 1.35 ± 0.04 and 3.78 ± 0.14 mmol/g/h, respectively. The specific rate of carbon dioxide generation was 3.41 ± 0.10 mmol/g/h. Small amounts of acetate and formate were detected in the effluent of the chemostat, namely, 0.08 ± 0.01 and 0.005 ± 0.002 mM, respectively. These values correspond to specific production rates of 0.003 and 0.0002 mmol/g/h for acetate and formate, respectively.

9.3.2. Simulation of oxygen gradient in the two-compartment system

Figure 9.2 shows the DOT profiles in the PFR during aerobic and anaerobic pulses. It can be seen that the use of an air-oxygen blend in the PFR was enough to maintain aerobic conditions. The

DOT in the chemostat was 0.25 mM. During the first 22 s of transit of the cells through the PFR, the DOT rapidly decreased to around 0.14 mM. This value was nearly constant during the remaining residence in the PFR. According to the mass transfer characteristics of the BioScope (Mashego *et al.* 2006), the q_{O2} in the PFR was 16 mmol/g/h, which means a 4 fold increase in oxygen uptake rate. A reduced DOT level in the STR and flushing of nitrogen through the BioScope gas channel were enough to deplete oxygen almost at the entrance of the PFR during the glucose pulse under anaerobic conditions (Figure 9.2).
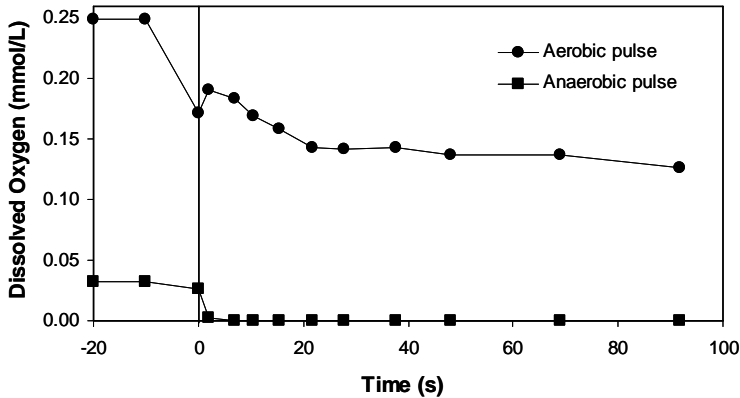
Figure 9.2: Dissolved oxygen concentration in the PFR during glucose pulses under fully aerobic or anaerobic conditions. The continuous vertical line indicates the samples taken previous to the perturbation of the glucose concentration.

9.3.3. Response of mixed-acid fermentation metabolism to an aerobic glucose gradient

The extracellular concentrations of glucose and the organic acids produced during an aerobic glucose gradient are shown in Figure 9.3. The extracellular glucose concentration increased from 0.13 ± 0.01 mM in the chemostat, to 16.5 ± 0.6 mM in the PFR after the glucose pulse and then decreased to 15.45 ± 0.20 mM after 92 s of exposure of *E. coli* to the glucose gradient (Figure 9.3a). Therefore, the calculated q_S value in the PFR was 15 ± 1 mmol/g/h, which is a 10 fold increase. Compared to the 4 fold increase in O_2-uptake this indicates fermentative metabolism. All the samples from the PFR were analyzed for organic acids, but only formate and acetate were detected (Figure 9.3). As shown in Figure 9.3b and 9.3c, both metabolites accumulated extracellularly already within 2 s after the glucose perturbation. During the first 10 s after the glucose pulse (phase I), acetate and formate were produced more rapidly than during the remaining 82 s of the experiment (phase II). The acetate concentration in the chemostat was 0.08 ± 0.01 mM and increased to 0.14 ± 0.01 mM during phase I in the PFR (i.e. 0.060 ± 0.001 mM of acetate were produced). During phase II, acetate concentration reached 0.17 ± 0.01 mM (i.e. 0.030 ± 0.002 mM of acetate were produced) (see Figure 9.3b).
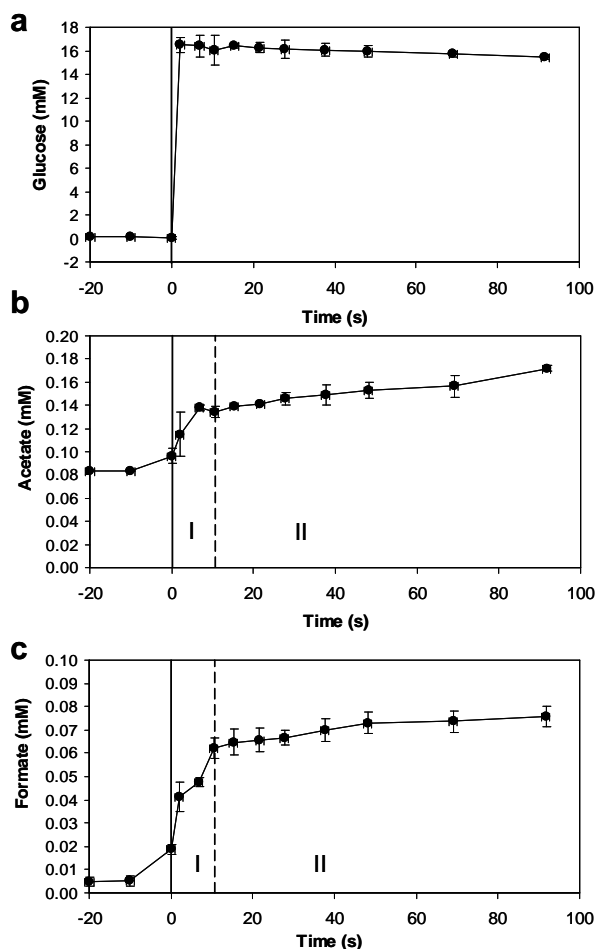
Figure 9.3: Extracellular concentration of glucose (a), acetate (b) and formate (c) in the PFR during exposure of *E. coli* cells to a glucose gradient under aerobic conditions. Error bars show the difference between duplicate experiments. The continuous vertical line indicates the samples taken previous to the perturbation. The dashed vertical line indicates the division in two distinctive phases of the microbial response to glucose/O$_2$ perturbations.

Formate was also found in very small concentrations in the chemostat (0.005 mM). A very fast accumulation of formate was observed during phase I in the PFR, reaching values of 0.066 $\pm$ 0.005 mM. At the end of phase II, formate concentration was 0.076 $\pm$ 0.004 mM (Figure 9.3c).

9.3.4. Response of mixed-acid fermentation metabolism to an anaerobic glucose gradient

In order to simulate the combined effects of moving from an aerobic, glucose-limited region to a glucose-rich, anaerobic zone in a large-scale bioreactor, anaerobic conditions in the PFR were

achieved as described previously. In contrast with the glucose pulses under aerobic conditions, the glucose excess under anaerobiosis caused the accumulation of all mixed-acid fermentation metabolites. The extracellular profiles of glucose and organic acids during this pulse experiment are shown in Figure 9.4. The product accumulation was much higher and no evident phases of their production during the glucose pulse were observed.
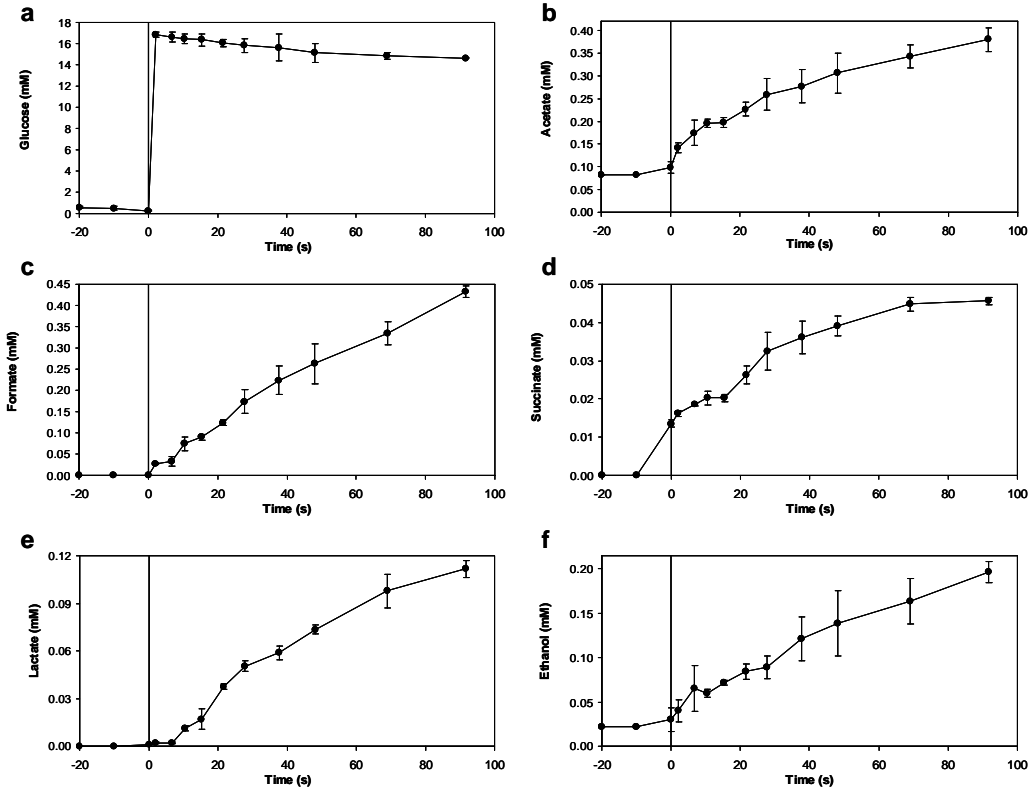
Figure 9.4: Extracellular concentration of glucose (a), acetate (b), formate (c), succinate (d), lactate (e) and ethanol (f) in the PFR during exposure of *E. coli* cells to a glucose gradient under anaerobic conditions. Error bars show the difference between duplicate experiments. The continuous vertical line indicates the samples taken previous to the perturbation.

The glucose concentration increased from 0.14 ± 0.01 mM in the chemostat to 16.84 ± 0.36 mM in the PFR after the pulse to reach 14.63 ± 0.75 mM (Figure 9.4a) in the last sampling port. Therefore, 2.22 ± 0.84 mM of glucose was consumed during the perturbation experiments, which is more than twofold the amount of glucose consumed during a glucose pulse under aerobic conditions. Therefore, the q_S value was 31 ± 3 mmol/g/h, which is a more than 20 fold increase compared to the steady-state. Formate and acetate were the most highly accumulated organic acids in response to a glucose gradient under anaerobic conditions, reaching values of 0.38 ± 0.02 and 0.43 ± 0.02 mM in the last sample point of the PFR (Figure 9.4b and 9.4c). Ethanol was the

third most highly accumulated metabolite, followed by lactate and succinate, whose maximum concentrations during the perturbation experiment were 0.20 ± 0.01, 0.11 ± 0.01, and 0.05 ± 0.01 mM (Figure 9.4c - f), respectively. The total products amounted to about 1 mM.

9.4. Discussion

The existence of local zones with elevated glucose concentrations in large-scale bioreactors is often combined with oxygen depletion (Lara *et al.* 2006a). However, the existence of DOT gradients does not depend on the presence of substrate gradients, as DOT fluctuations can also occur in batch cultures (Lara *et al.* 2006b). Depending on the operational conditions, DOT gradients can also exist in small-scale fermentors, as shown by Garcia *et al.* (2009), who used a fluorescence reporter in *E. coli* to detect oxygen limitations in a STR lab-scale bioreactor. The effects of DOT gradients on mammalian (Serrato *et al.* 2004) and bacterial (Lara *et al.* 2006b; Lara *et al.* 2006c; Sandoval-Basurto *et al.* 2005) cultures have been studied and are known to have a profound influence in the performance of cultures. Despite the relatively well-studied response of cultures to glucose gradients, the scale-down studies published to date have not effectively dissected the effects of glucose gradients from anaerobiosis. Moreover, in such studies, the first sample was typically taken after 14 s of exposure to regions with high glucose concentration (Bylund *et al.* 1998; Enfors *et al.* 2001; Xu *et al.* 1999) and at 28, 36 and 52 s of residence time in the PFR. The typical scale-down system to evaluate the effects of substrate gradients is the STR-PFR configuration (Lara *et al.* 2006a), in which a glucose pulse is added at the entrance of the PFR. The sudden increase in glucose uptake after a glucose pulse in scale-down studies (for instance, from 2.8 in the STR to 8.9 mmol/g/h after 40.5 s in the PFR; (Xu *et al.* 1999)) can cause a rapid depletion of oxygen, and hence oxygen limitation has been assumed to occur in the PFR section. However, no direct measurement of oxygen depletion in the PFR section of the scale-down systems has been documented previously, making it difficult to draw conclusions about the direct effect on cells upon exposure to a substrate or oxygen gradient. In the present study, the effects of glucose gradients and anaerobiosis were dissected by employing a STR connected to a mini-PFR in which the concentration of dissolved oxygen can be measured and manipulated. The STR was operated as chemostat in a steady-state mode at a dilution rate of 0.1 h^{-1}, which was similar to the feeding rates found in typical *E. coli* cultures (Lara *et al.* 2008). The characteristics of the BioScope allowed the effective exchange of gasses with the culture broth, and fully aerobic or anaerobic conditions were achieved and monitored (Figure 9.2).

When *E. coli* cells were exposed to a glucose gradient under fully aerobic conditions, the strongest effect was the increase in q_S and q_{O2} and the immediate accumulation of acetate (Figure 9.3b). A comparison of the specific glucose uptake rates (q_S) in the chemostat and during pulse experiments is shown in Table 9.1. The value of q_S increased from 1.35 mmol/g/h in the chemostat to 15.3 mmol/g/h in the PFR following the aerobic glucose pulse, which is an increase of about 11 fold. The latter value of q_S can sustain a specific growth rate higher than 1 h^{-1} (after calculations presented by (Carlson and Srienc 2004)), and is well above the critical value for triggering overflow metabolism. For instance, it has been reported (Kayser *et al.* 2005) that

acetate production by *E. coli* in chemostat cultures started when q_S reached a value of 0.64 g/g/h (ca. 10.7 mmol/g/h). Figure 9.5a shows a comparison of the specific production rates of organic acids in pulse experiments under aerobic conditions, during phases I and II. The specific production rate of acetate in the chemostat was 0.003 mmol/g/h, and it increased to 4.71 ± 0.30 mmol/g/h during the first phase of the pulse experiment. During phase II, it decreased to 0.53 ± 0.01 mmol/g/h. Acetate is mainly produced in *E. coli* by action of the phosphotransacetylase (PTA) and acetate kinase (ACK) enzymes. Both are constitutive enzymes in *E. coli* (Clark 1989; Wolfe 2005), and our results show that this pathway is immediately inducible by glucose overflow. The enzyme pyruvate oxidase (PoxB) converts pyruvate into acetate and also plays an important role in acetate production by *E. coli* W3110, both aerobically (Phue *et al.* 2005) and under oscillating DOT conditions (Lara *et al.* 2006b). Therefore, it is possible that PoxB is also present in *E. coli* under aerobic conditions and rapidly induced by a glucose pulse.

Table 9.1: Specific glucose (q_S) and oxygen (q_{O2}) uptake rate during exposure of *E. coli* cells to a glucose gradient under fully aerobic and anaerobic conditions

Condition	q_S [mmol/g/h]	q_{O2} [mmol/g/h]
Chemostat	1.35	3.78
Aerobic Pulse	15 ± 1	16
Anaerobic Pulse	31 ± 3	-

Formate also accumulated rapidly (as early as 2 s after the glucose pulse) during the exposure of *E. coli* culture to the aerobic glucose gradient (Figure 9.3c). Formate production in *E. coli* is expected under oxygen-limited conditions, as part of the fermentative metabolism (Clark 1989), but not under aerobic conditions, as in this experiment. The specific production rate of formate in the chemostat was 0.0002 mmol/g/h. Other authors have also reported the production of formate by *E. coli* in fully aerobic cultures (Castan and Enfors 2002; Lara *et al.* 2006b; Lara *et al.* 2006c; Sandoval-Basurto *et al.* 2005). The exact mechanism for this phenomenon is not yet known, but authors have related formate accumulation to DNA release into the media, probably due to cell rupture (Castan and Enfors 2002). It should be noted that the *pfl* gene, that codes for the enzyme responsible for formate production from pyruvate (pyruvate-formate lyase, PFL), is reported to be expressed only under anaerobic conditions. The regulation of PFL is rather complex, however, it is known that there exists a basal level of PFL in *E. coli* even under aerobic conditions (Pecher *et al.* 1982). Our results show that formate accumulates in response to glucose overflow under fully aerobic conditions and imply that there is a basal level of PFL in the *E. coli* strain used under aerobic conditions. This might occur due to a similar mechanism of overflow metabolism which leads to acetate production. The sudden increase in glucose uptake could have caused a transient accumulation of intracellular pyruvate, which in turn could have led to formate by PFL. Formate accumulation during the aerobic glucose pulse can also be divided into two phases. During the first phase, it accumulated at a rate of 5.36 ± 0.06 mmol/g/h, but then the specific production rate rapidly decreased during phase II to a value of 0.19 ± 0.03 mmol/g/h. Formate production in the

aerobic conditions of the experiment must has been originated from the basal PFL present in cells. This indicates that PFL must be present at relatively high amounts, and that it is very sensitive to glucose overflow, as formate was produced at similar rates as acetate during phase I of the pulse experiment (Figure 9.5a). Formate can be converted to CO_2 and H_2 by the formate hydrogenlyase (FHL) enzyme complex (Clark 1989), which is formed of four enzymes (Sawers 1994). Selenium acts directly as cofactor of the FHL complex (Axley *et al.* 1991; Gladyshev *et al.* 1994). It has been demonstrated that a lack or inadequate amount of this metal in the culture medium has conducted to formate accumulation, whereas the addition of this cofactor effectively prevented formate accumulation (Sandoval-Basurto *et al.* 2005; Soini *et al.* 2008).
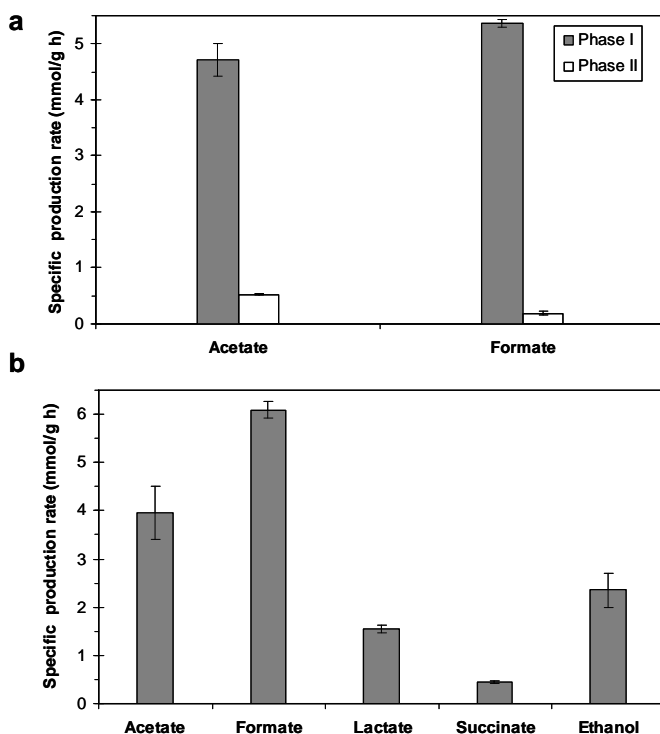
Figure 9.5: Specific production rates of the mixed-acid fermentation products in response to a glucose gradient under fully aerobic (a) or anaerobic (b) conditions. Error bars show the difference between duplicate experiments. Specific acetate and formate production rates in the chemostat were 0.003 and 0.0002 mmol/g/h.

As summarized in Table 9.1, the q_S value increased 11 times, whereas the oxygen uptake rate increased 4 fold from 3.78 in the STR to 15.6 mmol/g/h in the PFR during the aerobic glucose pulse. This latter value corresponds to the maximum oxygen uptake rate for the W3110 strain, according to data compiled elsewhere (Carlson and Srienc 2004). During exposure to the glucose gradient under anaerobic conditions all the mixed-acid fermentation final products were detected.

Formate and acetate accumulated to the highest concentrations. The specific production rates of formate and acetate were 6.09 ± 0.18 and 3.95 ± 0.55 mmol/g/h, respectively (Figure 9.5b). Glucose overflow, combined with the step-change to anaerobic conditions enhanced the production of formate and acetate, as their specific production rates were much higher than under aerobic conditions (Figure 9.5a and 9.5b). This is in agreement with the higher glucose uptake rate during anaerobic glucose pulses, which was almost 3 fold higher than during aerobic pulses (Table 9.1). It is well known that *E. coli* consumes glucose at higher rates under anaerobic than under aerobic conditions. This is due to the fact that under anaerobic conditions, the bulk of energy is obtained from the glycolysis (Gennis and Stewart 1996). Furthermore, formate and lactate are directly produced from pyruvate, whereas acetate can be produced also from pyruvate under anaerobic conditions by PoxB (Clark 1989; Lara *et al.* 2006b). Also, an increased demand for pyruvate may increase the glucose uptake rate, since one mole of phosphoenol pyruvate (PEP) is converted to pyruvate per mole of glucose that is internalized through the phosphotransferase system in *E. coli* (De Anda *et al.* 2006). The value of q_S for the anaerobic glucose pulse is well within the values reported by Carlson and Srienc (2004). Ethanol and lactate also accumulated rapidly in the PFR during the anaerobic glucose pulse at rates of 2.35 ± 0.36 and 1.56 ± 0.08 mmol/g/h, respectively (Figure 9.5b). Succinate was produced at a relatively low specific rate of 0.45 ± 0.03 mmol/g/h.

The residence time of cells in the PFR (92 s) can be considered insufficient for completion of induction, transcription, translation and activation events necessary for enzyme synthesis. Altogether, these processes can take place in a time frame of several minutes (Stephanopoulos *et al.* 1998). During the exposure of fully aerobically, glucose-limited cultivated *E. coli* cells to a glucose gradient under anaerobic conditions, all the mixed-acid fermentation metabolites were immediately detected (in < 5 s). This means that organic acids were produced by enzymes already present in the cells even under fully aerobic conditions, as was the situation prevailing in the chemostat. Ethanol was also detected early after the glucose pulse in the PFR. The *adhE* gene, coding for the fermentative ADH is known to be induced only under anaerobic conditions (Clark 1989). However, our results suggest that at least a low basal level of ADH should be present in *E. coli* even under fully aerobic conditions. The enzyme responsible for lactate synthesis, the lactate dehydrogenase (LDH) is known to be present in *E. coli* under both, aerobic and anaerobic conditions (Mat-Jan *et al.* 1989). Induction of LDH under aerobic conditions requires acidification of the medium. It is possible that during the glucose pulse under aerobic conditions, the amounts of acetate and formate produced did not significantly decrease the pH of the culture and in consequence, LDH was not induced and lactate was not detected.

During the 92 s exposure of *E. coli* cells to a glucose gradient under aerobic conditions in the PFR, 1.06 mM of glucose were consumed (6.38 CmM), whereas 0.08 mM of acetate (0.15 CmM) and 0.06 mM of formate (0.06 CmM) were produced. This means that 3.29 % of the consumed carbon was wasted as fermentation by-products due to the glucose gradient. In contrast, when the glucose gradient was combined with anaerobiosis, 2.22 mM of glucose (13.29 CmM) were consumed in the PFR. In this case, 0.43 mM of formate (0.43 CmM), 0.28 mM of acetate (0.56 CmM), 0.16 mM of ethanol (0.33 CmM), 0.11 mM of lactate (0.33 CmM) and 0.03 mM of succinate (0.13 CmM) were produced. Overall, this means that 13.4 % of the carbon consumed

was diverted to fermentation products during simultaneous depletion of oxygen depletion and glucose excess. The consequences of these effects in large-scale cultures where cells are continuously encountering glucose and dissolved oxygen gradients are obvious. It has been estimated that the region of oxygen limitation resulting from a high glucose concentration field in a large-scale, fed-batch bioreactor is of ~ 10 % of the total working volume (Enfors *et al.* 2001). If we assume a mean circulation time of 50 s as is commonly found in large-scale microbial cultures (Lara *et al.* 2006a), then it is reasonable to establish that cells will spend at least 10 % of the circulation time (i.e., 5 s) in an oxygen-depleted, glucose-rich region. The experimental set-up used in this work, and the design of the PFR allowed us to observe that overflow metabolism due to a glucose gradient under fully aerobic conditions resulted in acetate accumulation as soon as 2 s after exposure to high glucose concentrations. Importantly, formate also accumulated within 2 s. When the glucose gradient was combined with anaerobiosis, all the other fermentation metabolites were also detected after 2 s of exposure of cells to the gradients. This means that even if the circulation time in a large-scale bioreactor could be decreased to 20 s (which correspond to a mixing time of around 80 s; (Lara *et al.* 2006a)), the presence of glucose (and probably dissolved oxygen) gradients will still cause diversion of carbon fluxes towards fermentative products, and a concomitant waste of the substrate. The accumulated fermentative products also will trigger transcriptional responses. Moreover, the local accumulation of organic acids can also lead to a local drop of pH, which can also negatively affect the performance of *E. coli* cultures (Amanullah *et al.* 2001).

If practical constraints do not allow improving mixing at the large-scale, the use of cellular engineering strategies can form an alternative solution to this problem. For instance, *E. coli* with a modified substrate transport system with a much lower uptake rate has been successfully cultured under very high glucose concentrations, displaying a minimal overflow metabolism (Lara *et al.* 2008). Due to slower glucose uptake rate, compared to wild type strains, such modified strains are expected to perform better under glucose gradients, as it can be expected that the high glucose concentration lead to less increase in their glucose transport rate (De Anda *et al.* 2006; Lara *et al.* 2008).

Another approach to overcome the effects of glucose gradients under aerobic or anaerobic conditions using cellular engineering is to block the undesired pathways that might not be essential for the cells due to the temporal exposure to changes in environmental conditions. Lara *et al.* (2006c) inactivated the genes responsible for the production of formate, lactate and acetate in *E. coli*. The modified strain showed a much better growth, recombinant protein production and less by-products accumulation when cultured under DOT oscillations. Our CSTR/PFR set-up is well suited to evaluate such engineered strains on small scale before their application on large scale.

9.5. Conclusions

In the present study, the rapid (< 2 s) dynamic response of fermentative metabolism of *E. coli* exposed to a glucose gradient under aerobic and anaerobic conditions was analyzed. The use of a special mini-PFR (BioScope) allowed the sampling in shorter time frame than had been possible in previous studies. In addition, the effect of glucose gradients was successfully dissected from dissolved oxygen depletion. It was found that the fully aerobic transit from a glucose-limiting to a glucose-rich region triggered the overflow metabolism very rapidly, and acetate and formate were detected as early as 2 s after exposure to the glucose-rich condition. When the glucose gradient was combined with anaerobiosis, many other mixed-acid fermentation metabolites were detected after 2 s of exposure to the gradients and their production rates were higher. Under aerobic conditions, the accumulation of by-products was faster during the first 10 s of residence in the glucose-rich region, which demonstrated that even very short exposures of cells to gradients in large-scale bioreactors can have a profound effect in the fermentation pathways and thus a detrimental outcome to process performance.

The study of cellular response to substrate gradients, in fully aerobic and fully anaerobic conditions, during short time frames is relevant, since it can help to better understand the metabolic effects of industrial fermentation scale-based broth heterogeneity and to establish leads for genetic interventions in order to design strains that show a better performance in large-scale cultures. Future studies on the transcriptional profiling of cell response to these environmental stresses in short time frames will be important to further understand the physiological effects in large-scale bioreactors. Finally, the combination of CSTR/PFR (BioScope) was shown to be successful in controlled application of glucose/(an)aerobic condition and is envisaged to be suitable for testing of engineered strains.

Acknowledgements

Chapter 10

Future Directions

The quantitative evaluation, identification/understanding and, ultimately the prediction of the behaviour of cellular systems represent the primary challenges in the postgenomic era. Approaches, mostly in a mathematical framework (metabolic engineering aspects through a kinetic model), are now becoming faster and more efficient through the use of systems biology tools mentioned in the Introduction chapter of the thesis. Yet one of the important bottlenecks is still the availability of suitable quantitative experimental technologies.

Analysis and quenching methods for metabolites: An example is from the field of metabolomics; more powerful chromatographic techniques are required. More important than the deficiencies in analysis approaches, sample preparation also has some limitations. For example a quenching method, which would show no leakage of metabolites (during quenching and further processing) and provide parallel quantification of as many metabolites as possible, is urgently required, especially for *Escherichia coli*, which is one of the most studied organisms. The differential method proposed in this thesis to circumvent leakage issues has the disadvantage that it is not applicable when the extracellular amount of the compound is much higher than the intracellular amount. A good example is studying the product transporters. The intracellular concentration of the product-of-interest is important, as shown for dicarboxylic acid cases in this thesis. More attention should be given to find a solution to this quenching/leakage problem in prokaryotes. Finding a global leakage-free quenching method, which is applicable to most of the organisms -not limited to a specific organism-, is of prime importance.

Quantification of dynamic fluxes: To study *in vivo* kinetics of enzymes, in addition to the metabolite information, data on fluxes is also needed. As shown in the thesis, rapid sampling devices e.g. BioScope are not suitable for providing flux data in a very short time frame (< 50 s). As a solution, yet not optimal, perturbation experiments were repeated in the bioreactor, where dissolved O_2 in the broth and O_2/CO_2 in the offgas are monitored. *In vivo* oxygen uptake rate was determined from dissolved O_2 probe kinetics and dissolved O_2 dynamics during the applied perturbation experiment (Chapter 5 and 7). In future this can be combined with offgas data as in Wu *et al.* (2003) and Bloemen *et al.* (2003), but now with including the effect of pH as well because *E. coli* cultures are run at pH 7 where produced bicarbonate concentration has a significant contribution in quantification of CO_2 production. Additionally, monitoring the temperature of the culture (off-control) during the perturbation can be beneficial to calculate the heat produced as function of time and hence time-resolved biological heat production rate. However this approach (perturbation in the bioreactor) is laborious and has the potential drawback of disturbing the steady-state culture (although *E. coli* did return to its steady-state, shown in Chapter 7). Attention should be given to find methods, which would provide dynamic flux data, e.g. ^{13}C labeling experiments. Performing a ^{13}C labeling experiment in the BioScope might offer such data, however calculation of fluxes from the isotopomer data might not be that straightforward. An alternative to stimulus pulse experiments would be acquiring metabolite and flux data at different steady-state conditions, as shown in Canales *et al.* (2010). However, then measurement of enzyme levels is required because each steady-state would be different. There quantitative proteomics will have an important role.

Cell lysis: It is shown here that *E. coli* cultures have significant cell lysis. The causes are not clear but there might be a relation to programmed cell death. Methods to avoid cell lysis would be economically very beneficial.

Single cell studies: Conventional methods for metabolite analysis do not consider the differences between cells (heterogeneous culture) and/or compartmentation (absent in prokaryotes). The main assumption in the current literature is the homogeneous population of cells, however microscopic analysis of reporter proteins suggests the presence of population heterogeneity (Okumoto *et al.* 2008). Therefore flux and/or metabolite measurements in single cells will be important for kinetic modeling. In their review on fluorescence resonance energy transfer (FRET) sensors, Okumoto *et al.* (2008) discussed the possible deployment of these sensors, used for monitoring the conformation of a protein, in microorganisms as well. They believe that FRET sensors can be adapted to high-throughput analysis to identify controlling steps in metabolic flux as well as these sensors can provide information on differences between individual cells or cell populations. This method might be limited in terms that only a few metabolites can be measured. There are other examples of single cell research such as Parkhomchuck *et al.* (2009) who used high-throughput screening to observe genome dynamics at a single-cell level in several different *E. coli* strains.

Focus not only on central metabolism: The present work focused mainly on central carbon metabolism. From an industrial point of view, secondary (or tertiary) regions of metabolism might be of interest depending on the desired product. However the available literature, including genome-scale reconstructions, is poor in this area. Efforts should be given to illuminate these parts of the pathways and additionally to incorporate other networks than metabolic, e.g. genetic regulation networks.

Product secretion at low pH: Production of organic acids by fermentation has gained attention as a result of the developed techniques in metabolic engineering, which bring the product yields comparable to yields from conventional production. Economically it is desirable to perform the fermentation process at low pH where the undissociated form of the acid is produced. This avoids the need for the auxiliary agents, which are required to control the pH of the fermentation process and to obtain undissociated acid in the downstream process. Chapter 2 shows that the anaerobic production of succinic acid at pH < 3 is thermodynamically feasible. However a key challenge here is to construct over-producing *industrial microorganisms* (not exotic like acidophilic archaea) that are able to grow at low pH. There understanding microbial acid resistance is of importance.

Thermodynamics: Applying a data-driven thermodynamics-based approach in *Saccharomyces cerevisiae* for classification of *in vivo* reaction kinetics revealed that the reactions classified as near-equilibrium are dominated by the thermodynamic driving force and described as "Q-linear kinetics" because of a negative linear relation between the mass action ratio and the flux of the enzyme (Canelas *et al.* 2010). This approach is party applied to *E. coli* data in Chapter 7, however a more comprehensive set of data, e.g. dynamic metabolite measurements of GAP,

DHAP, pentose phosphate pathway intermediates, is required to analyze each reaction individually to estimate their apparent *in vivo* K_{eq}.

Bibliography

US Department of Energy, 2004. Top Value Added Chemicals from Biomass Gas. In: Werpy T, Petersen G, editors. Washington, DC: USDOE.

Alberty RA. 1998. Calculation of standard transformed formation properties of biochemical reactants and standard apparent reduction potentials of half reactions. Archives of Biochemistry and Biophysics 358(1):25-39.

Alberty RA. 2003. Thermodynamics of Biochemical Reactions. New Jersey: Wiley.

Amanullah A, McFarlane CM, Emery AN, Nienow AW. 2001. Scale-down model to simulate spatial pH variations in large-scale bioreactors. Biotechnology and Bioengineering 73(5):390-399.

Axley MJ, Bock A, Stadtman TC. 1991. Catalytic properties of an *Escherichia coli* formate dehydrogenase mutant in which sulfur replaces selenium. Proceedings of the National Academy of Sciences of the United States of America 88(19):8450-8454.

Bailey JE. 1991. Toward a science of metabolic engineering. Science 252(5013):1668-1675.

Ballesta JP, Schaechter M. 1972. Dependence of the rate of synthesis of phosphatidylethanolamine and phosphatidylglycerol on the rate of growth of *Escherichia coli*. Journal of Bacteriology 110(1):452-453.

Beauprez J. 2010. Metabolic modelling and engineering of *Escherichia coli* for succinate production [PhD Thesis]. Ghent: Ghent University.

Benson SW. 1976. Thermochemical Kinetics, Methods for Estimation of Thermochemical Data and Rate Parameters. New York: Wiley.

Blattner FR, Plunkett Gr, Bloch C, Perna N, Burland V, Riley M, Collado-Vides J, Glasner J, Rode C, Mayhew G, Gregor J, Davis N, Kirkpatrick H, Goeden M, Rose D, Mau B, Shao Y. 1997. The complete genome sequence of *Escherichia coli* K-12. Science 277(5331):1453-1474.

Bloemen HHJ, Wu L, van Gulik WM, Heijnen JJ, Verhaegen MHG. 2003. Reconstruction of the O_2 uptake rate and CO_2 evolution rate on a time scale of seconds. AIChE Journal 49(7):1895-1908.

Bolten CJ, Kiefer P, Letisse F, Portais JC, Wittmann C. 2007. Sampling for metabolome analysis of microorganisms. Analytical Chemistry 79(10):3843-3849.

Bolten CJ, Wittmann C. 2008. Appropriate sampling for intracellular amino acid analysis in five phylogenetically different yeasts. Biotechnology Letters 30(11):1993-2000.

Bratbak G, Dundas I. 1984. Bacterial dry matter content and biomass estimations. Applied and Environmental Microbiology 48(4):755-757.

Brauer MJ, Yuan J, Bennett BD, Lu W, Kimball E, Botstein D, Rabinowitz JD. 2006. Conservation of the metabolomic response to starvation across two divergent microbes. Proceedings of the National Academy of Sciences of the United States of America 103(51):19302-19307.

Bremer H, Dennis PP. 1996. Modulation of chemical composition and other parameters of the cell by growth rate. In: Neidhardt FC, Curtiss R, Ingraham JL, Lin ECC, Low KB, Magasanik B, Reznikoff WS, Riley M, Schaechter M, Umbarger HE, editors. *Escherichia coli* and *Salmonella*. Cellular and molecular biology. Washington DC: American Society for Microbiology. p 1527-1542.

Buchholz A, Hurlebaus J, Wandrey C, Takors R. 2002. Metabolomics: quantification of intracellular metabolite dynamics. Biomolecular Engineering 19(1):5-15.

Buchholz A, Takors R, Wandrey C. 2001. Quantification of intracellular metabolites in *Escherichia coli* K12 using liquid chromatographic-electrospray ionization tandem mass spectrometric techniques. Analytical Biochemistry 295(2):129-137.

Burgard AP, Vaidyaraman S, Maranas CD. 2001. Minimal reaction sets for *Escherichia coli* metabolism under different growth requirements and uptake environments. Biotechnology Progress 17(5):791-797.

Burgstaller W. 1997. Transport of small ions and molecules through the plasma membrane of filamentous fungi. Critical Reviews in Microbiology 23(1):1-46.

Buziol S, Bashir I, Baumeister A, Claaβen W, Noisommit-Rizzi N, Mailinger W, Reuss M. 2002. New bioreactor-coupled rapid stopped-flow sampling technique for measurements of metabolite dynamics on a subsecond time scale. Biotechnology and Bioengineering 80(6):632-636.

Bylund F, Castan A, Mikkola R, Veide A, Larsson G. 2000. Influence of scale-up on the quality of recombinant human growth hormone. Biotechnology and Bioengineering 69(2):119-128.

Bylund F, Collet E, Enfors SO, Larsson G. 1998. Substrate gradient formation in the large-scale bioreactor lowers cell yield and increases by-product formation. Bioprocess and Biosystems Engineering 18(3):171-180.

Bylund F, Guillard F, Enfors SO, Traegardh C, Larsson G. 1999. Scale-down of recombinant production: a comparative study of scaling performance. Bioprocess and Biosystems Engineering 20(5):377-389.

Calhoun MW, Oden KL, Gennis RB, de Mattos MJ, Neijssel OM. 1993. Energetic efficiency of *Escherichia coli*: effects of mutations in components of the aerobic respiratory chain. Journal of Bacteriology 175(10):3020-3025.

Canelas A, Ras C, Ten Pierick A, van Gulik W, Heijnen J. 2010. Finding simplicity in the midst of complexity: a data-driven thermodynamics-based framework for classification and quantification of *in vivo* enzyme kinetics. Submitted.

Canelas AB, Ras C, ten Pierick A, van Dam JC, Heijnen JJ, van Gulik WM. 2008a. Leakage-free rapid quenching technique for yeast metabolomics Metabolomics 4(3):226-239.

Canelas AB, ten Pierick A, Ras C, Seifar RM, van Dam JC, van Gulik WM, Heijnen JJ. 2009. Quantitative evaluation of intracellular metabolite extraction techniques for yeast metabolomics. Analytical Chemistry 81(17):7379-7389.

Canelas AB, van Gulik WM, Heijnen JJ. 2008b. Determination of the cytosolic free NAD/NADH ratio in *Saccharomyces cerevisiae* under steady-state and highly dynamic conditions. Biotechnology and Bioengineering 100(4):734-743.

Carlson R, Srienc F. 2004. Fundamental *Escherichia coli* biochemical pathways for biomass and energy production: creation of overall flux states. Biotechnology and Bioengineering 86(2):149-162.

Carson D, Pieringer RA, Daneo-Moore L. 1979. Effect of growth rate on lipid and lipoteichoic acid composition in *Streptococcus faecium*. Biochimica et Biophysica Acta 575(2):225-233.

Castan A, Enfors SO. 2002. Formate accumulation due to DNA release in aerobic cultivations of *Escherichia coli*. Biotechnology and Bioengineering 77(3):324-328.

Chang A, Scheer M, Grote A, Schomburg I, Schomburg D. 2009. BRENDA, AMENDA and FRENDA the enzyme information system: new content and tools in 2009. Nucleic Acids Research 37:D588-D592.

Chapman AG, Fall L, Atkinson DE. 1971. Adenylate energy charge in *Escherichia coli* during growth and starvation. Journal of Bacteriology 108(3):1072-1086.

Chassagnole C, Noisommit-Rizzi N, Schmid JW, Mauch K, Reuss M. 2002. Dynamic modeling of the central carbon metabolism of *Escherichia coli*. Biotechnology and Bioengineering 79(1):53-73.

Chemler JA, Fowler ZL, McHugh KP, Koffas MA. 2009. Improving NADPH availability for natural product biosynthesis in *Escherichia coli* by metabolic engineering. Metabolic Engineering 12(2):96-104.

Chou IC, Voit EO. 2009. Recent developments in parameter estimation and structure identification of biochemical and genomic systems. Mathematical Biosciences 219(2):57-83.

Clark DP. 1989. The fermentation pathways of *Escherichia coli*. FEMS Microbiology Reviews 5(3):223-234.

Connett RJ. 1985. *In vivo* glycolytic equilibria in dog gracilis muscle. Journal of Biological Chemistry 260(6):3314-3320.

Datsenko KA, Wanner BL. 2000. One-step inactivation of chromosomal genes in *Escherichia coli* K-12 using PCR products. Proceedings of the National Academy of Sciences of the United States of America 97(12):6640-6645.

De Anda R, Lara AR, Hernandez V, Hernandez-Montalvo V, Gosset G, Bolivar F, Ramirez OT. 2006. Replacement of the glucose phosphotransferase transport system by galactose permease reduces acetate accumulation and improves process performance of *Escherichia coli* for recombinant protein production without impairment of growth rate. Metabolic Engineering 8(3):281-290.

de Koning W, van Dam K. 1992. A method for the determination of changes of glycolytic metabolites in yeast on a subsecond time scale using extraction at neutral pH. Analytical Biochemistry 204(1):118-123.

De Mey M, Maertens J, Boogmans S, Soetaert WK, Vandamme EJ, Cunin R, Foulquié Moreno MR. 2010a. Promoter knock-in: a novel rational method for the fine tuning of genes. BMC Biotechnology 10:26.

De Mey M, Maertens J, Lequeux GJ, Soetaert WK, Vandamme EJ. 2007. Construction and model-based analysis of a promoter library for *E. coli*: an indispensable tool for metabolic engineering. BMC Biotechnology 7:34.

De Mey M, Taymaz-Nikerel H, Baart G, Waegeman H, Maertens J, Heijnen JJ, van Gulik WM. 2010b. Catching prompt metabolite dynamics in *Escherichia coli* with the BioScope at oxygen rich conditions. Metabolic Engineering 12(5):477-487.

Dennis PP, Bremer H. 1974. Macromolecular composition during steady-state growth of *Escherichia coli* B/r. Journal of Bacteriology 119(1):270-281.

Durot M, Bourguignon PY, Schachter V. 2009. Genome-scale models of bacterial metabolism: reconstruction and applications. FEMS Microbiology Reviews 33(1):164-190.

Edwards JS, Palsson BO. 2000. The *Escherichia coli* MG1655 *in silico* metabolic genotype: Its definition, characteristics, and capabilities. Proceedings of the National Academy of Sciences of the United States of America 97(10):5528-5533.

Emmerling M, Dauner M, Ponti A, Fiaux J, Hochuli M, Szyperski T, Wüthrich K, Bailey JE, Sauer U. 2002. Metabolic flux responses to pyruvate kinase knockout in *Escherichia coli*. Journal of Bacteriology 184(1):152-164.

Enfors SO, Jahic M, Rozkov A, Xu B, Hecker M, Jurgen B, Kruger E, Schweder T, Hamer G, O'Beirne D, Noisommit-Rizzi N, Reuss M, Boone L, Hewitt C, McFarlane C, Nienow A, Kovacs T, Tragardh C, Fuchs L, Revstedt J, Friberg PC, Hjertager B, Blomsten G, Skogman H, Hjort S, Hoeks F, Lin HY, Neubauer P, van der Lans R, Luyben K, Vrabel P, Manelius A. 2001. Physiological responses to mixing in large scale bioreactors. Journal of Biotechnology 85(2):175-185.

Farmer IS, Jones CW. 1976. The energetics of *Escherichia coli* during aerobic growth in continuous culture. European Journal of Biochemistry 67(1):115-122.

Feist AM, Henry CS, Reed JL, Krummenacker M, Joyce AR, Karp PD, Broadbelt LJ, Hatzimanikatis V, Palsson BO. 2007. A genome-scale metabolic reconstruction for *Escherichia coli* K-12 MG1655 that accounts for 1260 ORFs and thermodynamic information. Molecular Systems Biology 3:121.

Feist AM, Herrgard MJ, Thiele I, Reed JL, Palsson BO. 2009. Reconstruction of biochemical networks in microorganisms. Nature Reviews Microbiology 7(2):129-143.

Feist AM, Palsson BO. 2008. The growing scope of applications of genome-scale metabolic reconstructions using *Escherichia coli*. Nature Biotechnology 26(6):659-667.

Finley SD, Broadbelt LJ, Hatzimanikatis V. 2009. Thermodynamic analysis of biodegradation pathways. Biotechnology and Bioengineering 103(3):532-541.

Fischer E, Sauer U. 2003. A novel metabolic cycle catalyzes glucose oxidation and anaplerosis in hungry *Escherichia coli*. Journal of Biological Chemistry 278(47):46446-46451.

Fischer E, Zamboni N, Sauer U. 2004. High-throughput metabolic flux analysis based on gas chromatography-mass spectrometry derived ^{13}C constraints. Analytical Biochemistry 325(2):308-316.

Fleischmann RD, Adams MD, White O, Clayton RA, Kirkness EF, Kerlavage AR, Bult CJ, Tomb JF, Dougherty BA, Merrick JM, et al. 1995. Whole-genome random sequencing and assembly of *Haemophilus influenzae* Rd. Science 269(5223):496-512.

Fleming RM, Thiele I, Nasheuer HP. 2009. Quantitative assignment of reaction directionality in constraint-based models of metabolism: Application to *Escherichia coli*. Biophysical Chemistry 145(2-3):47-56.

Fogler S. 1991. Elements of chemical reaction engineering. New Jersey: Prentice-Hall International Editions.

Garcia JR, Cha HJ, Rao G, Marten MR, Bentley WE. 2009. Microbial nar-GFP cell sensors reveal oxygen limitations in highly agitated and aerated laboratory-scale fermentors. Microbial Cell Factories 8:6.

Gennis RB, Stewart V. 1996. Respiration. In: Neidhardt F, editor. *Escherichia coli* and *Salmonella*. Cellular and Molecular Biology. Washington, DC: American Society for Microbiology Press. p 217-261.

Gladyshev VN, Khangulov SV, Axley MJ, Stadtman TC. 1994. Coordination of selenium to molybdenum in formate dehydrogenase H from *Escherichia coli*. Proceedings of the National Academy of Sciences of the United States of America 91(16):7708-7711.

Goeddel DV, Kleid DG, Bolivar F, Heyneker HL, Yansura DG, Crea R, Hirose T, Kraszewski A, Itakura K, Riggs AD. 1979. Expression in *Escherichia coli* of chemically synthesized genes for human insulin. Proceedings of the National Academy of Sciences of the United States of America 76(1):106-10.

Goldberg RN, Tewari YB, Bhat TN. 2004. Thermodynamics of enzyme-catalyzed reactions-a database for quantitative biochemistry. Bioinformatics 20(16):2874-2877.

Gonzalez B, Francois J, Renaud M. 1997. A rapid and reliable method for metabolite extraction in yeast using boiling buffered ethanol. Yeast 13(14):1347-1355.

Grisolia S, Carreras J. 1975. Phosphoglycerate mutase from yeast, chicken breast muscle, and kidney (2, 3-PGA-dependent). Methods in Enzymology 42:435-450.

Gutowski SJ, Rosenberg H. 1975. Succinate uptake and related proton movements in *Escherichia coli* K12. Biochemical Journal 152(3):647-654.

Han L, Enfors SO, Haggstrom L. 2003. *Escherichia coli* high-cell-density culture: carbon mass balances and release of outer membrane components. Bioprocess and Biosystems Engineering 25(4):205-212.

Hardiman T, Meinhold H, Hofmann J, Ewald JC, Siemann-Herzberg M, Reuss M. 2009. Prediction of kinetic parameters from DNA-binding site sequences for modeling global transcription dynamics in *Escherichia coli*. Metabolic Engineering 12(3):196-211.

Hayashi K, Morooka N, Yamamoto Y, Fujita K, Isono K, Choi S, Ohtsubo E, Baba T, Wanner BL, Mori H, Horiuchi T. 2006. Highly accurate genome sequences of *Escherichia coli* K-12 strains MG1655 and W3110. Molecular Systems Biology 2:2006 0007.

Heijnen JJ. 1994. Thermodynamics of microbial growth and its implications for process design. Trends in Biotechnology 12(12):483-492.

Heijnen JJ. 2002. Stoichiometry and kinetics of microbial growth from a thermodynamic perpective. In: Ratledge C, Kristiansen B, editors. Basic Biotechnology. 2nd edition ed. Cambridge: Cambridge University Press.

Heijnen JJ. 2005. Approximative kinetic formats used in metabolic network modeling. Biotechnology and Bioengineering 91(5):534-545.

Heldal M, Norland S, Tumyr O. 1985. X-ray microanalytic method for measurement of dry matter and elemental content of individual bacteria. Applied and Environmental Microbiology 50(5):1251-1257.

Hempfling WP, Mainzer SE. 1975. Effects of varying the carbon source limiting growth on yield and maintenance characteristics of *Escherichia coli* in continuous culture. Journal of Bacteriology 123(3):1076-1087.

Henry CS, Broadbelt LJ, Hatzimanikatis V. 2007. Thermodynamics-based metabolic flux analysis. Biophysical Journal 92(5):1792-1805.

Henry CS, Jankowski MD, Broadbelt LJ, Hatzimanikatis V. 2006. Genome-scale thermodynamic analysis of *Escherichia coli* metabolism. Biophysical Journal 90(4):1453-1461.

Herbert D, Phipps PJ, Strange RE. 1971. Chemical analysis of microbial cells. In: Norris JR, Ribbons DW, editors. Methods in microbiology. London, United Kingdom: Academic Press. p 209-344.

Hiller J, Franco-Lara E, Papaioannou V, Weuster-Botz D. 2007a. Fast sampling and quenching procedures for microbial metabolic profiling. Biotechnology Letters 29(8):1161-1167.

Hiller J, Franco-Lara E, Weuster-Botz D. 2007b. Metabolic profiling of *Escherichia coli* cultivations: evaluation of extraction and metabolite analysis procedures. Biotechnology Letters 29(8):1169-1178.

Holms H. 1996. Flux analysis and control of the central metabolic pathways in *Escherichia coli*. FEMS Microbiology Reviews 19(2):85-116.

Hong SH, Lee SY. 2001. Metabolic flux analysis for succinic acid production by recombinant *Escherichia coli* with amplified malic enzyme activity. Biotechnology and Bioengineering 74(2):89-95.

Hoque MA, Ushiyama H, Tomita M, Shimizu K. 2005. Dynamic responses of the intracellular metabolite concentrations of the wild type and *pykA* mutant *Escherichia coli* against pulse addition of glucose or NH_3 under those limiting continuous cultures. Biochemical Engineering Journal 26(1):38-49.

Hua Q, Yang C, Baba T, Mori H, Shimizu K. 2003. Responses of the central metabolism in *Escherichia coli* to phosphoglucose isomerase and glucose-6-phosphate dehydrogenase knockouts. Journal of Bacteriology 185(24):7053-7067.

Ingledew WJ, Poole RK. 1984. The respiratory chains of *Escherichia coli*. Microbiology Reviews 48(3):222-271.

Ishii N, Nakahigashi K, Baba T, Robert M, Soga T, Kanai A, Hirasawa T, Naba M, Hirai K, Hoque A, Ho PY, Kakazu Y, Sugawara K, Igarashi S, Harada S, Masuda T, Sugiyama N, Togashi T, Hasegawa M, Takai Y, Yugi K, Arakawa K, Iwata N, Toya Y, Nakayama Y, Nishioka T, Shimizu K, Mori H, Tomita M. 2007. Multiple high-throughput analyses monitor the response of *E. coli* to perturbations. Science 316(5824):593-597.

Jamalzadeh E, Ras C, Verheijen PJT, van Gulik WM, Heijnen JJ. 2010. Fumaric acid uptake is facilitated by protein in *Saccharomyces cerevisiae* under anaerobic conditions. in preparation.

Jankowski MD, Henry CS, Broadbelt LJ, Hatzimanikatis V. 2008. Group contribution method for thermodynamic analysis of complex metabolic networks. Biophysical Journal 95(3):1487-1499.

Jantama K, Haupt MJ, Svoronos SA, Zhang XL, Moore JC, Shanmugam KT, Ingram LO. 2008. Combining metabolic engineering and metabolic evolution to develop nonrecombinant

strains of *Escherichia coli* C that produce succinate and malate. Biotechnology and Bioengineering 99(5):1140-1153.

Johansson L, Lindskog A, Silfversparre G, Cimander C, Nielsen KF, Liden G. 2005. Shikimic acid production by a modified strain of *E. coli* (W3110.shik1) under phosphate-limited and carbon-limited conditions. Biotechnology and Bioengineering 92(5):541-552.

Kayser A, Weber J, Hecht V, Rinas U. 2005. Metabolic flux analysis of *E. coli* in glucose-limited continuous culture. I. Growth-rate-dependent metabolic efficiency at steady state. Microbiology 151(3):693-706.

Keruchenko JS, Keruchenko ID, Gladilin KL, Zaitsev VN, Chirgadze NY. 1992. Purification, characterization and preliminary X-ray study of fumarase from *Saccharomyces cerevisiae*. Biochimica et Biophysica Acta 1122(1):85-92.

Keseler IM, Bonavides-Martinez C, Collado-Vides J, Gama-Castro S, Gunsalus RP, Johnson DA, Krummenacker M, Nolan LM, Paley S, Paulsen IT, Peralta-Gil M, Santos-Zavaleta A, Shearer AG, Karp PD. 2009. EcoCyc: A comprehensive view of *Escherichia coli* biology. Nucleic Acids Research 37:D464-D470.

Kim HU, Kim TY, Lee SY. 2008. Metabolic flux analysis and metabolic engineering of microorganisms. Molecular BioSystems 4(2):113-120.

Kimball E, Rabinowitz JD. 2006. Identifying decomposition products in extracts of cellular metabolites. Analytical Biochemistry 358(2):273-280.

Kiser RC, Niehaus WG, Jr. 1981. Purification and kinetic characterization of mannitol-1-phosphate dehydrogenase from *Aspergillus niger*. Archives of Biochemistry and Biophysics 211(2):613-621.

Kishore N, Tewari YB, Goldberg RN. 1998. An investigation of the equilibrium of the reaction {L-aspartate(aq) + 2-oxoglutarate(aq) = oxaloacetate(aq) + L-glutamate(aq)}. Journal of Chemical Thermodynamics 30(11):1373-1384.

Kizer L, Pitera DJ, Pfleger BF, Keasling JD. 2008. Application of functional genomics to pathway optimization for increased isoprenoid production. Applied and Environmental Microbiology 74(10):3229-3241.

Klein-Marcuschamer D, Santos CN, Yu H, Stephanopoulos G. 2009. Mutagenesis of the bacterial RNA polymerase alpha subunit for improvement of complex phenotypes. Applied and Environmental Microbiology 75(9):2705-2711.

Kresnowati MT, Suarez-Mendez C, Groothuizen MK, van Winden WA, Heijnen JJ. 2007. Measurement of fast dynamic intracellular pH in *Saccharomyces cerevisiae* using benzoic acid pulse. Biotechnology and Bioengineering 97(1):86-98.

Kresnowati MT, Suarez-Mendez CM, van Winden WA, van Gulik WM, Heijnen JJ. 2008. Quantitative physiological study of the fast dynamics in the intracellular pH of *Saccharomyces cerevisiae* in response to glucose and ethanol pulses. Metabolic Engineering 10(1):39-54.

Kresnowati MT, van Winden WA, Almering MJ, ten Pierick A, Ras C, Knijnenburg TA, Daran-Lapujade P, Pronk JT, Heijnen JJ, Daran JM. 2006. When transcriptome meets metabolome: fast cellular responses of yeast to sudden relief of glucose limitation. Molecular Systems Biology 2:49.

Krömer JO, Wittmann C, Schroder H, Heinzle E. 2006. Metabolic pathway analysis for rational design of L-methionine production by *Escherichia coli* and *Corynebacterium glutamicum*. Metabolic Engineering 8(4):353-369.

Kummel A, Panke S, Heinemann M. 2006. Systematic assignment of thermodynamic constraints in metabolic network models. BMC Bioinformatics 7:512.

Kuyper M, Winkler AA, van Dijken JP, Pronk JT. 2004. Minimal metabolic engineering of *Saccharomyces cerevisiae* for efficient anaerobic xylose fermentation: a proof of principle. FEMS Yeast Research 4(6):655-664.

Kwon YK, Lu W, Melamud E, Khanam N, Bognar A, Rabinowitz JD. 2008. A domino effect in antifolate drug action in *Escherichia coli*. Nature Chemical Biology 4(10):602-608.

Lang VJ, Leystralantz C, Cook RA. 1987. Characterization of the Specific Pyruvate Transport System in *Escherichia coli* K-12. Journal of Bacteriology 169(1):380-385.

Lange HC, Eman M, van Zuijlen G, Visser D, van Dam JC, Frank J, de Mattos MJ, Heijnen JJ. 2001. Improved rapid sampling for *in vivo* kinetics of intracellular metabolites in *Saccharomyces cerevisiae*. Biotechnology and Bioengineering 75(4):406-415.

Lange HC, Heijnen JJ. 2001. Statistical reconciliation of the elemental and molecular biomass composition of *Saccharomyces cerevisiae*. Biotechnology and Bioengineering 75(3):334-344.

Lara AR, Caspeta L, Gosset G, Bolivar F, Ramirez OT. 2008. Utility of an *Escherichia coli* strain engineered in the substrate uptake system for improved culture performance at high glucose and cell concentrations: an alternative to fed-batch cultures. Biotechnology and Bioengineering 99(4):893-901.

Lara AR, Galindo E, Ramirez OT, Palomares LA. 2006a. Living with heterogeneities in bioreactors: understanding the effects of environmental gradients on cells. Molecular Biotechnology 34(3):355-381.

Lara AR, Leal L, Flores N, Gosset G, Bolivar F, Ramirez OT. 2006b. Transcriptional and metabolic response of recombinant *Escherichia coli* to spatial dissolved oxygen tension gradients simulated in a scale-down system. Biotechnology and Bioengineering 92(2):372-385.

Lara AR, Taymaz Nikerel H, Mashego MR, van Gulik WM, Heijnen JJ, Ramirez OT, van Winden WA. 2009. Fast dynamic response of the fermentative metabolism of *Escherichia coli* to aerobic and anaerobic glucose pulses. Biotechnology and Bioengineering 104(6):1153-1161.

Lara AR, Vazquez-Limon C, Gosset G, Bolivar F, Lopez-Munguia A, Ramirez OT. 2006c. Engineering *Escherichia coli* to improve culture performance and reduce formation of by-products during recombinant protein production under transient intermittent anaerobic conditions. Biotechnology and Bioengineering 94(6):1164-1175.

Larsson G, Tornkvist M. 1996. Rapid sampling, cell inactivation and evaluation of low extracellular glucose concentrations during fed-batch cultivation. Journal of Biotechnology 49(1-3):69-82.

Larsson G, Tornkvist M, Wernersson ES, Tragardh C, Noorman H, Enfors SO. 1996. Substrate gradients in bioreactors: Origin and consequences. Bioprocess Engineering 14(6):281-289.

Lawson JW, Veech RL. 1979. Effects of pH and free Mg^{2+} on the K_{eq} of the creatine kinase reaction and other phosphate hydrolyses and phosphate transfer reactions. Journal of Biological Chemistry 254(14):6528-6537.

Lee KH, Park JH, Kim TY, Kim HU, Lee SY. 2007. Systems metabolic engineering of *Escherichia coli* for L-threonine production. Molecular Systems Biology 3:149.

Lee YH, Tsao GT. 1979. Dissolved oxygen electrodes. Advances in Biochemical Engineering Berlin: Springer. p 35-86.

Leger C, Heffron K, Pershad HR, Maklashina E, Luna-Chavez C, Cecchini G, Ackrell BA, Armstrong FA. 2001. Enzyme electrokinetics: energetics of succinate oxidation by fumarate reductase and succinate dehydrogenase. Biochemistry 40(37):11234-11245.

Lin HY, Neubauer P. 2000. Influence of controlled glucose oscillations on a fed-batch process of recombinant *Escherichia coli*. Journal of Biotechnology 79(1):27-37.

Link H, Anselment B, Weuster-Botz D. 2008. Leakage of adenylates during cold methanol/glycerol quenching of *Escherichia coli*. Metabolomics 4(3):240-247.

Link H, Anselment B, Weuster-Botz D. 2010. Rapid media transition: An experimental approach for steady state analysis of metabolic pathways. Biotechnology Progress 26(1):1-10.

Liu X, Ng C, Ferenci T. 2000. Global adaptations resulting from high population densities in *Escherichia coli* cultures. Journal of Bacteriology 182(15):4158-4164.

Lowry OH, Carter J, Ward JB, Glaser L. 1971. The effect of carbon and nitrogen sources on the level of metabolic intermediates in *Escherichia coli*. Journal of Biological Chemistry 246(21):6511-6521.

Luo B, Groenke K, Takors R, Wandrey C, Oldiges M. 2007. Simultaneous determination of multiple intracellular metabolites in glycolysis, pentose phosphate pathway and tricarboxylic acid cycle by liquid chromatography-mass spectrometry. Journal of Chromatography A 1147(2):153-164.

Maharjan RP, Ferenci T. 2003. Global metabolite analysis: the influence of extraction methodology on metabolome profiles of *Escherichia coli*. Analytical Biochemistry 313(1):145-154.

Mashego MR, Jansen ML, Vinke JL, van Gulik WM, Heijnen JJ. 2005. Changes in the metabolome of *Saccharomyces cerevisiae* associated with evolution in aerobic glucose-limited chemostats. FEMS Yeast Research 5(4-5):419-430.

Mashego MR, Rumbold K, De Mey M, Vandamme E, Soetaert W, Heijnen JJ. 2007a. Microbial metabolomics: Past, present and future methodologies. Biotechnology Letters 29(1):1-16.

Mashego MR, van Gulik WM, Heijnen JJ. 2007b. Metabolome dynamic responses of *Saccharomyces cerevisiae* on simultaneous rapid perturbations in external electron acceptor and electron donor. FEMS Yeast Research 7(1):48-66.

Mashego MR, van Gulik WM, Vinke JL, Heijnen JJ. 2003. Critical evaluation of sampling techniques for residual glucose determination in carbon-limited chemostat cultures of *Saccharomyces cerevisiae*. Biotechnology and Bioengineering 83(4):395-399.

Mashego MR, van Gulik WM, Vinke JL, Visser D, Heijnen JJ. 2006. *In vivo* kinetics with rapid perturbation experiments in *Saccharomyces cerevisiae* using a second-generation BioScope. Metabolic Engineering 8(4):370-383.

Mashego MR, Wu L, van Dam JC, Ras C, Vinke JL, van Winden WA, van Gulik WM, Heijnen JJ. 2004. MIRACLE: mass isotopomer ratio analysis of U-13C-labeled extracts. A new method for accurate quantification of changes in concentrations of intracellular metabolites. Biotechnology and Bioengineering 85(6):620-628.

Maskow T, von Stockar U. 2005. How reliable are thermodynamic feasibility statements of biochemical pathways? Biotechnology and Bioengineering 92(2):223-230.

Mat-Jan F, Alam KY, Clark DP. 1989. Mutants of *Escherichia coli* deficient in the fermentative lactate dehydrogenase. Journal of Bacteriology 171(1):342-348.

Mavrovouniotis ML. 1990. Group contributions for estimating standard gibbs energies of formation of biochemical compounds in aqueous solution. Biotechnology and Bioengineering 36(10):1070-1082.

Mavrovouniotis ML. 1991. Estimation of standard Gibbs energy changes of biotransformations. Journal of Biological Chemistry 266(22):14440-14445.

McKinlay JB, Vieille C, Zeikus JG. 2007. Prospects for a bio-based succinate industry. Applied Microbiology and Biotechnology 76(4):727-740.

Mendoza-Vargas A, Olvera L, Olvera M, Grande R, Vega-Alvarado L, Taboada B, Jimenez-Jacinto V, Salgado H, Juarez K, Contreras-Moreira B, Huerta AM, Collado-Vides J, Morett E. 2009. Genome-wide identification of transcription start sites, promoters and transcription factor binding sites in *E. coli*. PLoS One 4(10):e7526.

Millard CS, Chao Y-P, Liao JC, Donnelly MI. 1996. Enhanced production of succinic acid by overexpression of phosphoenolpyruvate carboxylase in *Escherichia coli*. Applied and Environmental Microbiology 62(5):1808-1810.

Mizoguchi H, Mori H, Fujio T. 2007. *Escherichia coli* minimum genome factory. Biotechnology and Applied Biochemistry 46(Pt 3):157-167.

Nanchen A, Schicker A, Sauer U. 2006. Nonlinear dependency of intracellular fluxes on growth rate in miniaturized continuous cultures of *Escherichia coli*. Applied and Environmental Microbiology 72(2):1164-1172.

Nasution U. 2007. A dynamic and steady state metabolome study of central metabolism and its relation with the penicillin biosynthesis pathway in *Penicillium chrysogenum* [PhD Thesis]. Delft: Delft University of Technology.

Nasution U, van Gulik WM, Proell A, van Winden WA, Heijnen JJ. 2006. Generating short-term kinetic responses of primary metabolism of *Penicillium chrysogenum* through glucose perturbation in the BioScope mini reactor. Metabolic Engineering 8(5):395-405.

Neidhardt FC. 1987. Chemical Composition of *Escherichia coli*. In: Neidhardt FC, editor. *Escherichia coli* and *Salmonella typhimurium*. Cellular and molecular biology. Washington: American Society for Microbiology. p 3-6.

Neidhardt FC, editor. 1996. *Escherichia coli* and *Salmonella*. Cellular and Molecular Biology. Washington, D.C.: ASM Press.

Neijssel OM, Teixeira de Mattos MJ. 1994. The energetics of bacterial growth: a reassessment. Molecular Microbiology 13(2):172-182.

Neubauer P, Haggstrom L, Enfors SO. 1995. Influence of substrate oscillations on acetate formation and growth yield in *Escherichia coli* glucose-limited fed-batch cultivations. Biotechnology and Bioengineering 47(2):139-146.

Nielsen J. 2001. Metabolic engineering. Applied Microbiology and Biotechnology 55(3):263-283.

Nielsen J, Jewett MC. 2008. Impact of systems biology on metabolic engineering of *Saccharomyces cerevisiae*. FEMS Yeast Research 8(1):122-131.

Nikerel IE. 2009. Managing complexity of cellular systems: theoretical tools for dynamic modeling of metabolic reaction networks [PhD Thesis]. Delft: Delft University of Technology.

Nikerel IE, van Winden WA, van Gulik WM, Heijnen JJ. 2006. A method for estimation of elasticities in metabolic networks using steady state and dynamic metabolomics data and linlog kinetics. BMC Bioinformatics 7:540.

Nikerel IE, van Winden WA, Verheijen PJ, Heijnen JJ. 2009. Model reduction and a priori kinetic parameter identifiability analysis using metabolome time series for metabolic reaction networks with linlog kinetics. Metabolic Engineering 11(1):20-30.

Okumoto S, Takanaga H, Frommer WB. 2008. Quantitative imaging for discovery and assembly of the metabo-regulome. New Phytologist 180(2):271-295.

Oldiges M, Kunze M, Degenring D, Sprenger GA, Takors R. 2004. Stimulation, monitoring, and analysis of pathway dynamics by metabolic profiling in the aromatic amino acid pathway. Biotechnology Progress 20(6):1623-1633.

Oldiges M, Takors R. 2005. Applying metabolic profiling techniques for stimulus-response experiments: Chances and pitfalls. Technology Transfer in Biotechnology: From Lab to Industry to Production 92:173-196.

Otero JM, Nielsen J. 2010. Industrial systems biology. Biotechnology and Bioengineering 105(3):439-460.

Palomares LA, Lara AR, Ramirez OT. 2010. Bioreactor scale-down. In: Flickinger MC, editor. Encyclopedia of Industrial Biotechnology: Bioprocess, Bioseparation, and Cell Technology. New York: John Wiley and Sons.

Panke O, Rumberg B. 1997. Energy and entropy balance of ATP synthesis. Biochimica Et Biophysica Acta-Bioenergetics 1322(2-3):183-194.

Park JH, Lee KH, Kim TY, Lee SY. 2007. Metabolic engineering of *Escherichia coli* for the production of L-valine based on transcriptome analysis and in silico gene knockout simulation. Proceedings of the National Academy of Sciences of the United States of America 104(19):7797-7802.

Parkhomchuk D, Amstislavskiy V, Soldatov A, Ogryzko V. 2009. Use of high throughput sequencing to observe genome dynamics at a single cell level. Proceedings of the National Academy of Sciences of the United States of America 106(49):20830-20835.

Pecher A, Blaschkowski HP, Knappe K, Bock A. 1982. Expression of pyruvate formate-lyase of *Escherichia coli* from the cloned structural gene. Archives of Microbiology 132(4):365-371.

Peng L, Arauzo-Bravo MJ, Shimizu K. 2004. Metabolic flux analysis for a *ppc* mutant *Escherichia coli* based on ^{13}C-labelling experiments together with enzyme activity assays and intracellular metabolite measurements. FEMS Microbiology Letters 235(1):17-23.

Perry R, Green D. 1997. Perry's Chemical Engineers' Handbook. New York: McGraw-Hill.

Petranovic D, Vemuri GN. 2009. Impact of yeast systems biology on industrial biotechnology. Journal of Biotechnology 144(3):204-211.

Phue JN, Noronha SB, Hattacharyya R, Wolfe AJ, Shiloach J. 2005. Glucose metabolism at high density growth of *E. coli* B and *E. coli* K: differences in metabolic pathways are responsible for efficient glucose utilization in *E. coli* B as determined by microarrays and Northern blot analyses. Biotechnology and Bioengineering 90(7):805-820.

Pramanik J, Keasling JD. 1997. Stochiometric model of *Escherichia coli* metabolism: incorporation of growth-rate dependent biomass composition and mechanistic energy requirements. Biotechnology and Bioengineering 56(4):398-421.

Pramanik J, Keasling JD. 1998. Effect of *Escherichia coli* biomass composition on central metabolic fluxes predicted by a stochiometric model. Biotechnology and Bioengineering 60(2):230-238.

Price ND, Reed JL, Palsson BO. 2004. Genome-scale models of microbial cells: evaluating the consequences of constraints. Nature Reviews Microbiology 2(11):886-897.

Rabinowitz JD, Kimball E. 2007. Acidic acetonitrile for cellular metabolome extraction from *Escherichia coli*. Analytical Chemistry 79(16):6167-6173.

Reed JL, Vo TD, Schilling CH, Palsson B. 2003. An expanded genome-scale model of *Escherichia coli* K-12. Genome Biology 4:R54.

Rispens P, Dellebar.Cw, Eleveld D, Helder W, Zijlstra WG. 1968. Apparent first dissociation constant of carbonic acid in plasma between 16 and 42.5 degrees. Clinica Chimica Acta 22(4):627-637.

Roels JA. 1983. Energetics and Kinetics in Biotechnology. Amsterdam: Elsevier Biochemical Press.

Rossell S. 2007. Unraveling the complexity of flux regulation: new insights through the quantitative description of regulatory processes [PhD Thesis]. Amsterdam: VU University Amsterdam.

Ruiz N, Kahne D, Silhavy TJ. 2006. Advances in understanding bacterial outer-membrane biogenesis. Nature Reviews Microbiology 4(1):57-66.

Sanchez AM, Bennett GN, San KY. 2005a. Efficient succinic acid production from glucose through overexpression of pyruvate carboxylase in an *Escherichia coli* alcohol dehydrogenase and lactate dehydrogenase mutant. Biotechnology Progress 21(2):358-365.

Sanchez AM, Bennett GN, San KY. 2005b. Novel pathway engineering design of the anaerobic central metabolic pathway in *Escherichia coli* to increase succinate yield and productivity. Metabolic Engineering 7(3):229-239.

Sander R. 2010. Henry's Law Constants. In: Linstrom PJ, Mallard WG, editors. NIST Chemistry WebBook, NIST Standard Reference Database Number 69. Gaithersburg MD: National Institute of Standards and Technology, http://webbook.nist.gov, (retrieved March 23, 2010).

Sandoval-Basurto EA, Gosset G, Bolivar F, Ramirez OT. 2005. Culture of *Escherichia coli* under dissolved oxygen gradients simulated in a two-compartment scale-down system: Metabolic response and production of recombinant protein. Biotechnology and Bioengineering 89(4):453-463.

Sanger F, Coulson AR. 1975. A rapid method for determining sequences in DNA by primed synthesis with DNA polymerase. Journal of Molecular Biology 94(3):441-448.

Sauer M, Porro D, Mattanovich D, Branduardi P. 2008. Microbial production of organic acids: expanding the markets. Trends in Biotechnology 26(2):100-108.

Sauer U, Lasko DR, Fiaux J, Hochuli M, Glaser R, Szyperski T, Wuthrich K, Bailey JE. 1999. Metabolic flux ratio analysis of genetic and environmental modulations of *Escherichia coli* central carbon metabolism. Journal of Bacteriology 181(21):6679-6688.

Sawers G. 1994. The hydrogenases and formate dehydrogenases of *Escherichia coli*. Antonie van Leeuwenhoek 66(1-3):57-88.

Schadel F, Franco-Lara E. 2009. Rapid sampling devices for metabolic engineering applications. Applied Microbiology and Biotechnology 83(2):199-208.

Schaefer U, Boos W, Takors R, Weuster-Botz D. 1999. Automated sampling device for monitoring intracellular metabolite dynamics. Analytical Biochemistry 270(1):88-96.

Schaub J, Mauch K, Reuss M. 2008. Metabolic flux analysis in *Escherichia coli* by integrating isotopic dynamic and isotopic stationary ^{13}C labeling data. Biotechnology and Bioengineering 99(5):1170-1185.

Schaub J, Reuss M. 2008. *In vivo* dynamics of glycolysis in *Escherichia coli* shows need for growth-rate dependent metabolome analysis. Biotechnology Progress 24(6):1402-1407.

Schaub J, Schiesling C, Reuss M, Dauner M. 2006. Integrated sampling procedure for metabolome analysis. Biotechnology Progress 22(5):1434-1442.

Schmalzriedt S, Jenne M, Mauch K, Reuss M. 2003. Integration of physiology and fluid dynamics. In: Scheper T, editor. Advances in Biochemical Engineering/Biotechnology. 2003/05/16 ed. Berlin Heidelberg: Springer-Verlag. p 19-68.

Schmid JW, Mauch K, Reuss M, Gilles ED, Kremling A. 2004. Metabolic design based on a coupled gene expression-metabolic network model of tryptophan production in *Escherichia coli*. Metabolic Engineering 6(4):364-377.

Schmidt K, Nielsen J, Villadsen J. 1999. Quantitative analysis of metabolic fluxes in *Escherichia coli*, using two-dimensional NMR spectroscopy and complete isotopomer models. Journal of Biotechnology 71(1-3):175-189.

Schmitz M, Hirsch E, Bongaerts J, Takors R. 2002. Pulse experiments as a prerequisite for the quantification of *in vivo* enzyme kinetics in aromatic amino acid pathway of *Escherichia coli*. Biotechnology Progress 18(5):935-941.

Schuetz R, Kuepfer L, Sauer U. 2007. Systematic evaluation of objective functions for predicting intracellular fluxes in *Escherichia coli*. Molecular Systems Biology 3:119.

Schwoppe C, Winkler HH, Neuhaus HE. 2002. Properties of the glucose-6-phosphate transporter from *Chlamydia pneumoniae* (HPTcp) and the glucose-6-phosphate sensor from *Escherichia coli* (UhpC). Journal of Bacteriology 184(8):2108-2115.

Schwoppe C, Winkler HH, Neuhaus HE. 2003. Connection of transport and sensing by UhpC, the sensor for external glucose-6-phosphate in *Escherichia coli*. European Journal of Biochemistry 270(7):1450-1457.

Seeholzer SH. 1993. Phosphoglucose isomerase: a ketol isomerase with aldol C2-epimerase activity. Proceedings of the National Academy of Sciences of the United States of America 90(4):1237-1241.

Seifar RM, Ras C, van Dam JC, van Gulik WM, Heijnen JJ, van Winden WA. 2009. Simultaneous quantification of free nucleotides in complex biological samples using ion pair reversed phase liquid chromatography isotope dilution tandem mass spectrometry. Analytical Biochemistry 388(2):213-219.

Serrano R. 1991. Transport across yeast vacuolar and plasma membranes. In: Broach JR, Pringle JR, Jones EW, editors. The molecular and cellular biology of the yeast *Saccharomyces*: genome dynamics, protein synthesis and energetics. New York: Cold Spring Harbor Laboratory Press. p 523-585.

Serrato JA, Palomares LA, Meneses-Acosta A, Ramirez OT. 2004. Heterogeneous conditions in dissolved oxygen affect N-glycosylation but not productivity of a monoclonal antibody in hybridoma cultures. Biotechnology and Bioengineering 88(2):176-188.

Siddiquee KAZ, Arauzo-Bravo MJ, Shimizu K. 2004. Metabolic flux analysis of *pykF* gene knockout *Escherichia coli* based on ^{13}C-labeling experiments together with measurements of enzyme activities and intracellular metabolite concentrations. Applied Microbiology and Biotechnology 63(4):407-417.

Soini J, Ukkonen K, Neubauer P. 2008. High cell density media for *Escherichia coli* are generally designed for aerobic cultivations - consequences for large-scale bioprocesses and shake flask cultures. Microbial Cell Factories 7:26.

Soupene E, van Heeswijk WC, Plumbridge J, Stewart V, Bertenthal D, Lee H, Prasad G, Paliy O, Charernnoppakul P, Kustu S. 2003. Physiological studies of *Escherichia coli* strain MG1655: growth defects and apparent cross-regulation of gene expression. Journal of Bacteriology 185(18):5611-5626.

Spura J, Reimer LC, Wieloch P, Schreiber K, Buchinger S, Schomburg D. 2009. A method for enzyme quenching in microbial metabolome analysis successfully applied to gram-positive and gram-negative bacteria and yeast. Analytical Biochemistry 394(2):192-201.

Stahlberg H, Muller DJ, Suda K, Fotiadis D, Engel A, Meier T, Matthey U, Dimroth P. 2001. Bacterial Na$^+$-ATP synthase has an undecameric rotor. EMBO Reports 2(3):229-233.

Stephanopoulos G. 1994. Metabolic engineering. Current Opinion in Biotechnology 5(2):196-200.

Stephanopoulos G. 1999. Metabolic fluxes and metabolic engineering. Metabolic Engineering 1(1):1-11.

Stephanopoulos G, Alper H, Moxley J. 2004. Exploiting biological complexity for strain improvement through systems biology. Nature Biotechnology 22(10):1261-1267.

Stephanopoulos G, Aristidou AA, Nielsen J. 1998. Metabolic Engineering: Principles and Methodologies. San Diego, CA, USA: Academic Press.

Stols L, Donnelly MI. 1997. Production of succinic acid through overexpression of NAD(+)-dependent malic enzyme in an *Escherichia coli* mutant. Applied and Environmental Microbiology 63(7):2695-2701.

Stouthamer A. 1973. A theoretical study on the amount of ATP required for synthesis of microbial cell material. Antonie van Leeuwenhoek 39(3):545-565.

Sud IJ, Schaechter M. 1964. Dependence of the content of cell envelopes on the growth rate of *Bacillus megaterium*. Journal of Bacteriology 88(6):1612-1617.

Sweere APJ, Luyben KCAM, Kossen NWF. 1987. Regime analysis and scale-down tools to investigate the performance of bioreactors. Enzyme and Microbial Technology 9(7):386-398.

Taymaz-Nikerel H, Borujeni AE, Verheijen PJT, Heijnen JJ, van Gulik WM. 2010a. Genome-derived minimal metabolic models for *Escherichia coli* MG1655 with estimated *in vivo* respiratory ATP stoichiometry. Biotechnology and Bioengineering 107(2):369-381.

Taymaz-Nikerel H, De Mey M, Baart G, Maertens J, Verheijen PJT, van Gulik WM, Heijnen JJ. 2010b. Flux and metabolite flexibility in central metabolism of aerobic glucose-limited *E. coli* to rapid glycolytic and gluconeogenic substrate pulses. In preparation.

Taymaz-Nikerel H, de Mey M, Ras C, ten Pierick A, Seifar RM, van Dam JC, Heijnen JJ, van Gulik WM. 2009. Development and application of a differential method for reliable metabolome analysis in *Escherichia coli*. Analytical Biochemistry 386(1):9-19.

Taymaz-Nikerel H, van Gulik WM, Heijnen JJ. 2010c. Rapid dynamics of *in vivo* flux-metabolite response in central and amino acid pathways in *E. coli*. Submitted.

Tempest DW, Meers JL, Brown CM. 1970. Influence of environment on the content and composition of microbial free amino acid pools. Journal of General Microbiology 64(2):171-185.

Teusink B, Passarge J, Reijenga CA, Esgalhado E, van der Weijden CC, Schepper M, Walsh MC, Bakker BM, van Dam K, Westerhoff HV, Snoep JL. 2000. Can yeast glycolysis be understood in terms of *in vitro* kinetics of the constituent enzymes? Testing biochemistry. European Journal of Biochemistry 267(17):5313-5329.

Theobald U, Mailinger W, Baltes M, Reuss M, Rizzi M. 1997. *In vivo* analysis of metabolic dynamics in *Saccharomyces cerevisiae*: I. Experimental observations. Biotechnology and Bioengineering 55(2):305-316.

Theobald U, Mailinger W, Reuss M, Rizzi M. 1993. *In vivo* analysis of glucose-induced fast changes in yeast adenine nucleotide pool applying a rapid sampling technique. Analytical Biochemistry 214(1):31-37.

Thiele I, Jamshidi N, Fleming RM, Palsson BO. 2009. Genome-scale reconstruction of *Escherichia coli*'s transcriptional and translational machinery: a knowledge base, its mathematical formulation, and its functional characterization. PLoS Computational Biology 5(3):e1000312.

Tran QH, Bongaerts J, Vlad D, Unden G. 1997. Requirement for the proton-pumping NADH dehydrogenase I of *Escherichia coli* in respiration of NADH to fumarate and its bioenergetic implications. European Journal of Biochemistry 244(1):155-160.

Tweeddale H, Notley-McRobb L, Ferenci T. 1998. Effect of slow growth on metabolism of *Escherichia coli*, as revealed by global metabolite pool ("Metabolome") analysis. Journal of Bacteriology 180(19):5109-5116.

van Dam JC, Eman MR, Frank J, Lange HC, van Dedem GWK, Heijnen SJ. 2002. Analysis of glycolytic intermediates in *Saccharomyces cerevisiae* using anion exchange chromatography and electrospray ionization with tandem mass spectrometric detection. Analytica Chimica Acta 460(2):209-218.

van der Heijden RTJM, Heijnen JJ, Hellinga C, Romein B, Luyben KCAM. 1994. Linear constraint relations in biochemical reaction systems: I. Classification of the calculability and the balanceability of conversion rates. Biotechnology and Bioengineering 43(1):3-10.

van Gulik WM. 2010. Fast sampling for quantitative microbial metabolomics. Current Opinion in Biotechnology 21(1):27-34.

van Gulik WM, Antoniewicz MR, deLaat WTAM, L VJ, Heijnen JJ. 2001. Energetics of growth and penicillin production in a high-producing strain of *Penicillium chrysogenum*. Biotechnology and Bioengineering 72(2):185-193.

van Gulik WM, de Laat WTAM, Vinke JL, Heijnen JJ. 2000. Application of metabolic flux analysis for the identification of metabolic bottlenecks in the biosynthesis of penicillin-G. Biotechnology and Bioengineering 68(6):602-618.

van Gulik WM, Heijnen JJ. 1995. A metabolic network stoichiometry analysis of microbial growth and product formation. Biotechnology and Bioengineering 48(6):681-698.

van Winden WA, van Dam JC, Ras C, Kleijn RJ, Vinke JL, van Gulik WM, Heijnen JJ. 2005. Metabolic-flux analysis of *Saccharomyces cerevisiae* CEN.PK113-7D based on mass isotopomer measurements of ^{13}C-labeled primary metabolites. FEMS Yeast Research 5(6-7):559-568.

van Winden WA, van Gulik WM, Schipper D, Verheijen PJT, Krabben P, Vinke JL, Heijnen JJ. 2003. Metabolic flux and metabolic network analysis of *Penicillium chrysogenum* using 2D [C-13, H-1] COSY NMR measurements and cumulative Bondomer simulation. Biotechnology and Bioengineering 83(1):75-92.

Varma A, Palsson BO. 1993. Metabolic capabilities of *Escherichia coli*: II. Optimal growth patterns. Journal of Theoretical Biology 165(4):503-522.

Vaseghi S, Baumeister A, Rizzi M, Reuss M. 1999. *In vivo* dynamics of the pentose phosphate pathway in *Saccharomyces cerevisiae*. Metabolic Engineering 1(2):128-140.

Veech RL, Raijman L, Dalziel K, Krebs HA. 1969. Disequilibrium in the triose phosphate isomerase system in rat liver. Biochemical Journal 115(4):837-842.

Vemuri GN, Eiteman MA, Altman E. 2002a. Effects of growth mode and pyruvate carboxylase on succinic acid production by metabolically engineered strains of *Escherichia coli*. Applied and Environmental Microbiology 68(4):1715-1727.

Vemuri GN, Eiteman MA, Altman E. 2002b. Succinate production in dual-phase *Escherichia coli* fermentations depends on the time of transition from aerobic to anaerobic conditions. Journal of Industrial Microbiology & Biotechnology 28(6):325-332.

Verduyn C, Postma E, Scheffers WA, van Dijken JP. 1992. Effect of benzoic acid on metabolic fluxes in yeasts: a continuous-culture study on the regulation of respiration and alcoholic fermentation. Yeast 8(7):501-517.

Verheijen PJT. 2010. Data Reconciliation and Error Detection. In: Smolke CD, editor. The Metabolic Pathway Engineering Handbook. Fundamentals. Boca Raton, FL: CRC Press.

Villas-Boas SG, Bruheim P. 2007. Cold glycerol-saline: the promising quenching solution for accurate intracellular metabolite analysis of microbial cells. Analytical Biochemistry 370(1):87-97.

Villas-Boas SG, Hojer-Pedersen J, Akesson M, Smedsgaard J, Nielsen J. 2005. Global metabolite analysis of yeast: evaluation of sample preparation methods. Yeast 22(14):1155-1169.

Visser D, van der Heijden R, Mauch K, Reuss M, Heijnen S. 2000. Tendency modeling: a new approach to obtain simplified kinetic models of metabolism applied to *Saccharomyces cerevisiae*. Metabolic Engineering 2(3):252-275.

Visser D, van Zuylen GA, van Dam JC, Eman MR, Proll A, Ras C, Wu L, van Gulik WM, Heijnen JJ. 2004. Analysis of *in vivo* kinetics of glycolysis in aerobic *Saccharomyces cerevisiae* by application of glucose and ethanol pulses. Biotechnology and Bioengineering 88(2):157-167.

Visser D, van Zuylen GA, van Dam JC, Oudshoorn A, Eman MR, Ras C, van Gulik WM, Frank J, van Dedem GW, Heijnen JJ. 2002. Rapid sampling for analysis of *in vivo* kinetics using the BioScope: a system for continuous-pulse experiments. Biotechnology and Bioengineering 79(6):674-681.

Vrabel P, van der Lans RGJM, Luyben KCAM, Boon L, Nienow A. 2000. Mixing in large-scale vessels stirred with multiple radial or radial and axial up-pumping impellers: modelling and measurements. Chemical Engineering Science 55(23):5881-5896.

Wang QZ, Chen X, Yang YD, Zhao XM. 2006. Genome-scale *in silico* aided metabolic analysis and flux comparisons of *Escherichia coli* to improve succinate production. Applied Microbiology and Biotechnology 73(4):887-894.

Wang Y, Chu J, Zhuang YP, Wang YH, Xia JY, Zhang SL. 2009. Industrial bioprocess control and optimization in the context of systems biotechnology. Biotechnology Advances 27(6):989-995.

Wiechert W. 2002. Modeling and simulation: tools for metabolic engineering. Journal of Biotechnology 94(1):37-63.

Wilcock AR, Goldberg DM. 1972. Kinetic determination of malate dehydrogenase activity eliminating problems due to spontaneous conversion of oxaloacetate to pyruvate. Biochemical Medicine 6(2):116-126.

Winder CL, Dunn WB, Schuler S, Broadhurst D, Jarvis R, Stephens GM, Goodacre R. 2008. Global metabolic profiling of *Escherichia coli* cultures: An evaluation of methods for quenching and extraction of intracellular metabolites. Analytical Chemistry 80(8):2939-2948.

Wisselink HW, Toirkens MJ, Wu Q, Pronk JT, van Maris AJA. 2009. Novel evolutionary engineering approach for accelerated utilization of glucose, xylose, and arabinose mixtures by engineered *Saccharomyces cerevisiae* strains. Applied and Environmental Microbiology 75(4):907-914.

Wittmann C. 2007. Fluxome analysis using GC-MS. Microbial Cell Factories 6:6.

Wittmann C, Kromer JO, Kiefer P, Binz T, Heinzle E. 2004. Impact of the cold shock phenomenon on quantification of intracellular metabolites in bacteria. Analytical Biochemistry 327(1):135-139.

Wold F, Ballou CE. 1957. Studies on the enzyme enolase. I. Equilibrium studies. Journal of Biological Chemistry 227(1):301-312.

Wolfe AJ. 2005. The acetate switch. Microbiology and Molecular Biology Reviews 69(1):12-50.

Wu H, Li ZM, Zhou L, Ye Q. 2007. Improved succinic acid production in the anaerobic culture of an *Escherichia coli PflB ldhA* double mutant as a result of enhanced anaplerotic activities in the preceding aerobic culture. Applied and Environmental Microbiology 73(24):7837-7843.

Wu L, Lange HC, van Gulik WM, Heijnen JJ. 2003. Determination of *in vivo* oxygen uptake and carbon dioxide evolution rates from off-gas measurements under highly dynamic conditions. Biotechnology and Bioengineering 81(4):448-458.

Wu L, Mashego MR, van Dam JC, Proell AM, Vinke JL, Ras C, van Winden WA, van Gulik WM, Heijnen JJ. 2005. Quantitative analysis of the microbial metabolome by isotope dilution mass spectrometry using uniformly ^{13}C-labeled cell extracts as internal standards. Analytical Biochemistry 336(2):164-171.

Wu L, van Dam J, Schipper D, Kresnowati MT, Proell AM, Ras C, van Winden WA, van Gulik WM, Heijnen JJ. 2006. Short-term metabolome dynamics and carbon, electron, and ATP balances in chemostat-grown *Saccharomyces cerevisiae* CEN.PK 113-7D following a glucose pulse. Applied and Environmental Microbiology 72(5):3566-3577.

Xu B, Jahic M, Blomsten G, Enfors S-O. 1999. Glucose overflow metabolism and mixed-acid fermentation in aerobic large-scale fed-batch processes with *Escherichia coli*. Applied Microbiology and Biotechnology 51(5):564-571.

Yalkowsky SH, He Y. 2003. Handbook of Aqueous Solubility Data: CRC Press.

Yano M, Izui K. 1997. The replacement of Lys620 by serine desensitizes *Escherichia coli* phosphoenolpyruvate carboxylase to the effects of the feedback inhibitors L-aspartate and L-malate. European Journal of Biochemistry 247(1):74-81.

Zamboni N, Sauer U. 2009. Novel biological insights through metabolomics and ^{13}C-flux analysis. Current Opinion in Microbiology 12(5):553-558.

Zelle RM, de Hulster E, van Winden WA, de Waard P, Dijkema C, Winkler AA, Geertman JMA, van Dijken JP, Pronk JT, van Maris AJA. 2008. Malic acid production by *Saccharomyces cerevisiae*: Engineering of pyruvate carboxylation, oxaloacetate reduction, and malate export. Applied and Environmental Microbiology 74(9):2766-2777.

Zhao J, Shimizu K. 2003. Metabolic flux analysis of *Escherichia coli* K12 grown on ^{13}C-labeled acetate and glucose using GC-MS and powerful flux calculation method. Journal of Biotechnology 101(2):101-117.

Zhou JW, Liu LM, Shi ZP, Du GC, Chen J. 2009. ATP in current biotechnology: Regulation, applications and perspectives. Biotechnology Advances 27(1):94-101.

List of Publications

Journal articles

Taymaz-Nikerel H, Borujeni AE, Verheijen PJT, Heijnen JJ, van Gulik WM. 2010. Genome-derived minimal metabolic models for *Escherichia coli* MG1655 with estimated *in vivo* respiratory ATP stoichiometry. Biotechnology and Bioengineering 107(2): 369-381.

De Mey M[§], Taymaz-Nikerel H[§], Baart G, Waegeman H, Maertens J, Heijnen JJ, van Gulik WM. 2010. Catching prompt metabolite dynamics in *Escherichia coli* with the BioScope at oxygen rich conditions. Metabolic Engineering 12(5): 477-487. *([§]Equal contribution)*

Lara AR[§], Taymaz-Nikerel H[§], Mashego M, van Gulik WM, Heijnen JJ, Ramírez OT, van Winden WA. 2009. Fast dynamic response of the fermentative metabolism of *Escherichia coli* to aerobic and anaerobic glucose pulses. Biotechnology and Bioengineering 104(6): 1153-1161. *([§]Equal contribution)*

Taymaz-Nikerel H, De Mey M, Ras C, ten Pierick A, Seifar RM, van Dam JC, Heijnen JJ, van Gulik WM. 2009. Development and application of a differential method for reliable metabolome analysis in *Escherichia coli*. Analytical Biochemistry 386(1): 9-19.

Taymaz H, Eraslan S, Toksoy Öner E, Alkan T, Ağırbaşlı M, Kırdar B. 2007. Sequence variations within the genes realated to hemostatic imbalance and their impact on coronary artery disease in Turkish population. Thrombosis Research 119(1): 55-62.

Taymaz-Nikerel H, van Gulik WM, Heijnen JJ. Rapid dynamics of *in vivo* flux and metabolite response in central and amino acid pathways in *E. coli*. *Submitted*.

Taymaz-Nikerel H[§], Jamalzadeh E[§], Borujeni AE, van Gulik WM, Heijnen JJ. A thermodynamic analysis of dicarboxylic acid production in microorganisms *([§]Equal contribution). In preparation.*

Taymaz-Nikerel H, De Mey M, Baart G, Maertens J, van Gulik WM, Heijnen JJ. Flux and metabolite flexibility in central metabolism of aerobic glucose-limited *E. coli* to rapid glycolytic and gluconeogenic substrate pulses. *In preparation.*

Taymaz-Nikerel H, De Mey M, Baart G, Maertens J, Foulquie-Moreno MR, Charlier D, van Gulik WM, Heijnen JJ. Comparative fluxome and metabolome analysis for overproduction of succinate. *In preparation.*

De Mey M, Taymaz-Nikerel H, van Dam J, van Winden W, Verheijen PJT, van Gulik WM, Heijnen JJ. Critical assessment of flux analysis from dynamic wash-in of U-^{13}C glucose into steady-state *E. coli* cells. *In preparation.*

Conference proceeding

Bernaerts K, Taymaz-Nikerel H, Heijnen JJ, van Gulik WM, Verheijen PJT. 2009. Identification of lin-log kinetics for the central carbon metabolism of *E. coli*. Proceeding of the Third

International Conference on Foundations of Systems Biology in Engineering (FOSBE 2009, Denver (Colorado), August 9-12, 2009), p.189-192 (CD-ROM).

Oral Presentations

In vivo estimation of energetic parameters of a metabolic network model for substrate limited growth of *E. coli*. Presented at 14th European Congress on Biotechnology (ECB), Barcelona, Spain, September 13-16, 2009.

Stimulus-response and ^{13}C labeling experiments for *in vivo* kinetic analysis of *E. coli*. Presented at KU Leuven Metabolomics and Metabolic Networks Summer School, Leuven, Belgium, September 7-11, 2009.

Metabolome analysis of *E. coli*: evaluation of sampling and quenching techniques. Presented at Fifth Kluyver Centre Symposium, Noordwijkerhout, The Netherlands, January 29-31, 2008.

Evaluation of experimental protocols for metabolome analysis in *Escherichia coli* K12 MG1655. Presented at Metabolic Engineering VI: From recDNA towards Engineering Biological Systems, Noordwijkerhout, The Netherlands, October 1-5, 2006.

Poster Presentations

Taymaz-Nikerel H, De Mey M, Baart G, Maertens J, van Gulik WM, Heijnen JJ. Analysis of short-term dynamic *in vivo* response of *E. coli* to alternative substrate perturbations. Presented at Metabolic Engineering VIII: Metabolic Engineering for Green Growth, Jeju Island, South Korea, June 13-18, 2010.

Taymaz-Nikerel H, Seifar RM, Ras C, ten Pierick A, van Gulik WM, Heijnen JJ. Dynamic *in vivo* response of aerobic chemostat cultivated *E. coli* to a substrate pulse. Presented at 14th European Congress on Biotechnology (ECB), Barcelona, Spain, September 13-16, 2009.

Lara AR, Taymaz-Nikerel H, Mashego M., van Gulik WM, Heijnen JJ, Ramírez OT, van Winden W. Dynamic response of fermentative metabolism of E*scherichia coli* to aerobic and anaerobic glucose pulses. Presented at XIII Congreso Nacional de Biotecnologia y Bioingenieria, Acapulco, Guerrero, Mexico, June 21-26, 2009.

Taymaz Nikerel H, De Mey M, Ras C, ten Pierick A, Seifar RM, van Dam J, Heijnen JJ, van Gulik WM. Development of an accurate method for intracellular metabolome analysis in *E. coli* for *in vivo* kinetic analysis. Presented at Metabolic Engineering VII: Health and Sustainability, Puerto Vallarta, Mexico, September 14-19, 2008.

Taymaz-Nikerel H, De Mey M, Ras C, ten Pierick A, Seifar RM, van Dam J, Heijnen JJ, van Gulik WM. 2009. Development and application of a differential method for reliable metabolome

analysis in *Escherichia coli*. Presented at The Fourth International Conference of the Metabolomics Society, Boston, MA, USA, September 2-6, 2008.

Taymaz-Nikerel H, Ras C, ten Pierick A, Seifar RM, van Dam J, van Gulik WM, Heijnen JJ. Reliable quantification of intracellular metabolites in *Escherichia coli*. Presented at Netherlands Biotechnology Congress-12, Ede, The Netherlands, March 13-14, 2008.

Baart GJE, Beauprez J, Maertens J, Moreno MRF, Mashego M, De Mey M, Taymaz H, Lequeux G, Bhagwat A, Donckels B, Van Horen E, Vancoppenolle E, Boogmans S, De Pauw D, Delmeire D, Bicalho B, van Gulik W, Vanrolleghem P, De Baets B, Cunin R, Charlier D, Heijnen JJ, Soetaert W and Vandamme EJ. Metabolic Engineering and Dynamic Modelling of *Escherichia coli* for the Production of Chemicals from Renewable Resources (MEMORE). Presented at 3rd International Conference on Renewable Resources and Biorefineries, Ghent, Belgium, June 4-6, 2007.

Taymaz H, Mashego MR, Vancoppenolle E, van Winden WA, van Gulik WM, Heijnen JJ. Evaluation of experimental protocols for metabolome analysis in *Escherichia coli* K12 MG1655. Presented at Metabolic Engineering VI: From recDNA towards Engineering Biological Systems, Noordwijkerhout, The Netherlands, October 1-5, 2006.

Curriculum vitae

Hilal Taymaz Nikerel was born on November 22, 1978 in Adana, Turkey and was raised up in Çorlu. After finishing her secondary education at Körfez Science High School in Kocaeli in 1996, she studied chemical engineering at Boğaziçi University in İstanbul with specialization on biochemical engineering (from 1996 to 2001). During the summer holidays in this period, she did internships in several factories. From 2001 to 2003 she carried out her master degree on chemical engineering at Boğaziçi University where she was also working as teaching/research assistant. Her master thesis was titled as "Contribution of Coagulation/ Fibrinolysis Factors to the Risk of Cardiovascular Disease: Their Genetic Determinants". In the following two years she continued to work as a teaching/research assistant in the same department. From 2005 to 2010 she worked as a PhD candidate in the Bioprocess Technology group at Delft University of Technology, The Netherlands under the supervision of Prof. dr. ir. J.J. Heijnen, the results of which are presented in this thesis.

Acknowledgements

I am here, at the point where I desired to be for a long time. Now my head may reach the sky :) I would like to express my gratitude to everyone who helped me, supported me, and was by my side through this amazing PhD journey.

Firstly dear Sef, who is a great teacher, professor, supervisor, ... I learned a lot from you and will always appreciate your attitude to your students. Thanks for accepting me in your group, your continuous motivation, all the discussions, all the help, never sending me away, being always there, especially at 7:45 am and being my inspiration. Dear Walter, my copromotor, daily supervisor. Thanks for being a good guide, creating time whenever I interrupt you, answering all my questions, correcting my manuscripts, giving your valuable touch to my texts, posters, presentations and lastly translating my propositions into Dutch. Dear Peter, thanks for your help with statistics, your valuable stories, sharing your "view of life" and finally for translating the summary of this thesis to Dutch.

Dear committee members Prof. Reuss, Prof. Teusink, Prof. de Winde, Prof. Teixeira de Mattos, Prof. Soetart and Prof. J. Pronk. Thanks for accepting to be a committee member, reading my thesis and giving your comments.

My project was a part of the big MEMORE project. I would like to thank all the members, Wim, Dominique, Gino, Joeri, Ellen, Hendrick, Peter, Gaspard, Jo, Aditya, Brecht, Daniel, Raymond, Perry, Sarah, Karl, for the nice discussions during the meetings (generally zipped but still helpful). And dear Marjan, who was the one uniting the project members, my experiment-mate. Thanks for all your support and help, our collaborative work that ended up in Chapters 4, 6, 7 and 8, always being positive, travelling from Gent *just for* sampling :)

Former and present members of the BPT group, which is a privilege that I was part, where anyone can find friendly atmosphere, scientific richness, and helpful people. Thanks to Wouter, Mlawule (for introducing me the lab), Uly, Penia, Roelco, Roeland, Chiara, Fredrick, Michiel, Andre (for your permanent welcome to my questions, always giving long but helpful answers, fruitful discussions), Emrah, Zheng (for the nice discussions), Lodewijk, Marjan, Evelien, Domenico, Marco, Sergio, Kristel, Rutger, Elaheh (for the collaborative work that ended up in Chapter 3), and later Aljoscha, Amit, Luisa, Rob and Katelijne. The nicest part of the rapid sampling experiments was the ice-creams or cakes eaten after the experiments, isn't it? Special thanks to who helped me carrying my dear heavy reactor. My bigger thanks go to Dirk and Rob for always helping in the laboratory, finding solutions to problems with the set-up, and Susan and Mario. The effort of MS team is visible throughout the thesis, without analysis/support by Jan, Cor, Angela, Johan, Reza and Zhen it would not be possible (sorry about the number of samples I provided). Thank you all for this great five years!

Dear Alvaro, thanks for the nice collaboration that ended up in Chapter 9. Also thanks for your encouragement through your e-mails from Mexico.

Dear students I worked with, especially thanks to Amin who has contributions in Chapter 2 and 3. Also to Tata, Shokoufeh, Mathijs and Armand. Although not all the results ended up in this thesis, it was nice experience to work with you in the lab.

All this work was supported by Sjaak (solving any problem I had), Astrid and Apilena (accepting my last-minute-ready fermentors for autoclave), Jos, Arno and other workshop team members, Herman, Hans (helping with computer related issues), Kees, Robert, Rowdy, secretaries Carla, Jenny, Miranda, Annette, and lastly and mostly Jenifer. Thank you all for making the Kluyver such a beautiful place.

My dear office-mates, Xiaonan, Fredrick, Mervin and Piotr. At different times of these five years sharing our nice office with you was great. Thank you for all the chats, discussions, and Mervin for explaining me the Dutch life. And thanks to friends and colleagues in the/outside of the department: Andre, Fanni, Chiara, Domenico, Valentina, Esengül, Sergio, Iris, Lucie, Joost, Barbara, Francesco, Esteban, Loesje, María, Carol, Carla, Margarida, Tania, Irina. Thank you for the great time we had during coffee breaks, lunches, barbeque parties, bike trips, squash games, bowling, aquaerobics/swimming, pub-quizzes, dinners, chats & drinks in 't Keldertje or Botanical Garden… Dear Esengül additional thanks for your help with the Dutch documents/rules and your nice laughter. And dear Chiara thanks for your continuous support, attached friendship and always smiling face.

During the years in Delft, I had opportunity to visit other countries, thanks to the conference organizers. One of the great trips was to China, organized by dear colleagues. It is an unforgettable memory, greetings to all BioTour 2008 attendees.

I would also like to thank to my dear Turkish friends, Çağrı, Aylin, Elif, Begüm, Şenol, Şafak, Muammer, Anıl, Tolga, Levent, Özlem, Özde, Pervin, Anıl, Fatma, Robert, Filiz, Ayhan. I had great time with the parties, kına geceleri, cinemas, watching football games/eurovisons, always delicious food thanks to Turkish cuisine and to our talents :). Thank you very much for all the pleasure! Dear Çağrı thanks for everything, both good and bad times we had together. I am curious about where your future will take place, because most probably we will be there too :). And dear Aylin, thanks for all the energy you gave, great organizations, and of course your hospitality will never be forgotten. And both of you, thanks for being my paranimfen, sitting next to me during *that* one hour.

I never felt alone with the supports from abroad, thanks to Elif, Hülya and Evren. My dear friends I know that you will always be there and I am grateful to your love, support, encouragement and confidence for me.

As time passes, importance of a great family becomes evident. My dear family, my father, my mother, my brother and my sister, çok çok teşekkürler. Herşey için, sonsuz desteğiniz için, sabrınız için, hiç bitmeyen güveniniz için, ve tabii ki hep hissettiğim ve yaşam kaynağım olan sevginiz için. İyi ki varsınız. And my dear family gets bigger with the presence of dear Bade and my dear future-nephew, thanks. And I also thank to my family-in-law, dear Nihat (will not hear but feel), Nezahat, Kerem and Zeynep for their support and belief in me.

And my most dearest, Emrah, my love, everlasting best friend, *I am only here* because of you. You are (and will be) all my reasons, you know. Teşekkürler!

Now it is time to sail to another sea..